SAPIENZA
UNIVERSITÀ DI ROMA

PhD Course in Biochemistry

XXII Cycle (Academic years 2016 – 2019)

Modulation of hydrogen sulfide metabolism: new pharmacological targets in cancer and amyotrophic lateral sclerosis therapy

Wassily Kandinsky — On White II, 1923

Ph.D. Student
Karim Zuhra

Tutor
Dr. Alessandro Giuffrè

PhD Coordinator
Prof. Stefano Gianni

December 2019

To my parents, for being always there.

"Life is nothing but an electron looking for a place to rest"

Albert Szent Györgyi

Acknowledgments

I would like to express my sincere gratitude to my supervisor Alessandro Giuffrè for the continuous support of my Ph.D. study and related research, for his patience and motivation. Our constant exchange of ideas and opinions significantly contributed to my personal and professional growth. A very special thanks goes to João B. Vicente for being my honorary supervisor, an elder brother, and for giving me the opportunity to join his group and to carry out part of my research at ITQB. What a cracking place where to work!

My sincere thanks to Gianluca Cestra and Michela Di Salvio, for welcoming me to their team, and giving me access to the laboratory and research facilities. Your scientific and moral support have been precious during the last two years. I have found in you two enthusiastic scientists and good friends.

Thank you to all my lab mates and all the Ph.D. students of Biochemistry, for their help and most of all for their friendship. A big thank you goes to Francesca Malagrinò, for the stimulating discussions, for the sleepless nights we were working together, and for all the fun we have had in the past three years. I am also grateful to Daniela Mastronicola for enlightening me the first glance of research.

A special mention goes to Matilde Trabuco, for being a tireless motivator. I could not have imagined having a better travel mate during this period of my life.

Last but not the least, I would like to thank all my friends, my sister Laila, my parents and all my family, which, besides giving me unlimited love and support, is partly responsible for my passion for science.

PUBBLICATIONS

- **N-Acetylcysteine serves as substrate of 3-mercaptopyruvate sulfurtransferase and stimulates sulfide metabolism in colon cancer cells.** Karim Zuhra, Catarina S. Tomé, Letizia Masi, Giorgio Giardina, Giulia Paulini, Francesca Malagrinò, Elena Forte, João B. Vicente, and Alessandro Giuffrè. *Cells 2019, 8(8): 828.*
- **Hydrogen sulfide oxidation: adaptive changes in mitochondria of SW480 colorectal cancer cells upon exposure to hypoxia.** Francesca Malagrinò, Karim Zuhra, Ludovica Mascolo, Daniela Mastronicola, João B. Vicente, Elena Forte and Alessandro Giuffrè. *Oxidative Medicine and Cellular Longevity, 2019, 2019:1*.
- **Hydrogen sulfide metabolism and signaling in the tumor microenvironment.** Alessandro Giuffrè, Catarina S. Tomé, Dalila G. F. Fernandes, Karim Zuhra, and João B. Vicente. *Advances in Experimental Medicine and Biology, in press*.
- **Screening pyridine derivatives against human hydrogen sulfide-synthesizing enzymes by orthogonal methods.** Karim Zuhra, Pedro M. F. Sousa, Giulia Paulini, Ana Rita Lemos, Zenta Kalme, Imants Bisenieks, Egils Bisenieks, Brigita Vigante, Gunars Duburs, Tiago M. Bandeiras, Luciano Saso, Alessandro Giuffrè and João B. Vicente. *Scientific Reports. 2019, 9(1):684*.
- **Hydrogen sulfide mediates ALS-related damages in *Drosophila melanogaster* models and human cells.** Karim Zuhra, Michela Di Salvio, Elena Forte, Alessandro Giuffrè, Gianluca Cestra. *Manuscript in preparation*

INDEX

SUMMARY

Summary

Hydrogen sulfide (H_2S) is an endogenously produced signaling molecule with a key role in human (patho)physiology. In human cells, H_2S is synthetized by cystathionine β-synthase (CBS), cystathionine γ-lysase (CSE) and 3-mercaptopyruvate sulfurtransferase (MST), and is oxidatively catabolized in the mitochondrion by sulfide:quinone oxidoreductase (SQR). H_2S homeostasis relies on a fine balance between its catabolism and biosynthesis. Dysregulation of H_2S metabolism has been associated to neurodegeneration and cancer.

Reprogramming of H_2S metabolism was shown to have pro-survival effects in cancer cells and, recently, N-acetylcysteine (NAC) was suggested to exert its antioxidant effects by increasing intracellular levels of persulfides and polysulfides (collectively known as "sulfane sulfur species"). In *paper 1*, the effect of NAC on the H_2S metabolism of SW480 colon cancer cells was investigated. After exposing cells to 10 mM NAC for 24 hours, both MST and SQR displayed enhanced expression and activity. Moreover, NAC has proven to persist inside colon cancer cells over the 24-hour treatment and to act as a substrate for human MST, as shown working on the isolated recombinant enzyme. Altogether, these findings demonstrate that NAC stimulates H_2S

metabolism in colon cancer cells and serves as substrate for human MST.

Hypoxia is currently recognized as a hallmark of the microenvironment of solid tumors, typically associated to malignant phenotypes. An increasing body of evidence suggests that H_2S can increase cell resistance to hypoxia, while supporting angiogenesis, energy metabolism and drug resistance in cancer. Available information on the role played by H_2S in the tumor microenvironment was reviewed in *paper 3*. In *paper 2*, working on SW480 colon cancer cells, the effect of hypoxia on the ability of cells to metabolize H_2S was evaluated by high resolution respirometry. Hypoxia was found to decrease the mitochondrial content and the overall H_2S-consuming activity of cells, while inducing a mitochondrial enrichment in SQR. These findings suggest that under hypoxic conditions cancer cells undergo adaptive changes to ensure higher intracellular H_2S levels with pro-survival effects and, concomitantly, protection of cell respiration from H_2S poisoning.

In the central nervous system, H_2S plays a central role in the regulation of numerous physiological processes, including neurotransmission and cytoprotection. Dysregulation of sulfide metabolism has been associated to cognitive disturbances like in Down's syndrome and neurodegeneration like in Parkinson's and Alzheimer's

disease. Recently, it was suggested an involvement of H_2S in the etiology of amyotrophic lateral sclerosis (ALS). In the provisional *paper 5*, working on *in vivo* (*Drosophila melanogaster*) and *in vitro* ALS models, the effect of H_2S on ALS-associated neurotoxicity was investigated. Of interest, knock down or pharmacological inhibition of the two H_2S-synthetizing enzymes CBS and CSE was found to result in ameliorative phenotypes. These results triggered additional, still on-going investigations aimed at elucidating the impact of H_2S in ALS and the underlined molecular mechanisms.

Given the role of H_2S in human (patho)physiology, there is an urgent need for inhibitors of the human H_2S-synthetizing enzymes with pharmacological potential. In *paper 4*, a small library of newly synthesized pyridine derivatives was screened for the ability of these compounds to inhibit the human CBS, CSE and MST, as recombinantly produced in *Escherichia coli* and purified. By combining a wide range of biophysical and biochemical techniques, two compounds with similar molecular scaffold were found to weakly inhibit both CBS and CSE. In this study, a robust methodological platform for compound screening was set-up, and two hit compounds were identified which will be used as a starting point for future screening campaigns.

The new knowledge acquired here, while deepening our understanding of the role of H_2S in human (patho)physiology and, more specifically, in tumorigenesis and neurodegeneration, will hopefully set the basis for innovative diagnostic and therapeutic approaches.

INTRODUCTION

Introduction

H_2S is a colorless gas with a typical smell of rotten eggs, known for its environmental hazard and toxicity. Yet, its beneficial properties have been known since the time of Romans, who used to bath in natural sulfur springs as a therapeutic treatment [1]. Sulfur containing water has indeed been shown to have anti-inflammatory, anti-bacterial, vasodilatory and anti-fungal action, highlighting the double-faced behavior of this gas [2]. An epidemiological study associated consumption of food enriched in organosulfur compounds, namely garlic and onions, to reduced cardiovascular disease incidence [3]. A few decades ago, the first finding that H_2S is endogenously produced in humans had turn on the spotlight on the possible involvement of this gaseous species in physiology [4]. Currently, H_2S, along with nitric oxide (NO) and carbon monoxide (CO), belongs to a group of gaseous signaling molecules, collectively known as "gasotransmitters", which regulate several physiological processes. Particularly, H_2S was found to modulate blood flow, cellular stress response, inflammation, immune response, apoptosis and energy metabolism. Conversely, dysregulation of H_2S metabolism has been associated to several pathologies, including metabolic, cardiovascular, neurodegenerative and oncological diseases [5].

In the following introduction, are reported the physico-chemical properties that make H_2S able to act as a chemical messenger as well as a substrate of the mitochondrial respiratory chain. Furthermore, it will be presented the tight balance governing H_2S metabolism, and the main diseases associated to the perturbation of this equilibrium. Eventually, it will be discussed whether pharmacological modulation of H_2S metabolism

represents a prospective strategy for therapeutic applications.

1. Physico-chemical properties of H_2S and sulfane sulfur species

Hydrogen sulfide is a weak acid with molecular formula H_2S and molecular weight of 34.08 $g \cdot mol^{-1}$. It is a potentially toxic, flammable and corrosive gas, with relatively high solubility in water (100 mM at 1 atm and 25 °C). Being a diprotic acid, in aqueous solutions H_2S is in equilibrium with its conjugate bases, hydrosulfide (HS^-) and sulfide (S^{2-}), according to $pK_{a1} \approx 7.0$ (H_2S/HS^-) and $pK_{a2} \approx 19$ (HS^-/S^{2-}) [6]. Despite its significant dipole moment (0.97 D) and polarizability, H_2S is relatively permeable to lipid bilayer and, therefore, able to diffuse from a cellular compartment to another, with no need of specific transporters [7]. H_2S speciation in cellular compartments occurs in a pH-dependent manner, existing mostly as deprotonated in the mitochondrion (pH ≈ 8), as H_2S in lysosomes (pH ≈ 4.7), and being partitioned in one third H_2S and two third HS^- in the cytosol (pH ≈ 7.4), where S^{2-} concentrations are negligible (Fig. 1) [5]. Hereafter, with the terms "hydrogen sulfide" and "sulfide" we will refer to H_2S, HS^- and S^{2-} as a whole.

Sulfur is a chalcogen element, in group 16 of the periodic table. Positioned immediately under the oxygen element, it displays an electronic configuration $1s^2 2s^2 2p^6 3s^2 3p^4$, corresponding to 6 valence electrons and a vacant 3d orbital, thus being able to assume any oxidation state between -2 and +6. In the form of sulfide, it is in its lowest oxidation state, thus making of H_2S a reducing specie with a marked nucleophilic character [8]. Particularly, H_2S was reported to be a direct scavenger of electrophiles such as reactive oxygen species (ROS) and reactive nitrogen species (RNS), thus exerting an antioxidative action in biological systems [9]. Its oxidation products,

persulfides (R-SSH) and polysulfides ($RS(S)_nH$ and $RS(S)_nSR$), are overall known as "sulfane sulfur species". They are characterized by two or more sulfur atoms arranged in a chain and are believed to serve as a pool of sulfide molecules, released 'on demand' under particular conditions [10]. Sulfane sulfur species are more reactive towards electrophiles than their corresponding thiol species [11], likely due to the unshared pairs of electrons on the atom adjacent to the nucleophilic atom (α-effect) [12, 13]. In recent years, a growing interest has emerged in sulfane sulfur species, such as cysteine persulfide (CysSSH) and glutathione persulfide (GSSH), which were proposed to be the actual mediators of some of the biological roles of H_2S [14].

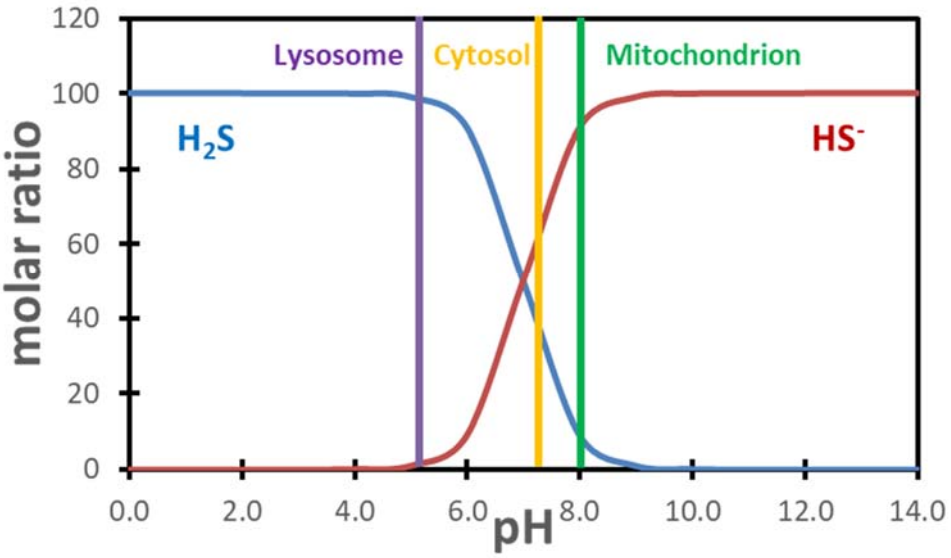

Figure 1. Speciation of sulfide in aqueous solution. Diagram of H_2S speciation in its conjugate bases and relative distribution in cellular compartments. Calculations were made using $pK(HS^-) = 7.0$ and $pK(S^{2-}) = 19$.

2. H_2S metabolism

Along with nitric oxide (NO) and carbon monoxide (CO), H_2S fulfils all criteria for being a gasotransmitter. These three molecules are endogenously produced, exert a signalling direct function without a second messenger and freely diffuse through biological membrane. It has been described a close relationship between the three gasotransmitters, which indeed exert complementary physiological functions and mutually regulate each other's metabolism [15]. Particularly, the physiological functions of H_2S are exerted within a narrow concentration window, this gaseous species being potentially toxic at higher or lower than physiological amounts [16]. Therefore, steady-state levels of H_2S must be kept under tight control through a fine regulation of its biosynthesis and catabolism [17]. Enzymes involved in H_2S metabolism are differently distributed in the organism, thus tuning sulfide availability according to the cellular district and body region [18]. Here is provided an overview of H_2S metabolism.

2.1 H_2S synthesis

2.1.1 Transsulfuration pathway

In mammals H_2S is synthetized by the two cytosolic enzymes cystathionine β-synthase (CBS) and cystathionine γ-lyase (CSE), and by 3-mercaptopyruvate sulfurtransferase (MST), partly localized in mitochondria. CBS and CSE are involved in the transsulfuration pathway, which is a branch of the methionine (Met) cycle (Fig. 2), converting dietary-derived Met into Cys. The first intermediate of this process is S-adenosylmethionine (AdoMet), a methyl donor essentially involved in all the methylation reactions in human physiology. The subsequent AdoMet de-methylation produces S-adenosylhomocysteine (AdoHcy), which, in turn, is hydrolysed to adenosine

and homocysteine (Hcy). The latter has two possible fates: i) entering the transsulfuration pathway or ii) being re-methylated to methionine, thus completing the cycle. In mammals, the transsulfuration pathway is irreversible and generates a range of bioactive sulfur compounds. Indeed, the final product Cys is a precursor for glutathione (GSH) and coenzyme A (CoA) biosynthesis. GSH together with its oxidized form (GSSG) is the most relevant low-molecular weight (LMW) antioxidant in humans, being highly represented in cellular systems (millimolar range). CoA is a transporter of acyl groups, involved in the fatty acids' metabolism and Kreb's cycle. The transsulfuration pathway is therefore a crossroad of different biochemical pathways and, certainly, its positive or negative modulation has a relevant impact on cellular homeostasis.

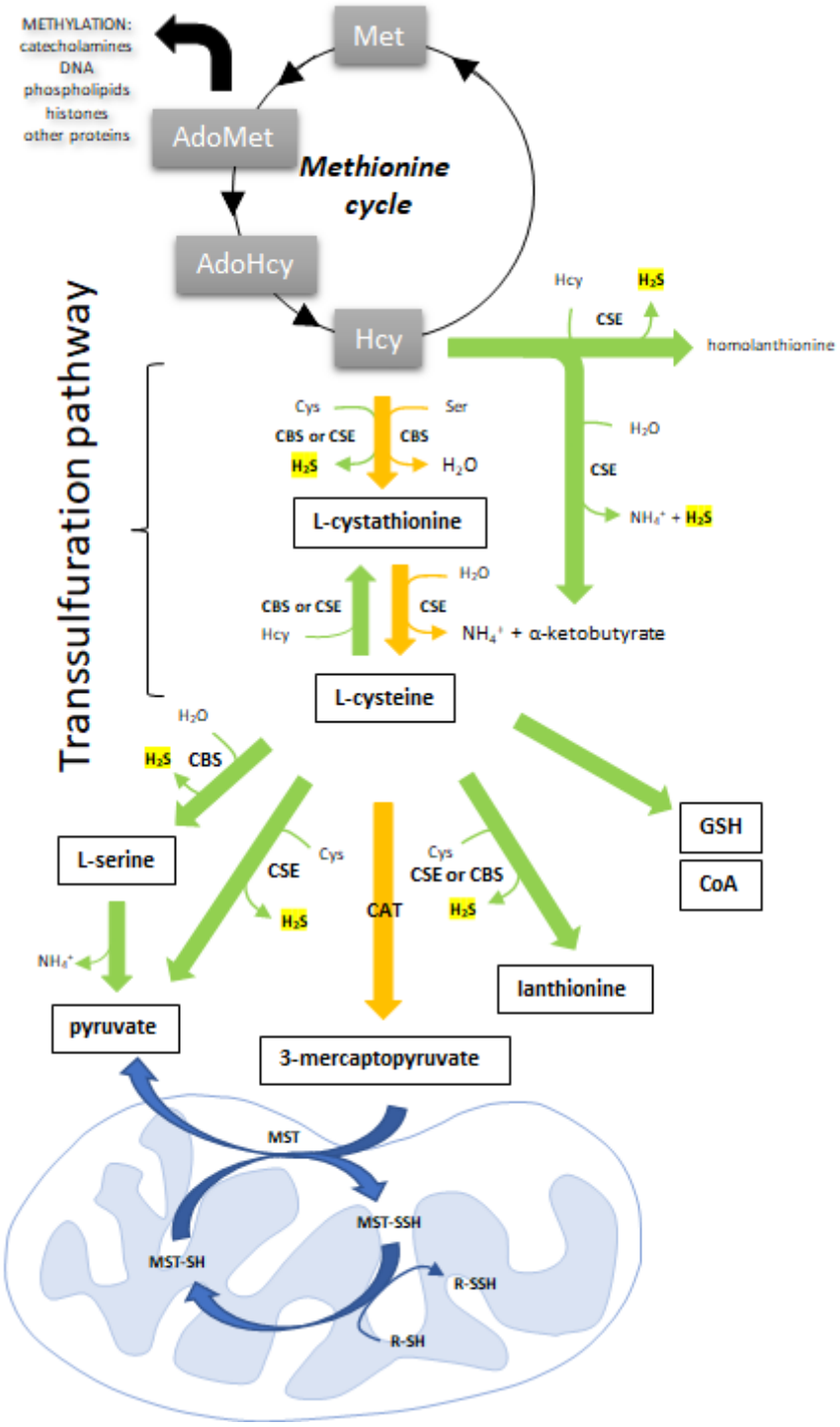
METHYLATION:
catecholamines
DNA
phospholipids
histones
other proteins
Met
AdoMet
Methionine cycle
AdoHcy
Hcy
Transsulfuration pathway
Hcy
H2S
CSE
homolanthionine
Cys
Ser
CBS or CSE
CBS
H2S
H2O
L-cystathionine
H2O
CSE
NH4+ + H2S
CBS or CSE
Hcy
CSE
NH4+ + α-ketobutyrate
L-cysteine
H2O
H2S
CBS
L-serine
CSE
Cys
H2S
CAT
Cys
CSE or CBS
H2S
GSH
CoA
NH4+
pyruvate
lanthionine
3-mercaptopyruvate
MST
MST-SSH
MST-SH
R-SSH
R-SH

Figure 2. Transsulfuration pathway. The transsulfuration (TS) is a branch the demethylation/remethylation cycle of methionine (black), overall leading to conversion of methionine to cysteine. Briefly, the first reaction of the TS is catalyzed by cystathionine β-synthase (CBS) and consists in the condensation of homocysteine (Hcy) and serine (Ser) into cystathionine, which in turn is converted into cysteine (Cys) by cystathionine γ-lyase (CSE). Subsequently, cysteine aminotransferase (CAT) converts Cys into 3-mercaptopyruvate, the substrate of 3-mercaptopyruvate sulfurtransferase (MST), partly localized in mitochondria. Beside the "canonical" reactions (orange), there is a variety of alternative reactions (green).

2.1.2 Cystathionine β-synthase

CBS catalyzes the first reaction of the two-steps transsulfuration pathway, which converts Hcy into Cys. The canonical reaction catalyzed by CBS is the condensation of L-serine and L-Hcy, yielding L-cystathionine and elimination of a H_2O molecule (Fig. 3A). However, due to its catalytical promiscuity, a range of alternative reactions take place according to substrates availability. For instance, similarly to its canonical reaction, CBS catalyzes the condensation of L-Hcy with L-Cys in place of L-serine, thus producing H_2S (Fig. 3C), whereas in the presence of L-cysteine alone CBS produces H_2S *via* β-replacement (Fig. 3D) [19, 20]. More recently it was reported that a further possible substrate is L-cystine (CysSSCys), leading the production of CysSSH (Fig. 3F), believed to be a mediator of the H_2S biological effects, along with others sulfane sulfur species [21].

The full-length CBS is enzymatically active as a homotetramer. Each monomer has 551 amino acids (61 kDa) and consists of an N-terminal heme-binding domain, a central pyridoxal 5'-phosphate (PLP)-binding domain and a C-terminal AdoMet-binding domain [22]. The catalytic active site is buried in a pocket of the PLP-binding domain, its accessibility being regulated by the AdoMet-binding domain. Particularly, it was reported that upon AdoMet

stimulation, CBS activity increases 3 to 5-fold, whereas the truncated CBS (45 kDa), lacking the regulatory domain, is constitutively activated [23]. At the N-terminus, the heme prosthetic group functions as a redox sensor, mediating CBS inactivation in the reduced (ferrous) state. Intriguingly, NO and CO bind tightly the ferrous heme, thus stabilizing the inactivated CBS and negatively modulating H_2S biosynthesis [24-27]. Another redox sensitive site is Cys_{346}, which has been reported to undergo an S-gluthationylation, resulting in a 3-fold increase of CBS enzymatic activity. This mechanism has been suggested to take place under oxidative conditions, thus increasing the transsulfuration-derived Cys availability and, consequently, promoting GSH biosynthesis [28]. Conversely, under reducing environment, the reduction of Cys disulfide (Cys_{272}–Cys_{275}) in the catalytic domain is responsible for an increase of CBS activity. This mechanism may occur as a response to hypoxia, a condition in which increased H_2S production has been extensively documented [29, 30].

CBS is generally viewed as a cytosolic enzyme, however under hypoxic conditions higher CBS levels were observed in mitochondria [31]. Moreover, the SUMOylated CBS was found to accumulate in cellular nuclei [32], overall supporting the idea that H_2S production can be locally modulated in particular conditions. CBS was abundantly found in liver, pancreas, kidney and brain [33, 34]. Particularly, it was reported that in the nervous system CBS is mainly expressed in glia and astrocytes rather than neurons, as shown on mice brain tissues [4, 35].

2.1.3 Cystathionine γ-lyase

CSE is a homotetrameric enzyme, composed of 405 amino acids monomers (44 kDa), each showing an N-terminal PLP-binding domain and a C-terminal domain [22]. CSE catalyzes the second step of the transsulfuration

pathway, converting the CBS-derived cystathionine into Cys, α-ketobutyrate and ammonia in an α,γ-elimination reaction (Fig. 3B). Similarly to CBS, CSE is catalytical versatile, being able to produce H_2S from L-Hcy γ-replacement (Fig. 3E). Intriguingly, CSE shares with CBS some common reactions, such as L-Cys and L-Hcy condensation (Fig 3C), L-Cys β-replacement (Fig. 3D) and L-cystine α,β-elimination (Fig. 3F) (reviewed in [5]). In view of this substrate promiscuity, it could be argued that the CBS and CSE have partially overlapping biological roles. Indeed, recently Kabil et al. have observed that chronic inhibition of CBS leads to CSE up-regulation, resulting in compensation of CBS catalytical deficiency and revealing a complementary rather than redundant role [36]. CSE activity has been reported to be Ca^{2+}-dependent, being negatively modulated by increased Ca^{2+} intracellular levels. However, so far, the molecular mechanism behind Ca^{2+}-mediated regulation remains elusive [37].

CSE has a mostly cytosolic cellular localization but, similarly to CBS, it has been reported to undergo translocation into mitochondria under hypoxic conditions [38]. CSE is abundantly expressed in the liver. Lower levels were detected in kidney and smooth muscle, while its expression in the brain is negligible as compared to CBS [16].

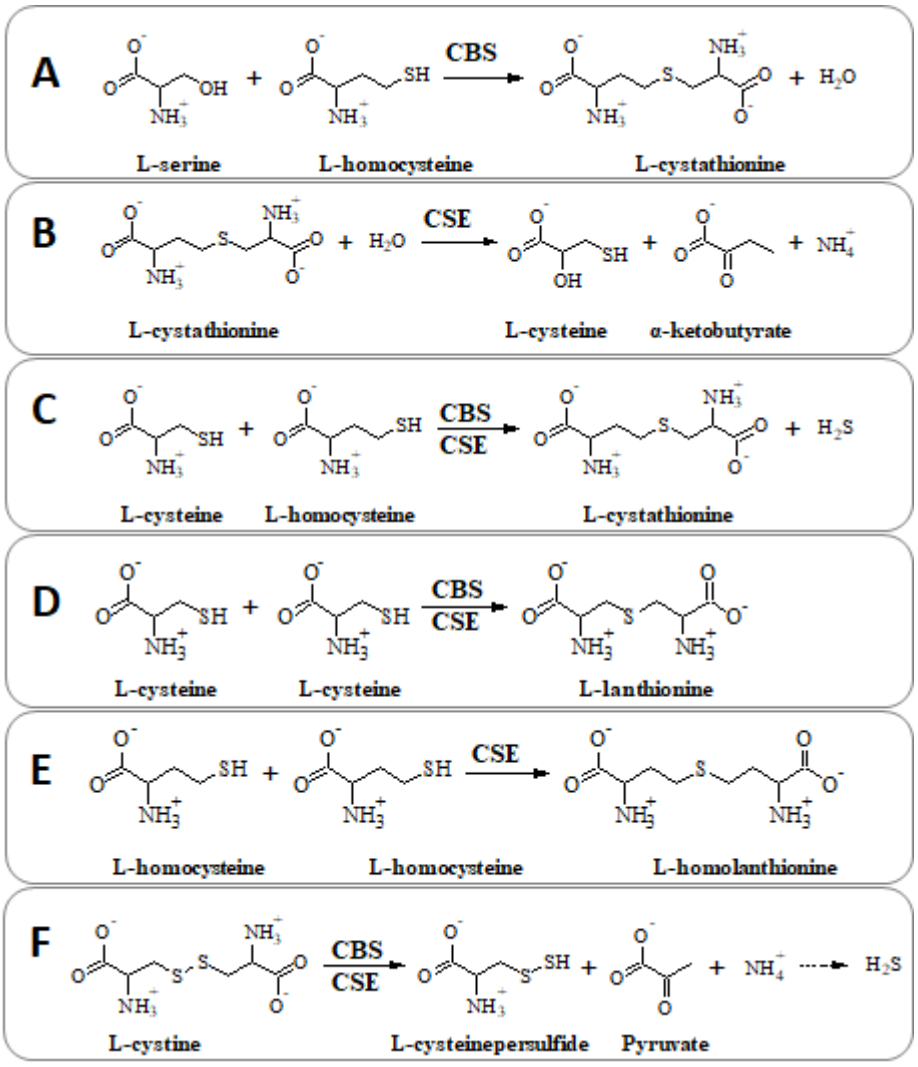

Figure 3. Catalytic promiscuity of cystathionine β-synthase (CBS) and cystathionine γ-lyase (CSE). Structure of metabolites and reaction scheme of H_2S biosynthesis by CBS and CSE as part of the transsulfuration pathway. In the panels A and B are represented the "canonical" reaction for CBS and CSE, respectively. Panels C – F show alternative reactions.

2.1.4 Mercaptopyruvate sulfurtransferase

MST is a 297 amino acids monomeric enzyme (33 kDa), made of two structurally similar domains separated by a cleft harbouring the active site. The substrate of MST is 3-mercaptopyruvate (3MP), a product of Cys transamination catalysed by cysteine aminotransferase (CAT; Fig. 4A). In the active site, 3MP transfers a sulfur atom to the catalytic Cys residue (Cys_{248}), thus generating pyruvate and a reactive enzyme-bound Cys persulfide (CysSSH) (Fig. 4B). Regeneration of the thiolic form of the active site occurs in the presence of a thiol reducing agent, such as thioredoxin, glutathione or Cys (Fig. 4C) [39, 40]. MST is a redox sensitive enzyme, and oxidative conditions are able to dramatically reduce its activity [41].

So far, two MST isoforms with comparable enzymatic activity have been identified: MST-1 localized in the cytosol, and MST-2 dually localized in cytosol and mitochondria. Compared to CBS and CSE, MST has a broader distribution in human tissues, being nearly ubiquitous [42].

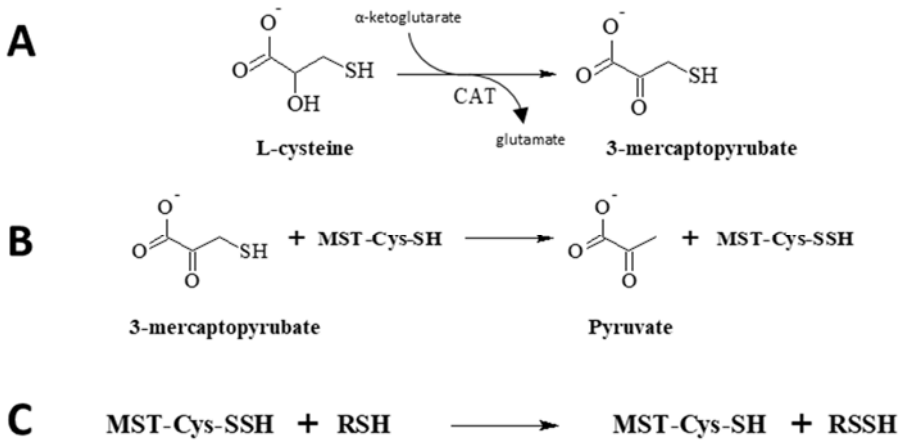

Figure 4. H_2S biosynthesis through the CAT/MST pathway. A) Cysteine aminotransferase (CAT) catalyzes the transamination between α-ketoglutarate and cysteine,

leading to formation of 3-mercaptopyruvate (3MP) and glutamate. B) 3-mercaptopyruvate sulfurtransferase (MST) converts 3MP into pyruvate, with the concomitant generation of an MST-bound Cys persulfide. C) MST is catalytically regenerated in the presence of a sulfur acceptor.

2.1.5 Gut microbiota

The gut microbiota is one of the major sources of sulfide in the organism [43]. Sulfur produced in the bowel has been shown to have a physiological role not only locally, but also at a systemic level [44]. In the intestine, the total sulfide level is high, reaching in the colorectal tract concentrations in the range of millimolar, an amount potentially lethal for local tissues [45]. To survive this extreme environment, colonocytes have developed a sophisticated enzymatic machinery, responsible for sulfide oxidative detoxification [46]. Dysregulation of this pathway may lead to chronic inflammation resulting in ulcerative colitis, Crohn's disease and cancer [47].

2.2 Human H_2S-catabolizing enzymes

In mammals, H_2S breakdown takes place mainly in the mitochondrion in a multistep process catalyzed by a group of enzymes, collectively known as "sulfide oxidizing unit" (SOU), which couples the oxidation of 2 sulfide molecule with the consumption of 1.5 molecule of dioxygen [46]. The four actors involved in this process are the inner mitochondrial membrane-associated enzyme sulfide:quinone oxidoreductase (SQR), the mitochondrial matrix enzymes persulfide dioxygenase (ETHE1) and thiosulfate sulfurtransferase (TST), and sulfite oxidase (SOx) located in the mitochondrial intermembrane space. The final products of H_2S breakdown are thiosulfate ($S_2O_3^{2-}$) and sulfate (SO_4^{2-}) [48]. The distribution of these enzymes is not

homogeneous in the organism, as they are more expressed where sulfide is likely to accumulate. Therefore, it is not surprising that the SOU enzymes are markedly expressed in the bowel region, particularly in the colorectal tract [49]. Sulfide metabolism is a fascinating example of the inclination of biological system to evolve, adopting strategies aimed at turning a potential threat into an opportunity [50]. Indeed, SOU couples sulfide detoxification with stimulation of the electron transport chain (ETC), thus stimulating OXPHOS and ATP production. Furthermore, H_2S has been proposed to act as an 'emergency' substrate when the Krebs cycle efficiency decreases and is insufficient to satisfy the energy needs [48]. In the following sections we will go through this intricate process, analysing the enzymes involved, their molecular mechanisms, the distribution of SOU in human tissues and, finally, the implications for cell bioenergetics.

2.2.1 An overview on the oxidative phosphorylation pathway

The OXPHOS is the end point of a complex metabolic pathway in which the 'dis-assembly line' of glucose, through glycolysis and Kreb's cycle, is coupled with energy production. Particularly, Kreb's cycle-derived electrons are shuttled to the inner mitochondrial membrane, where the four complexes (I-IV) of ETC generate an electron flux culminating with the production of ATP. In the first step, NADH and succinate donate electrons to Complex I (NADH:ubiquinone dehydrogenase) and Complex II (succinate dehydrogenate), respectively. By means of coenzyme Q (CoQ), the electrons are then transferred to Complex III (cytochrome bc_1), cytochrome *c*, Complex IV (cytochrome *c* oxidase or CcOx), and eventually to the final acceptor O_2, which is reduced to H_2O. Complexes I, III and IV are proton pumps, overall translocating from the mitochondrial matrix to the intermembrane space 10

protons (from oxidation of one molecule of NADH) or 6 protons (from oxidation of one molecule of succinate/$FADH_2$). The electrochemical gradient generated across the inner mitochondrial membrane is the driving force used by Complex V (ATP synthase) to produce ATP (Fig. 5).

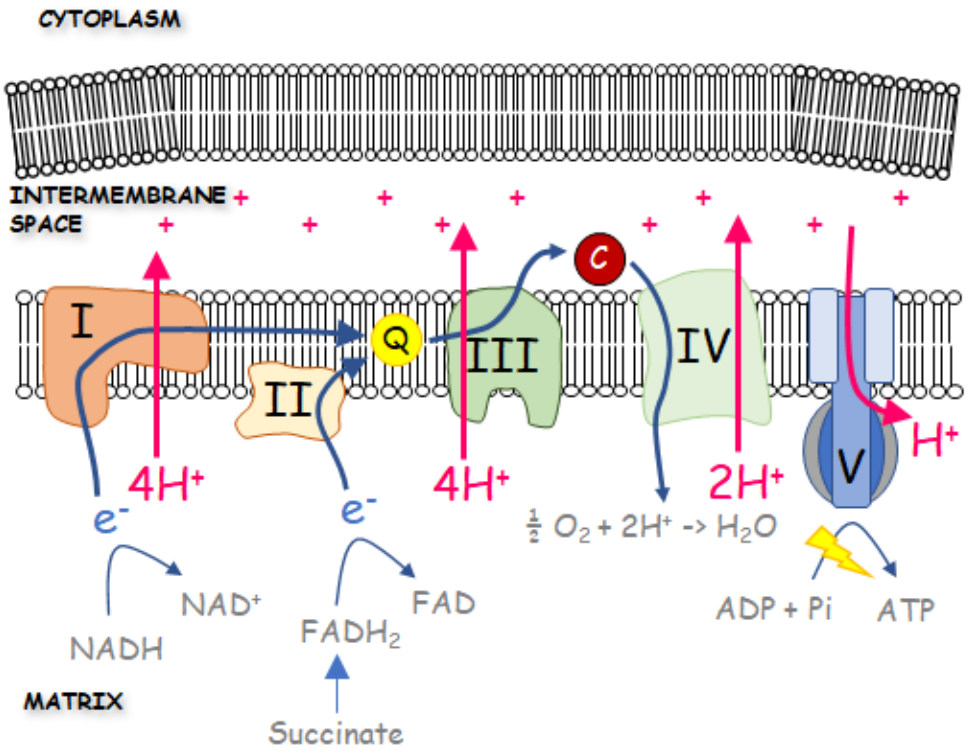

Figure 5. Oxidative phosphorylation (OXOHOS) pathway. Schematic representation of the OXPHOS pathway. The Kreb's cycle-derived substrates, NADH and succinate, transfer electrons to complex I and II, respectively. The electrons are hence transferred, through coenzyme Q (Q), to complex III, cytochrome *c* (C), complex IV and oxygen (O_2), which is eventually reduced to H_2O. Complexes I, III and IV pump protons from the mitochondrial matrix side to the intermembrane space, thus generating an electrochemical gradient used by Complex V to produce ATP.

2.2.2 SOU

SQR is the enzyme catalysing the first and rate-limiting reaction of sulfide oxidative breakdown, by transferring a sulfur atom to an acceptor, most likely GSH. Concomitantly, sulfide-derived electrons are transferred to a flavin adenine dinucleotide (FAD) cofactor and injected into the ETC through CoQ, leading to reduction of 0.5 molecule of O_2 [51]. SQR is an integral membrane protein of 450 amino acids (50 kDa). Its active site, accessible from the mitochondrial matrix, harbours a Cys disulfide (Cys_{201}/Cys_{379}) flanked by a FAD moiety [52]. The GSH persulfide (GSSH) produced by SQR acts as a substrate for ETHE1, which consumes 0.5 molecule of O_2 per molecule of GSSH [53]. In the presence of GSSH, the sulfite can be oxidized to thiosulfate by TST or, alternatively, to sulfate by SOx, a heme- and molybdenum-containing enzyme, which uses a H_2O molecule as an oxygen atom donor and cytochrome *c* as electron acceptor (Fig. 6) [51]. Overall, mitochondrial H_2S oxidation stimulates energy production and is associated to consumption ~ 0.75 O_2 molecules (0.25 by CcOX and 0.5 by ETHE1) per molecule of H_2S [46].

As mentioned, the limiting reaction is catalyzed by SQR, thus SOU efficiency strictly depends on SQR expression. This enzyme is widespread in the organism, and it is abundantly found in the kidney, colorectal tract, whereas its expression in the brain is generally low [17, 49].

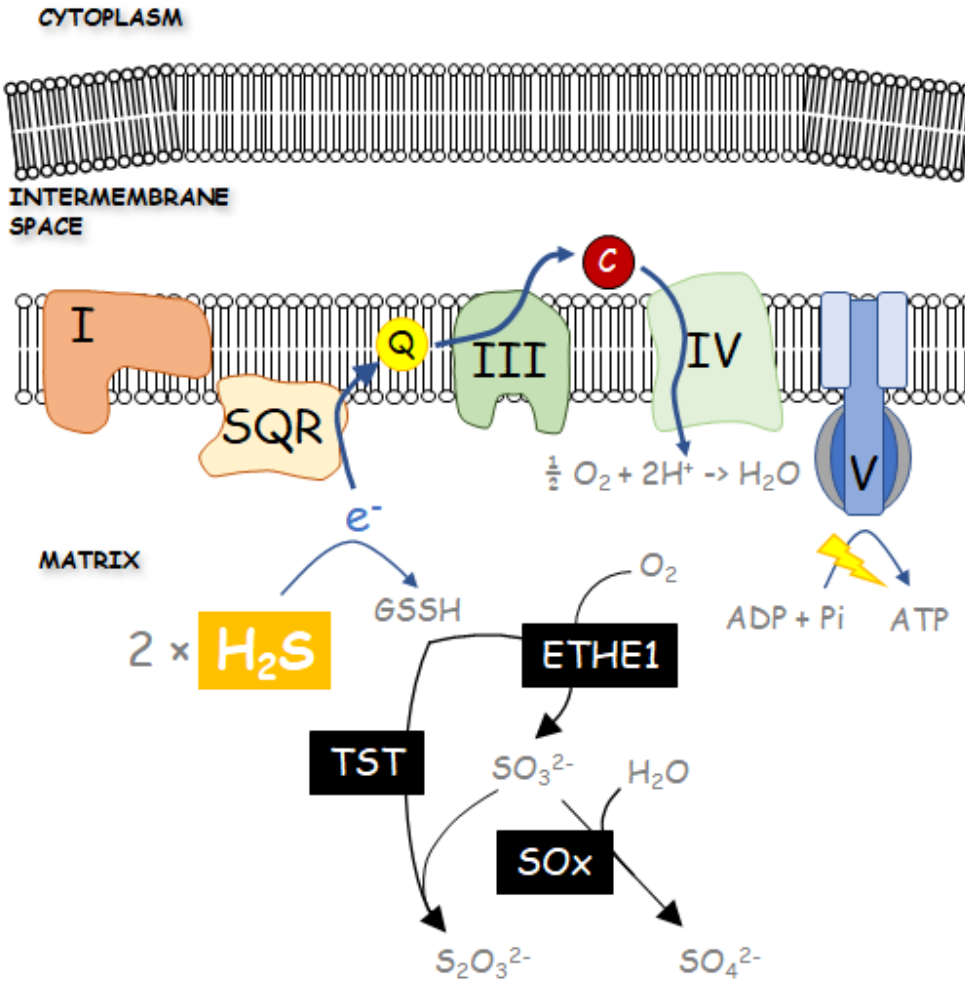

Figure 6. Sulfide oxidizing unit (SOU). Schematic representation of H_2S oxidative breakdown pathway. H_2S-derived electrons are injected by sulfide:quinone oxidoreductase (SQR) in the electron transport chain, thus stimulating ATP production and consuming 0.5 molecules of oxygen (O_2) every 2 H_2S molecules. Concomitantly, SQR transfers a sulfur atom to glutathione (GSH), which is pesulfidated to GSSH. Persulfide dioxygenase (ETHE1) oxidizes the GSSH-derived sulfur to sulfite (SO_3^{2-}). This reaction consumes 1 O_2 molecule. Thiosulfate sulfurtransferase (TST), using a GSSH-derived sulfur, further oxidizes SO_3^{2-} to thiosulfate ($S_2O_3^{2-}$). Alternatively, SO_3^{2-} can be oxidized to sulfate (SO_4^{2-}) by sulfite oxidase (SOx), which uses H_2O as a source of oxygen atoms. Overall this process

couples sulfide oxidation with energy production, consuming 0.75 O_2 molecules per molecule of H_2S.

3. H_2S role in patho-physiology

3.1 H_2S-mediated signaling

A hallmark of gasotransmitters is their ability to tightly bind heme moiety of target proteins, such as haemoglobin and CcOx. Unlike CO and NO, in which case this mechanism has been thoroughly described, the reaction of hemeproteins with sulphide has been studied in less detail. The biological role of gasotransmitters is often strictly linked one each other, as their regulation is mutually dependent (as reviewed in [5]). Their interplay has been documented in different body systems, including the cardiovascular and nervous ones. The relevant role of gasotransmitters is proven by the increasing evidence associating dysregulation of their metabolism to different pathologies, like cardiovascular, neurodegenerative and oncological diseases [5, 54-56]. H_2S signalling is prevalently accomplished through protein persulfidation, a post-translational modification which, along with phosphorylation, has been emerging as a major route for protein functional modulation [57]. It consists on the transfer of a sulfur atom to a protein thiol from a sulfur donor, such as GSSH or CysSSH [14]. Sulfane sulfur species are by-products of H_2S-metabolizing enzymes, namely CBS, CSE, MST and SQR (already discussed in section 2). Recently, it has been proposed that the mitochondrial isoform of cysteinyl-tRNA synthetases (CARSs), is one of the main source of CysSSH [58]. Indeed, as Cys concentration is 3-fold higher in the mitochondrion, this organelle might be the principal source of sulfane sulfur species [38], which are then transferred to the cytoplasm [59]. A clear advantage of persulfidation is its reversibility in the presence of reducing agents like low molecular weight

thiols, such as GSH or Cys [60]. However, it should be noted that not all solvent-exposed protein thiols are susceptible to persulfidation, as the reactivity of a target Cys is crucially modulated by its surroundings [57]. The effect of sulfide in biological systems has been described to have a bell-shape character, exerting beneficial properties within a narrow window of concentration. Increased H_2S production has been associated with a number of diseases, like cancer, cardiovascular and neurological disturbs [15, 54, 61]. Exposure to elevated sulfide levels was reported to impair mitochondrial respiration, thus leading cytotoxicity and cell death [62]. Conversely, too low sulfide levels have been associated to neurodegeneration [63]. The following sections will focus on the role of H_2S on cell bioenergetics, cytoprotection, neuromodulation and the involvement of H_2S in cancer development and neurodegeneration.

3.2 Bioenergetic role

Persulfidation is a main route of H_2S signalling, involved in the regulation of different metabolic pathways, including energy metabolism. For instance, the mitochondrial inner membrane protein ATP synthase (complex V) was found to be persulfidated in its active state, thus suggesting a potential role of sulfide in the regulation of this enzyme activity [64]. Moreover, glyceraldehyde-3-phosphate dehydrogenase (GAPDH) activity was reported to be positively modulated through persulfidation. In support of this observation, authors reported a significant decrease of GAPDH activity in CSE knock out mice, revealing an involvement of H_2S in the stimulation of glycolysis [65]. However, some concerns were raised about the biological role of GAPDH persulfidation, as the isolated enzyme was found to be associated to enzymatic deactivation rather than activation [66]. H_2S has a bimodal effect

on cellular bioenergetics, being a potent inhibitor of CcOx (K_I = 0.2 μM at pH 7.4), thus acting as an ETC promotor or suppressor in a concentration-dependent manner [67]. Despite its relatively low K_I, impairment of ETC in cells or isolated mitochondria occurs in the H_2S concentration range of tens of micromolar. This apparent discrepancy has been firstly clarified with the finding that mitochondria are equipped with SOU, which detoxifies cells from an excess of H_2S [53]. Oxidative sulfide breakdown has been extensively described in mammals, where this pathway is coupled with energy production [48]. However, as reported by Lagoutte et al., the relevance of H_2S as an ETC substrate is quite limited in terms of energy production and its role should be considered marginal in physiological conditions. Conversely, it acquires more importance when Krebs cycle-derived electron donors are insufficient to guarantee an adequate electron flux [46]. This may happen in cancer cells, which undergo a metabolic switch favouring glycolysis over the more efficient OXPHOS pathway [68, 69].

3.3 Cancer biology

The biology of cancer is a complex matter, due to the adaptability of tumoral cells to different environments and tissues. Despite the great variety of cancer types, remarkable efforts aimed at identifying some common features outlining the phenotypic profile of tumors. These “cancer hallmarks” include high proliferative rate, apoptosis evasion, mitochondrial dysregulation, and cellular bioenergetics reprogramming. In addition to this, the surrounding tumor microenvironment seems to play a relevant role in shaping the cancer response to environmental conditions [70]. The involvement of H_2S in cancer biology has been extensively studied and it has been shown to influence, directly or indirectly, tumoral growth at all levels (as reviewed in [54]). For

instance, ROS overproduction resulting from mitochondrial dysregulation has been shown to stimulate and promote cancer initiation, progression, invasion, metastasis, and chemoresistance [71]. On the other hand, excessively high ROS levels may compromise cell functions, leading to apoptosis and cell death [72, 73]. Therefore, in order to tolerate this potentially adverse environment, cancer cells reprogram their metabolism and boost their antioxidant defence [74]. In this respect, H_2S seems to play an important role as witnessed by the higher sulfide levels found in different cancer types [54]. Increased H_2S production, due to overexpression of H_2S-sysnthetizing enzymes, was documented in colorectal, ovarian, breast, melanoma and prostate cancer cells [75-77]. In human colorectal cancer cells HCT116, CBS knock-down or its pharmacological inhibition markedly reduced cellular proliferation, migration and tumor xenograft growth [77]. Accordingly, CBS overexpression correlated with ROS levels reduction in ovarian cancer cells, while its inhibition has been shown to lead to oxidative stress and cytotoxicity [78]. CSE is abundantly expressed in breast cancer, promoting cellular proliferation and metastasis [79]. The Cys prodrug *N*-acetylcysteine (NAC) has been shown to increase resistance to anticancer therapy by exerting an antioxidant effect [80]. Intriguingly, Ezerina et al demonstrated that the molecular mechanism behind the cytoprotective action of NAC is related to its ability to enhance the production of H_2S and sulfane sulfur species [81]. H_2S has been shown to positively modulate *via* persulfidation the lactate dehydrogenase activity and to act as substrate of ETC, overall supporting cancer bioenergetics [82]. Upregulation of CBS and MST has been associated to resistance to commonly used chemotherapeutics, as shown for different cancer types [78, 83, 84]. Accordingly, in chemoresistant cancer cells it was observed an increased Cys import, correlating with enhanced H_2S-synthesizing enzymes activity [74].

Exposure of colon cancer cell lines to NaHS, a fast releaser of H_2S, or treatment with NAC, abrogated the pro-apoptotic effect of β-phenyethyl isothiocyanate [85]. The evasion to apoptosis has been proposed to be a key element in tumor progression and a potential target for cancer treatment [85-88]. Particularly, Sen et al. have shown that the anti-apoptotic role of NF-κB is mediated by protein persulfidation [88, 89]. Currently it is believed that NF-κB plays a crucial role in the link between chronic inflammation and cancer progression by strongly influencing the tumoral microenvironment [90].

3.4 Tumor microenvironment

Although tumorigenesis has been traditionally viewed as a cell self-directed process, currently it has been recognized the fundamental role of the tumoral microenvironment, including the surrounding blood vessels, signaling molecules and the extracellular matrix (ECM). [91, 92]. ECM provides a physical scaffold supporting neoplastic expansion. Its remodelling, exerted by metalloprotease (MMPs), has been proposed to play an important role in tumor proliferation and migration [92]. Interestingly, exposure to exogenous sulfide donors has been reported to enhance cancer cells proliferation together with MMPs upregulation, suggesting a role for H_2S in ECM remodelling [88, 93]. Because of their higher metabolic rate as compared to the surrounding healthy tissues, neoplastic cells are typically associated to neovascular formation, a common way for solid tumors to fulfil the increased demand of nutrients and O_2 [94]. In this respect, H_2S has been reported to mediate the pro-angiogenic effect of the vascular endothelial growth factor (VEGF), thus stimulating proliferation and migration of endothelial cells [95]. Particularly, experimental evidence supports the involvement in this process of K_{ATP} channels opening by persulfidation [95, 96]. Nutrients and O_2 deprivation is believed to be one

of the stimuli leading to activation of angiogenesis, and the role of hypoxia in neovascular formation, tumor malignancy and drug resistance has been extensively studied [97]. A master regulator of the transcriptional responses to hypoxia is the hypoxia-inducible factor (HIF), mediating cellular proliferation and migration, evasion to apoptosis, metabolic reprogramming, metalloprotease upregulation and angiogenesis [98, 99]. Interestingly, it was observed that the majority of the responses associated to low O_2 availability is somewhat overlapping with some of the cellular signalling pathways activated by H_2S [100]. This suggests an intimate interplay between the two gaseous species. Several lines of evidence have shown that H_2S induces HIF upregulation [95, 101-103], suggesting that sulfide could be implicated in integrating the hypoxia-induced response [41]. Indeed, hypoxia has been shown to positively modulate H_2S levels by reducing its mitochondrial catabolism and enhancing its production, hence sulfide was proposed to act as an O_2 sensor (as reviewed by [30]). Mitochondria seem to play a crucial role in hypoxia signalling pathway, as they are the main source of ROS, which are directly involved in HIF accumulation [104]. Interestingly, it has been reported that under hypoxic conditions, CSE translocates from the cytosol to mitochondria, where its activity is boosted by the approximately 3-fold higher concentration of Cys [38]. Moreover, it has been shown that, upon hypoxic conditions, CBS escapes Lon protease-mediated degradation and thus accumulates in mitochondria [31]. It has been suggested that the resulting increased H_2S levels provide protection to mitochondria in hypoxic conditions [105, 106]. On the other hand, this mechanism must be kept under tight control as it can be a double-edged sword. Indeed, the shortage of O_2 is responsible for i) reduction of SOU activity, resulting in increased CcOx sensitivity to H_2S

[107] and ii) promotion of a metabolic switch favouring glycolysis rather than OXPHOS [108], overall being a potential threat for cellular bioenergetics.

3.5 From neuroprotection to neurodegeneration

The cytoprotectant role of H_2S in the nervous system has been thoroughly investigated (as reviewed in [61]). It is well recognized that sulfide exerts an antioxidant and anti-aging effect at different levels. H_2S is a reducing species and, as such, at physiological concentrations it is able to directly scavenge ROS [109]. Indeed, it has been reported that its potency in peroxynitrite scavenging is qualitatively and quantitatively comparable to that of GSH [110]. GSH is a first-line antioxidant as witnessed by its high intracellular concentration (in the millimolar range), while H_2S may directly contribute to cytoprotection mostly at extracellular level, where GSH is absent [16]. Interestingly, H_2S has proven to play an important role in regulating GSH availability by i) stimulating the Cys transporter and the cystine/glutamate antiporter and ii) enhancing the activity of γ-glutamylcysteine synthetase involved in GSH biosynthesis [111, 112]. At a transcriptional level, H_2S exerts its neuroprotective effect by activating the antioxidant Keap1-NRF2 pathway *via* persulfidation of Keap1 [113]. The crucial role of H_2S as neuroprotectant is confirmed by the co-existence of the three H_2S-syntetizing enzymes in the nervous system [16]. Dysregulation of sulfide metabolism has been associated to several neurological diseases. Decreased sulfide levels have been associated to Huntington's disease, where depletion of CSE and low disposal of Cys were suggested to contribute to neuronal death [114]. Administration of exogenous sulfide to mouse models of Alzheimer's disease (AD) has been shown to be effective in reducing inflammation and improving spatial memory, suggesting a potential therapeutic application of H_2S releasers [115]. Protein

persulfidation has been demonstrated to enhance the catalytical activity of parkin, a neuroprotective protein which was found to be abundantly de-sulfhydrated in brains of patients with Parkinson's disease (PD) [116]. In accordance with its bell-shaped character, elevated intracellular concentrations of sulfide might be toxic as well, interfering with different cellular functions and resulting in mental aberrations [61]. Sulfide accumulation was described for ethylmalonic encephalopathy, an inborn mitochondrial disease characterized by developmental delay and intellectual disorders [117]. CBS overexpression has been reported in Down's syndrome (DS) patients and suggested to contribute to cognitive dysfunction in DS children and maybe to the onset of AD in DS adults [118]. Recently, a relationship was established between H_2S and amyotrophic lateral sclerosis (ALS), a fatal disease characterized by a progressive motoneurons degeneration, resulting in muscle atrophy. High sulfide levels were measured in spinal fluid of ALS patients and mouse spinal cord cell culture, where CBS appeared to play a major role [119]. The pathological processes underlying motoneurons death are mostly unknown, and the possible involvement of H_2S in the etiology of ALS is likely but needs to be further assessed.

4. Modulation of H_2S metabolism as a therapeutic strategy

Given that both increased or decreased H_2S levels have been associated to pathology, a plausible therapeutic strategy would be the use of sulfide donors or inhibitors of H_2S biosynthesis, depending on the type of disease. In cancer cells, exogenous H_2S-donors (up to tens of micromolar) proved to enhance cellular proliferation and migration, while higher concentrations (up to hundreds of micromolar) were shown to be cytotoxic [41, 120]. In some neurological diseases like PD and AD, low-dosage injection of sulfide donors

was shown to protect from neuronal damage and improve behavioural tests in animal models (as reviewed in [63]). Alternatively, boosting sulfide biosynthesis may prove beneficial for pharmacological applications. For instance, recently Ezerina et al. have suggested that the cytoprotectant and antioxidant effect of NAC results from enhanced production of sulfane sulfur species [81]. H_2S was suggested to provide protection to various cancer types, where its increased metabolism was shown to promote cellular proliferation, migration and chemoresistance. Although various studies have highlighted the role of CSE and MST in cancer biology [54, 121], CBS has shown to be the most promising pharmacological target [41]. Aminooxyacetic acid (AOAA) has been commonly used as CBS inhibitor ($IC_{50} \approx 8$ μM) [122]. Treatment with AOAA caused impairment of cell proliferation and migration of colon cancer cell lines, nearly mimicking CBS silencing [77]. Similarly, AOAA-induced cytotoxicity was confirmed in ovarian, breast and pancreatic cancer cells [78, 123, 124]. In *vivo*, pharmacological inhibition of CBS caused regression of both colon and breast cancer [77, 123]. Despite CBS inhibition by AOAA has proven to be effective, major concerns were raised about AOAA selectivity, as it inhibits other PLP-dependent enzymes, including CSE [122]. Recently, it was found that benserazide, a drug approved for the treatment of PD, was reported to inhibit CBS ($IC_{50} \approx 30$ μM) with a good selectivity, exerting an antitumoral action both in *vitro* and in *vivo* [125]. CBS dysregulation was described also in the central nervous system and suggested to play a role in the etiology of different pathologies, including ALS [119, 126]. The patho-physiological role of CBS seems to be particularly relevant, the enzyme being at the crossroad of different biochemical pathways. Hence, the importance of finding new and selective inhibitors of CBS.

OBJECTIVES

Objectives

Hydrogen sulfide (H_2S) is one of the gaseous signaling molecules, also known as "gasotransmitters", which has been shown to play a key role in the regulation of numerous (patho)physiological processes. In human cells, H_2S is endogenously produced by cystathionine β-synthase (CBS), cystathionine γ-lysase (CSE) [127] and 3-mercaptopyruvate sulfurtransferase (MST) [39], and is oxidatively catabolized in the mitochondrion [128]. The maintenance of a tight balance between H_2S biosynthesis and breakdown is crucial, as high levels of H_2S can result in mitochondrial dysfunction. This balance is partly achieved through a crosstalk between H_2S and other gaseous molecules, namely oxygen (O_2), nitric oxide (NO) and carbon monoxide (CO) [5]. Currently, it is believed that part of the biological roles of H_2S are mediated by protein persulfidation, a post-translational modification whereby a sulfur atom is transferred to a protein thiol, and more in general by "sulfane sulfur species", reactive species containing zero-valent (S^0) sulfur atoms, such as persulides and polysulfides [57]. Unbalanced biosynthesis or catabolism of H_2S was found to be associated with neurodegeneration and cancer [54, 129]. Hence, the importance of exploring the impact of H_2S metabolism in human diseases in the perspective of developing innovative pharmacological interventions.

A growing body of literature indicates that endogenous H_2S promotes proliferation, drug resistance and bioenergetics in cancer cells. Oxidative stress caused by reactive oxygen species (ROS) is a typical feature of tumor cells, associated to some cancer hallmarks such as evasion from apoptosis, mitochondrial dysfunction and propensity to

metastatization [71]. On the other hand, many oncological drugs acts by inducing high intracellular ROS levels and thereof promoting cancer cell death together with unwanted side effects. The supplementation of antioxidant drugs as a preventative strategy to reduce the side effects of chemotherapy unfortunately has proven to negatively affect cancer treatment [130]. Recently, it was proposed that the mechanism of action of N-acetylcysteine (NAC), a widely used pharmacological antioxidant, involves the stimulation of sulfane sulfur species production [81]. Therefore, NAC could provide protection to tumor cells by boosting sulfur metabolism, in line with the role of H_2S and sulfane sulfur in cancer biology. To test this hypothesis, we investigated the effect of NAC on H_2S metabolism by working both on SW480 colon cancer cells and recombinant human MST (*paper 1*).

It is increasingly recognized the role of tumor microenvironment at all stages of cancer development, favoring progression, migration and propensity to metastatization. The milieu of solid tumors is typically characterized by low O_2 tension, a condition which seems to have implications in the progression of neoplasia [131]. In this respect, H_2S was suggested to act as an O_2 sensor, being upregulated upon low O_2 availability and mediating some of the hypoxia-induced adaptive changes [30, 105]. This prompted us to investigate the ability of tumoral cells to dispose H_2S under hypoxic conditions by evaluating the influence of hypoxia on the mitochondrial catabolism of H_2S. To this purpose, we performed high-resolution respirometric measurements on a SW480 colon cancer cells (*paper 2*). An additional task was to provide a critical review of the literature dealing with the role played by H_2S in the tumor microenvironment (*paper 3*).

The emerging role of H_2S as neuromodulator has proven to be relevant in human patho-physiology, as attested by the still growing body of literature questioning whether dysregulation of sulfide metabolism contributes to neurodegeneration [129]. Indeed, altered H_2S signaling has been reported for Huntington's, Alzheimer's and Parkinson's disease [61]. Recently, amyotrophic lateral sclerosis (ALS) was reported to be associated with increased H_2S levels [119]. However, the literature dealing with H_2S metabolism and ALS is much poorer than that for other neurological diseases. Therefore, one goal of the present thesis has been to gain insight into the functional role of H_2S in ALS pathogenesis, by combining work on in *vivo* (*Drosophila melanogaster*) and in *vitro* (HeLa cells) models (*paper 5*).

Finally, despite the role of H_2S in human pathology has been extensively documented, currently there are no available potent and selective inhibitors against human CBS, CSE and MST, suitable for pharmacological applications. Therefore, an additional goal of this thesis project was to set up a high-throughput platform for drug discovery employing a multimethodological approach, with the declared aim of searching for inhibitors against the three human H_2S-synthetizing enzymes (*paper 4*).

MATERIALS AND METHODS

1. Materials

1.1 *Chemicals*

Acetyl coenzyme A (A2056), benserazide (B7283), 7-azido-4-methylcoumarin (7AzC, L511455), reduced β-nicotinamide adenine dinucleotide (NADH, disodium salt, N8129), Dulbecco's Modified Eagle Medium (DMEM) cell culture medium (D6546), CelLytic™MT cell lysis reagent (C2978), coenzyme Q_1 (CoQ_1, C7956), D-lactic dehydrogenase (LDH, L2395), 5,5'-dithiobis-(2-nitrobenzoic acid) (DTNB, D8130), L-cysteine (Cys, C1276), L-homocysteine (Hcy, H6503), *N*-acetylcysteine (NAC, A7250), metaphosphoric acid (239275), 2-mercaptoethanol (805740), sodium 3-mercaptopyruvate dihydrate (3MP, 90374), *N*-ethylmaleimide (NEM, 34115-M), oxaloacetate (O7753), perchloric acid (PCA, 77232), protease inhibitor cocktail (P8340), rabbit polyclonal antibody against human SQR (HPA017079) and CBS (SAB1411562), anti-rabbit peroxidase secondary antibody (A6154), rotenone (R8875), sodium sulfide nonahydrate ($Na_2S \cdot 9H_2O$, 431648), sodium sulfite (S0505), thiazolyl blue tetrazolium bromide (MTT, M2128), trypan blue (T98154) were purchased from Sigma. The bicinchoninic acid assay (BCA) kit and rabbit polyclonal antibody against human MST (PA528779) were from Thermo Fisher Scientific. Mouse monoclonal antibody against human CSE (SC-365381) was purchased from Santa Cruz Biotechnology. Fetal bovine serum (FBS), L-glutamine, streptomycin and penicillin were from Biowest. Mini-PROTEAN TGX stain-free precast gels, the Clarity Western ECL substrate and the Laemmli protein sample buffer were purchased from Bio-Rad. Bovine serum albumin was from AppliChem. Anti-TIAR antibody (610352) was from BD Biosciences, whereas the anti-mouse secondary antibody (green) from Hybridoma, GYY4137 from CAYMAN, the Protein Thermal Shift Dye Kit™

from Applied Biosystems and the SPR Amine Coupling Kit, type 2 from GE Healthcare.

1.2 *Human cell lines*

The human colon cancer cell line SW480 (ATCC no. CCL228™) and the human cervix adenocarcinoma cell line HeLa (ATCC no. CCL-2™) were purchased from the American Type Culture Collection.

1.3 *Expression vectors*

The pET28b plasmid containing human CBS cDNA with restriction sites for NdeI and XhoI and a premature stop codon at position 409, yielding an N-terminally His-tagged protein devoid of the C-terminal 143 residues corresponding to the AdoMet binding domain. The plasmid confers kanamycin resistance and encodes for the truncated $CBS_{\Delta 409\text{-}551}$ (tCBS).

The pET28b plasmid containing human CSE cDNA with restriction sites for NdeI and XhoI, yielding an N-terminally His-tagged protein. The plasmid confers kanamycin resistance and encodes for the hCSE.

The pET28b plasmid containing human MST cDNA with restriction sites for NdeI and XhoI, yielding an N-terminally His-tagged protein. The plasmid confers kanamycin resistance and encodes for the hMST.

1.4 *Drosophila fly stocks*

All fly stocks were purchased from the Bloomington Drosophila Stock Centre. Oregon flies were used as healthy control. Stocks #51370 were transgenic flies overexpressing wtTDP43 specifically in the eyes, under the GAL4-GMR system. Stocks #36767 and #41877 were transgenic flies expressing dsRNA for RNAi of CBS under GAL4-UAS binary system. Stocks

#36766 and #41876 were transgenic flies respectively producing dsRNA for RNAi of CSE under GAL4-UAS binary system.

2. Methods

2.1 Human cell cultures and treatment

2.1.1 Human cells culture

The human cell lines SW480 and HeLa were grown in DMEM containing 4.5 $g \cdot L^{-1}$ glucose, supplemented with 2 mM L-glutamine, 10% (v/v) heat-inactivated FBS, 100 $U \cdot mL^{-1}$ penicillin and 100 $\mu g \cdot mL^{-1}$ streptomycin. Cells were typically cultured in 25 cm^2- or 75 cm^2-flasks at 37 °C, 20% O_2 (v/v), 5% CO_2 (v/v) and were subcultured every two/three days at approximately 70-80% confluence.

2.1.2 N-acetylcysteine (NAC) treatment

SW480 cells were seeded in five 25 cm^2-flasks (1×10^6 cells/flask) and grown at 37 °C and 5% CO_2. After 24 h, the culture medium was replaced with fresh medium as such (control) or supplemented with 10 mM NAC, and further incubated for 24 h. Cells were harvested by trypsinization, washed with fresh culture medium and centrifuged at 1,000 ×g for 5 min, yielding typically 2–3 $\times 10^7$ cells per condition. Under the tested conditions, 10 mM NAC proved not to be cytotoxic, as evaluated with the trypan blue dye exclusion test (section 2.1.5) and the MTT viability assay (section 2.1.6).

2.1.3 Hypoxic treatment

SW480 cells at 50-60% confluence were incubated in the Galaxy 14 S (Eppendorf) incubator at 1% O_2 (v/v), 37 °C, 5% CO_2 (v/v). After 24 h, cells

were harvested, washed in fresh culture medium, counted with the trypan blue dye exclusion test, centrifuged at 1,000 ×g for 5 min and resuspended in fresh medium at a final density of 8×10^6 cells·mL^{-1}.

2.1.4 Sodium arsenite treatment

75×10^3 cells/well of HeLa cells grown in DMEM were seeded on top of sterile 12-mm glass coverslips (final volume of 1 mL), positioned on the bottom of a 24-well plate, and grown overnight at 37 °C and 5% CO_2. The day after, cells were treated for 6 hours with 25 μM, 50 μM, 100 μM or no benserazide, an inhibitor of the H_2S-sythetizing enzyme CBS. Afterwards, sublethal oxidative stress was induced by treating cells with 1 mM sodium arsenite (NaAs) for 30 min at 37 °C. Cells were then washed three times in pre-filtered PBS, fixed with 500 μL of 4% *p*-formaldeide for 20 min and incubated at 4 °C in PBS overnight.

2.1.5 Trypan blue dye exclusion test

The trypan blue dye exclusion test is commonly used to estimate cell viability. The assay relies on the ability of trypan blue to stain with blue colour broken cells, whereas living cells do not incorporate the dye. Briefly, 50 μL of the cell suspension was diluted 1:1 (v/v) with trypan blue dye and gently resuspended. Cells were then counted using a Neubauer counting chamber.

2.1.6 MTT viability assay

The thiazolyl blue tetrazolium bromide (MTT) assay is widely used to evaluate cell viability and proliferation. MTT is a water-soluble tetrazolium salt which in eukaryotic cells is reduced by mitochondrial succinate dehydrogenase, leading to formation of purple formazan crystals. Briefly,

5,000 cells/well were seeded in a 96-well plate, in a final volume of 200 µl of DMEM. After 24 h-incubation at 37 °C and 5% CO_2, the medium was replaced with fresh medium as such (control) or supplemented with 10 mM NAC. After 24 hour-incubation, the medium was replaced with medium supplemented with 0.5 $mg \cdot mL^{-1}$ MTT, and further incubated for 2.5 hours. Subsequently, the medium was soaked away with a vacuum pump and replaced with 100 µl dimethyl sulfoxide (DMSO), and samples were incubated in an orbital shaker for 10 min, at room temperature and in the dark, in order to solubilize the coloured formazan crystals. Cell viability was estimated colorimetrically by measuring with an Appliskan plate-reader the absorbance at 570 nm-*minus*-690 nm.

2.1.7 Total protein extraction

Cells were harvested by trypsinization and centrifugation at 1,000 ×g for 5 min at 20 °C, washed in PBS and lysed using the CelLytic™MT cell lysis reagent in the presence of 1% v/v protease inhibitor cocktail. After 15-min incubation in an orbital shaker at 4°C and 400 RPM, cells were centrifuged at 10,000 ×g for 10 min and the resulting supernatant was stored at -80 °C.

2.1.8 Isolation of mitochondria

The protocol used to isolate mitochondria was adapted from [132]. Cells were harvested by trypsinization and centrifugation (1,000 ×g for 5 min at 4 °C). The pelleted cells were washed twice in cold PBS, resuspended in 1 mL of hypotonic buffer (3.5 mM Tris HCl pH 7.8, 2.5 mM NaCl, 0.5 mM $MgCl_2$, 1% v/v protease inhibitors cocktail) and kept on ice for 1 hour. The sample was then transferred to a pre-chilled glass-teflon tissue grinder and homogenized with 100 strokes. Afterwards, 100 µL of hypertonic buffer (350 mM Tris HCl

pH 7.8, 250 mM NaCl, 50 mM $MgCl_2$) were added to the homogenate, which was gently resuspended, followed by centrifugation at 1,000 ×g for 5 min at 4 °C to pellet unbroken cells, debris and nuclei. The supernatant was kept on ice, while the pellet was resuspended in isotonic buffer (35 mM Tris HCl pH 7.8, 25 mM NaCl, 5 mM $MgCl_2$, 1% protease inhibitor) and centrifuged a second time at 1,000 ×g for 5 min at 4 °C. The supernatants from both centrifugations were pooled and centrifuged at 20,000 ×g for 30 min at 4 °C. The mitochondria-enriched pellet was solubilized in 150 µL of 10 mM Tris HCl pH 7.4, 250 mM sucrose, 1 mM EDTA, 0.5% (w/v) N-lauryl maltoside, as reported in [66]. The efficiency of mitochondrial isolation was verified by Western blot using SQR as mitochondrial marker.

2.2 **Sulfide and thiols quantification**

2.2.1 Preparation of sulfide and thiols stock solutions

Stock solutions of sulphide were prepared by dissolving Na_2S crystals in degassed ultra-pure (Milli-Q®) water under a N_2 atmosphere, as reported in [8]. Sulfide concentration was then measured spectrophotometrically with the Ellman's reagent (5,5'-dithiobis-2-nitrobenzoic acid [DTNB]), which generates two molecules of the yellow compound 5-thio-2-nitrobenzoate anion (NTB^-) per molecule of H_2S. Briefly, in a 1 mL-quartz cuvette were dispensed 850 µL of ultra-pure water supplemented with 100 µL of 5 mM DTNB solubilized in 100 mM HEPES pH 7.5. After blank acquisition, at least three consecutive kinetic runs were collected, each following the addition of 1 µL of the Na_2S solution. The observed change in absorbance (ΔA) was used to determine the concentration of the Na_2S solution using the molar extinction coefficient ε_{412} = 14,150 $M^{-1} \cdot cm^{-1}$, as recommended by the manufacturer, and by dividing the obatined value by 2 [133]. Thiol compounds, namely Cys, NAC, GSH and 3MP,

were solubilised in Tris HCl buffer, pH 8, and titrated as reported above. Unlike H_2S, the final value was not divided by 2, as the stoichiometry of the reaction between DTNB and thiol compounds other than H_2S is 1:1. Finally, solutions of sulfide or thiol compounds were diluted to the desired working concentration.

2.2.2 Thiol quantification by reverse phase high performance liquid chromatography (RP-HPLC)

In this method adapted from [134], thiol compounds from a biological sample were first derivatized with DTNB and then quantified with RP-HPLC. In contrast to NTB^-, showing an absorption maximum at 412 nm, DTNB derivatives of alkyl thiols are detected at 330 nm. Herein, SW480 cells treated with or without NAC (section 2.1.2) were harvested and washed twice in PBS. The pellet was resuspended in 250 µL ultra-pure (Milli-Q®) water, kept on ice for 30 min and then lysed by three cycles of freeze-thawing. Lysates were mixed with 250 µl of 3.34% meta phosphoric acid and, after vortexing, were incubated for 30 min on ice, followed by centrifugation at 12,000 ×g for 10 min at 4 °C. The supernatant was filtered and 120 µL of the deproteinized solution were mixed with 60 µL of 0.3 M Na_2HPO_4 and 90 µL of 1 mM DTNB. NAC quantification was performed at room temperature by injecting 100 µL of DTNB-derivatized samples into a PrevailTM C8 column (150 × 4.6 mm – 5 µm) (Grace) connected to a double pump HPLC apparatus (Azura ASM 2.1L; Knauer) equipped with an UV-Vis detector (Azura ASM 2.1L; Knauer). Injections were performed automatically using an HT300L autosampler (HTA). The elution was monitored by recording the signal at 331 nm using the following mobile phase: 20 mM NaH_2PO_4 pH 4.9 (Buffer A) and 100% methanol (Buffer B). The flow rate was 1 $mL \cdot min^{-1}$ and the concentration of buffer B was varied during the elution as follows: 2% B for 10 mL, then the

concentration of B was raised to 40% in a steep gradient of 2 mL, kept at 40% for 1 mL to allow the elution of the unreacted excess of DTNB, then brought back to 2% in a 2 mL reverse gradient and kept at 2% for 7 mL before injection of the next sample. Calibrations were performed by injecting standards of NAC, GSH and Cys at known concentrations after derivatization with DTNB.

2.3 **Bacterial cell cultures**

2.3.1 Generation of competent cells

Escherichia coli BL21-Gold (DE3) cells (1 mL) were grown overnight at 37 °C in 100 mL of Luria Bertani broth (LB). Cells were then incubated at 37 °C and 220 RPM until the optical density at 600 nm (OD_{600}) reached 0.4 - 0.6, and then further incubated for 30 min on ice and centrifuged at 4,000 ×g for 20 min at 4 °C. The supernatant was discarded, the pellet gently resuspended in 10 mL of a cold solution of 0.1 M $CaCl_2$ and then further incubated on ice for 2 hours. Eventually, cells were centrifuged at 4,000 ×g for 20 min at 4 °C, the supernatant discarded, and the pellet was resuspended in 20% glycerol and frozen at -80°C in 100-µl aliquots.

2.3.2 Transformation of competent cells

50 µL of competent cells were gently mixed with 2.5 µl of the plasmid (pET28b_hCBS$_{\Delta 409\text{-}551}$, pET28b_hCSE or pET28b_hMST) and incubated on ice for 30 min. The cell suspension was then incubated at 42 °C for 45 seconds, followed by 2-min incubation on ice. Afterwards, 600 µl of sterile LB were added and cells were incubated at 37 °C for 45 min (750 RPM). Finally, 200-300 µl of transformed cells were plated on a Petri dish containing LB-agar with the appropriate antibiotics and incubated at 37 °C overnight. On the day after, the plate was stored at 4 °C until use.

2.3.3 Recombinant protein expression

A preinocule was obtained by incubating overnight, under stirring and at 37 °C, a single colony of the transformed cells in 250 mL of LB medium containing kanamycin (50 μg·mL^{-1}). On the day after, two liters of M9 medium containing the same antibiotic were inoculated with 20 mL of the preinocule and incubated at 37 °C and 180 RPM until the OD_{600} value reached 0.4 - 0.6. Hence, protein expression was induced with 500 μM of isopropyl-1-thio-ß-D-galactopyranoside (IPTG) and, only in the case of CBS, 75 mg·L^{-1} δ-aminolevulinic acid were added to stimulate heme biosynthesis. The suspension was incubated overnight at 20°C and 160 RPM, followed by harvesting and storing at -45°C until use.

2.4 **Purification of recombinant proteins**

The cell pellet (typically 6 g) was thawed and resuspended in 10 ml of buffer A (50 mM potassium phosphate buffer [KPi], pH 7.0, 300 mM KCl, 0.5 mM tris(2-carboxyethyl)phosphine [TCEP], 10% glycerol), supplemented with 1 mg·mL^{-1} lysozyme (AppliChem), 1 mM phenylmethylsulfonyl fluoride (PMFS; Roche), and DNase I (AppliChem). The suspension was incubated on ice for 15 min, followed by sonication (8 cycles of 30 s separated by 1 min-cooling period) and centrifugation at 18,000 RPM for 10 min at 4°C, using a JA-20 rotor. The supernatant was supplemented with 10 mM imidazole and loaded at 2.5 mL·min^{-1} onto a 5-mL HisTrap FF crude column (GE Healthcare), pre-equilibrated with 15 volumes of buffer B (Buffer A supplemented with 10 mM imidazole) at a rate of 2.5 mL·min^{-1}. Protein purification was carried out using ÅKTA Prime fast performance liquid chromatography system (GE Healthcare) equipped with UV-Vis detector.

2.4.1 tCBS purification

Purification of tCBS was carried out as reported in [26]. The protein was eluted in two fractions with 30 volumes of a linear gradient of buffer C (Buffer A supplemented with 500 mM imidazole) up to 50% and, subsequently, 100%. The fractions containing tCBS were identified based on the A280/A430 ratio, pooled, concentrated and then loaded onto a S200 column.

2.4.2 CSE purification

The protocol used for hCSE purification was adapted from [22]. The protein was eluted with a linear gradient of buffer C up to 80%. The fractions containing hCSE, identified based on the A280/A430 ratio, were pooled, concentrated and then loaded onto a S200 column.

2.4.3 MST purification

The protocol used for hMST purification was adapted from [39]. The protein was eluted with a linear gradient of buffer C up to 40%. The fractions containing hMST, identified based on the A280/A430 ratio, were pooled, concentrated and then loaded onto a S200 column.

The pooled samples were concentrated with an Amicon Ultra-15 centrifugal filter unit with an Ultracel-30 membrane (Millipore). The obtained sample was loaded onto a HiLoad 26/600 Superdex S200 column (GE Healthcare), previously equilibrated with buffer A, and eluted in buffer A at a rate of 0.8 $mL \cdot min^{-1}$. The purity of the isolated proteins was evaluated by SDS-PAGE and their concentration by the Bradford method.

2.5 **Protein quantification**

2.5.1 Bradford method

The Bradford assay is a colorimetric method commonly used to determine protein concentration. The assay relies on the ability of Coomassie Brilliant Blue to stain protein sample under acidic conditions, leading to generation of a blue solution. The main advantage of using the Bradford method is its compatibility with the reducing agents commonly used during the protein purification procedure. However, a main disadvantage is its incompatibility with some detergents. The assay was performed in 96-well plates, in which each well received 5 µL of protein sample and 200 µL of the Bradford reagent. The calibration curve was made with bovine serum albumin (BSA) at increasing concentration (ranging from 0 to 10 $mg \cdot mL^{-1}$). After incubating the plate at 25 °C for 5 min, the absorbance at 595 nm was measured using a plate reader (Appliskan Multimode).

2.5.2 Bicinchoninic acid (BCA) assay

The BCA assay is another colorimetric method widely used to determine protein concentration. The BCA method relies on the ability of proteins to reduce Cu^{2+} to Cu^{1+} under alkaline conditions. Cu^{1+} forms in amounts proportional to the protein amount and is chelated by BCA, thus forming a purple complex. Unlike the Bradford method, BCA is compatible with many detergents commonly used to obtain cell lysates. The assay was performed in 96-well plates, in which each well received 5 µL of protein sample and 200 µL of BCA reagents. The calibration curve was made with BSA at increasing concentration (ranging from 0 to 2 $mg \cdot mL^{-1}$). After incubating the plate at 37 °C for 30 min, the absorbance at 562 nm was measured using a plate reader (Appliskan Multimode).

2.6 **Protein immunodetection**

2.6.1 Western blot analysis

Cell extracts were obtained as reported in section 2.1.7 or 2.1.8, and total protein content was evaluated by the BCA method. Proteins were separated on an SDS-PAGE Mini-PROTEAN TGX stain-free precast gels (Bio-Rad). The gel formulation includes trihalo compounds, which lead to UV fluorescence emission upon reaction with proteins [135], allowing to estimate the total protein load in a gel lane for normalization purposes, using a ChemiDoc MP imaging system (Bio-Rad). After transfer onto a PVDF membrane, proteins were blocked for 1 h with blocking solution (PBS, 0.1% Tween 20 [v/v], 3% BSA [w/v]) and then incubated overnight at 4 °C with antibodies against human SQR or MST. After three washing steps with PBS-T, the membranes were incubated for 1 h with horseradish peroxidase-conjugated secondary antibody, followed by three washing steps with PBS-T and detection by enhanced chemiluminescence (Clarity Western ECL Substrate, Biorad). Densitometric analysis was performed using Image Lab software (Biorad), followed by normalization of the target protein band intensity to the total protein load determined as described above.

2.6.2 Detection of stress granules by immunofluorescence

Following the treatment described in section 2.1.4, HeLa cells were permeabilized with 0.25% Triton in PBS. Samples were incubated with the blocking solution for 1 hour. Each sample was incubated for 2 hours in humidity chamber with anti-TIAR antibody (1:100 in blocking solution), a marker commonly used to detect stress granules (SGs). After three washing steps, samples were further incubated with secondary antibody diluted 1:200 in blocking solution, followed by three additional washing steps. Eventually, coverslips were mounted onto microscope slides with 3 μL of Vectashield

mounting medium with DAPI (Vector Laboratories). Microscopy was performed by means of a Carl Zeiss Axioplan fluorescence microscope using Image J software and images were analysed with Photoshop CS4. SGs formation was evaluated by randomly capture images of at least 100 cells. Once the observational window was established, the same limits were applied for all conditions and replicates. Total cell number was evaluated by nuclear staining with DAPI, while cells labelled with anti-TIAR immunostaining were considered positive for SGs formation.

2.7 **Enzymatic activity assays**

2.7.1 Citrate synthase assay

The citrate synthase assay, adapted from [136], is a commonly used method to estimate the mitochondrial mass in a cellular sample. Citrate synthase is an enzyme of the Krebs cycle catalysing the conversion of acetyl-CoA and oxaloacetate (OAA) into citrate and CoA. The latter has a free thiol group which is reactive towards DTNB, forming the yellow product 5-thio-2-nitrobenzoic acid (TNB). Briefly, SW480 cells were lysed as reported in 2.1.7. In a 1 mL-quartz cuvette was dispensed a reaction mixture containing 100 mM Tris HCl, pH 8.1, 0.5 mM OAA, 0.1 mM DTNB and 0.3 mM acetyl-CoA in a final volume of 1 mL. The reaction was triggered by adding the cell lysate (typically 0.05 – 0.16 mg) and the subsequent increase in absorbance was followed at 412 nm (ε_{412}=13.600 M^{-1} cm^{-1}) at 25°C using a Cary 60 UV-VIS spectrophotometer equipped with stirring system.

2.7.2 MST activity assay in cell lysates

The MST activity assay was adapted from [137]. In the presence of 3MP and a sulfur acceptor, MST produces H_2S and pyruvate in a 1:1 stoichiometry.

MST activity was therefore evaluated by quantifying the amount of pyruvate produced over a given time (1h) by MST in the presence of an excess of the substrates. Pyruvate was quantified spectrophotometrically from the amount of NADH enzymatically oxidized in the presence of LDH. Briefly, cell lysates (typically, in the range of 0.56 – 0.36 mg total protein) were obtained as described in section 2.1.7, and dispensed into Eppendorf tubes containing 100 mM Tris HCl pH 8.0, 50 mM sodium sulfite, 10 mM 2-mercaptoethanol (acting as a sulfur atom acceptor [39]) and 10 mM 3MP, in a final volume of 1 mL. The Eppendorf tubes were incubated at 37 °C in a thermal shaker for 1 h. Afterwards, the reaction was stopped by addition of 446 mM PCA. The sample was kept on ice for 10 min, followed by a 10-min centrifugation at 10,000 ×g at 4 °C and collection of the supernatant. Pyruvate in the supernatant was then quantified by carrying out an LDH assay in a final volume of 1.095 mL at 37 °C. The starting solution contained 100 mM Tris HCl pH 8.0, 6.4 mM NEM, 224 µM NADH, and 50 µL of the supernatant. NEM was present to block the residual (unreacted) 3MP which is also a substrate of LDH [137]. NADH oxidation was triggered by adding 7U LDH and followed as an absorbance decrease at 340 nm (ε = 6.22 $mM^{-1}cm^{-1}$). Data were normalized to total protein content (quantified with the BCA method) and expressed as nmol of pyruvate generated per minute per mg of protein.

2.7.3 SQR activity assay in mitochondrial preparations

The SQR activity assay was adapted from [138]. Measurements were carried out in a Cary 60 spectrophotometer (Agilent Technologies) equipped with a stirring and a Peltier temperature control system. Assays were performed at 37 °C in a final volume of 1 mL. Briefly, 961 µL of 100 mM potassium phosphate buffer at pH 7.5 were poured into a quartz cuvette, covered with a 200

μL layer of mineral oil and degassed under a N_2 atmosphere for a few minutes. The reaction mixture contained 30 μL of mitochondrial extract (typically, in the range of 37.5 – 139 μg total protein) obtained as described in section 2.1.8, 58 μM CoQ_1, 1 mM sodium sulfite, 2 mM sodium cyanide (to inhibit complex IV) and 4 μM rotenone (to prevent H_2S-derived reverse electron flow through complex I). The reaction was triggered by adding 96 μM H_2S and the reaction rates were determined by following the reduction of CoQ_1 at 278 nm ($\Delta\varepsilon_{ox\text{-}red}$ = 12 $mM^{-1}cm^{-1}$). Data were normalized to the total protein content (quantified with the BCA method) and expressed as nmol of CoQ_1 reduced per minute per mg of protein.

2.7.4 Fluorimetric activity assays of isolated H_2S-synthetizing enzymes

Activity assays on isolated recombinant human H_2S-producing enzymes were adapted from [39, 139, 140]. The assays were carried out in 96-well black plates, using the H_2S-selective fluorescent probe 7-azido-4-methyl-cumarin (7AzC) and a plate reader (Thermo Scientific Appliskan or FLUOstar Optima BMG Labtech). The reaction mixture contained 200 mM Tris-HCl pH 8.0, 50 μM 7AzC, tCBS (1.12 μg/well) or MST (10 μg/well), supplemented with their respective substrates, in a final volume of 250 μL. CBS activity was assayed in the presence of 0.5 mM Hcy and 50 μM PLP. After incubating the protein with Hcy and PLP for 10 min at 37 °C, the reaction was triggered by adding 10 mM Cys. The MST activity assay was carried out in the presence of 20 mM of a sulfur acceptor (NAC or Cys) and triggered with 0.5 mM 3MP. The increase in fluorescence (λ_{exc} = 340 nm; λ_{em} = 460 nm) was monitored over 90 min at 37 °C. Data were analysed using Excel and the H_2S-producing activity was calculated from the initial slope of the fluorescence increase.

2.7.5 Colorimetric activity assays of the isolated H_2S-synthetizing enzymes

The colorimetric methylene blue method, adapted from [125], was used to assay the activity of the H_2S-syntetizing enzymes. This assay consists in the reaction of one molecule of H_2S with two molecules of N,N-dimethyl-p-phenylenediamine (NNDPD) in the presence of ferric chloride ($FeCl_3$), leading to formation of methylene blue. For CBS- and CSE-catalyzed H_2S production assays, the reaction mixture contained tCBS (10 μg/well) or CSE (30 μg/well) in 50 mM Tris-HCl pH 8.0, and 5 μM PLP, in a final volume of 110 μL. In the case of tCBS, 2 mM Hcy was also added. After keeping the plate on ice for 30 min, the reactions by tCBS and CSE were respectively triggered by adding either Cys (10 mM final concentration) alone or plus Hcy (2 mM final concentration), The plate was sealed with vinyl adhesive films and incubated for 2 h at 37 °C. Regarding MST, a 110 μL-reaction mixture contained 30 μg/well MST in 50 mM Tris-HCl pH 8.0, and 10 mM dithiothreitol. After keeping the plate on ice for 30 min, the reaction was triggered by adding 1.5 mM sodium 3-mercaptopyruvate. The plate was sealed with vinyl adhesive films and incubated for 1 h at 37 °C. After the above-mentioned incubation times, the plates with the reaction mixtures containing CBS, CSE and MST were kept on ice for 15 min. Then, 110 μl of 4% zinc acetate were dispensed to each well by punching a hole through the strip with a gas-tight Hamilton syringe. After 15-min incubation on ice, the films were removed and 15 μl of 60 mM NNDPD (3.6 mM final concentration) and 15 μl of 90 mM $FeCl_3$ (5.4 mM final concentration) were dispensed to each well (final volume: 250 μl). The plate was incubated for 10 min at room temperature in the dark and the absorbance measured afterwards at 690 nm. Data were acquired using the plate reader Thermo Scientific Appliskan Multimode.

2.8 **H_2S consumption evaluation by high resolution respirometry**

High resolution respirometric assays, adapted from [46], were performed by using an Oxygraph-2k (OROBOROS Instruments, Innsbruck, Austria). This instrument is provided with two 1.5 mL-chambers, each equipped with O_2 Clark-type electrodes measuring the O_2 concentration (μM) and the O_2 consumption rate (OCR) ($nM \cdot s^{-1}$) in real time. Herein, 4 x 10^6 SW480 cells, obtained as described in 2.1.3, were injected into the Oroboros chambers pre-equilibrated with DMEM supplemented with FBS. Cells were kept under stirring at 37 °C and basal respiration was monitored for at least 10 min, followed by addition of 5 μM rotenone, an inhibitor of Complex I. Subsequently, by means of the Tip-2k micropump, controlled amounts of a sulfide solution (3-5 mM) were injected into the two chambers at increasing rate (10 nL s^{-1}, 20 nL s^{-1}, 40 nL s^{-1}, 80 nL s-1 and 160 nL s^{-1}). Each sulfide injection lasted 180 s and was restarted only after restoration of the O_2 consumption rate measured in the absence of sulfide. The extramitochondrial O_2 consumption, was evaluated by blocking mitochondrial respiration with 5 μM antimycin A prior to injecting sulfide, under otherwise identical experimental conditions. OCR was acquired using DatLab software (Oroboros Instruments). The extramitochondrial contribution was then subtracted from the maximal OCR measured at the highest non-inhibitory (for CcOX) rate of sulfide injection. The resulting value was used to calculate the maximal sulfide-oxidizing activity employing the H_2S:O_2 stoichiometric coefficient (1.33) reported in [46]. Data were normalized to cell number and citrate synthase activity.

2.9 **Ligand-protein binding assays**

2.9.1 Differential scanning fluorimetry (DSF)

DSF allows to gain information on ligand binding to a target protein from the observed changes in the protein thermal denaturation profile [141]. Using 96-to-1536-well plates in an RT-PCR instrument, thermal protein denaturation is monitored by means of a fluorescent dye that emits light upon binding to the buried hydrophobic amino acid residues that become exposed as the protein unfolds at increasing temperatures. Typically, thermal denaturation profiles are sigmoidal and the protein melting temperature (T_m) is estimated from the inflection point. Ligand binding is evaluated from the ability of a given compound to either stabilize or destabilize the target protein, which is respectively reflected in an increase or a decrease in the T_m. Here, DSF measurements were carried out in 384-well plates in an Applied Biosystems QuantStudio™ 7 Flex Real-Time PCR. The compounds were assayed by mixing in each well 14 µl of tCBS (2 µg/well; ~2 µM), CSE (1 µg/well; ~1 µM), or MST (2 µg/well; ~3 µM) in buffer A (10 mM HEPES, 150 mM NaCl, 1 mM TCEP, pH 7.2), with 2 µl of compound solution (typically 2 mM in 10% DMSO, yielding a final compound concentration of 200 µM). The microplate was incubated at 4 °C for 2 hours to favour possible interactions with the target proteins. Prior to the measurement, the fluorescent dye was pre-diluted in buffer A to a 5x working concentration, and 4 µl of the dye solution were dispensed into each well. The microplate was sealed with optical adhesive covers (Applied Biosystems) and centrifuged for 30 s at 500 ×g. Using the QuantStudio™ 7 Flex Real-Time PCR System, the microplates were incubated at increasing temperatures, from 20 °C to 90 °C with increments of 1 °C·min^{-1}. Protein unfolding was monitored with the ROX filter (excitation wavelength = 580 ± 10 nm and emission wavelength = 623 ± 14 nm). Data from triplicate curves were averaged and, for tCBS and MST, the melting temperatures were determined by fitting the data to biphasic sigmoidal curves (for CSE, please

see the Results section). For statistical validation of the DSF assays towards these protein targets, control assays were performed employing 200 μM AOAA as negative control both for tCBS and CSE, and 2 mM 3-mercaptopyruvate for MST, with the compound-free enzymes being used as positive controls.

2.9.2 Far-UV circular dichroism

Far-UV circular dichroism (CD) thermal denaturation curves were recorded in a Jasco J-815 spectropolarimeter equipped with a Jasco CDF-426S Peltier temperature controller, in a quartz cuvette with a light path length of 0.1 cm. CSE was diluted to 0.15 $mg \cdot mL^{-1}$ in 50 mM NaPi buffer, 300 mM NaCl, 0.5 mM TCEP, 10% glycerol, pH 7.5, while tCBS and MST were diluted to 0.2 $mg \cdot mL^{-1}$ in 10 mM Hepes buffer, 150 mM NaCl, 1 mM TCEP, pH 7.2. CD spectropolarimeter experimental setup: λ = 222 nm; temperature range, 20–90 °C; slope, 1 $°C \cdot min^{-1}$; data pitch, 0.5 min; data integration time, 1 s; bandwidth, 1 nm; nitrogen flow, 4 $L \cdot min^{-1}$. Thermal denaturation curves were analysed with Graphpad (Prism), fitting the data to a monophasic (tCBS and CSE) or biphasic (MST) sigmoidal curve.

2.9.3 Surface plasmon resonance (SPR)

Putative interactions of the tested compounds with tCBS, CSE, and MST were investigated by surface plasmon resonance (SPR). Assays were carried out in a Biacore 4000 instrument (GE Healthcare) at 25 °C. tCBS, CSE and MST were diluted to 5 $\mu g \cdot mL^{-1}$ (tCBS) or 10 $\mu g \cdot mL^{-1}$ (CSE and MST) in their corresponding immobilization buffer (10 mM sodium acetate pH 5.8 for CBS, and 10 mM Bis-Tris pH 6.0 for CSE and MST) and immobilized onto CM5 sensor chips using the standard amine coupling procedure. HBS-N,

which consisted of 10 mM Hepes pH 7.4 and 150 mM NaCl, was used as the background buffer. Prior to immobilization, the carboxymethylated surface of the chip was activated with 20 mM 1-ethyl-3-(3-dimethylaminopropyl)-carbodiimide and 5 mM N-hydroxysuccinimide for 1.5 min. Proteins were coupled to the surface with a 5-to-10 min injection time at a flow rate of 10 $\mu L \cdot min^{-1}$ in order to reach 5,000 to 10,000 response units (RU). The remaining activated carboxymethylated groups were blocked with a 5-min lasting injection of 1 M ethanolamine pH 8.5. Compounds (analytes) were directly diluted in running buffer (10 mM HEPES, 150 mM NaCl, 1 mM TCEP, 0.1 mM EDTA, 0.05% (v/v) TWEEN-20, 5 mM MgCl2, pH 7.2.) and injected at four different concentrations using 2-fold dilution series, the highest concentration tested being 200 µM. Interactions were qualitatively assessed from the obtained plots of steady-state analyte binding levels against the concentration, making use of the provided Biacore 4000 evaluation software (GE Healthcare).

2.10 Maintenance and phenotypic characterization of Drosophila flies

Drosophila flies were bred on a standard cornmeal, yeast, glucose agar medium at 25°C. The Oregon and GMR-GAL4-wtTDP43 (stock #51370) lines were used as healthy and ALS model, respectively. Transgenic stocks producing dsRNA for RNAi of CBS or CSE *Drosophila* homologs under UAS control were UAS-CBSRNAi1 (stock # 36767), UAS-CBSRNAi2 (stock # 41877), UAS-CSERNAi1 (stock # 36766) and UAS-CSERNAi3 (stock # 41876). In order to generate the lines GMR-TDP43/UAS-CBSRNAi1, GMR-TDP43/UAS-CBSRNAi2, GMR-TDP43/UAS-CSERNAi1 and GMR-TDP43/UAS-CSERNAi3, males from the RNAi stocks were allowed to mate with virgin females GMR-TDP43 over 10 days. Phenotypic studies were carried out on F1

progeny flies, which were daily observed and transferred to fresh food. Eye images were captured by means of a microscope Carl Zeiss Stemi 508 equipped with axiocam 105 color, using Zen 2 core software. Images were analysed with Photoshop CS4.

2.11 **Statistical analysis**

Enzymatic activity assays, as well as SPR and DSF assays, were statistically validated using Z'-factor to assess the quality of the methods. Data were analysed in terms of Z-score and coefficient of variation (CV). A |Z-score| = 3 was taken as threshold value to consider a screened compound as effective. Data analyses were performed using Excel (Microsoft).

RESULTS AND DISCUSSION

PAPER 1

N-acetylcysteine serves as substrate of 3-mercaptopyruvate sulfurtransferase and stimulates sulfide metabolism in colon cancer cells

Karim Zuhra[1,2], Catarina S. Tomé[3], Letizia Masi[1], Giorgio Giardina[1], Giulia Paulini[1], Francesca Malagrinò[1], Elena Forte[1,*], João B. Vicente[3,*], Alessandro Giuffrè[2,*]

[1] Department of Biochemical Sciences, Sapienza University of Rome, Piazzale Aldo Moro 5, I-00185 Rome, Italy; karim.zuhra@uniroma1.it; letizia.masi94@gmail.com; giorgio.giardina@uniroma1.it; paulini.giulia@gmail.com; francesca.malagrino@uniroma1.it; elena.forte@uniroma1.it;

[2] CNR Institute of Molecular Biology and Pathology, Piazzale Aldo Moro 5, I-00185 Rome, Italy; alessandro.giuffre@uniroma1.it

[3] Instituto de Tecnologia Química e Biológica António Xavier (ITQB NOVA), Avenida da República (EAN), 2780-157 Oeiras, Portugal; ctome@itqb.unl.pt; jvicente@itqb.unl.pt

***** Correspondence: elena.forte@uniroma1.it (EF); jvicente@itqb.unl.pt (JBV); alessandro.giuffre@uniroma1.it (AG);

Cells. 2019 Aug 4;8(8). pii: E828. doi: 10.3390/cells8080828.

Received: 9 July 2019; Accepted: 2 August 2019; Published: 4 August 2019

ABSTRACT

Hydrogen sulfide (H_2S) is an endogenously produced signaling molecule. The enzymes 3-mercaptopyruvate sulfurtransferase (MST), partly localized in mitochondria, and the inner mitochondrial membrane-associated sulfide:quinone oxidoreductase (SQR), besides being respectively involved in the synthesis and catabolism of H_2S, generate sulfane sulfur species such as persulfides and polysulfides, currently recognized as mediating some of the H_2S biological effects. Reprogramming of H_2S metabolism was reported to support cellular proliferation and energy metabolism in cancer cells. As oxidative stress is a cancer hallmark and *N*-acetylcysteine (NAC) was recently suggested to act as an antioxidant by increasing intracellular levels of sulfane sulfur species, here we evaluated the effect of prolonged exposure to NAC on the H_2S metabolism of SW480 colon cancer cells. Cells exposed to NAC for 24 hours displayed increased expression and activity of MST and SQR. Furthermore, NAC was shown to i) persist at detectable levels inside the cells exposed to the drug for up to 24 hours and ii) sustain H_2S synthesis by human MST more effectively than cysteine, as shown working on the isolated recombinant enzyme. We conclude that prolonged exposure of colon cancer cells to NAC stimulates H_2S metabolism and that NAC can serve as a substrate for human MST.

ABBREVIATION

H_2S: hydrogen sulfide; CBS: cystathionine β-synthase; CSE: cystathionine γ-lyase; MST: 3-mercaptopyruvate sulfurtransferase; 3MP: 3-mercaptopyruvate; GSH: glutathione; Cys: cysteine; SQR: sulfide:quinone oxidoreductase; GSSH: glutathione persulfide; ROS: reactive oxygen species; Cys-SSH:

cysteine persulfide; NAC: *N*-acetylcysteine; 5-FU: 5-fluorouracil; 7AzC: 7-azido-4-methylcoumarin; BCA: bicinchoninic acid; CoQ1: co-enzyme Q_1; DMEM: Dulbecco's Modified Eagle Medium; DTNB: 5,5'-dithiobis-(2-nitrobenzoic acid); LDH: lactate dehydrogenase; NEM: *N*-ethylmaleimide; PCA: perchloric acid; *N*-AceCysSSH: *N*-acetylcysteine persulfide.

1. INTRODUCTION

Hydrogen sulfide (H_2S) is an endogenously produced signaling molecule involved in the regulation of several physiological processes, such as blood flow, inflammation, neurotransmission, apoptosis, redox homeostasis, energy metabolism and stress response [1-3]. The signaling function of H_2S is mainly accomplished by mediating cysteine thiol persulfidation of target proteins [3-6]. Recently, protein persulfidation has emerged as a physiologically relevant modification taking place both during protein synthesis and post-translationally in a considerable fraction of the proteome in mammalian cells [6, 7]. Along with thiosulfate, persulfides and polysulfides generated from proteins or low-molecular-weight thiol-containing molecules are H_2S-derived species containing zero-valent sulfur (S^0), commonly referred to as "sulfane sulfur". It was recently demonstrated that these species are not only much more abundant in the cell than previously thought but also, due to their elevated nucleophilicity [8], more reactive with e.g. protein thiols or reactive oxygen species (ROS) than H_2S or their parental thiol compounds [9]. Therefore, many of the biological effects attributed to H_2S are currently believed to be mediated by sulfane sulfur species [10-13], whose antioxidant and cytoprotective action has been clearly established (reviewed e.g. in [14]).

Moreover, sulfane sulfur species like persulfides have an increased affinity for exogenous toxins with respect to their thiol counterparts [15-17].

Steady-state levels of H_2S and related species in blood and tissues are kept in balance through a tight regulation of H_2S biosynthesis and catabolism [18]. In mammals, H_2S is enzymatically produced by the two predominantly cytosolic enzymes cystathionine β-synthase (CBS) and cystathionine γ-lyase (CSE) [4] from the transsulfuration pathway and by 3-mercaptopyruvate sulfurtransferase (MST) [19]. Two isoforms of MST have been reported: MST-1, exclusively localized in the cytosol (35 kDa), and MST-2, present both in the cytosol and mitochondria (33 kDa) [20]. MST converts into pyruvate the 3-mercaptopyruvate (3MP) generated by cysteine aminotransferase, yielding a persulfidated Cys248 (human MST numbering) at the protein active site. The sulfane sulfur atom is then transferred from the persulfidated protein to an acceptor —such as cysteine (Cys), homocysteine, glutathione (GSH), dihydrolipoic acid or thioredoxin [19, 21] — leading to the formation of the corresponding persulfide (R-SSH) [19], that can eventually release H_2S. MST is therefore a recognized source of both H_2S and sulfane sulfur species in the cell. Unlike H_2S biosynthesis, which takes place both at the cytosolic and mitochondrial level, H_2S catabolism occurs essentially in the mitochondrion, where sulfide:quinone oxidoreductase (SQR) —a flavoenzyme associated to the inner membrane— catalyzes the oxidation of H_2S. The reaction leads to formation of a protein-bound persulfide [22, 23] that in turn can donate its sulfane sulfur atom to sulfite or, more likely, GSH, yielding thiosulfate [24] or glutathione persulfide (GSSH), respectively [25]. SQR is thus another intracellular source of sulfane sulfur species. As SQR uses coenzyme Q as the acceptor of the electrons derived from H_2S oxidation, SQR-mediated breakdown of H_2S stimulates oxidative phosphorylation and, thus, ATP

synthesis, which makes H_2S the first known inorganic substrate of the mitochondrial electron transport chain [24, 27]. This mitochondrial sulfide oxidizing activity varies considerably between different cell types, ranging from undetectable in neuroblastoma cells to high in colonocytes [28], the latter being physiologically exposed to the high H_2S levels produced by the gut microbiota [29]. Indeed, Libiad and co-authors have recently demonstrated that colonic crypts at the host-microbiota interface display an apical localization of H_2S oxidation pathway enzymes, whereas this localization pattern is lost in the epithelium of colorectal cancer [30].

Several human pathologies, including neurodegenerative, cardiovascular and oncological diseases, are known to be associated with altered H_2S metabolism (reviewed in [2, 6]), and the enzymes responsible for H_2S biosynthesis are currently recognized as potential pharmacological targets [31-33]. H_2S and related species, including sulfane sulfur species, seem to play a major role in cancer biology [34, 35]. In colorectal cancer cell lines, CBS-derived H_2S was suggested to support cellular proliferation, promote angiogenesis and maintain cell energy metabolism by stimulating both oxidative phosphorylation and glycolysis [36]. Accordingly, silencing or pharmacological inhibition of CBS significantly reduced cellular proliferation and migration, and tumor xenograft growth [36]. Furthermore, increased expression of CBS and CSE was documented in different cancer types, such as colorectal, ovarian, breast, prostate and melanoma, and was shown to contribute to cancer progression, energy metabolism and drug resistance [35, 37, 38]. MST too was found to be upregulated in different cancer types, namely, colorectal cancer [39], renal carcinoma [40], astrocytoma and melanoma [41]. However, the studies on the role of MST in cancer are scarcer and only in recent years MST, with its ability to produce sulfane sulfur species

and its partial mitochondrial localization [2], was proposed as a potential target in cancer biology [42]. Recently, Libiad and colleagues reported increased SQR expression in colon cancer patient samples relatively to the surrounding normal tissue, and found a correlation between increased SQR expression and the degree of malignancy in human colorectal cancer tissues and cell lines [30]. Moreover, in the SW480 colorectal cancer cell line, an increase in mitochondrial levels of SQR has been proposed to afford an adaptive response upon exposure to hypoxia, a common feature within the tumor microenvironment [43].

The association between altered mitochondrial metabolism, dysregulated cell redox homeostasis and carcinogenesis is well documented (reviewed in [44]). The mitochondrial respiratory chain is a major source of ROS which are known to have opposite effects on cancer development, depending on their abundance in the cell. While at lower levels ROS can promote cancer survival and progression by causing DNA damage and activating pro-oncogenic signaling pathways [45], at excessively high levels they can induce cell death [46]. Common anticancer drugs owe their efficacy, but also their unwanted side effects, to their ability to generate oxidative stress in cancerous as well as in healthy tissues ([47, 48, 49]). Therefore, targeting the ROS signaling pathways and redox mechanisms involved in cancer development was suggested as a potential strategy to prevent both cancer formation and the adverse effects of antitumoral drugs [50]. However, it is still controversial whether supplementation of antioxidants has an impact on limiting cancer incidence or the side effects of chemotherapy. Clinical trials have shown that antioxidants may not be beneficial and might even produce adverse effects in terms of cancer prevention and treatment (reviewed in [51-53]). One of the most widely used antioxidant drug is *N*-acetylcysteine (NAC),

which has been extensively studied not only for its ROS scavenging action [54], but also (unfortunately, with rather disappointing results) for its presumed cytoprotective effects against anticancer drugs [55, 56] and cancer preventive action [57-59]. Despite the wide use of NAC, the molecular mechanisms underlying the antioxidant action of this drug are not yet fully clear. Although it is generally accepted that NAC exerts its effect acting as a precursor of Cys and, thus, in turn, of GSH, it seems that the rate of intracellular deacetylation of NAC to Cys is insufficient to sustain increased GSH biosynthesis [60]. Accordingly, some studies have shown that NAC supplementation, while providing protection against oxidative stress, does not affect GSH levels [61]. Recently, Ezerina et al. proposed that NAC-derived Cys enhances mitochondrial levels of sulfane sulfur species and suggested that these species are the actual mediators of the antioxidants effects of NAC [62]. This study prompted us to investigate the effect of NAC on H_2S metabolism in colorectal cancer cells. By combining work on the SW480 cell line and on recombinant human MST, we observed that NAC not only promotes increased expression and activity of MST and SQR, both involved in the production of sulfane sulfur species, but is also an effective substrate for MST.

1. MATERIALS AND METHODS

2.1 Materials

The human colon cancer cell line SW480 was purchased from the American Type Culture Collection (ATCC no. CCL228™). Acetyl coenzyme A (A2056), 7-azido-4-methylcoumarin (7AzC, L511455), reduced β-nicotinamide adenine dinucleotide (NADH, disodium salt, N8129), Dulbecco's Modified Eagle Medium (DMEM) cell culture media (D6546), CelLytic™MT cell lysis

reagent (C2978), coenzyme Q_1 (CoQ_1, C7956), D-lactic dehydrogenase (LDH, L2395), 5,5'-dithiobis-(2- nitrobenzoic acid) (DTNB, D8130), L-cysteine (Cys, C1276), *N*-acetylcysteine (NAC, A7250), metaphosphoric acid (239275), 2-mercaptoethanol (805740), sodium 3-mercaptopyruvate dihydrate (3MP, 90374), *N*-ethylmaleimide (NEM, 34115-M), oxaloacetate (O7753), perchloric acid (PCA, 77232), protease inhibitor cocktail (P8340), rabbit polyclonal antibody against human SQR (HPA017079) and CBS (SAB1411562), anti-rabbit peroxidase secondary antibody (A6154), rotenone (R8875), sodium sulfide nonahydrate ($Na_2S \cdot 9H_2O$, 431648), sodium sulfite (S0505) were purchased from Sigma (Saint Louis, MO, USA). The bicinchoninic acid assay (BCA) kit and rabbit polyclonal antibody against human MST (PA528779) were purchased from Thermo Fisher Scientific (Waltham, MA, USA). Mouse monoclonal antibody against human CSE (SC-365381) was purchased from Santa Cruz Biotechnology (Santa Cruz, CA, USA). Fetal bovine serum (FBS), L-glutamine, streptomycin and penicillin were purchased from Biowest (Riverside, MO, USA). Mini-PROTEAN TGX Stain-Free Precast Gels, the Clarity Western ECL substrate and the Laemmli protein sample buffer were purchased from Bio-Rad (Hercules, CA, USA). Bovine serum albumin was purchased from AppliChem (Darmstadt, Germany).

2.2 Preparation of sulfide stock solutions

Sulfide stock solutions were prepared by dissolving Na_2S crystals in degassed ultra-pure (Milli-Q®) water under a N_2 atmosphere, as reported in [8]. Sulfide concentration was then measured spectrophotometrically with DTNB as reported in [64], using the molar extinction coefficient $\varepsilon_{412} = 14{,}150\ M^{-1} \cdot cm^{-1}$ as recommended by the manufacturer. The concentration of sulfide was then adjusted to 50 mM by dilution with degassed ultra-pure (Milli-Q®) water in a

gas-tight glass syringe. For simplicity, sulfide solutions, though containing H_2S, HS^- and S^{2-} in different proportions depending on the pH, here will be referred to as "H_2S solutions".

2.3 Cell culture and isolation of mitochondria

SW480 colorectal cancer cells were cultured in DMEM containing 4.5 $g \cdot L^{-1}$ glucose, supplemented with 2 mM L-glutamine, 10% (v/v) heat-inactivated FBS, 100 $U \cdot mL^{-1}$ penicillin and 100 $\mu g \cdot mL^{-1}$ streptomycin. For each studied condition, cells were seeded in five 25 cm^2 flasks (1×10^6 cells/flask) and grown at 37 °C and 5% CO_2. After 24 h, the culture medium was replaced with fresh medium (control) or medium supplemented with 10 mM NAC, and further incubated for 24 h. After trypsinization, cells were washed with fresh culture medium, counted using the trypan blue dye exclusion test, and centrifuged at 1,000 ×g for 5 min, yielding usually 2–3 × 10^7 cells per condition. Under the tested conditions, 10 mM NAC proved not to be cytotoxic.

Mitochondrial preparations were obtained as described in [65] with modifications. The cell pellet was washed twice in cold PBS, resuspended in 1 mL of hypotonic buffer (3.5 mM Tris HCl pH 7.8, 2.5 mM NaCl, 0.5 mM $MgCl_2$, 1% v/v protease inhibitors cocktail) and kept on ice for 1 hour. The sample was then transferred to a pre-chilled glass-teflon tissue grinder and homogenized with 100 strokes. Immediately afterwards, 100 µL of hypertonic buffer (350 mM Tris HCl pH 7.8, 250 mM NaCl, 50 mM $MgCl_2$) were added to the homogenate, which was carefully resuspended, followed by centrifugation at 1,000 ×g for 5 min at 4 °C to pellet unbroken cells, debris and nuclei. The supernatant was kept on ice, while the pellet was resuspended in isotonic buffer (35 mM Tris HCl pH 7.8, 25 mM NaCl, 5 mM $MgCl_2$, 1% protease inhibitor) and centrifuged a second time at 1,000 ×g for 5 min at 4 °C, to minimize heavy

contaminants. The supernatants from both centrifugations were pooled and centrifuged at 20,000 ×g for 30 min at 4 °C. The mitochondria-enriched pellet was solubilized in 150 µL of 10 mM Tris HCl pH 7.4, 250 mM sucrose, 1 mM EDTA, 0.5% (w/v) *N*-lauryl maltoside, as reported in [66].

2.4 Human MST expression and purification

Recombinant human MST was expressed and purified as described in Yadav et al. [19].

2.5 SQR activity assay in mitochondrial preparations

The SQR activity assay was adapted from [67]. Measurements were carried out in a Cary 60 spectrophotometer (Agilent Technologies, Santa Clara, CA, USA) equipped with stirring and a Peltier temperature control system. Assays were performed at 37 °C in a final volume of 1 mL. Briefly, 961 µL of 100 mM potassium phosphate buffer at pH 7.5 were poured into a quartz cuvette, covered with a 200 µL layer of mineral oil and degassed under a N_2 atmosphere for a few minutes. The reaction mixture contained 30 µL of mitochondrial extract (typically, in the range of 37.5 – 139 µg total protein), 58 µM CoQ_1, 1 mM sodium sulfite, 2 mM sodium cyanide (to inhibit complex IV) and 4 µM rotenone (to prevent H_2S-derived reverse electron flow through complex I). The reaction was triggered by adding 96 µM H_2S and the reaction rates were determined by following the reduction of CoQ_1 at 278 nm ($\Delta\varepsilon_{ox\text{-}red}$ = 12 $mM^{-1}cm^{-1}$). Data were normalized to total protein (quantified with the BCA method) and were expressed as nmol of CoQ_1 reduced per minute per mg of protein.

2.6 MST activity assay in cell lysates

The MST activity was assayed in cell lysates as described in [68] with modifications. In the presence of 3MP and a sulfur acceptor, MST produces H_2S and pyruvate in a 1:1 stoichiometry. MST activity was therefore evaluated by quantifying the amount of pyruvate produced over a given time (1h) by MST in the presence of an excess of the substrates. Pyruvate was quantified spectrophotometrically from the amount of NADH enzymatically oxidized in the presence of LDH. Briefly, cells were harvested by centrifugation and lysed using the CelLytic™MT reagent and the protease inhibitors cocktail from Sigma, according to the manufacturer instructions. Cell lysates (typically, in the range of 0.56–0.36 mg total protein) were dispensed into eppendorf tubes containing 100 mM Tris HCl pH 8.0, 50 mM sodium sulfite, 10 mM 2-mercaptoethanol (acting as a sulfur atom acceptor [19]) and 10 mM 3MP, in a final volume of 1 mL. The eppendorf tubes were incubated at 37 °C in a thermal shaker for 1 h. Afterwards, the reaction was stopped by addition of 446 mM PCA. The sample was kept on ice for 10 min, followed by a 10-min centrifugation at 10,000 ×g at 4 °C and collection of the supernatant. Pyruvate in the supernatant was then quantified by carrying out an LDH assay in a final volume of 1.095 mL at 37 °C. The starting solution contained 100 mM Tris HCl pH 8.0, 6.4 mM NEM, 224 µM NADH, and 50 µL of the supernatant. NEM was present to block the residual 3MP which is also a substrate of LDH [68]. NADH oxidation was triggered by adding 7U LDH and followed as an absorbance decrease at 340 nm (ε = 6.22 $mM^{-1}cm^{-1}$). Data were normalized to total protein content (quantified with BCA method) and expressed as nmol of pyruvate generated per minute per mg of protein.

2.7 Recombinant human MST activity assay

Activity assays on isolated recombinant human MST were adapted from [19, 33, 69]. The assays were carried out in 96-well black plates, using the H_2S-selective fluorescent probe 7AzC and a Thermo Scientific Appliskan plate reader. The reaction mixture, in 200 mM Tris-HCl pH 8.0, contained 10 µg of recombinant human MST per well, 50 µM 7AzC, and NAC (or Cys) at varied concentrations. The reaction was triggered by adding 3MP in a total assay volume of 250 µL. The increase in fluorescence (λ_{exc} = 340 nm; λ_{em} = 460 nm) was monitored over 90 min at 37 °C. Kinetic parameters for Cys and NAC were determined at concentrations ranging from 0 to 40 mM in the presence of 0.5 mM 3MP. Conversely, kinetic parameters for 3MP were determined at concentrations ranging from 0 to 2 mM in the presence of 20 mM NAC or Cys. Prior to use, the solutions of NAC, Cys and 3MP were adjusted to pH 8.0 and their concentration determined by spectrophotometric titrations with DTNB, using the molar extinction coefficient ε_{412nm} = 14,150 $M^{-1} \cdot cm^{-1}$. Data were analyzed using Excel and the MST activity was calculated from the initial slope of the fluorescence increase.

2.8 Evaluation of mitochondrial content by the citrate synthase assay

Cells were harvested and lysed as described in section 2.6. Cell extracts were then assayed spectrophotometrically for citrate synthase in 100 mM Tris-HCl, 0.3 mM acetyl-CoA, 0.1 mM DTNB and 0.5 mM oxaloacetate, as described in [70].

2.9 Immunoblotting assays

Cells were lysed as described in section 2.6 and proteins quantified using the BCA method. Samples were separated on SDS-PAGE Mini-PROTEAN

TGX Stain-Free Precast Gels (Bio-Rad, Hercules, CA, USA). The gel formulation includes trihalo compounds, which lead to UV fluorescence emission upon reaction with proteins [71], allowing to estimate the total protein load in a gel lane for normalization purposes, using a ChemiDoc MP imaging system (Bio-Rad, Hercules, CA, USA). After transfer onto a PVDF membrane, proteins were blocked for 1 h with PBS-T (phosphate buffered saline with 0.1% Tween 20 [v/v]) containing 3% bovine serum albumin (BSA, w/v) and then incubated overnight at 4 °C with antibodies against human SQR or MST. After three washing steps with PBS-T, the membranes were incubated for 1 h with horseradish peroxidase-conjugated secondary antibody, followed by three washing steps with PBS-T and detection by enhanced chemiluminescence (Clarity Western ECL Substrate, Biorad, Hercules, CA, USA). Specific bands were analyzed using Image Lab software (Biorad, Hercules, CA, USA), followed by normalization of the target protein band intensity to the total protein load determined as described above.

2.10 NAC quantification by reverse phase high performance liquid chromatography (RP-HPLC)

This method was adapted from [72]. Cells were harvested as described in section 2.3 and washed twice in PBS. The pellet was resuspended in 250 µL ultra-pure (Milli-Q®) water, kept on ice for 30 min and then lysed by three cycles of freeze-thawing. Lysates were mixed with 250 µL of 3.34% meta phosphoric acid and, after vortexing, were incubated for 30 min on ice, followed by centrifugation at 12,000 ×g for 10 min at 4 °C. The supernatant was filtered and 120 µL of the deproteinized solution were mixed with 60 µL of 0.3 M Na_2HPO_4 and 90 µL of 1 mM DTNB. NAC quantification was performed at room temperature by injecting 100 µL of DTNB-derivatized samples into a

Prevail™ C8 column (150 × 4.6 mm – 5 µm) (Grace) connected to a double pump HPLC apparatus (Azura ASM 2.1L; Knauer) equipped with an UV-Vis detector (Azura ASM 2.1L; Knauer). Injections were performed automatically using an HT300L autosampler (HTA). The elution was monitored by recording the signal at 331 nm using the following mobile phase: 20 mM NaH_2PO_4 pH 4.9 (Buffer A) and 100% methanol (Buffer B). The flow rate was 1 $mL \cdot min^{-1}$ and the concentration of buffer B was varied during the elution as follows: 2% B for 10 mL, then the concentration of B was raised to 40% in a steep gradient of 2 mL, kept at 40% for 1 mL to allow the elution of the unreacted excess of DTNB, then brought back to 2% in a 2 mL reverse gradient and kept at 2% for 7 mL before injection of the next sample. Calibrations were performed by injecting standards of NAC, GSH and Cys at known concentrations after derivatization with DTNB. For each condition, two experimental duplicates were tested, and each duplicate was injected twice. The derivatization buffer and a derivatized lysate of untreated cells were injected as controls.

2. RESULTS

3.1 Effect of NAC on expression levels of H_2S metabolism enzymes

SW480 colorectal cancer cells were grown in DMEM alone or supplemented with 10 mM NAC. After 24 hours, the expression levels of CBS, CSE, MST and SQR were evaluated in the cell lysates by immunoblotting. Whereas cell exposure to NAC had no effect on the expression of CBS and CSE (Supplementary Figure S1), as compared to control cells, NAC-treated cells displayed increased expression of both MST isoforms (overall accounting for an increment of 61 ± 16 %, Figures 1A and 1B) and SQR (by 36 ± 17 %, Figures 1C and 1D). In a control experiment with cells grown for 24 hours in

DMEM supplemented with 10 mM Cys instead of NAC, a decrease in both MST and SQR expression (by 24 ± 10 % and 28 ± 9 %, respectively) was observed (Supplementary Figure S2). As compared to the control, NAC did not affect cellular viability and proliferation, while treatment with cysteine proved to be cytotoxic at the tested conditions, causing impairment of cellular growth of ≈30%.

3.2 Effect of NAC on MST activity

Prompted by the increased MST expression levels observed upon cell exposure to NAC, we evaluated the MST activity in lysates of NAC-treated cells. As described in section 2.6, the activity was evaluated by quantifying spectrophotometrically in an LDH-coupled assay the amount of pyruvate produced over 1h by MST in the presence of excess of 3MP and 2-mercaptoethanol. A representative trace of pyruvate quantitation is shown in figure 2A. In the assay, the starting solution contained a diluted aliquot of the deproteinized MST reaction mixture with the produced pyruvate, and NEM to block unreacted 3MP. As expected, the absorbance at 340 nm increased after addition of NADH. Upon addition of LDH, partial oxidation of NADH was detected as an absorbance decrease, and pyruvate could be quantified from the NADH being oxidized. In line with their enhanced MST expression levels, NAC-treated cells displayed higher MST activity than control cells (112.4 ± 9.5 $nmol \cdot min^{-1} \cdot mg^{-1}$ *vs* 92.1 ± 7.9 $nmol \cdot min^{-1} \cdot mg^{-1}$, Figure 2B). A blank control lacking the MST reaction mixture, and thus pyruvate, exhibited no changes in absorbance upon addition of LDH (*not shown*).

3.3 Effect of NAC on SQR activity

The H_2S oxidizing activity of SQR was evaluated in mitochondrial preparations of NAC-treated and control cells by monitoring spectrophotometrically the H_2S-induced reduction of exogenous CoQ_1 (see section 2.5). The efficiency of mitochondria isolation was preliminarily confirmed with immunoblotting assays revealing the presence of SQR in the mitochondrial preparations, but not (at least to detectable levels) in the cytosolic fraction (Supplementary figure S3). A representative SQR activity assay is shown in figure 3A. The mitochondrial preparation was preincubated with the mitochondrial electron transport chain inhibitors rotenone and cyanide, respectively to prevent re-oxidation of the reduced CoQ_1 by Complex I through reverse electron transfer [28] or by Complex III and IV through forward electron transfer to O_2 [67]. The SQR-mediated H_2S:CoQ_1 oxidoreductase activity of NAC-treated cells was 25.8 ± 2.7 nmol·min^{-1}·mg^{-1}, whereas that of untreated cells was 17.2 ± 4.6 nmol·min^{-1}·mg^{-1} (Figure 3B). A blank control lacking the mitochondrial extract exhibited no changes in absorbance upon addition of H_2S (*not shown*).

3.4 Effect of NAC on mitochondrial mass

Citrate synthase (CS) activity measurements were carried out as a validated surrogate marker of mitochondrial mass [70]. NAC-treated and control cells exhibited very similar CS activity (respectively 11.3 ± 1.4 μM·min^{-1}·mg^{-1} and 10.4 ± 1.9 μM·min^{-1}·mg^{-1}, Figure S4).

3.5 Kinetics of H_2S production by recombinant human MST with NAC as a substrate

The H_2S-synthesizing activity of recombinant human MST was evaluated in the presence of 3MP using the H_2S selective fluorescent probe

7AzC [69]. In these assays, the ability of NAC to function as a substrate for MST was evaluated in comparison with Cys, a known physiological substrate of the enzyme [19]. The K_M and V_{max} values for NAC or Cys were independently determined at fixed concentration of 3MP. A hyperbolic dependence of MST activity on the substrate concentration was observed for both NAC and Cys (Figure 4A). Accordingly, data were fitted to the Michaelis-Menten model, yielding the apparent K_M and V_{max} values reported in Table 1. As compared to Cys, NAC yielded a 2.5-fold higher V_{max} and a 1.9-fold higher K_M, thereby accounting for a 1.3-fold higher catalytical efficiency (V_{max}/K_M). To evaluate the effect on MST activity of the simultaneous presence of the two substrates, H_2S production by MST was determined in the presence of Cys and NAC together. As shown in Figure S5, no significant changes in the enzyme activity were observed in the presence of both Cys and NAC, as compared to NAC alone. With either NAC or Cys at saturating concentrations, MST activity displayed clear sigmoidal dependence on 3MP concentration (Figure 4B), and both the V_{max} and K_M values for 3MP were in the same order of magnitude (Table 1). In these assays too, NAC was confirmed to account for a higher catalytic efficiency (1.4-fold), as compared to Cys.

3.6 HPLC quantification of intracellular NAC

SW480 cells were treated with DMEM supplemented with 10 mM NAC for 5 minutes, 2 hours, 6 hours or 24 hours. After harvesting, cell lysates were deproteinized and thiol compounds were derivatized with DTNB. In each sample, NAC was determined simultaneously with Cys and GSH by using a simple and sensitive RP-HPLC method (Figure 5A), as reported in the Materials and Methods (section 2.10). For each analyte the calibration curves were linear at least up to 120 μM. Under the working conditions, NAC

displayed good stability and a retention time (about 7 min) sufficiently distinct from those of Cys and GSH (about 3 min and 5 min, respectively). No significant interference from endogenous substances was observed at the retention times of the studied compounds. As shown in figure 5B, under the tested conditions the intracellular levels of NAC remained detectable and essentially constant from 2 to 24 hours.

3. DISCUSSION

Several lines of evidence have shown that mitochondrial dysfunction is interrelated with cancer hallmarks, such as metastatic propensity, cell death evasion, dysregulated bioenergetics and genome instability (reviewed in [44]). Altered redox balance is a common feature to cancer cells, which usually exhibit persistently high ROS levels in comparison to their normal counterparts [73]. Cancer cells are therefore endowed with an enhanced antioxidant system which protect them from oxidative damage and likely contribute to drug resistance [74]. ROS modulation has long appeared as a possible strategy to fight cancer by either preventing malignant transformation or killing cancerous cells. However, the consequences of pharmacological ROS modulation *in vivo* are hard to predict [73]. While it has been proposed that targeting ROS with antioxidant compounds could prevent carcinogenesis, upregulation of ROS by anticancer drugs does suppress vulnerable cancer cells, but it also affects normal tissues thereby contributing to the several side effects typically associated to antitumoral chemotherapy.

Reprogramming of sulfur metabolism has been reported as a common mechanism to different cancer types (reviewed in [2, 75]). In cancer cells, enzymes involved in H_2S synthesis, such as CBS, CSE and MST [76] were

found to be overexpressed [36, 37, 39-41, 77, 78], and growing evidence suggests that H_2S and related reactive sulfide species, including sulfane sulfur species, play a role in cancer biology [9, 34]. While H_2S appears to favor cancer cell survival and proliferation by stimulating cell bioenergetics and neo-angiogenesis, among other effects, sulfane sulfur species could potentiate the cell antioxidant defense system, by both scavenging free radicals and enhancing the activity of antioxidant enzymes such as glutathione peroxidase, glutathione reductase and superoxide dismutase [79, 80]. (Per/poly)sulfides are indeed more nucleophilic than the corresponding thiols and their reactivity towards ROS increases with the length of the sulfane sulfur chain [14]. In this context, it is of relevance that NAC, a commonly used antioxidant drug, was recently proposed to exert its antioxidant activity precisely by promoting sulfane sulfur production [62, 81, 82]. Therefore, while NAC supplementation may appear as an appealing strategy to ameliorate the oxidative stress imposed by alkylating/oxidative chemotherapeutic drugs, chronic exposure to NAC may actually confer unwanted protective effects to cancer cells.

In the present study, working on SW480 colorectal cancer cells, we explored the effect of prolonged (24 h) exposure to NAC on H_2S metabolism, particularly on its synthases (CBS, CSE and MST) and SQR, the enzyme catalyzing the limiting step of mitochondrial sulfide oxidation. Cell exposure to NAC resulted in increased expression levels of both MST (≈60%) (Figure 1B) and SQR (≈40%) (Figure 1D), whereas neither CBS nor CSE expression levels varied significantly (Figure S1). Such changes in protein expression were not observed when cells were exposed to Cys in place of NAC under otherwise identical experimental conditions (Figure S2), which argues against the idea that the observed effects are due to the Cys derived from intracellular NAC deacetylation [83, 84]. This was further corroborated by the observation

that, while NAC treatment did not affect the cellular proliferation rate, exposure to cysteine resulted in ≈30% decreased cell viability. This observation neatly fits with the reported cytotoxicity of cysteine both in cell culture media [85, 86] and as a dietary supplement of animal models, particularly as compared to *N*-acetylcysteine [87]. In this respect, the downregulation of both MST and SQR could be related to the cysteine-mediated cytotoxicity.

The NAC-induced enhancement of MST and SQR expression levels points to changes in mitochondrial H_2S metabolism. With the aim of exploring the correlation between increased expression levels and enzymatic activity, a functional approach was undertaken by measuring MST and SQR activity in cell and mitochondrial extracts, respectively. As compared to controls, NAC-treated cells displayed, respectively, ≈20% and ≈50% increase in MST and SQR activity (Figure 2B and 3B), in line with the increased expression levels of these enzymes. Considering that NAC exposure did not result in changes in the mitochondrial mass (Figure S4), NAC seems to induce a mitochondrial enrichment in MST and SQR, likely boosting the mitochondrial (per/poly)sulfide metabolism. In agreement with a previous report [62], we speculate that the enhanced production of mitochondrial reactive sulfide species and their physical proximity to the electron transport chain, a main source of ROS, could be at the basis of the antioxidant function of NAC.

Besides the regulatory effect of NAC on MST and SQR expression, we tested whether NAC could stimulate the production of sulfane sulfur species by directly sustaining MST activity, acting as a sulfane sulfur accepting co-substrate, similarly to Cys or homocysteine [19]. Working on the recombinant human MST, we found that the enzyme can use NAC as a substrate to sustain H_2S synthesis with a higher K_M but also a higher V_{max} when compared to Cys,

overall accounting for a ≈30% higher catalytic efficiency (V_{max}/K_M) (Table 1). This higher catalytic efficiency was confirmed by measuring the enzymatic activity at varied 3MP concentrations and fixed concentration of NAC (Figure 4B; Table 1). Combined NAC and Cys acting as sulfane sulfur acceptors yielded a comparable MST activity to that measured with NAC alone, approximately the double of the activity with Cys alone (Figure S5). Therefore, NAC and Cys do not display synergic or additive effects on H_2S generation by MST and probably compete for the same binding site on the protein. Given the higher reactivity of (per/poly)sulfides with electrophiles compared to their thiolic counterpart [15, 88, 89], it is likely that NAC persulfide (*N*-AceCysSSH) —the expected product of the reaction of MST with NAC— can directly contribute to ROS scavenging, as already reported for cysteine persulfide (CysSSH, [80]). It is important to note that, in addition to affording protection from oxidative stress, *N*-AceCysSSH may also increase the drug detoxifying capacity of cancer cells, thus promoting chemoresistance. Indeed, acetylation of cysteine-S-drug conjugates by microsomal NAT8 into the corresponding mercapturate is a crucial step for drug excretion in the urine [16, 17]. On this basis, it is envisaged that conjugation of MST-derived *N*-AceCysSSH with an exogenous alkylating/oxidative drug will prompt the latter for its excretion. Therefore, our results suggest that NAC supplementation may help cancer cells not only evade the oxidative stress derived from anticancer drug, but even increase their drug resistance.

The physiological relevance of the reaction between NAC and MST might be questioned because cell-internalized NAC was reported to be deacetylated into cysteine [83, 84], though at significant rates only in kidneys and much less in other organs [84]. To address this question, we evaluated the residual amount of NAC in treated SW480 cells by RP-HPLC at different

exposure times to NAC and found that, under our working conditions, the intracellular levels of NAC remained detectable and essentially constant over at least 24 h-treatment (Figure 5B). This shows that in our experimental setting, despite possible reactions with acylases, NAC persists as such inside the cells for a considerable time, allowing its reaction with MST and other protein targets.

In summary, this is to our knowledge the first study in which the effect of prolonged cell exposure to NAC on H_2S metabolism has been evaluated in colon cancer cells. The evidence collected with SW480 colorectal cancer cells shows that i) treatment with NAC promotes increased expression and activity of mitochondrial enzymes (MST and SQR) involved in the production and consumption of H_2S and sulfane sulfur species and ii) NAC can act as a direct sulfane sulfur-accepting co-substrate for MST, being likely persulfidated (Figure 6). The relevance of these findings in cancer biology needs to be assessed, particularly whether the ability of colorectal cells to resist oxidative stress and develop chemoresistance could be promoted by NAC through mitochondrial metabolic reprogramming of H_2S and related reactive species.

AUTHOR CONTRIBUTIONS

Conceptualization, A.G., J.B.V and E.F.; investigation, K.Z., C.S.T., L.M. , G.P. and G.G.; data analysis, K.Z., C.S.T., L.M., G.P. and G.G.; writing—original draft preparation, K.Z., J.B.V. and A.G.; writing—review and editing, K.Z., J.B.V., A.G., C.S.T., E.F., L.M., G.P. and G.G; supervision, A.G., E.F. and J.B.V.; funding acquisition, A.G. and J.B.V; supervision and methodological support (with regard to the activities carried out by K.Z.), F.M.;

FUNDINGS

This research was funded by Ministero dell'Istruzione, dell'Università e della Ricerca of Italy (PNR-CNR Aging Program 2012–2014 and PRIN 20158EB2CM_003), by iNOVA4Health Research Unit (LISBOA-01-0145-FEDER-007344), which is cofunded by Fundação para a Ciência e Tecnologia / Ministério da Ciência e do Ensino Superior, through national funds, and by FEDER under the PT2020 Partnership Agreement, is acknowledged by CST and JBV. This work has received funding from the European Union's Horizon 2020 research and innovation program under grant agreement No 810856.

TABLES AND FIGURES

Table 1. Kinetic parameters of human MST.

	$K_{M\,(A)}$	$V_{max\,(A)}$	$V_{max}/K_{M\,(A)}$	$K_{M\,(3MP)}$	$V_{max\,(3MP)}$	$V_{max}/K_{M\,(3MP)}$
	mM	*RFU·min^{-1}*	*RFU·min^{-1}·mM^{-1}*	*mM*	*RFU·min^{-1}*	*RFU·min^{-1}·mM^{-1}*
Cys	6.0 ± 1.0	15,136 ± 839	2,523	0.57 ± 0.04	81,560 ± 3,972	143,088
NAC	11.4 ± 1.0	37,178 ± 1,442	3,261	0.49 ± 0.02	95,396 ± 2,487	194,686

(A) Values determined at varying concentration of Cys or NAC and fixed concentration of 3MP.
(3MP) Values determined at varying concentration of 3MP and fixed concentration of either Cys or NAC.

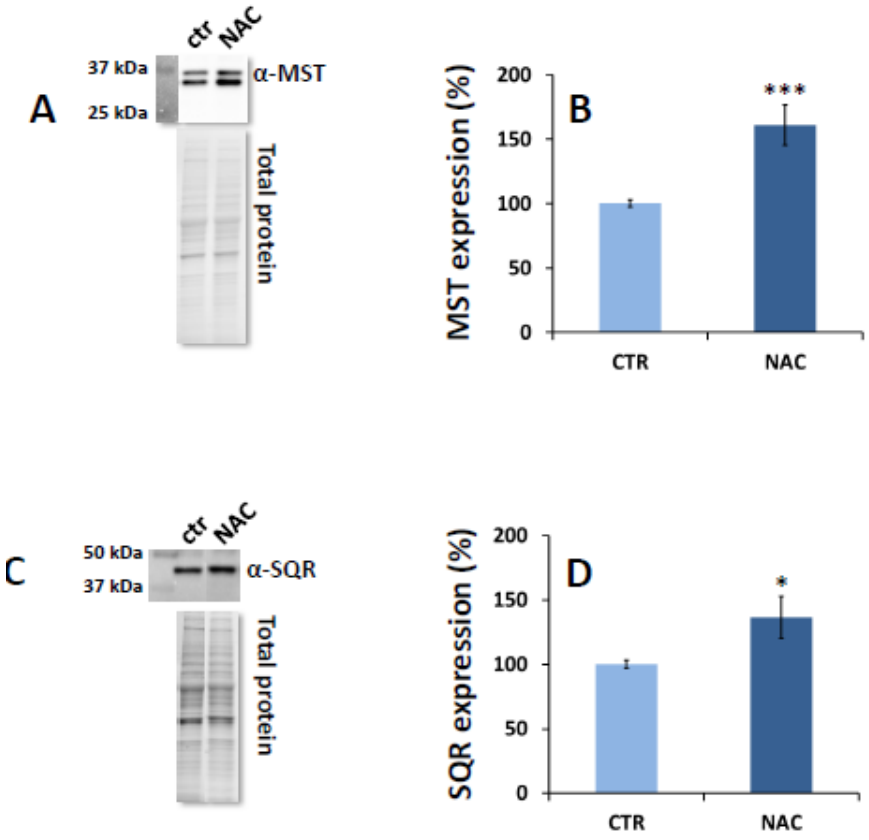

Figure 1. Effect of NAC on MST and SQR expression. (Panel A) Representative Western blot analysis of MST expression in SW480 cells grown for 24 h in DMEM alone (control) or supplemented with 10 mM NAC (NAC). The blots are shown together with their corresponding total protein load quantitation by stain-free imaging technology (see Materials and Methods). (Panel B) MST expression levels as normalized to total protein. Data represent the mean value ± SEM of 6 repeats, each carried out in technical duplicate. ***$P \leq 0.001$. (Panel C) Similarly to panel A, representative Western blot analysis of SQR expression. (Panel D) SQR expression levels as normalized to total

protein. Data represent the mean value ± SEM of 5 repeats, each carried out in technical duplicate. *P ≤ 0.05.

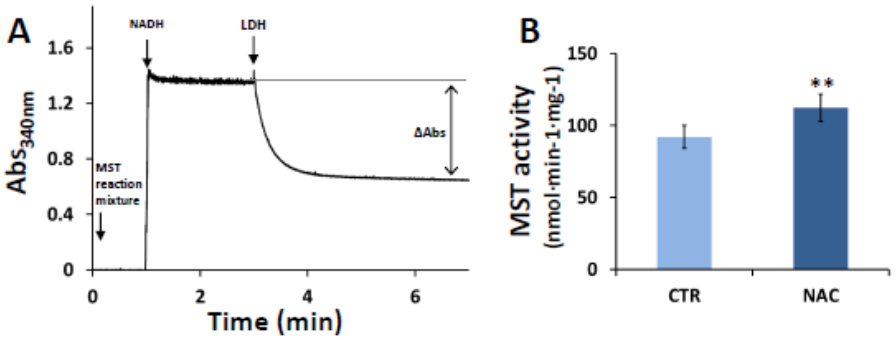

Figure 2. MST activity in cell lysates. (Panel A) Representative spectrophotometric trace of MST activity measured by LDH-coupled assay. The measurement was carried out at 37 °C under stirring conditions (see Materials and Methods). The starting solution contained the deproteinized MST activity mixture in Tris HCl 100 mM (pH 8.0) containing 6.4 mM NEM to block unreacted 3MP. After addition of 224 µM NADH followed by addition of 7 U LDH, the pyruvate concentration was estimated from the NADH being oxidized accounting for the decrease in absorbance measured at 340 nm. (Panel B) MST activity normalized to total protein. Data represent the mean value ± SD of 5 repeats. **P ≤ 0.01.

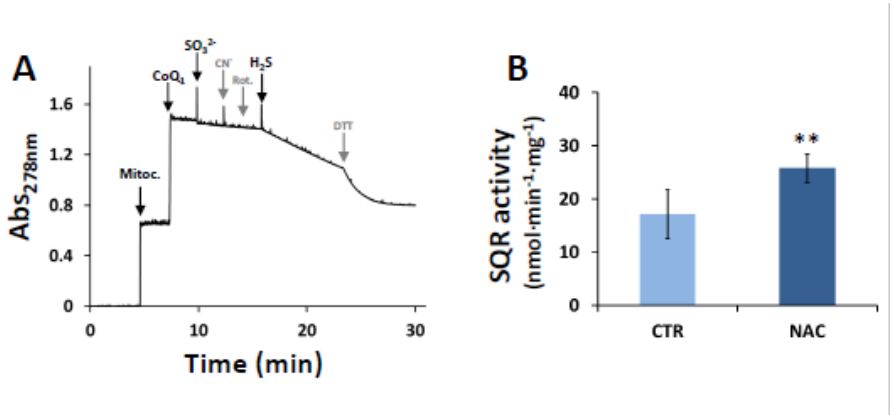

Figure 3. SQR activity of mitochondrial extracts. (Panel A) Representative spectrophotometric trace of SQR activity. The measurement was carried out at 37 °C under stirring. The starting solution contained the mitochondrial protein extract in 100 mM potassium phosphate buffer (pH 7.5) in anaerobic conditions (see Materials and Methods). Then, 58 µM CoQ1, 1 mM sodium sulfite, 2 mM sodium cyanide and 4 µM rotenone were sequentially added. SQR enzymatic activity was triggered by adding 96 µM H_2S, and the reaction rate was estimated by following the reduction of CoQ1 at 278 nm. Afterwards, CoQ1 was fully reduced by addition of dithiothreitol (DTT). (Panel B) SQR activity normalized to total protein. Data represent the mean value ± SD of 5 repeats. **P ≤ 0.01.

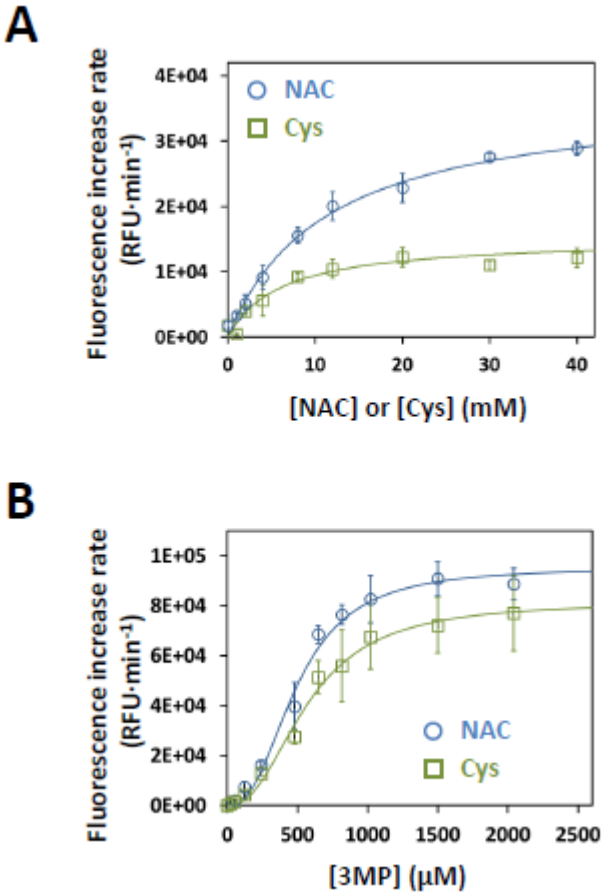

Figure 4. Kinetics of H_2S generation by MST. (Panel A) H_2S-synthesizing activity of MST measured at varying concentrations of Cys or NAC. The reaction mixture contained 10 µg recombinant human MST, 0–40 mM NAC (blue) or Cys (green), 50 µM 7AzC and 0.5 mM 3MP in a total assay volume of 250 µL, as described in Materials and Methods. Buffer: 200 mM Tris-HCl pH 8.0 Data represent the mean values ± SD of at least two independent experiments, each in technical triplicate. (Panel B) H_2S-synthesizing

activity of MST measured at varying concentrations of 3MP. The reaction mixture contained 0–2 mM 3MP, 20 mM of NAC (blue) or Cys (green). Other experimental conditions as reported in panel A. Data represent the mean values ± SD of at least two independent experiments, each in technical triplicate.

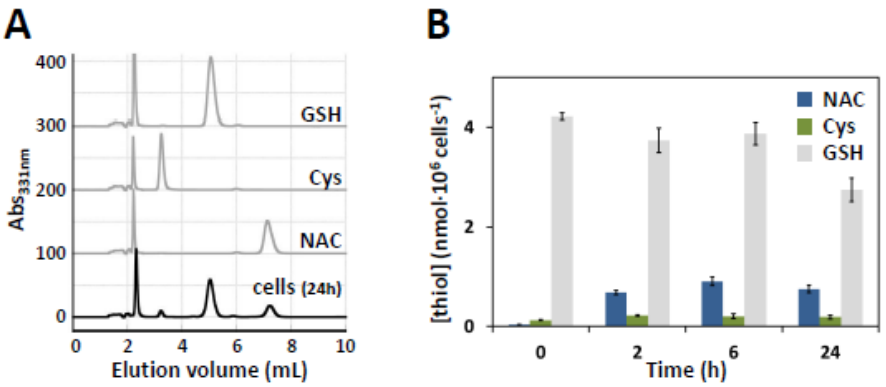

Figure 5. Intracellular NAC quantification by RP-HPLC. (Panel A) SW480 colon cancer cells were treated with 10 mM NAC for 5 min, 2 h, 6 h and 24 h. Cell lysates were deproteinized and NAC was quantified by RP-HPLC simultaneously with Cys and GSH after DTNB derivatization. Representative chromatograms are shown. Calibrations (in gray) were performed by injecting standard solutions of GSH, Cys and NAC at known concentrations. In black it is reported a representative chromatogram obtained with cells treated with NAC for

24 h. (Panel B) Data represent the mean values ± SD of two biological duplicates, each in technical duplicate.

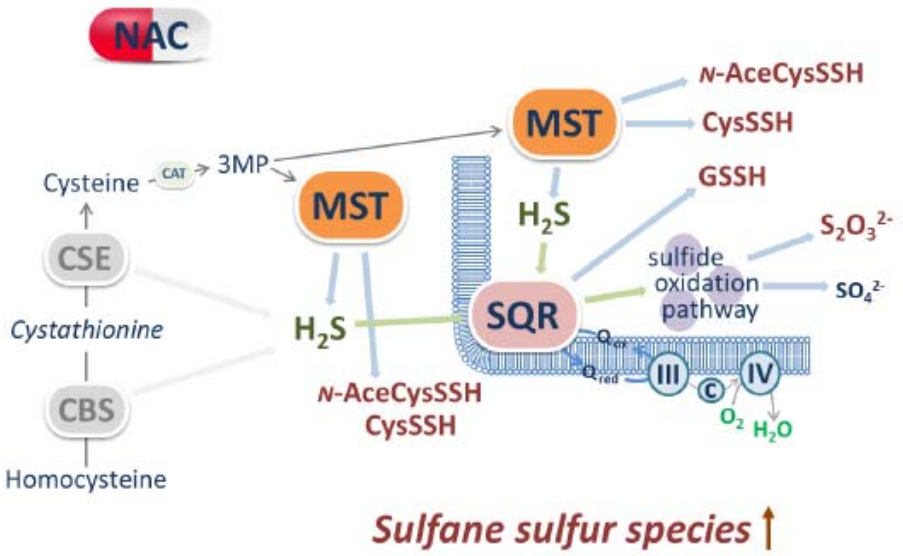

Figure 6. Schematic representation of the effects of NAC on H_2S metabolism. CBS: cystathionine β-synthase; CSE: cystathionine γ-lyase; MST: 3-mercaptopyruvate sulfurtransferase; 3MP: 3-mercaptopyruvate; SQR: sulfide:quinone oxidoreductase; GSSH: glutathione persulfide; ROS: reactive oxygen species; Cys-SSH: cysteine persulfide; *N*-AceCysSSH: *N*-acetylcysteine persulfide.

Supplementary informations

Supplementary Figure S1. Effect of NAC on CBS and CSE expression.

Supplementary Figure S2. Effect of Cys on MST and SQR expression.
interaction between human CSE and pyridine derivatives
Supplementary Figure S3. Efficiency of mitochondria isolation.
interaction between human MST and pyridine derivatives
Supplementary Figure S4. Effect of NAC on mitochondrial content.
Supplementary Figure S5. Effect of combined NAC and Cys on MST activity.

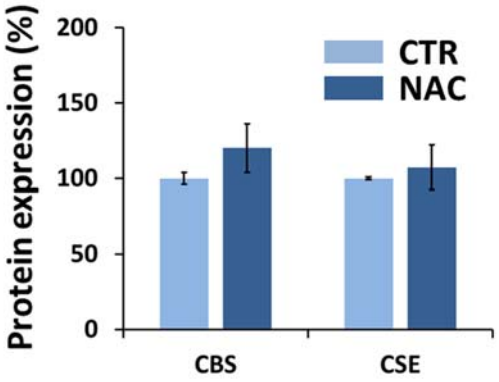

Figure S1. Effect of NAC on CBS and CSE expression. Western blot analysis of CBS and CSE expression in NAC-treated and control SW480 cells. Data represent the mean value ± SEM of 3 repeats, each carried out in technical duplicate.

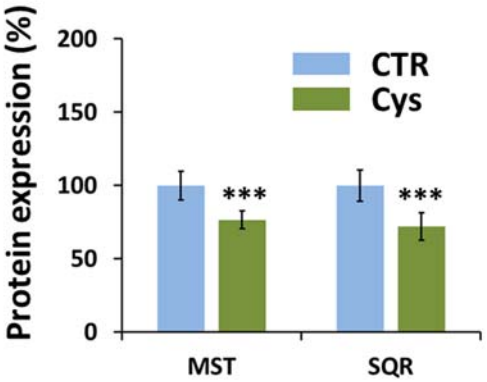

Figure S2. Effect of Cys on MST and SQR expression. Western blot analysis of MST and SQR expression in SW480 cells grown for 24 h in DMEM alone (control) or supplemented with 10 mM Cys-supplemented medium (Cys). Data represent the mean value ± SEM of 4 repeats, each carried out in technical duplicate

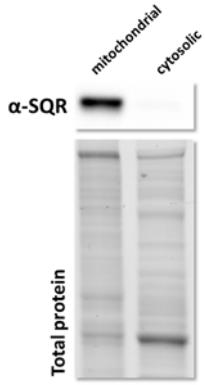

Figure S3. Efficiency of mitochondria isolation. Representative Western blot analysis of SQR to test the efficiency of mitochondria isolation. Data were normalized

to their corresponding total protein load, quantitated by stain-free imaging technology (see Materials and Methods).

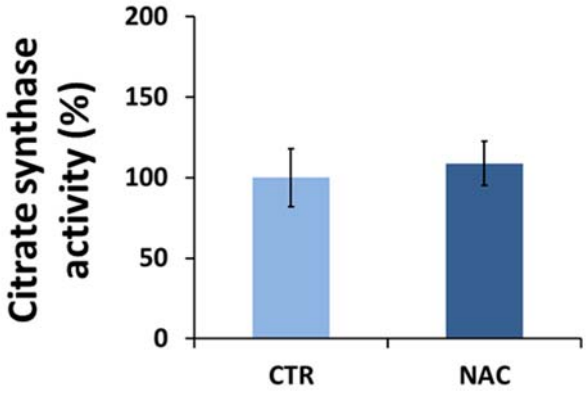

Figure S4. Effect of NAC on mitochondrial content. Mitochondrial content in NAC-treated and control SW480 cells was estimated by performing citrate synthase activity assays on cell lysates. Data represent the mean value ± SD of 5 repeats.

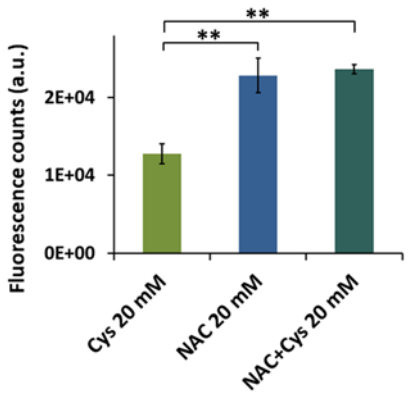

Figure S5. Effect of combined NAC and Cys on MST activity. H2S-synthesizing activity of the recombinant human MST, as measured in the presence of 20 mM Cys (light green), 20 mM NAC (blue), or a combination of 20 mM Cys and 20 mM NAC (dark green). Buffer: 200 mM Tris-HCl pH 8.0. In addition to NAC and/or Cys, the reaction mixture contained 10 µg recombinant human MST, 50 µM 7AzC, 0.5 mM 3MP in a total assay volume of 250 µL, as described in Materials and Methods. Data represent the mean values ± SD of 3 independent experiments, each in technical triplicate. **P ≤ 0.01.

RESULTS AND DISCUSSION
PAPER 2

Hydrogen sulfide oxidation: adaptive changes in mitochondria of SW480 colorectal cancer cells upon exposure to hypoxia

Francesca Malagrinò[a,b], Karim Zuhra[a,b], Ludovica Mascolo[a], Daniela Mastronicola[a], João B. Vicente[c,*], Elena Forte[a], Alessandro Giuffrè[b,*]

[(a)] Department of Biochemical Sciences, Sapienza University of Rome, Rome, Italy

[(b)] CNR Institute of Molecular Biology and Pathology, Rome, Italy

[(c)] Instituto de Tecnologia Química e Biológica António Xavier, Universidade Nova de Lisboa, Oeiras, Portugal

*Corrispondence:
Dr. Alessandro Giuffrè, Institute of Molecular Biology and Pathology (IBPM), National Research Council of Italy (CNR), Piazzale Aldo Moro 5, I-00185 Rome, Italy. alessandro.giuffre@uniroma1.it
Dr. João B. Vicente, Instituto de Tecnologia Química e Biológica António Xavier, NOVA University of Lisbon, Av. da República (EAN), 2780-157 Oeiras, Portugal. jvicente@itqb.unl.pt

Oxid Med Cell Longev. 2019 Jan 29;2019:8102936. doi: 10.1155/2019/8102936. eCollection 2019.

Received: 26 September 2018; Accepted: 10 December 2018; Published: 29 January 2019

ABSTRACT

Hydrogen sulfide (H_2S), a known inhibitor of cytochrome *c* oxidase (CcOX), plays a key signaling role in human (patho)physiology. H_2S is synthesized endogenously and mainly metabolized by a mitochondrial sulfide-oxidizing pathway comprising sulfide:quinone oxidoreductase (SQR), whereby H_2S-derived electrons are injected into the respiratory chain stimulating O_2 consumption and ATP synthesis. Under hypoxic conditions, H_2S has higher stability and is synthesized at higher levels with protective effects for the cell. Herein, working on SW480 colon cancer cells, we evaluated the effect of hypoxia on the ability of cells to metabolize H_2S. The sulfide-oxidizing activity was assessed measuring by high-resolution respirometry the stimulatory effect of sulfide on rotenone-inhibited cell respiration in the absence or presence of antimycin A. Compared to cells grown under normoxic conditions (air O_2), cells exposed for 24 h to hypoxia (1% O_2) displayed a 1.3-fold reduction in maximal sulfide-oxidizing activity and 2.7-fold lower basal O_2 respiration. Based on citrate synthase activity assays, mitochondria of hypoxia-treated cells were 1.8-fold less abundant, and displayed 1.4-fold higher maximal sulfide-oxidizing activity and 2.6-fold enrichment in SQR as evaluated by immunoblotting. We speculate that under hypoxic conditions mitochondria undergo these adaptive changes to protect cell respiration from H_2S poisoning.

ABBREVIATIONS: H_2S, hydrogen sulfide; SQR, sulfide:quinone oxidoreductase; NO, nitric oxide; CO, carbon monoxide; CcOX, cytochrome *c* oxidase; CBS, cystathionine β-synthase; CSE, cystathionine γ-lyase; MST, 3-mercaptopyruvate sulfurtransferase; SO_4^{2-}, sulfate; $S_2O_3^{2-}$, thiosulfate;

DTNB, 5,5'-dithiobis-(2-nitrobenzoic acid); PBS-T, phosphate buffered saline with 0.1% Tween 20 (v/v); OCR, oxygen consumption rate.

1. INTRODUCTION

Hydrogen sulfide (H_2S) has been increasingly recognized as a key signaling molecule in human (patho)physiology. While being able to regulate cell redox homeostasis and other crucial physiological functions at low (nM) concentrations [142-145], at higher (μM) levels H_2S exerts toxicity both inhibiting O_2 consumption by cytochrome *c* oxidase (CcOX) in the mitochondrial electron transport chain [146] and impairing O_2 transport/storage through covalent modification of the heme porphyrin ring in globins (reviewed in [147]). It is therefore crucial that cells tightly control H_2S bioavailability to prevent toxicity.

In humans, at least three enzymes are directly involved in H_2S synthesis (reviewed in [142, 148, 149]): cystathionine β-synthase (CBS) and cystathionine γ-lyase (CSE), belonging to the transulfuration pathway, and the mitochondrial enzyme 3-mercaptopyruvate sulfurtransferase (MST). Of these, CBS is inhibited with relatively high affinity by nitric oxide (NO) and carbon monoxide (CO), particularly in the presence of the allosteric stimulator S-adenosyl-L-methionine [150-154]. H_2S breakdown is instead mostly accomplished by a mitochondrial enzymatic pathway that couples the oxidation of H_2S into thiosulfate ($S_2O_3^{2-}$) and sulfate (SO_4^{2-}) to ATP synthesis [155]. The first step of sulfide breakdown is catalyzed by the membrane-associated sulfide:quinone oxidoreductase (SQR). This flavoprotein transfers electrons from H_2S to coenzyme Q in the mitochondrial electron transfer chain, thus making of H_2S the first inorganic substrate able to sustain mitochondrial

respiration [156]. Concomitantly, SQR transfers the H_2S sulfur atom to an acceptor, leading to formation of glutathione persulfide (GSSH) [157, 158] or, less likely, $S_2O_3^{2-}$ [128, 159]. Differences in the SQR substrate specificity were recently reported comparing the soluble with the nanodisc-incorporated enzyme [160]. Three additional enzymes, persulfide dioxygenase (ETHE1), thiosulfate sulfurtransferase and sulfite oxidase, cooperate with SQR in the mitochondrial sulfide oxidation pathway, to oxidize H_2S into SO_4^{2-} and $S_2O_3^{2-}$. To process 1 H_2S molecule, mitochondria overall consume ~0.75 O_2 molecules (0.25 by CcOX plus 0.5 by ETHE1, [161]). Besides being metabolized through the mitochondrial sulfide-oxidizing pathway, H_2S can be oxidized by several metalloproteins such as globins, heme-based sensors of diatomic gaseous molecules, catalase and peroxidases (see [149] and references therein) or be catabolized by the cytosolic thiol methyltransferase [162].

In vivo, H_2S can therefore exert a dual effect on cell bioenergetics, at lower concentrations stimulating *via* SQR mitochondrial respiration and thus ATP synthesis, or causing a reversible inhibition of CcOX at higher concentrations (reviewed in [163-166]). Notably, the sulfide oxidizing activity varies considerably between different cell types and tissues, spanning from undetectable, as e.g., in neuroblastoma cells, to high, as observed in colonocytes [156, 161, 167]. The high H_2S detoxifying ability of colonocytes is perhaps not surprising as these cells are physiologically exposed to the fairly high H_2S levels produced by the gut microbiota (reviewed in [45]).

Among other diseases, cancer has been increasingly associated with alterations of H_2S metabolism [168-170]. In particular, CBS has been shown to be overexpressed in cell lines and samples of colorectal cancer [171] and

other cancer types [78, 172-174]. In colorectal cancer cell lines, CBS-derived H_2S was proposed to promote cell proliferation and angiogenesis, and to sustain cellular bioenergetics by stimulating both oxidative phosphorylation and glycolytic ATP synthesis. The enzyme is therefore currently recognized as a drug target [168, 170, 175]. CSE and CSE-derived H_2S have been recognized as key elements in melanoma progression [176]. All three H_2S-synthesizing enzymes have been posited to contribute to the correlation between increased H_2S production and tumor stage and grade in bladder urothelial cell carcinoma [177]. Moreover, Szczesny and co-workers [174] observed higher expression levels of all three H_2S-generating enzymes and increased H_2S-producing activity in lung adenocarcinoma samples as compared to adjacent normal lung tissue. A link between H_2S production and mitochondrial DNA repair was proposed and inhibition of CBS and CSE by aminooxyacetic acid or siRNA-mediated depletion of CBS, CSE or MST in the lung adenocarcinoma A549 cell line resulted in compromised integrity of mitochondrial DNA. Irrespectively of the downstream mechanisms linking increased H_2S levels and cell proliferation and/or tumor progression, it remains to be established how cancer cells circumvent the potentially toxic effects of increased H_2S.

Hypoxia is a common factor in the microenvironment of solid tumors that has been recognized to be associated to drug-resistance and promote cancer progression, metastasization and angiogenesis (see [178] for a review). The effect of hypoxia on cancer metabolism has been extensively investigated (reviewed in [179-181]). Among other changes, hypoxic cells undergo a reduction in mitochondrial mass, resulting from reduced biogenesis of this organelle and enhanced mitophagy [182-184]. Because mitochondria are the main site of sulfide oxidation, in the absence of compensatory mechanisms,

hypoxic cells are expected to display a reduced ability to detoxify sulfide. The intricate interplay between H_2S and O_2 has been extensively investigated (reviewed in [185, 186]). As O_2 facilitates both the chemical and enzymatic oxidative decomposition of H_2S into persulfides and polysulfides, at low O_2 tension a higher stability of H_2S is expected. Furthermore, hypoxic/ischemic conditions have been reported to enhance H_2S synthesis, through: up-regulation or stimulation of the sulfide-synthesizing enzymes [187, 188]; accumulation of CBS in mitochondria, likely augmenting the H_2S mitochondrial levels [189], and release of CO-mediated inhibition of CBS and CSE [190, 191]. Hypoxia is thus expected to increase H_2S bioavailability, a condition that can have opposite physiological consequences. Indeed, while H_2S has been shown to be protective against ischemia injuries [192, 193], the enhanced biosynthesis and chemical stability of H_2S, combined with the reduced content in mitochondria (the main sites of sulfide disposal), may increase the risk of H_2S toxicity in hypoxic cells.

This information prompted us to investigate in the present study the effect of hypoxia on the mitochondrial sulfide-oxidizing activity and SQR expression in colorectal cancer cells.

2. MATERIALS AND METHODS

2.1 Materials

The human colon cancer cell line SW480 was purchased from the American type Culture Collection (ATCC *no. CCL228*™). Sodium sulfide nonahydrate ($Na_2S·9H_2O$, 431648), 5,5'-dithiobis-(2-nitrobenzoic acid) (DTNB), acetyl coenzyme A, oxaloacetate, CelLytic™MT cell lysis reagent, protease inhibitor cocktail (P8340) and rabbit polyclonal antibody against

human SQR (HPA017079) were purchased from Sigma. The bicinchoninic acid assay (BCA) kit was from Thermo Fisher Scientific. Cell culture media and antibiotics were from Sigma, Euroclone or Gibco. Mini-PROTEAN TGX Stain-Free Precast Gels, the Clarity Western ECL substrate and the Laemmli protein sample buffer were purchased from Bio-Rad. Bovine serum albumin was from AppliChem.

2.2 Preparation of sulfide stock solutions

Stock solutions of Na_2S were prepared by quickly washing with degassed ultra-pure (Milli-Q®) water the surface of a Na_2S crystal, and then dissolving it in degassed Milli-Q water under N_2 atmosphere, as reported in [194]. The concentration of Na_2S in solution was measured spectrophotometrically using 5,5'-dithiobis-(2-nitrobenzoic acid) (DTNB) according to [195] in a Cary 60 UV-VIS spectrophotometer. The concentration of Na_2S was then adjusted to 3-5 mM by dilution with degassed ultra-pure (Milli-Q®) water in a gas-tight glass syringe.

2.3 Cell culture

The human colon cancer cell line SW480 was maintained in Dulbecco's Modified Eagle Medium (DMEM) containing 4.5 $g \cdot L^{-1}$ glucose, supplemented with 2 mM L-glutamine, 10% (v/v) heat-inactivated fetal bovine serum (FBS), 100 $U \cdot mL^{-1}$ penicillin and 100 $\mu g \cdot mL^{-1}$ streptomycin. Cells at 37 °C and 5% CO_2 in 25 cm^2 or 75 cm^2 flasks were grown under normoxic conditions (air O_2) or incubated for 24 h under hypoxic conditions (1% O_2) in a Galaxy 14 S incubator (Eppendorf) designed to maintain cell cultures at controlled O_2 tension. After trypsinization, the cells were washed in the culture medium, counted using the trypan blue dye exclusion test, centrifuged at 1000 x g for 5

min and resuspended in fresh medium at a final density of 8 x 10^6 cells·mL^{-1}. Trypan blue-positive cells were always less than 5%. Cells grown under air conditions or exposed to hypoxia are respectively referred to as 'normoxic' and 'hypoxia-treated' cells.

2.4 Measurements of the mitochondrial sulfide-oxidizing activity

The mitochondrial sulfide-oxidizing activity of tested cells was evaluated as described in [165], by measuring the stimulatory effect of sulfide on cellular O_2 consumption. Measurements were carried out at 37 °C, using a high-resolution respirometer (Oxygraph-2k, Oroboros Instruments, Innsbruck, Austria), equipped with two 1.5-mL chambers and a micropump (TIP-2k) allowing for steady injections of relatively small amounts of sulfide into the chambers. According to [165], in these assays, sulfide is injected into a cell suspension at increasing flux (determined by the pump rate) and the mitochondrial sulfide-detoxifying activity is evaluated from the observed stimulation of cellular O_2 consumption. Indeed, upon increasing the rate of sulfide injection, the concentration of sulfide in solution and, in turn, the sulfide-sustained cellular O_2 consumption increase until the concentration of injected sulfide becomes inhibitory for CcOX. In colorectal cancer cells SQR-mediated sulfide detoxification was shown to promote both forward electron transfer to O_2 via quinol:cytochrome *c* reductase (Complex III)/cytochrome *c*/CcOX and reverse electron transfer through Complex I [161]. Therefore, measurements were herein carried out in the presence of rotenone, a known inhibitor of Complex I, to prevent electrons derived from SQR-mediated sulfide oxidation to be partially diverted from O_2 reduction with consequent underestimation of the mitochondrial sulfide-oxidizing activity. Herein the assays were typically conducted in FBS-supplemented cell medium under

stirring as follows. A suspension of four million cells was added into the respirometer chamber, and the basal respiration was measured for ~10 min. Afterwards, following the addition of 5 μM rotenone resulting in O_2 consumption inhibition, a solution of 3 - 5 mM sulfide was injected for time intervals of 180 s at increasing rates (10 $nL \cdot s^{-1}$, 20 $nL \cdot s^{-1}$, 40 $nL \cdot s^{-1}$, 80 $nL \cdot s^{-1}$ and 160 $nL \cdot s^{-1}$) and the effect on O_2 consumption was measured. Control experiments were carried out in the presence of both rotenone (5 μM) and antimycin A (5 μM), an inhibitor of Complex III. The latter assays allowed us to evaluate the effect of sulfide on extra-mitochondrial and non-enzymatic O_2 consumption and thus obtain by subtraction (from the experiments performed in the absence of antimycin A) the genuine mitochondrial O_2 consumption activity due to sulfide oxidation and from it an estimate of the H_2S-oxidizing activity, considering that ~1.33 molecules of H_2S per O_2 molecule are reportedly consumed by the mitochondrial sulfide oxidizing pathway [161].

2.5 Evaluation of mitochondrial content by the citrate synthase assay

Cells were harvested and lysed using the CelLytic™MT cell lysis reagent and protease inhibitor cocktail from Sigma according to the manufacturer instructions. Cell extracts were assayed spectrophotometrically for citrate synthase in 100 mM Tris-HCl, 0.3 mM acetyl-CoA, 0.1 mM DTNB and 0.1 mM oxaloacetate, as described in [196].

2.6 Immunoblotting assays

Cells were harvested, lysed as described in the previous section and, after total protein content determination by the bicinchoninic acid method, proteins (20 μg per lane) were separated by SDS-PAGE using Mini-PROTEAN TGX Stain-Free Precast Gels (Bio-Rad). The formulation of these

gels includes trihalo compounds which lead to UV fluorescence emission upon reaction with proteins [197], allowing to estimate for normalization purposes the total protein load in a gel lane, using a ChemiDoc MP imaging system (Bio-Rad) without resorting to staining procedures or protein housekeepers**.** Proteins commonly used as housekeepers, such as glyceraldehyde 3-phosphate dehydrogenase and β-actin, indeed are known to change their expression levels under hypoxia [198, 199]. Afterwards, the proteins separated by SDS-PAGE were transferred onto a polyvinylidene difluoride membrane using a Trans-Blot SD Semi-Dry Electrophoretic Transfer Cell (from Bio-Rad) at 180 mA for 30 min. The membrane was blocked with PBS-T (phosphate buffered saline with 0.1% Tween 20 [v/v]) containing 3% bovine serum albumin (BSA, w/v) and then incubated overnight at 4 °C with the antibody against human SQR (1:150, in PBS-T with 3% BSA (w/v)). After three washing steps with PBS-T (15 min), the membrane was incubated with horseradish peroxidase-conjugated secondary antibody (1:5000, in PBS-T with 3% BSA (w/v)), followed by three washing steps with PBS-T (15 min) and detection by enhanced chemiluminescence (Clarity Western ECL Substrate, Biorad). Finally, the blotted membrane was subjected to densitometric analysis using Image Lab software (Biorad), followed by normalization of the target protein band intensity to the total protein load determined as described above.

2.7 Data analysis

Oxygen consumption rates (OCR) were calculated using the software DatLab4 (Oroboros Instruments, Austria). Data are reported as mean ± standard error of the mean (SEM). Statistical significance (P) was estimated using the Student's *t*-test in Microsoft Excel. *$P \leq 0.05$ and ***$P \leq 0.001$ were considered significant.

3. RESULTS

Colorectal cancer SW480 cells were either grown under normoxic (air O_2) conditions or exposed for 24 h to hypoxia (1% O_2), and their sulfide-oxidizing activity was assayed by high-resolution respirometry, according to [165], as described in the Materials and Methods. A representative oxygraphic trace acquired with untreated ('normoxic') cells is shown in Figure 1a. The trace shows that ~80% of oxygen consumption was blocked by addition of the Complex I inhibitor rotenone, added to prevent sulfide oxidation through reversal of Complex I activity, as described in [161, 200]. Sulfide was then injected five times at increasing rates into the oxygraphic chamber via a micropump. The first four injections led to stimulation of O_2 consumption, pointing to a fully operative mitochondrial sulfide-oxidizing pathway in the tested cells (Figures 1a and 1b). The stimulation persisted for the entire duration (3 minutes) of sulfide injection, after which the O_2 consumption rate (OCR) declined back to the value measured in the absence of sulfide. The decline took a few minutes, as if some sulfide persisted in solution, sustaining cell respiration even after the injection was stopped. The extent of O_2 consumption stimulation by sulfide increased with the rate of sulfide injection (up to 80 $nL \cdot s^{-1}$, Figures 1a and 1c). However, upon further increasing the injection rate (to 160 $nL \cdot s^{-1}$) a decline in OCR was observed already before sulfide injection was stopped, likely due to CcOX inhibition by sulfide, as suggested previously [165].

For comparison, the measurements described above were carried out on the same cells after 24 h-exposure to hypoxic conditions. A representative oxygraphic trace is shown in Figure 1b. Hypoxia-treated cells displayed a lower basal respiratory activity compared to untreated cells (6.3 ± 0.5 nM $O_2 \cdot s^{-}$

[1] vs 17.1 ± 1.1 nM $O_2 \cdot s^{-1}$ per million cells). Yet, as observed for normoxic cells, after rotenone addition a progressive stimulation of cell respiration was observed upon injecting sulfide at increasing rate (Figures 1b and 1d), until the amount of injected sulfide exceeded the detoxifying activity of the cells, and C*c*OX inhibition occurred, leading to impairment of cell respiration (see last sulfide injection in Figure 1b, top).

To evaluate the contribution of mitochondria to the observed sulfide-oxidizing activity, we used antimycin A, a known inhibitor of Complex III that blocks quinol oxidation in the respiratory chain and thus prevents sulfide oxidation by mitochondria [165]. As shown in Figures 1a and 1b (bottom traces), in the presence of rotenone, antimycin A considerably prevented O_2 consumption stimulation by sulfide in both normoxic and hypoxia-treated cells, proving that under the tested conditions sulfide oxidation occurs mostly at the mitochondrial level. The effect of sulfide on mitochondrial O_2 consumption was quantitatively evaluated by subtracting the OCR values measured during sulfide injection in the presence of both rotenone and antimycin A from those measured at identical sulfide injection rates in the presence of rotenone only (see legend to Figure 1 for more details). According to this analysis, at the highest non-inhibitory (for C*c*OX) injection rate sulfide sustained a mitochondrial O_2 consumption of 9.7 ± 1.2 nM $O_2 \cdot s^{-1}$ and 7.3 ± 0.8 nM $O_2 \cdot s^{-1}$ per million cells, in normoxic and hypoxia-treated cells, respectively. Considering that the mitochondrial sulfide-oxidizing pathway overall was reported to consume ~1.33 molecules of H_2S per O_2 molecule [161], a mitochondrial sulfide-oxidizing activity of 12.8 ± 1.5 and 9.7 ± 1.1 nM $H_2S \cdot s^{-1}$ per million cells was estimated for normoxic and hypoxia-treated cells, respectively (Figure 2a). To evaluate the mitochondrial content in the

tested cells, we carried out citrate synthase activity assays, a validated surrogate biomarker of mitochondrial content ([201] and references therein). Normoxic and hypoxia-treated cells displayed, respectively, a citrate synthase activity of 1.1 ± 0.1 μmol·min^{-1}·10^6 cells^{-1} and 0.6 ± 0.1 μmol·min^{-1}·10^6 cells^{-1} (Figure 2b), consistent with a reduction in the mitochondrial content upon exposure to hypoxia [182-184]. The measured citrate synthase activity was used to normalize the calculated mitochondrial sulfide-oxidizing activity, which proved to be in hypoxia-treated cells ~1.4-fold higher than in normoxic cells (Figure 2c). Finally, we have assayed by immunoblotting combined with 'stain-free' imaging technology the SQR expression level in the tested cells (Figure 3a) and found that hypoxia-treated cells display 1.4-fold higher SQR protein levels than normoxic cells (Figure 3b). Considering that hypoxia-treated cells have a lower mitochondrial content (based on citrate synthase activity assays, Figure 2b), we estimate that the mitochondria of hypoxia-treated cells contain 2.6-fold more SQR than those of normoxic cells (Figure 3c).

4. DISCUSSION

O_2 and H_2S are key molecules in living systems, able to control each other's availability and regulate numerous processes in human (patho)physiology. As reviewed in [185], the interplay between H_2S and O_2 is intricate and based on several mechanisms: i) direct reaction between the two; ii) O_2-dependent H_2S breakdown through the mitochondrial sulfide-oxidizing pathway; iii) H_2S-mediated stimulation or inhibition of mitochondrial O_2 consumption; iv) O_2-dependent regulation of expression and cellular re-localization of the H_2S-synthesizing enzymes, and v) O_2-dependent control of

CO-mediated inhibition of H_2S production by CBS. H_2S has indeed been recognized as an O_2 sensor [202]. Despite this, to our knowledge no studies have been conducted yet to explore the effect of prolonged exposure to hypoxia on the cell ability to dispose of H_2S, which represented the main objective of the present study.

Under hypoxic conditions, H_2S plays a key protective role against ischemia/reperfusion damages [192, 193] through only partly understood molecular mechanisms including induction of antioxidant and vasorelaxation effects on microcirculation. Moreover, H_2S appears to mediate the repair of damaged mitochondrial DNA [174], occurring in ischemia/reperfusion, and to protect from hypoxia-induced proteostasis disruption, as demonstrated in *Caenorhabditis elegans* [203]. In knockdown experiments with Hepa1-6 cells, H_2S-mediated protection during O_2 deprivation was found to require SQR [204], pointing to a key role of H_2S catabolism in the cellular protective responses to hypoxia. Consistently, under hypoxic conditions, thiosulfate, a major product of H_2S oxidation, has been shown to exert protective effects against ischemia/reperfusion damage [204-206] and also to generate H_2S [207]. In this context, it is noteworthy that H_2S is able to mimic hypoxia-induced responses such as vasodilation [208], neo-angiogenesis [209] and expression of the hypoxia inducible factor (HIF-1α, [210]), a master gene regulator promoting cell survival under hypoxic conditions shown to stimulate CBS expression in hypoxia [187]. The occurrence of H_2S under hypoxic conditions is therefore likely part of a more general adaptive response adopted by the cells to ensure survival and protection from damages resulting from O_2 deprivation (and possible reoxygenation).

In hypoxic cells, H_2S bioavailability therefore needs to be finely regulated for this gaseous molecule to occur at physiologically protective yet non-poisonous levels. In this regard, it seems relevant to gain insight into the regulation of H_2S production and breakdown at low O_2 tensions. Previous studies focused on the H_2S-synthesizing enzymes have shown that, under hypoxic conditions, H_2S synthesis is enhanced [185] through multiple mechanisms [187-191] (see Introduction). In addition, H_2S breakdown via both chemical and enzymatic reaction pathways is negatively affected by low O_2 tensions. Evidence for a lower mitochondrial sulfide-oxidizing activity at lower O_2 concentrations was initially provided in [211] working on immortalized cells derived from alveolar macrophages and, then, corroborated by Abou-Hamdan *et al*. in a more recent investigation on CHO cells [212].

In the present study, using SW480 colorectal cancer cells as a model, we tested the effect of prolonged (24 h) exposure to 1% O_2 on the cellular ability to dispose of sulfide at mitochondrial level. Exposure to hypoxia lead to a notable (2.7-fold) reduction in basal respiration and to a marked (1.8-fold) decrease in the mitochondrial content (Figure 2b), as previously documented and suggested to result from enhanced mitophagic activity and reduced organelle biogenesis [182-184]. Hypoxia-treated cells also display a lower ability to dispose of H_2S as compared to normoxic cells (Figure 2a). However, considering the above-mentioned decrease in mitochondrial content, the sulfide-detoxifying capacity of hypoxia-treated cells normalized to their minor mitochondrial content, actually turned out to be 1.4-fold higher than that of untreated cells, pointing to an enhanced sulfide disposal capacity of mitochondria in hypoxia-treated cells. To gain further insight, we analyzed the SQR expression by immunoblotting, employing ‘stain-free’ imaging

technology for total protein quantitation and normalization purposes. Using this approach, we made the somewhat puzzling observation that hypoxia-treated cells, though displaying slightly reduced overall sulfide-oxidizing activity, have modestly (~1.4-fold) increased SQR levels. Interestingly, normalizing the SQR expression to the mitochondrial content revealed that, in line with their enhanced sulfide-oxidizing capacity, mitochondria of hypoxia-treated SW480 cells have ~2.6-fold higher levels of SQR than those of normoxic cells. Altogether, these results are intriguing in that they suggest that mitochondria in hypoxia-treated cells display lower mass but are enriched in SQR. The increased SQR levels could have a protective role in hypoxic cells preventing mitochondria to be poisoned by enhanced production of sulfide (Figure 4).

5. CONCLUSIONS

This is to our knowledge the first study in which the effect of prolonged cell exposure to hypoxia on the mitochondrial sulfide-oxidizing activity has been evaluated. The evidence collected in SW480 colorectal cancer cells shows that hypoxia-treated cells metabolize sulfide with overall reduced maximal efficacy and have reduced mitochondrial content, but mitochondria are better equipped to dispose of H_2S. Physiologically, this may represent a regulatory mechanism to ensure higher protective H_2S levels, while protecting mitochondria from H_2S toxicity.

DATA AVAILABILITY

The data used to support the findings of this study are available from the corresponding authors upon request.

FUNDING STATEMENT

This work was partially supported by Ministero dell'Istruzione, dell'Università della Ricerca of Italy (PNR-CNR Aging Program 2012–2014 and PRIN 20158EB2CM_003 to AG). iNOVA4Health Research Unit (LISBOA-01-0145-FEDER-007344), which is cofunded by Fundação para a Ciência e Tecnologia / Ministério da Ciência e do Ensino Superior, through national funds, and by FEDER under the PT2020 Partnership Agreement, is acknowledged by JBV.

FIGURES

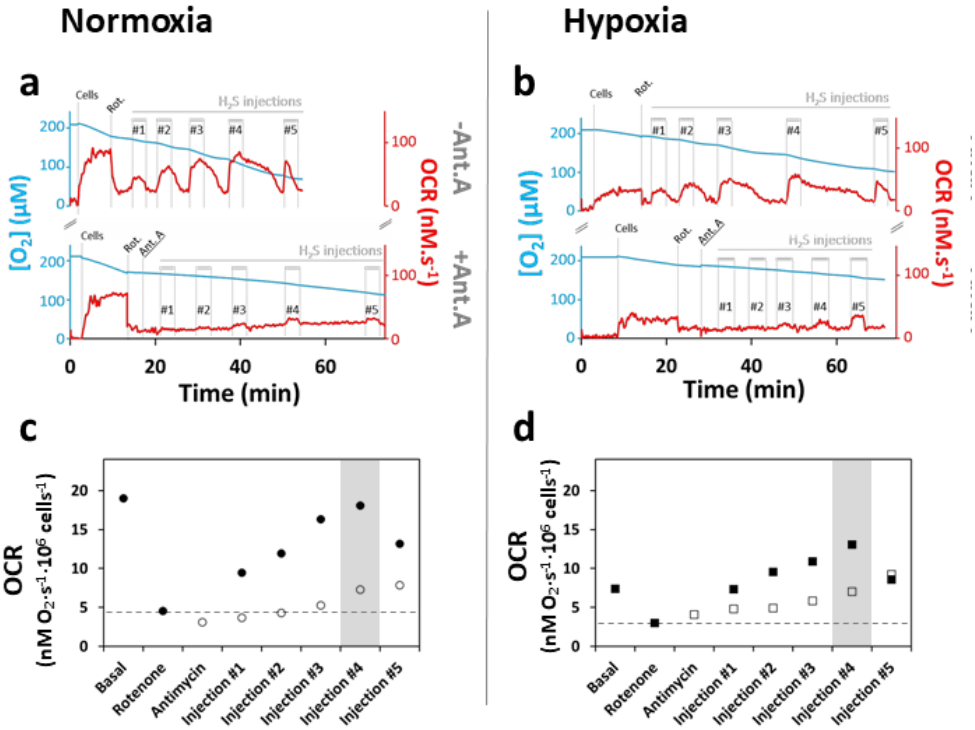

Figure 1. Stimulation of O_2 consumption by sulfide. Representative oxygen consumption traces (blue) and corresponding O_2 consumption rate (OCR, red traces) acquired with normoxic (*Panel a*) or hypoxia-treated SW480 cells (*Panel b*), following the addition of: cells (4 x 10^6), rotenone (Rot., 5 µM) either alone (top traces) or plus antimycin A (Ant. A, 5 µM, bottom traces), and subsequent injection of a sulfide solution (3-5 mM) at increasing rates (10 nL·s^{-1}, 20 nL·s^{-1}, 40 nL·s^{-1}, 80 nL·s^{-1} and 160 nL·s^{-1}, corresponding respectively to injections #1 to #5). *Panels c* and *d*, OCR values obtained from the oxygraphic traces (blue) respectively shown in *Panels a* and *b*, measured at basal condition and upon sulfide injection at

increasing rates after addition of rotenone alone (full symbols) or rotenone plus antimycin A (hollow symbols).

Mitochondrial H_2S consumption in normoxic cells was calculated by determining the OCR measured at the highest non-inhibitory H_2S injection rate (highlighted with grey bar in *Panel c*) and subtracting the OCR measured after the addition of rotenone (dashed line in *Panel c*), yielding $\Delta OCR_{(-Ant)}$. Then, the ΔOCR at the corresponding sulfide injection in the antimycin A-containing measurement was calculated in the same manner, yielding $\Delta OCR_{(+Ant)}$. By calculating $\Delta OCR_{(-Ant)}$ - $\Delta OCR_{(+Ant)}$, the genuine mitochondrial H_2S-dependent OCR (OCR_{mitH2S}) was determined. Finally, OCR_{mitH2S} was multiplied by 1.33 to account for the number of H_2S molecules consumed per O_2 molecule, yielding an estimated sulfide oxidizing activity of 12.7 nM $H_2S \cdot s^{-1} \cdot 10^6$ $cells^{-1}$. Employing the same procedure for cells exposed to hypoxia (*Panels b* and *d*), an activity of 9.5 nM $H_2S \cdot s^{-1} \cdot 10^6$ $cells^{-1}$ was estimated.

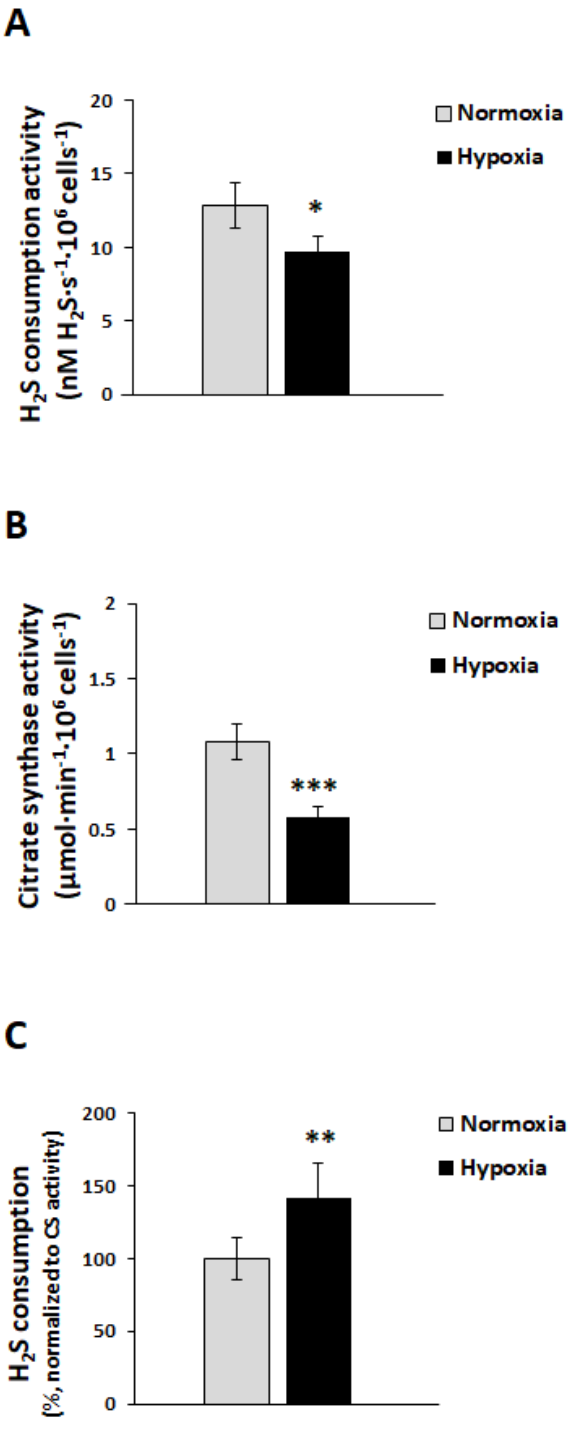
A
H2S consumption activity
(nM H2S·s-1·10^6 cells-1)
20
15
10
5
0
*
Normoxia
Hypoxia
B
Citrate synthase activity
(µmol·min-1·10^6 cells-1)
2
1.5
1
0.5
0
***
Normoxia
Hypoxia
C
H2S consumption
(%, normalized to CS activity)
200
150
100
50
0
**
Normoxia
Hypoxia

Figure 2. Effect of hypoxia on mitochondrial sulfide consumption. *Panel a*: mean values of maximal estimated sulfide consumption activity (calculated as described in the legend to Figure 1c), measured in normoxic (n = 9, grey bar) and hypoxia-treated (n = 8, black bar) cells. *Panel b*: citrate synthase activity in normoxic (n = 13, grey bar) and hypoxia-treated (n = 10, black bar) cell lysates. *Panel c*: maximal sulfide consumption activity normalized to the citrate synthase activity, as measured in normoxic (grey bar) and hypoxia-treated (black bar) cells. *P ≤ 0.05, ***P ≤ 0.001.

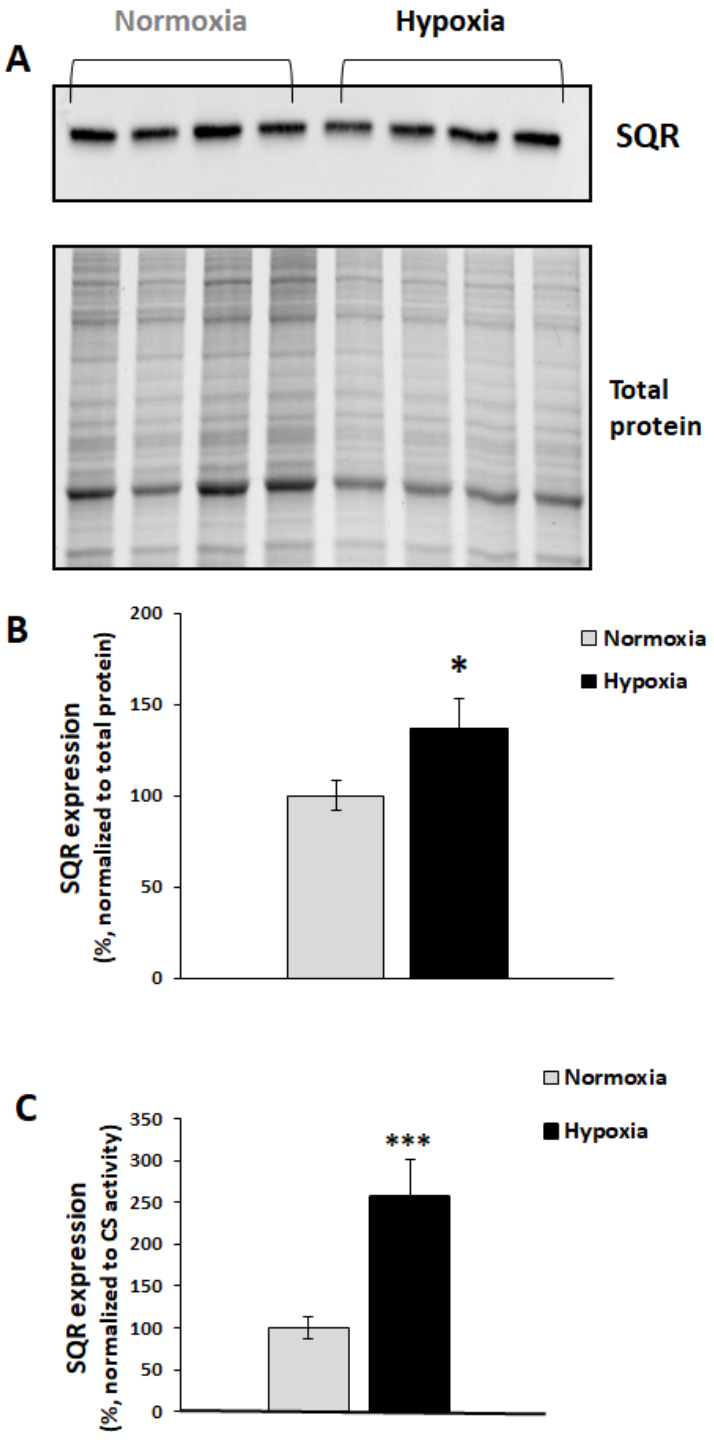
A
Normoxia
Hypoxia
SQR
Total protein
B
SQR expression (%, normalized to total protein)
200
150
100
50
0
*
Normoxia
Hypoxia
C
SQR expression (%, normalized to CS activity)
350
300
250
200
150
100
50
0
***
Normoxia
Hypoxia

Figure 3. Effect of hypoxia on SQR expression. Representative Western blot analyzing SQR expression in normoxic and hypoxia-exposed SW480 cells (*Panel a*), with the corresponding total protein load quantitation by stain-free imaging technology (see Materials and Methods). SQR levels in normoxic (n = 4 in triplicate, grey bars) and hypoxia-treated cells (n = 4 in triplicate, black bars), as normalized to total protein (*Panel b*) or citrate synthase activity (*Panel c*). *P ≤ 0.05, ***P ≤ 0.001.

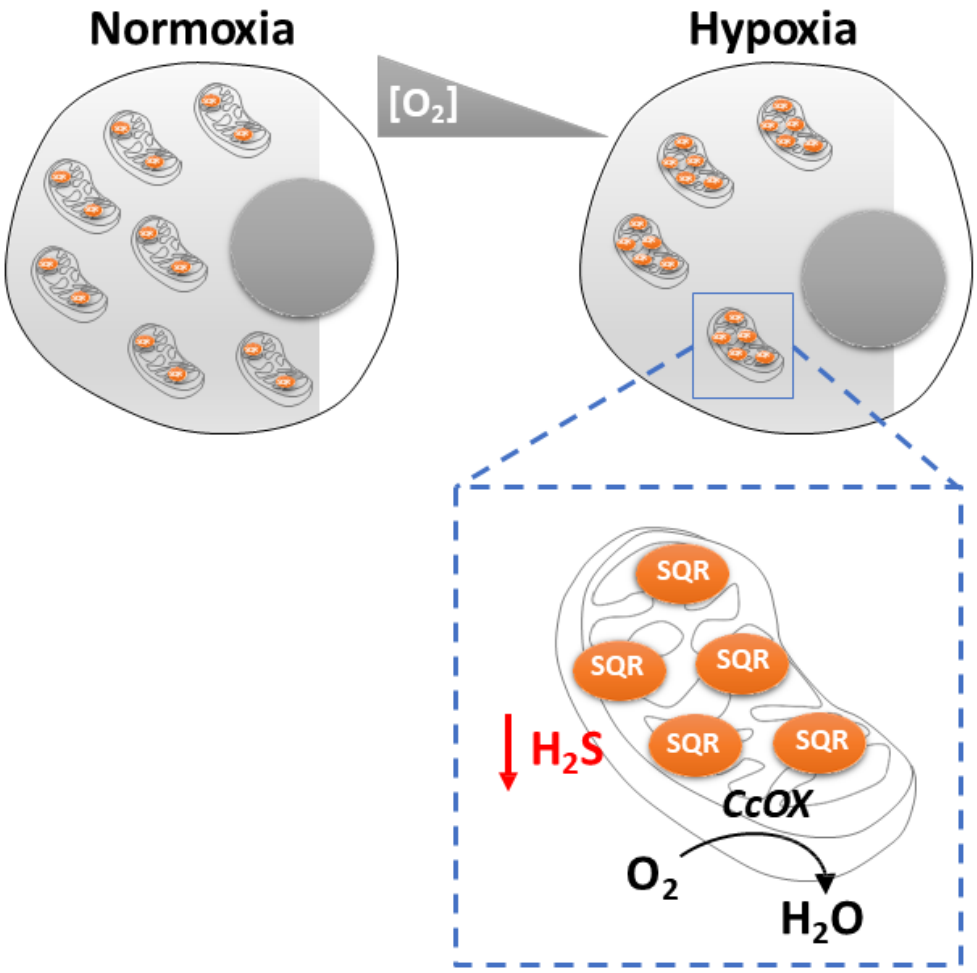

Figure 4. Adaptive changes occurring in mitochondria in response to hypoxia. Upon prolonged exposure to hypoxia, mitochondria become less abundant, but enriched in sulfide:quinone oxidoreductase (SQR). Consistently, their maximal sulfide-oxidizing activity increases, while overall decreasing in the cell. These changes are proposed to occur to prevent H_2S inhibition of cytochrome *c* oxidase (CcOX) and thus protect cell respiration from H_2S poisoning.

RESULTS AND DISCUSSION
PAPER 3

Hydrogen sulfide metabolism and signaling in the tumor microenvironment

Alessandro Giuffrè*[1], Catarina S. Tomé[2], Dalila G. F. Fernandes[2], Karim Zuhra[1,3], and João B. Vicente*[2]

1 - CNR Institute of Molecular Biology and Pathology, Rome, Italy

alessandro.giuffre@uniroma1.it

2 - Instituto de Tecnologia Química e Biológica António Xavier, NOVA University of Lisbon, Av. da República (EAN), 2780-157 Oeiras, Portugal

3 - Department of Biochemical Sciences, Sapienza University of Rome, Rome, Italy

* correspondence: alessandro.giuffre@uniroma1.it; jvicente@itqb.unl.pt

Advances in Experimental Medicine and Biology, in press

ABSTRACT

Hydrogen sulfide (H_2S), while historically perceived merely as a toxicant, has progressively emerged as a key regulator of numerous processes in mammalian physiology, exerting its signaling function essentially through interaction with and/or modification of proteins, targeting mainly cysteine residues and metal centers. As a gaseous signaling molecule that freely diffuses across aqueous and hydrophobic biological milieu, it has been designated the third 'gasotransmitter' in mammalian physiology. H_2S is synthesized and detoxified by specialized endogenous enzymes that operate under a tight regulation, ensuring homeostatic levels of this otherwise toxic molecule. Indeed, imbalances in H_2S levels associated with dysfunctional H_2S metabolism have been growingly correlated various human pathologies, from cardiovascular and neurodegenerative diseases to cancer. Several cancer cell lines and specimens have been shown to naturally overexpress one or more of the H_2S-synthesizing enzymes. The resulting increased H_2S levels have been proposed to promote cancer development through the regulation of various cancer-related processes, which led to the interest of pharmacologically targeting H_2S metabolism. Herein are summarized some of the key observations that place H_2S metabolism and signaling pathways at the forefront of the cellular mechanisms that support the establishment and development of a tumor within its complex and challenging microenvironment. Special emphasis is given to the mechanisms whereby H_2S helps shaping cancer cell bioenergetic metabolism and affords resistance and adaptive mechanisms to hypoxia.

1. Hydrogen sulfide and cancer

Nothing says more about the excitement and interest of a research field than the lack of a profound knowledge despite a massive accumulation of data in the literature. The link between hydrogen sulfide metabolism in human physiology and cancer is certainly characterized by inferred proposals based essentially on scattered yet sometimes converging phenomenological data. Yet, different trends can be observed and summarized. Indeed, several excellent reviews have been already published on the topic [41, 54, 75]. Herein, we attempted to provide an overview of the role that hydrogen sulfide metabolism and signaling pathways may play in shaping the tumor microenvironment in its numerous defining aspects. Besides summarizing the phenomenological data linking H_2S metabolism with cancer and highlighting key elements of H_2S metabolism and signaling pathways, emphasis is given on the role of the latter in relation to two major aspects of the tumor microenvironment: cellular bioenergetics (Section 4) and hypoxia (Section 5).

Hydrogen sulfide (H_2S) was historically merely considered a toxic gas until its recognition in the early 21st century as an endogenously generated relevant signaling molecule in mammalian physiology regulating numerous processes within the cardiovascular, respiratory, digestive and central nervous systems (reviewed e.g. in [16]). Its particular physicochemical properties allow H_2S to freely diffuse across biological milieu and exert its regulatory and signaling functions mostly through modification of target proteins (detailed below). The reactivity and potential toxicity of H_2S demand a fine balance between its biosynthesis and breakdown, the respective metabolic pathways functioning under

a tight regulation. The balance between deleterious and beneficial effects of H_2S obeys to a conceptual bell-shaped model where homeostatic H_2S levels operate in a narrow range of optimal concentrations, whereas too low or too high H_2S may lead to dysfunction and toxicity at a cellular and/or systemic level. Besides H_2S, the related reactive sulfur species (RSS [60]) persulfides (RSSH) and polysulfides ($RS_{(n)}SH$), partly generated by H_2S metabolism enzymes, have been growingly demonstrated to have equally relevant roles in signaling that extend to the etiology of pathological conditions [6, 21, 60, 213].

Multiple cause-effect links have been growingly established between altered hydrogen sulfide metabolism and/or signaling and human disease, particularly cancer. Pivotal studies on ovarian and colorectal cancer have reported a clear overexpression of H_2S-synthesizing cystathionine β-synthase (CBS) in cancer cell lines and tumor samples with respect to non-tumorigenic cells or normal tumor-adjacent tissue [77, 78]. Soon followed a similar association between cancer and increased expression of any or all the enzymatic H_2S sources: CBS, cystathionine γ-lyase (CSE) and 3-mercaptopyruvate sulfurtransferase (MST). To date, increased expression of either or all H_2S-synthesiszing enzymes has been demonstrated for colorectal, ovarian, breast, prostate, gastric cancer, as well as lung adenocarcinoma, melanoma, hepatocellular carcinoma, urothelial cell carcinoma of bladder, astrocytoma, neuroblastoma, and glioma (reviewed e.g. in [41, 75]). In line with the increased H_2S production resulting from induction of H_2S-synthesizing enzymes in cancer cells, Libiad and co-workers have recently reported a higher expression and differences in the cellular localization of enzymes involved in H_2S catabolism [214].

Thus far, the full extent of the implications of altered H_2S metabolism to cancer progression is still a matter of significant dedicated research efforts. While many observations derived from cell biology studies on tumor samples and cellular and animal models bring together common threads concerning the effect of altered H_2S metabolism on cancer, strong molecular studies are lagging behind.

Moreover, as pointed out by Cao and co-workers, several studies employ non-physiological concentrations of H_2S donors, unspecific inhibitors that may affect other enzymes than those synthesizing H_2S and cause changes in other metabolites other than H_2S derived from or consumed by the H_2S metabolism pathways [41]. Nevertheless, mounting evidence posits key roles of H_2S and related RSS in the modulation of several recognized characteristics of cancer, such as dysregulation of cell growth and signaling pathways towards uncontrolled proliferation, evasion of apoptosis, stimulation of angiogenesis, subversion of cell energy limitations, genome instability, and tumor enhanced inflammation. In line with the scope of this book, it becomes logic that H_2S metabolic and signaling pathways help shaping the adaptive changes within the tumor microenvironment that favor its progression (Figure 1). Indeed, increased H_2S production by cancer cells naturally overexpressing H_2S-synthesizing enzymes has been shown to stimulate cellular bioenergetics at the levels of mitochondrial respiration, ATP production and glycolysis (detailed in Section 4) (e.g.[5, 48]). The role of H_2S in promoting neoangiogenesis allows replenishing the tumor microenvironment with the nutrients and oxygen that become scarce with the dysregulated proliferation and growth. Both CBS and CSE have been implicated in controlling angiogenesis in colorectal, ovarian and breast cancer, likely involving the H_2S-mediated

persulfidation of ATP-sensitive potassium K_{ATP} channels [96, 215], as well as the phosphoinositide-3-kinase/protein kinase B (PI3K/Akt) and the mitogen activated protein kinase (MAPK) signaling pathways [95, 216, 217]. The link between the mutual regulation of H_2S metabolism and hypoxia, and angiogenesis in the context of the tumor microenvironment is detailed in Section 5.

The evasion of apoptosis and cell cycle acceleration have also been linked to the H_2S-mediated persulfidation of key players in the corresponding signaling cascades, typically activating the respective protein targets. The role of H_2S metabolism in evading apoptosis has been demonstrated for gastric and colorectal cancer, hepatoma and neuroblastoma [85-88], chiefly involving the CSE-H_2S axis in the persulfidation and consequent modulation of protein targets of key pathways (associated also with inflammation) such as: the Keap1-transcription factor nuclear factor erythroid 2-related factor (Nrf2) [113], the nuclear factor kappa-light-chain-enhancer of activated B cells (NF-κB) [88], and the extracellular-regulated kinase (ERK) activator kinase 1 (MEK1)-ERK. CBS has been proposed to take part in ferroptosis resistance mechanisms, possibly contributing to evasion of this alternative non-apoptotic cell death mechanism [218].

The genome instability of cancer cells triggers the activation of several mechanisms, including DNA repair pathways, possibly by activation of e.g. the MEK1-ERK-Poly [ADP-ribose] polymerase 1 (PARP-1) pathway, whose activity was found to be diminished in the liver and kidney of a CSE knock-out mouse model [217]. Szczesny and co-workers have also demonstrated that MST silencing in A549 lung adenocarcinoma cells attenuates the mitochondrial DNA repair rate upon damage [219].

Another key element for the tumor proliferation concerns the acquisition of resistance to common chemotherapeutic agents. H_2S-synthesizing enzymes have been implicated in the development of chemoresistance phenotypes in colorectal, ovarian and liver cancer cell lines [78, 84, 220]. Moreover, the proposal of cysteine-dependent chemoresistance mechanisms in ovarian cancer is based on an enhanced cysteine flux in chemoresistant cancer cells that relies on increased cystine import and enhanced intracellular cysteine catabolism likely via H_2S-synthesizing enzymes [221].

Whereas numerous reports point to a pro-cancer effect of increased expression and activity of H_2S-synthesizing enzymes, it should be noted that exogenous addition of H_2S either with sulfide salts or slow releasers may have anti-cancer effects, depending on the dose and exposure time [222, 223]. This is not surprising taking into account the proposed bell-shape model that dictates how H_2S, depending on its levels, acts as a signaling molecule or a toxin in human physiology. Indeed, this model simply appears to be shifted in several cancer cell models and patient samples to hint for a higher H_2S metabolic flux in cancer that overall contributes to shape the tumor microenvironment and promote tumor growth and proliferation. This dual nature of H_2S in cancer, nevertheless, offers different options for pharmaceutical therapeutic interventions, either through the development of inhibitors for H_2S-synthesising enzymes [75, 125, 219, 224], or through the development of H_2S-releasing drugs [222, 223, 225], including naturally derived compounds such as components from garlic extracts [226, 227].

2. Human H_2S metabolism

The dual role of H_2S in physiology implies a fine tune of sulfide metabolism to maintain its homeostatic levels. In mammals, besides the contribution of gut microbiota metabolism and dietary per-/polysulfides breakdown, a group of enzymes specialized in the synthesis and catabolism of H_2S regulates the sulfide pool (Figure 2).

2.1. H_2S synthesis

Endogenous H_2S is produced mainly by three enzymes: cystathionine β-synthase (CBS), cystathionine γ-lyase (CSE) and 3-mercatopyruvate sulfurtransferase (MST). The tissue distribution of the three enzymes (and thus their contribution to H_2S production) differs: CBS is mainly found in liver, pancreas, kidney and nervous system; CSE is mainly found in liver, kidney and smooth muscle; MST has a broader distribution, being present in most tissues [42]. While the main cellular localization is considered cytosolic for CBS and CSE and mitochondrial for MST, pathophysiological stimuli can dictate translocation of these enzymes into different cell compartments or even the extracellular milieu. While MST can additionally be detected in the cytosol [228], CBS and CSE can be found extracellularly or in the mitochondria upon, for instance, oxidative damage [31, 38].

MST participates in the cysteine catabolism pathway, producing H_2S as a product of its reaction with 3-mercaptopyruvate (3MP). It is a monomeric protein (297 amino acids; 33 kDa) composed of two structurally nearly identical domains

between which lies the 3MP binding site and a catalytic cysteine residue (Cys_{248}) [39]. Upon reaction with 3MP, Cys_{248} (Cys-SH) becomes persulfidated (Cys-SSH) and prone to react with reductant molecules (such as glutathione, L-homocysteine or thioredoxin) that release H_2S upon accepting the sulfane sulfur atom.

CBS and CSE are both PLP-dependent homotetrameric proteins. CBS monomers (551 amino acids; 61 kDa) consist of three domains: an N-terminal heme-binding domain, a central pyridoxal 5'-phosphate (PLP)-binding domain, and a C-terminal S-adenosyl-L-methionine (AdoMet)-binding domain [23]. CSE monomers (405 amino acids; 44 kDa) consist of an N-terminal PLP-binding domain and a C-terminal domain [22]. The canonical reactions catalyzed by CBS and CSE constitute the transsulfuration pathway (Figure 2): CBS catalyzes the condensation of L-homocysteine and L-serine to yield cystathionine; CSE then converts cystathionine into L-cysteine, α-ketobutyrate and ammonia. Production of H_2S by CBS and CSE results from alternative reactions that use L-cysteine and/or L-homocysteine as substrates. Similarly to its canonical reaction, CBS can catalyze the condensation of L-homocysteine and L-cysteine to yield cystathionine, releasing H_2S instead of H_2O. Also in the presence of L-cysteine, CBS and CSE produce H_2S *via* β-replacement/β-elimination or α,β-elimination, respectively. CSE catalyzes the same alternative reactions as CBS, and can additionally use L-homocysteine in β-replacement/β-elimination reactions that yield H_2S. The extent of H_2S generation by CBS and CSE thus depends on the equilibrium between canonical *versus* alternative reactions, which in turn is affected by tissue expression levels, substrate availability and regulation at protein level. Indeed, CBS activity can be modulated by post-translational modifications and allosteric

regulators. Glutathionylation at Cys_{346} increases CBS activity and is thought to serve as a redox sensor to boost the transsulfuration pathway under oxidative conditions towards formation of cysteine and, ultimately, glutathione [28]. A CXXC motif in the catalytic domain of CBS ($C_{272}PGC_{275}$) is also thought to act as a redox sensor, modulating enzyme activity upon reduction of the two cysteine thiols or their oxidation to a disulfide [29]. The two flanking domains of CBS also have a regulatory function. The C-terminal domain adopts an autoinhibitory conformation in the resting enzyme, blocking the entrance of the catalytic site [229]. Binding of the allosteric activator AdoMet to each C-terminal domain of adjacent monomers triggers their dimerization, facilitating the access of substrates to the active site and activating the protein [229, 230]. The N-terminal domain binds a heme moiety that mediates CBS regulation through changes in its redox and ligand state. Reduction of the heme promotes enzyme inactivation. This ferrous form is also able to bind NO and CO that displace its endogenous ligands (Cys_{52} and His_{65}), inhibiting CBS [24-27]. The forty N-terminal residues in CBS constitute an intrinsically disordered peptide suggested to represent a second heme binding site (*via* Cys_{15} and His_{22}), although its physiological relevance is not clear [231]. Interestingly, despite the distance between both regulatory domains (>30 Å), an intercommunication between heme- and AdoMet-modulation is observed, with AdoMet binding enhancing CO- and NO-mediated inhibition [26]. The sequential reactions of CBS and CSE in the transsulfuration pathway and the fact that they share the same substrates in H_2S-generating reactions implies that regulation of one enzyme will affect the other through substrate/product accumulation/depletion, which will favor one biochemical pathway over the other.

Besides, it has been shown that inhibition of CBS may result in overall higher H_2S production through CSE which presents a higher catalytic efficiency using the same H_2S-originating substrates [232].

2.2. H_2S catabolism

In mammals, the sulfide-oxidizing pathway – comprising four mitochondrial enzymes – is responsible for H_2S catabolism. The first irreversible and limiting step in H_2S degradation is catalyzed by sulfide:quinone oxidoreductase (SQR). SQR oxidizes H_2S, transferring the sulfur atom to an acceptor molecule (such as glutathione) that becomes persulfidated, and using coenzyme Q (CoQ) as an electron acceptor. SQR is an integral membrane flavoprotein (450 amino acids; 50 kDa), located at the inner mitochondrial membrane. The active site is accessible through the matrix-facing surface, where H_2S reacts with a catalytic disulfide (Cys_{201}/Cys_{379}) and the extracted electrons are transferred via a flavin adenine dinucleotide (FAD) cofactor to a CoQ molecule bound to hydrophobic pocket accessible from the membrane-facing surface [52]. In the second step of H_2S catabolism, the glutathione persulfide released by SQR is taken up by persulfide dioxygenase (ETHE1) that catalyzes the oxygenation of the sulfane sulfur and yields sulfite using a non-heme iron cofactor. In the only crystal structure of human ETHE1, a cysteinyl sulfinic acid (C_{247}-SO_2H) is present 15Å away from the active site, although the catalytic relevance of this observation is still unknown [233]. SQR-derived persulfidated glutathione and ETHE1-derived sulfite can be further converted to thiosulfate by thiosulfate

sulfurtransferase (Rhod). In the last step of H_2S catabolism, sulfite oxidase (SOx) converts sulfite to sulfate, using molybdenum and heme-iron as cofactors, a water molecule as oxygen donor and cytochrome c as electron acceptor [51]. The coupling of the mitochondrial H_2S oxidation pathway with the respiratory chain through SQR-mediated reduction of CoQ at low sulfide concentrations, and the H_2S-mediated inhibition of complex IV at high sulfide concentrations suggests implications on cellular bioenergetics upon different pathophysiological conditions (detailed in Section 4).

3. H_2S-mediated signaling

As mentioned above, H_2S exerts its numerous signaling and regulatory functions mainly by interacting with and/or directly modifying target proteins by two distinct mechanisms: (i) interaction with metal centers, mostly heme moieties, and (ii) protein persulfidation.

3.1. H_2S and heme proteins

As a small signaling molecule, H_2S can interact with heme proteins. These reactions are, however, very complex and determined by many factors, such as the H_2S concentration, the redox and ligation state of the heme iron, the environment of the heme pocket, the protonation state of the bound sulfide and the presence/absence of O_2 or reducing agents in solution, as reviewed e.g. in [5, 14].

H_2S can bind to heme-Fe(III) as such or as HS^- (deprotonated state of H_2S), generating heme-Fe(III)-H_2S or heme-Fe(III)-HS^-, respectively. The stability of each adduct depends on the protein residues in the heme surroundings: nonpolar

residues can stabilize heme-Fe(III)-H_2S by limiting the deprotonation of the ligand; in contrast, basic residues can mediate the deprotonation of the H_2S, yielding heme-Fe(III)-HS^-. Moreover, bound sulfide can reduce heme-Fe(III), which can result in the heme-Fe(II)-$HS\cdot$ radical adduct. The reduced heme-Fe(II)-$HS\cdot$ species can further react with excess $HS^-/HS\cdot$ or O_2/H_2O to originate, polysulfides or thiosulfate, respectively.

Alternatively, H_2S can react with a heme-Fe(II)-O_2 complex likely *via* a heme-Fe(IV)=O ferryl intermediate, yielding a sulfheme derivative, with the sulfur atom being incorporated into one of the pyrrole rings of the porphyrin. The reaction is favored in the presence of H_2O_2, thus implicating the formation of higher valent heme iron intermediates [14, 234, 235]. Although the mechanistic details of sulfheme formation are still to be fully clarified, these reactions have been described for different heme proteins such as globins (particularly hemoglobin and myoglobin), heme-based sensors, peroxidases and catalase (reviewed e.g. in [235]). Formation of the sulfheme derivative of hemoglobin (Hb), designated by sulfhemoglobin, results from the insertion of a sulfur atom into the heme B pyrrole. This derivative is irreversible and has lower O_2 affinity, thus being considered to contribute to sulfide-derived toxicity [235]. Alternatively, the accumulation of ferric hemoglobin (metHb) in the blood, designated as methemoglobinemia, has been suggested to protect against sulfide toxicity in mice, by promoting sulfide disposal [236]. Furthermore, Hb can also be a source of physiologically relevant sulfane sulfur products resulting from sulfide oxidation, namely thiosulfate and glutathione persulfide [237].

The historical hallmark of H_2S interacting with heme proteins concerns the inhibition of mitochondrial cytochrome *c* oxidase (CcOX). Indeed, CcOX is considered the main target of the three gasotransmitters (H_2S, NO, and CO), being inhibited through different mechanisms and with different kinetics [24, 238]. CO only binds to fully-reduced heme a_3-Cu_B active site, whereas NO-mediated inhibition can proceed *via* binding to the single-electron reduced active site [239] through two reaction pathways, depending on the oxygen tension and electron flux [240, 241]. The mechanism whereby H_2S inhibits CcOX does not involve binding to ferrous heme a_3. Rather, it is hypothesized that CcOX in turnover with O_2 is primarily targeted by H_2S at the oxidized and reduced Cu_B, followed by intramolecular sulfide transferred to ferric a_3 [24, 62]. Irrespectively of the mechanism, H_2S mediated CcOX inhibition is fast, potent and reversible.

3.2. Persulfidation of protein cysteine residues

As put forward in Section 1, many of the signaling effects commonly attributed to H_2S have been growingly assigned to per- and polysulfides. Formation of protein-bound persulfides occurs through the modification of cysteine side chains of target proteins, often upon reaction with free reactive low-molecular weight (LMW) persulfides (RSSH), such as glutathione persulfide (GSSH) and cysteine persulfide (CysSSH) (Figure 3) [242-244]. Such sulfane sulfur containing metabolites are actually generated both by H_2S biosynthetic and catabolic enzymes, namely through: production of CysSSH (or homocysteine persulfide, HcySSH) by CBS and CSE using cystine (or homocystine) and by MST using cysteine (or homocysteine) as sulfur-accepting co-substrate, and

production of GSSH by SQR or by MST [245]. The CBS- and CSE-catalyzed CysSSH-producing reactions result also in longer polythiolated products that can react with glutathione to yield GSSH [246]. Other possibilities to generate protein-bound cysteine persulfides include the reaction of oxidized cysteine residues directly with H_2S, or the reaction of protein-bound cysteine thiols with sulfhydryl radical (generated by reaction of H_2S with metal centers) and subsequently with O_2. Protein persulfidation requires the appropriate environment surrounding the target cysteine, a favorable cellular redox status and free glutathione/cysteine/H_2S availability [5]. A recent report [58] posits that mammalian cysteinyl-tRNA synthetases (CARSs), in particular the mitochondrial isoform CARS2, are the main source of free and protein-bound CysSSH (and $CysSS_{(n)}H$), the latter resulting from co-translational insertion of previously per- or polysulfidated cysteine (Figure 3). It is also suggested that CySSH is formed in the mitochondria, prior to being released into the cytosol to exert its effects. Whereas CARS2 is possibly the major CysSSH source under physiological conditions, CBS and CSE still play a major role in CysSSH synthesis in pathophysiological conditions. In the latter case, cystine levels are increased in line with oxidative and electrophilic stress, such as in cancer, where the glutamate/cystine xCT antiporter is often up-regulated [21, 58]. Besides its signaling and regulatory function, persulfidation also protects thiol-containing residues against irreversible chemical modification by oxidants and electrophiles [242]. For cellular signaling, a key advantage of a post-translational modification such as persulfidation is that this modification is reversed by reaction of the resulting derivatives with reducing agents (*e.g.* glutathione), proteins (*e.g.* thioredoxin or glutaredoxin) or via re-formation of a

disulfide bond initiated by nucleophilic attack [60]. Deficiency in persulfidated proteins has been associated with various pathologies, like cancer and cardiovascular disease [5, 129]. Moreover, it has been proposed that free LMW persulfides have a higher affinity than their thiol counterparts to form *s*-conjugates with exogenous toxins [6, 247]. The fact that cancer cells have higher expression of H_2S-synthesizing enzymes and likely overproduce LMW persulfides owing to the oxidative environment could endow cancer cells with chemoresistance mechanisms to cope with the toxicity of oxidative alkylating drugs.

4. Effect of H_2S on cellular bioenergetics

Cellular bioenergetics is a trademark of the dual role of H_2S in human physiology. Indeed, H_2S has a bell-shaped effect on bioenergetics, contributing to ATP synthesis at lower concentrations while being cytotoxic and potentially lethal at higher levels (Figure 4). The detailed molecular mechanisms behind its toxicity are not yet fully understood, but it is well recognized that it reversibly binds the heme moiety of CcOX, resulting in mitochondrial respiration impairment [24]. Although CcOX inhibition occurs with a relatively low K_i value (K_i = 0.2 μM at pH 7.4), as reported working on isolated enzyme [67], inhibition of the electron transport chain using isolated mitochondria or cultured cells is usually observed at much higher concentrations (up to tens of micromolar) [248]. Consistently, mammalian cells are equipped with the sulfide oxidizing pathway, able to couple energy production with sulfide detoxification [46]. As mentioned in Section 2, the rate-limiting reaction of this pathway is catalyzed by sulfide:quinone

oxidoreductase (SQR), which transfers a sulfur atom to an acceptor such as GSH and concomitantly the sulfide-derived electrons to coenzyme Q (CoQ). H_2S oxidation by SQR thus supplies electron equivalents to the mitochondrial electron transport chain and consequently stimulates ATP production via oxidative phosphorylation [51]. From a methodological point of view, the sulfide oxidizing activity of living cells or isolated mitochondria can be studied by following O_2 consumption at increasing concentration of H_2S administered as e.g. sodium sulfide (Na_2S). Because of its cytotoxicity at high concentrations, sulfide is usually supplied with a continuous infusion at a selected rate rather than a single bolus. Sulfide-dependent oxidation consumption can be arrested by inhibiting complex III with antimycin or complex IV with cyanide, as sulfide-derived electrons enter to the electron chain transport at CoQ level [48, 249]. Notably, the oxidizing activity varies among different cell types, ranging from undetectable in nervous system cells to high in colon cells. Indeed, colonocytes are physiologically exposed to high sulfide concentrations (in the range of millimolar) produced by the gut microbiota. Therefore, it is not surprising that the sulfide oxidizing pathway enzymes are significantly expressed and precisely localized in colonic tissue [214] and that the corresponding sulfide disposal activity is possibly the maximal in the organism [250]. Overall, this process couples the oxidation of H_2S with ATP production, consuming ~ 0.75 O_2 molecules (0.25 by CcOX and 0.5 by ETHE1) per molecule of H_2S [46]. In terms of energy yield, this process displays a relatively low efficiency, particularly because of the supplemental consumption of O_2 by ETHE1. On the other hand, considering that H_2S is highly diffusible through biological membranes and its bioavailability is tightly controlled by the

interplay between H_2S-synthesizing and the H_2S-consuming enzymes, it has been suggested that this molecule may act mainly as an 'emergency' substrate of the electron transport chain when O_2 supply is insufficient to fulfil the energy demand [24, 48]. Enhanced sulfide metabolism has been extensively associated to cancer survival by stimulation of energy supply [54]. For instance, both the cytosolic enzymes CBS and CSE were reported to accumulate in mitochondria when cells are exposed to hypoxic conditions, a common factor within the tumor microenvironment. The resulting increase in mitochondrial sulfide availability was suggested to support ATP production and provide protection against oxidative stress [31, 251]. Isolated mitochondria from HCT 116 colorectal cancer cells treated with cysteine displayed an enhanced electron transport, which was suppressed by shRNA mediated CBS silencing or its pharmacological inhibition with aminooxyacetic acid (AOAA). This observation suggested that CBS, but not CSE, significantly contributes to cancer cell respiration [77]. Consistently, in ovarian cancer cells CBS inhibition resulted in mitochondrial impairment with concomitant overproduction of reactive oxygen species (ROS) [78]. Probably, among the three H_2S-synthetizing enzymes, the most relevant for mitochondrial bioenergetics at physiological conditions is MST [252, 253]. Currently, two MST isoforms are known, with comparable enzymatic activity, MST-Iso1 localized in the cytosol and MST-Iso2, which exists both in the cytosol and in mitochondria [228]. The interest for this enzyme arose from its privileged localization, from where the produced H_2S is readily available as a substrate for the electron transport chain via SQR. Indeed, it has been shown in isolated liver mitochondria and cultured murine hepatoma cells that mitochondrial bioenergetics is stimulated

upon treatment with low concentration of the MST substrate 3MP. Basal cellular bioenergetics was reduced upon silencing of either MST or SQR, supporting the hypothesis that mitochondrial respiration is in part sustained by the 3MP-derived sulfide and its oxidation catalyzed by SQR [254]. Beyond its ability to act as a metabolic fuel, H_2S-mediated protein persulfidation has been shown to be involved, at different levels, in the regulation of cellular bioenergetics. Indeed, it was discovered that the mitochondrial inner membrane protein ATP synthase (complex V) is physiologically regulated by persulfidation and this post-translational modification may maintain this enzyme in its activated state [64] (Figure 4). This notwithstanding, it is worth mentioning that tumors undergo a well-known energy metabolism reprogramming (Warburg effect), promoting glycolysis instead of the more efficient oxidative phosphorylation pathway, even under aerobic conditions [68, 69]. Indeed, cancer cells seem to express the isoform A of lactate dehydrogenase (LDH-A), that catalyzes the conversion of pyruvate to lactate, more than they express LDH-B, that catalyzes the opposite reaction, thus resulting in a lower ratio NAD^+/NADH [255]. Recently, it was observed that colon cancer cells treated with a sulfide releaser display increased lactate levels and, consistently, higher LDH-A catalytic activity, which was shown to be positively modulated via persulfidation. Accordingly, H_2S-mediated stimulation of glycolysis, and also of oxidative phosphorylation, seems to be LDH-A-dependent, thus making H_2S a pivotal regulator of cancer bioenergetics [220] (Figure 4). Modulation of glycolysis through persulfidation of glyceraldehyde-3-phosphate dehydrogenase (GAPDH) mediated by H_2S or related sulfane sulfur species has been proposed, although opposite effects regarding enzyme activation/inactivation

have been reported [65, 66] (Figure 4). H_2S has been shown to stimulate mitochondrial ATP production in human endothelial cells (ECs), resulting in enhanced proliferation and migration. Conversely, MST pharmacological inhibition or its silencing suppresses microvessel growth [252]. Interestingly, ECs stimulation induced by treatment with vascular endothelial growth factor (VEGF) is abrogated in the presence of inhibitors of CSE or K_{ATP}, suggesting that this process is at least in part mediated by K_{ATP} channels opening by persulfidation as introduced in Section 1 [95]. The pro-angiogenic action of H_2S thus indirectly promotes solid tumor bioenergetics by increasing nutrients supply, including glucose and O_2. In summary, H_2S seems to be a polyhedral actor being involved at different levels on cellular bioenergetics, stimulating mitochondrial ATP production, glycolysis and angiogenesis. On the other hand, in line with its Janus-faced character, at higher concentration it impairs the electron transport chain resulting in mitochondrial respiration failure.

5. H_2S and hypoxia in the tumor microenvironment

The microenvironment of solid tumors is typically characterized by low O_2 tension. Hypoxia, while representing a challenge for cancer cells in some respects, in many others is beneficial, promoting cancer progression. O_2 deprivation has been recognized not only to promote cancer development and spreading by stimulating neoangiogenesis and metastasization, but also to increase resistance of cancer cells to treatments with chemotherapeutic agents or irradiation (see [178] for a review). Though based on a rather limited number of studies, there is growing

evidence that H_2S plays a role in cancer cells under hypoxic conditions, as reviewed below.

Hypoxia has drastic effects on gene expression and metabolism in cancer cells (reviewed in [256-258]) (Figure 5A). Hypoxia-inducible factor-1 (HIF-1) is a master regulator of gene expression in response to changes in O_2 levels. This transcription factor regulates the expression of numerous genes, many of which are involved in fundamental processes occurring in cancer cells [259]. Under normoxic conditions, HIF-1α is targeted by prolyl-hydroxylases and committed to degradation. These hydroxylases, however, are inhibited under hypoxic conditions which thereby promote accumulation of HIF-1α [260]. HIF-1α was found to be up-regulated by H_2S in *Caenorhabditis elegans* under normoxic conditions [261], but down-regulated by H_2S under hypoxia in several human cell lines [262]. The latter observation was confirmed and expanded in another study [263] where H_2S, exogenously administered as NaHS, proved to reduce HIF-1α protein levels in different human cell lines (HEK293T, Hep3B and EA.hy926) under both hypoxia and hypoxia-mimetic conditions in a dose- and time-dependent manner (Figure 5A). The same authors investigated the molecular mechanism of HIF-1α down-regulation by H_2S and found that H_2S does not work at the transcriptional level, as shown by real-time PCR analysis, or stimulating the ubiquitin-proteasomal degradation pathway, but rather inhibits the translation of HIF-1α by promoting phosphorylation of the eukaryotic translation initiation factor 2α (eIF2α). eIF2α is a component of the eIF-2 complex that is required to start protein synthesis. When eIF2α is phosphorylated at Ser51, formation of the eIF-2 complex is impaired and HIF-1α translation inhibited [260] (Figure 5A). To be noted that repression of HIF-

1α translation by H_2S via phosphorylated eIF2α was shown to take place under hypoxic but not hypoxia-mimetic conditions. To add further complexity, a mutual control between HIF-1α and H_2S seems to occur at low O_2 tension as HIF-1α was shown to stimulate CBS expression in hypoxia [264].

The hypoxic microenvironment is known to increase resistance of cancer cells not only to chemotherapeutic agents, but also to radiation-induced killing [265]. Working on human hepatoma HepG2 cells, both endogenously produced and exogenous H_2S was reported to play a role in enhancing cancer cell radioresistance in hypoxia [266]. Compared to control cells not treated with H_2S-donors or inhibitors of H_2S synthesis, irradiated hypoxic cells were found to display reduced damages in the presence of NaHS and elevated damages in the presence of the inhibitors of H_2S-synthesis AOAA and propargylglycine (PPG). The radioprotective effect of NaHS was shown to be concentration dependent up to 100 μM and suggested to involve activation of the K_{ATP} channels, as shown using the selective inhibitor glibenclamide.

Neoangiogenesis, the development of new blood vessels, is a well-known strategy through which tumoral cells support their proliferation. A drawback of such a strategy, however, is that blood flow through these newly formed vessels is less constant than in the normal vasculature. Due to blood flow intermittence, tumoral cells are exposed to alternating conditions of hypoxia and re-oxygenation which are known to boost the formation of ROS, eventually leading to oxidative damage. Under these conditions, H_2S is likely to play a protective role. H_2S is indeed known to protect cells against ischemia/reperfusion damages [193, 267] through a variety of mechanisms to date only partly understood. Apart from

exerting its well-known vasodilative and antioxidant effects, H_2S was reported to protect from hypoxia-induced proteostasis disruption, as shown working on *Caenorhabditis elegans* [203], and from mitochondrial DNA damages [219] which are known to occur in response to ischemia/reperfusion. A functional H_2S catabolism seems to be required to assure protection from hypoxia, as shown by knocking SQR down in Hepa1-6 cells [204]. Accordingly, some studies highlighted a protective role of thiosulfate, one of the products of H_2S catabolism, against ischemia/reperfusion damage [204, 268, 269]. Under hypoxic (but not under normoxic) conditions, H_2S either endogenously produced or exogenously administered as NaHS was also found to sustain energy metabolism in vascular smooth-muscle cells via stimulation of mitochondrial ATP production [38]. In this context, it is noteworthy that the H_2S-precursor cysteine was recently reported to favor in several ovarian cancer cell lines adaptation to hypoxic conditions and resistance to the widely used chemotherapeutic agent carboplatin [221]. In the same study, cysteine was found to be the prevalent thiol compound in the ascitic fluid from patients with advanced ovarian cancer, and higher levels of cysteine and homocysteine (another precursor of H_2S) were intriguingly found in the serum of patients with ovarian cancer compared to healthy individuals.

Based on the evidence presented above, under hypoxic conditions, cancer cells seem to benefit from endogenously produced or exogenous H_2S in many regards, and H_2S can be viewed as contributing to adaptation of cancer cells to their harsh microenvironment. However, the occurrence of H_2S under hypoxia does not always represent a benefit for cancer cells in that hypoxia, under some circumstances, can exaggerate some of the detrimental effects of H_2S. For

instance, in the ovarian cancer cell lines A2780, it was found that the H_2S released from the donor GYY4137 induces disruption of calcium homeostasis causing endoplasmic reticulum stress and, ultimately, apoptosis, the effect being more pronounced in hypoxic than in normoxic conditions [270].

For cancer cells, particularly under hypoxic conditions, it is imperative to finely control H_2S bioavailability so that H_2S exerts its protective effects without inducing cytotoxicity. Control of intracellular H_2S levels in hypoxia relies on multiple processes and is based on a rather intricate interplay between H_2S and O_2 which led to recognition of H_2S as an O_2 sensor [271]. As reviewed in [30], O_2 can affect H_2S bioavailability not only by directly reacting with H_2S, but also regulating the protein levels and cellular localization of the H_2S-synthesizing enzymes, the efficacy of H_2S breakdown through the mitochondrial sulfide-oxidizing pathway and even the availability of inhibitors of H_2S synthesis, such as carbon monoxide (CO). On the other hand, H_2S can regulate O_2 levels either enhancing or inhibiting mitochondrial O_2 consumption (see section 4). Hypoxia is therefore expected to have a strong influence on H_2S bioavailability. O_2 deprivation not only is expected to result into a higher chemical stability of H_2S, but it was also shown to stimulate H_2S synthesis by enhancing the expression of H_2S-synthesizing enzymes [251, 264], releasing inhibition of CBS and CSE by CO [272, 273] and accumulating CBS in mitochondria [31] (Figure 5B). The effect of hypoxia on mitochondrial H_2S breakdown was also investigated in a few studies. Working initially on immortalized cells derived from alveolar macrophages [211] and, then, on CHO cells [107], the mitochondrial sulfide-oxidizing activity was measured at different O_2 tensions and found to be lower at

lower O_2 concentration, as expected. A more recent investigation assessed the effects of chronic (24 hour) exposure to hypoxia (1% O_2) on the ability of cells to dispose sulfide at mitochondrial level, using SW480 colorectal cancer cells as a model [249]. In line with previous studies [108, 274, 275], hypoxia was found to reduce the mitochondrial mass and the overall ability of cells to dispose sulfide. However, considering their lower mitochondrial content, hypoxia-treated cells were found to contain mitochondria with higher maximal sulfide-detoxifying capacity and higher SQR levels, compared to untreated cells. The hypoxia-induced enrichment in SQR of mitochondria was suggested to have a protective role, preventing poisoning of mitochondria by enhanced production of sulfide under hypoxic conditions [249] (Figure 5B). All in all, in hypoxic cancer cells H_2S is expected to occur at higher levels, as a result of its higher chemical stability, enhanced synthesis and diminished breakdown through the mitochondrial pathway. The higher bioavailability of H_2S could be beneficial for cancer cells, as long as they undergo adaptive mechanisms preventing H_2S toxicity.

Summing up, hypoxia as a common feature of tumor microenvironment has a strong impact on the bioavailability of H_2S, which in turn appears to play a role in adaptation of cancer cells to hypoxic conditions, further pointing to the H_2S-producing and -consuming enzymes as possible drug targets. Experimental research in this field is still in its infancy and complicated by the fact that not only hypoxia and H_2S can cause different effects between normal and tumoral cells, and even between different kinds of tumoral cells [276], but sometimes different observations are made depending on the experimental design used to set-up hypoxic conditions. More efforts are therefore needed to shed light on the intricate

interplay between H_2S and hypoxia in the framework of cancer biology, a promising research field with a great potential in terms of development of innovative anti-cancer strategies.

ACKNOWLEDGMENTS

The Authors are grateful for funding from Ministero dell'Istruzione, dell'Università e della Ricerca of Italy (PNR-CNR Aging Program 2012–2014 and PRIN 20158EB2CM_003). iNOVA4Health Research Unit (LISBOA-01-0145-FEDER-007344), which is cofunded by Fundação para a Ciência e Tecnologia / Ministério da Ciência e do Ensino Superior, through national funds, and by FEDER under the PT2020 Partnership Agreement, is acknowledged by CST and JBV.

FIGURES

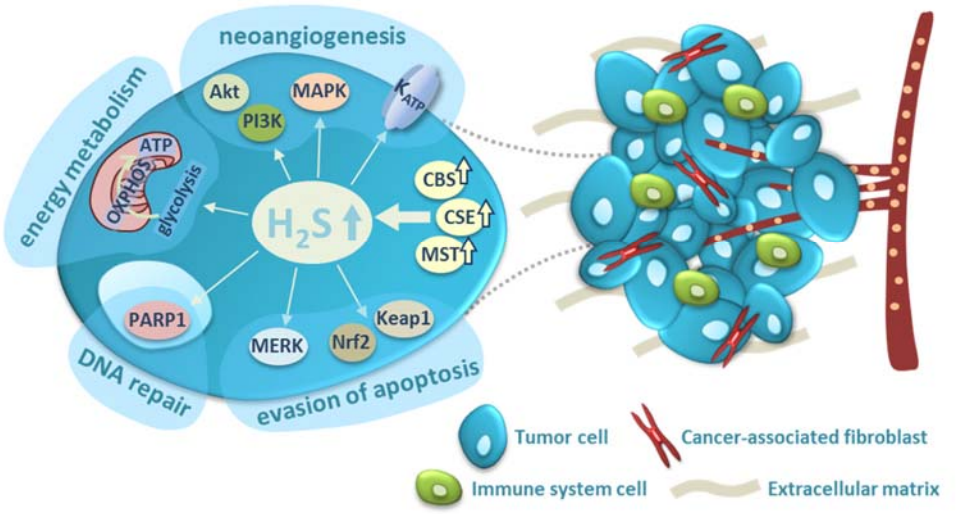

Figure 1. Effects of hydrogen sulfide within the tumor microenvironment. Hydrogen sulfide (H_2S)-synthesizing enzymes (cystathionine β-synthase, CBS, cystathionine γ-lyase, CSE, and 3-mercaptopyruvate sulfurtransferase, MST) have been reported to be upregulated in different cancer cell lines and specimens. The resulting increased H_2S production has been proposed to contribute to modulate the cancer cells adaptation within the complex tumor microenvironment, mainly through persulfidation of key protein targets in signaling pathways that regulate numerous processes, e.g.: neoangiogenesis via the PI3K/Akt and MAPK pathways and by modulation of K_{ATP} channels; evasion of apoptosis via the MERK and Keap1/Nrf2 pathways; DNA repair via the MERK/PARP1 pathway. H_2S also stimulates the tumor cell bioenergetics by directly injecting electrons into the mitochondrial electron

transfer chain through sulfide:quinone oxidoreductase, by persulfidation of ATP synthase keeping it in the active state, and by stimulation of glycolysis, particularly by persulfidation of lactate dehydrogenase A.

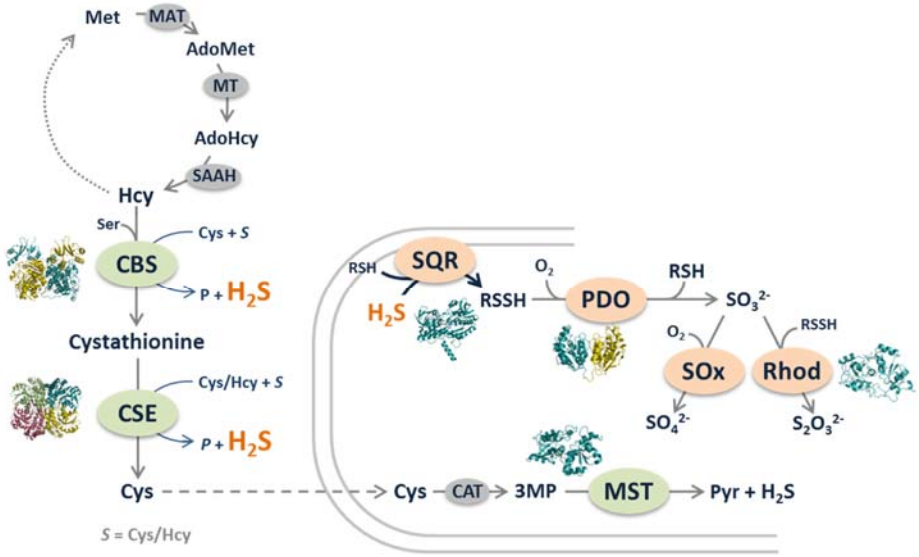

Figure 2. Metabolic pathways of H_2S synthesis and catabolism. Enzymatic production of H_2S is accomplished by cystathionine β-synthase (CBS), cystathionine γ-lyase (CSE) and mercaptopyruvate sulfurtransferase (MST). CBS and CSE participate in the transsulfuration pathway that converts homocysteine into cysteine. Both enzymes catalyze alternative reactions that use cysteine and/or homocysteine as substrates and yield H_2S. MST participates in the cysteine catabolic pathway, where it converts 3-mercaptopyruvate (derived from cysteine via cysteine aminotransferase,

CAT) into pyruvate and releases H_2S. Enzymatic breakdown of H_2S is accomplished by the sulfide oxidizing pathway, comprising four mitochondrial enzymes. The first irreversible and rate-limiting step of H_2S catabolism is catalyzed by sulfide:quinone oxidoreductase (SQR) that transfers the sulfur atom to an acceptor (RSH); persulfide dioxygenase (PDO) oxidizes the resulting persulfide (RSSH) and oxygenates the sulfane sulfur to yield sulfite (SO_3^{2-}). Sulfite can be further oxidized by thiosulfate sulfurtransferase (Rhod) to thiosulfate ($S_2O_3^{2-}$) or by sulfite oxidase (SOx) to sulfate (SO_4^{2-}). MAT: methionine-adenosyl transferase; MT: methyltransferase; SAHH: S-adenosyl homocysteine hydrolase; CAT: cysteine aminotransferase. Protein three-dimensional structures were generated from PDB entries 4COO (CBS), 2NMP (CSE), 4JGT (MST), 6M5P (SQR), 4CHL (PDO) and 2ORA (Rhod).

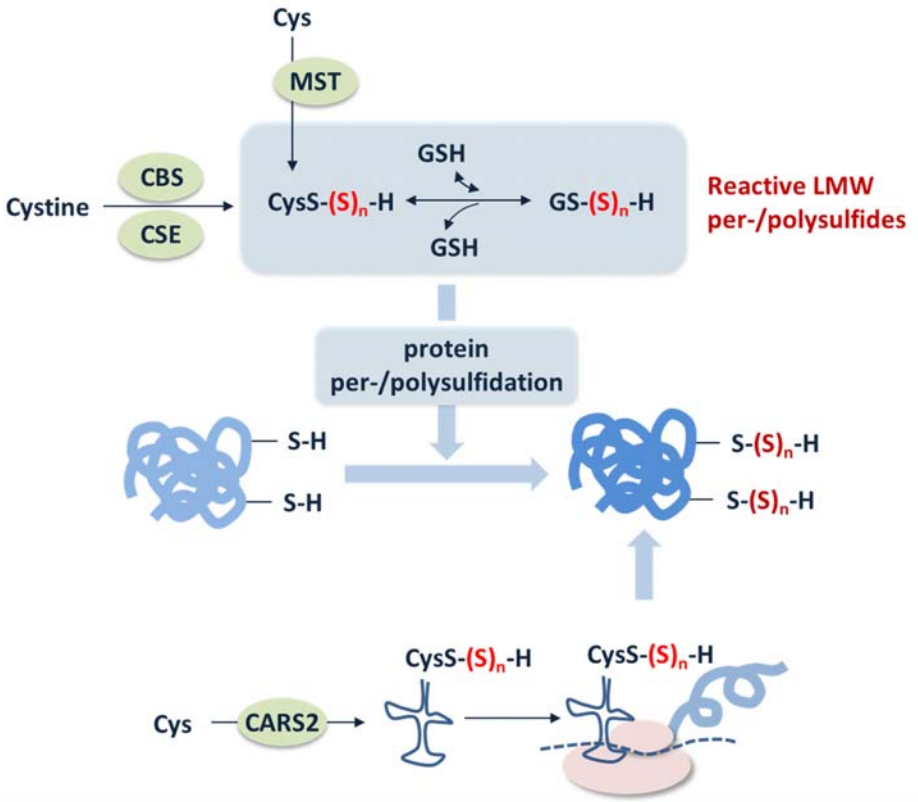

Figure 3. H_2S-mediated signaling via protein persulfidation. Persulfidation of protein cysteine residues can occur through two plausible mechanism: posttranslational modification of cysteine residues or co-translational incorporation of cysteine persulfide (CysSSH) through CysSSH-bound tRNA derived from the mitochondrial protein cysteinyl-tRNA synthetase (CARS2). Cystathionine β-synthase (CBS), cystathionine γ-lyase (CSE) and 3-mercatopyruvate sulfurtransferase (MST) generate CysSSH from either cystine (CBS and CSE) or cysteine (MST). CysSSH can then react with gluthatione (GSH), yielding glutathione persulfide

(GSSH). Sulfane sulfur can next be reversibly transferred to other thiols (such as GSH or protein-SH) to form the corresponding persulfide/polysulfide species. Mammalian CARS2, the other (main) source of persulfides, catalyzes the synthesis of tRNA-bound persulfides from cysteine, followed by its incorporation into the nascent protein, upon translation.

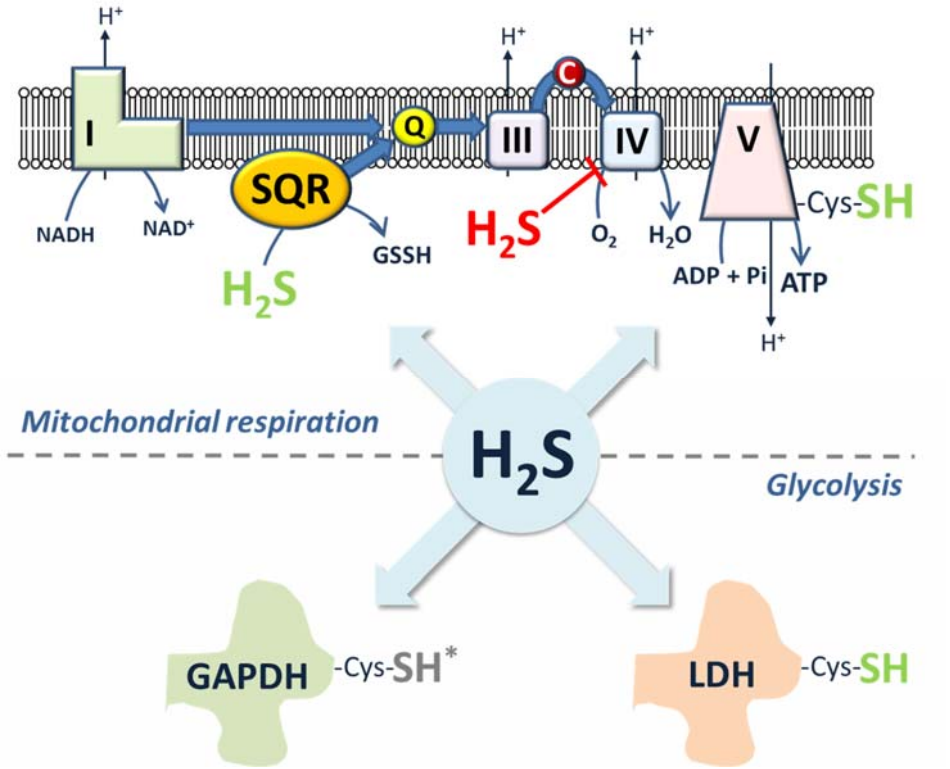

Figure 4. H_2S effect on cellular bioenergetics. At low concentrations H_2S stimulates the mitochondrial electron transport chain by acting as a metabolic

fuel. H_2S-derived electrons are transferred to coenzyme Q (CoQ) by sulfide:quinone oxidoreductase (SQR). CoQ is then re-oxidized by complex III and electrons are shuttled via cytochrome *c* to complex IV, where O_2 is eventually reduced to H_2O. Complexes I, III and IV contribute to generating a proton electrochemical gradient which is the driving force for ATP synthesis catalyzed by ATPase (complex V). H_2S stimulates directly complex V activity by persulfidation, which contributes to maintain the enzyme in its catalytically active conformation. At higher concentrations H_2S binds cytochrome *c* oxidase (complex IV), thus leading to impairment of electron transfer. In the cytosol, H_2S modulates the activity of the glycolytic enzymes by mediating persulfidation of glyceraldehyde-3-phosphate dehydrogenase (GAPDH; with opposite effects reported) and lactate dehydrogenase (LDH).

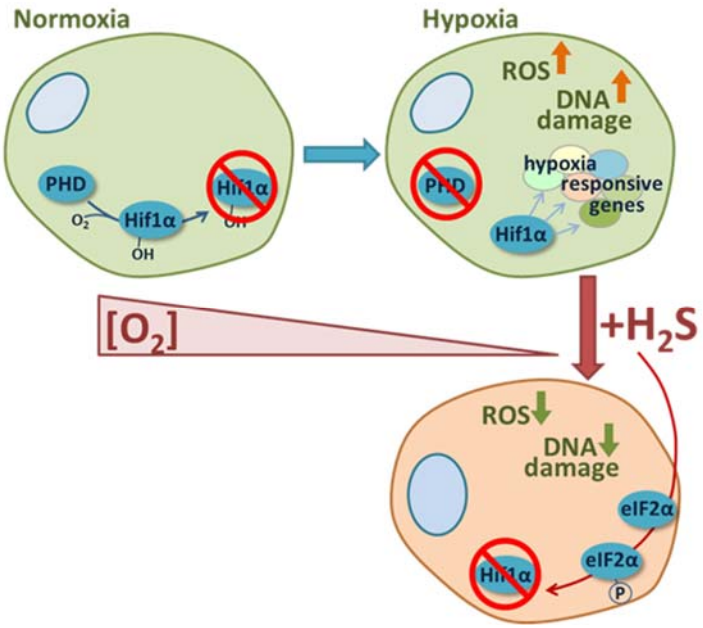

Figure 5: H_2S and hypoxia. A) The master gene regulator hypoxia-inducible factor-1α (HIF-1α), while being committed by prolyl-hydroxylases (PHD) to ubiquitin-mediated proteasomal degradation under normoxic conditions, under hypoxic conditions tends to accumulate in the cell in response to PHD inhibition. In hypoxia, however, in addition to affording protection from oxidative stress and DNA damage, H_2S downregulates HIF-1α synthesis via phosphorylation of the eukaryotic translation initiation factor 2α (eIF2α). B) Hypoxia up-regulates the expression of the H_2S-synthesizing enzymes cystathionine β-synthase (CBS) and cystathionine γ-lyase (CSE) and promotes their partial translocation into mitochondria, where 3-mercaptopyruvate sulfurtransferase (MST) is partly located. Concomitantly, mitochondria

become less abundant, but enriched in the H_2S-consuming enzyme sulfide:quinone oxidoreductase (SQR) to protect the electron transport chain from H_2S poisoning.

RESULTS AND DISCUSSION
PAPER 4

Screening Pyridine Derivatives against Human Hydrogen Sulfide-synthesizing Enzymes by Orthogonal Methods

Karim Zuhra[1,2,3], Pedro M. F. Sousa[4], Giulia Paulini[3], Ana Rita Lemos[4], Zenta Kalme[5], Imants Bisenieks[5], Egils Bisenieks[5], Brigita Vigante[5], Gunars Duburs[5], Tiago M. Bandeiras[1,4], Luciano Saso[6], Alessandro Giuffrè[2,*], and João B. Vicente[1,*]

1 - Instituto de Tecnologia Química e Biológica António Xavier, Universidade Nova de Lisboa, Oeiras, Portugal

2 - CNR Institute of Molecular Biology and Pathology, Rome, Italy

3 - Department of Biochemical Sciences, Sapienza University of Rome, Italy

4 - Instituto de Biologia Experimental e Tecnológica, Oeiras, Portugal

5 - Latvian Institute of Organic Synthesis, Riga, Latvia.

6 - Department of Physiology and Pharmacology "Vittorio Erspamer", Sapienza University of Rome, Italy

*** Correspondence:**

Dr. João B. Vicente

Instituto de Tecnologia Química e Biológica António Xavier

Universidade Nova de Lisboa

Av. da República (EAN)

2780-157 Oeiras, Portugal

Phone: +351-214469662

Email: jvicente@itqb.unl.pt

Dr. Alessandro Giuffrè,
Institute of Molecular Biology and Pathology (IBPM)
National Research Council of Italy (CNR)
Piazzale Aldo Moro 5, I-00185 Rome, Italy
Phone: +39-06-49910944;
Email: alessandro.giuffre@uniroma1.it

Sci Rep. 2019 Jan 24;9(1):684. doi: 10.1038/s41598-018-36994-w.

Received: 26 March 2018; Accepted: 26 November 2018; Published: 24 January 2019

ABSTRACT

Biosynthesis of hydrogen sulfide (H_2S), a key signalling molecule in human (patho)physiology, is mostly accomplished by the human enzymes cystathionine β-synthase (CBS), cystathionine γ-lyase (CSE) and 3-mercaptopyruvate sulfurtransferase (MST). Several lines of evidence have shown a close correlation between increased H_2S production and human diseases, such as several cancer types and amyotrophic lateral sclerosis. Identifying compounds selectively and potently inhibiting the human H_2S-synthesizing enzymes may therefore prove beneficial for pharmacological applications. Here, the human enzymes CBS, CSE and MST were expressed and purified from *Escherichia coli*, and thirty-one pyridine derivatives were synthesized and screened for their ability to bind and inhibit these enzymes. Using differential scanning fluorimetry (DSF), surface plasmon resonance (SPR), circular dichroism spectropolarimetry (CD), and activity assays based on fluorimetric and colorimetric H_2S detection, two compounds (C30 and C31) sharing structural similarities were found to weakly inhibit both CBS and CSE: 1 mM C30 inhibited these enzymes by approx. 50% and 40%, respectively, while 0.5 mM C31 accounted for CBS and CSE inhibition by approx. 40% and 60%, respectively. This work, while presenting a robust methodological platform for screening putative inhibitors of the human H_2S-synthesizing enzymes, highlights the importance of employing complementary methodologies in compound screenings.

INTRODUCTION

Once merely regarded as a toxic substance for virtually all life forms, hydrogen sulfide (H_2S) was discovered to be in fact a 'gasotransmitter' in mammalian physiology (similarly to nitric oxide, NO, and carbon monoxide, CO), i.e., an endogenously produced signalling molecule that regulates a myriad of processes like blood flow, cellular stress response, inflammation, apoptosis and energy metabolism [15, 277]. H_2S is endogenously synthesized by specialized enzymes. Yet, it can be also produced by the gut microbiota as an intermediate or end-product of microbial metabolic pathways, or be released from persulfides and polysulfides, endogenously produced or derived from dietary intake (reviewed in [278]). The human enzymes that synthesize H_2S are cystathionine β-synthase (CBS) and cystathionine γ-lyase (CSE) from the transsulfuration branch of the methionine cycle, and 3-mercaptopyruvate sulfurtransferase (MST) [127]. The signalling function of H_2S is mostly related to the ability of this molecule to modify target proteins by mediating the persulfidation of cysteine thiols or direct interaction with metal centers, particularly heme moieties (reviewed in [213, 279]). Being potentially toxic, H_2S needs to be disposed via a mitochondrial sulfide oxidation pathway in many cell types [127, 280] and proposedly via haemoglobin in red blood cells [237]. The production and breakdown of H_2S are kept under tight regulatory control at all levels, transcriptional, translational and post-translational, by complex mechanisms which also involve the other two 'gasotransmitters', as reported for CBS [24-26, 36, 232, 281]. Indeed, the relevance of H_2S homeostasis is attested by the still growing association between altered H_2S metabolism and human pathologies, from cardiovascular and

neurodegenerative diseases to cancer (reviewed in [54, 129]). Decreased endogenous H_2S production, due to CSE knock-out or pharmacological inhibition, leads to hypertension and early development of atherosclerosis (reviewed in [282]). H_2S has also been implicated in neuronal disorders. Indeed, a correlation between elevated H_2S levels and amyotrophic lateral sclerosis (ALS) in human patients was reported [119], while CSE deficiency was found to mediate neurodegeneration in Huntington's disease [114]. Furthermore, several lines of evidence have shown a close correlation between increased expression of CBS and CSE and different cancer types, namely colorectal, ovarian, breast, prostate and melanoma [75-77], where increased H_2S production was suggested to promote cellular proliferation and energy metabolism [77], and contribute to drug resistance [78, 283]. Accordingly, in the human colorectal cancer cell line HCT 116, shRNA-mediated silencing of CBS or its pharmacological inhibition by aminooxyacetic acid (AOAA) significantly impaired cellular proliferation and migration, and tumor xenograft growth [77].

Given this association between H_2S metabolism and human disease, several studies have aimed to identify compounds selectively targeting the human H_2S-synthesizing enzymes [75]. This notwithstanding, currently there are no available potent and selective inhibitors of CBS, CSE and MST suitable for pharmacological applications. AOAA, commonly referred to as a selective CBS inhibitor, inhibits also CSE (and with even higher potency than CBS), as well as several other pyridoxal 5'-phosphate (PLP)-dependent enzymes [122]. Propargylglycine, a well-studied inhibitor of human CSE, though displaying an IC_{50} in the tens of micromolar range, requires millimolar concentrations to fully

inhibit the enzyme *in vivo* [122], and only non-selective and weak substrate-like inhibitors have so far been reported for human MST, none of them suitable for biological studies [284].

Compound screening campaigns have been reported mostly for CBS, but also for CSE and MST. Regarding CBS, screening studies have either focused on direct inhibition of the purified recombinant protein [122, 285], or on cell lines that endogenously overexpress CBS [125, 286]. Recently, benserazide was reported to inhibit CBS activity with good selectivity, to impair colon cancer cell proliferation *in vitro*, and tumor growth *in vivo* [125]. As for CSE, a screening has been reported, where a few compounds were observed to inhibit CSE, although they lacked specificity, as they also inhibited CBS [22, 122]. Recently, Hanaoka and co-workers performed a compound screening against mouse MST and identified four pyrimidone derivatives with high inhibitory effect against purified MST and MST-overexpressing cells [284]. Despite the potential interest on these newly discovered compounds, there is still the need to discover selective high affinity inhibitors for all three H_2S-synthesizing enzymes.

High-throughput screening campaigns typically employ orthogonal methods that complement the information from each other and progressively narrow down the number of tested compounds from up to millions of compounds to a few lead molecules [287]. Biophysical methodologies that allow to directly evaluate the interaction between a target protein and the screened compounds are often used as a first line of screening, particularly if it is unfeasible, due to technical and/or budgetary reasons, to employ an enzymatic activity assay in a high-throughput fashion (reviewed e.g. in [288]). First line screening

methodologies include differential scanning fluorimetry (DSF, also known as thermal scanning assay), surface plasmon resonance (SPR), nuclear magnetic resonance (NMR), and fluorescence polarization. Once hit compounds are identified in the first line of screening, complementary methodologies, such as *in vitro* activity assays, isothermal calorimetry and X-ray crystallography, ensue to validate lead molecules and feed information into the pipeline for compound optimization. High-throughput H_2S-detecting methods have thus far commonly employed the fluorescence assay based on the 7-azido-4-methylcoumarin (AzMC) dye. AzMC is selectively reduced by H_2S to 7-amino-4-methylcoumarin with concomitant increase in fluorescence [139]. Despite its specificity, AzMC not only reacts with H_2S slowly, but is also prone to chemical interference [125]. Other approaches have been recently reported based on non-commercially available H_2S probes (e.g. [289]). The colorimetric methylene blue method is one of the most commonly used methods for H_2S measurement. The method is based on the reaction of H_2S with *N,N*-dimethyl-*p*-phenylenediamine (NNDPD), followed by iron chloride ($FeCl_3$)-mediated formation of the methylene blue dye, which is detected by visible absorption spectroscopy [290].

Herein, we employed a combination of orthogonal biophysical and functional assays to screen a library of synthetic pyridine derivatives against the human H_2S-synthesizing enzymes CBS, CSE and MST. Both SPR and DSF didn't detect any strongly interacting compound. An activity-based screening using the H_2S-detecting AzMC fluorescent probe indicated positive hits. However, a counter-screen with the colorimetric methylene blue method revealed direct interference of the tested compounds with AzMC, thus rebutting the finding of

positive hits, and allowed the identification of two compounds weakly inhibiting CBS and CSE. The experimental setup herein presented offers a robust platform for future compound screenings targeting the three human H_2S-synthesizing enzymes.

RESULTS

Synthesis of pyridine derivatives

Thirty-one pyridine derivatives (Table 1 and Figure 1) were synthesized and characterized as reported in the Materials and Methods section, employing condensation and heterocyclization reactions. Some of the prepared compounds were used for further transformation to water soluble salts. Compounds purity was at least 95 %.

Interaction with human CBS, CSE and MST analyzed by differential scanning fluorimetry (DSF) and surface plasmon resonance (SPR)

The newly synthesized derivatives were assayed by two complementary biophysical techniques, namely DSF and SPR, for their ability to bind to the H_2S-synthesizing human enzymes tCBS, CSE and MST, recombinantly expressed and purified from *E. coli*. For each target protein, the DSF assays were preliminarily optimized in terms of protein and dye concentration, resulting in the following conditions (final volume: 20 µL in each well): tCBS (2 µg/well; ~2 µM), CSE (1 µg/well; ~1 µM) or MST (2 µg/well; ~3 µM); final dye concentration: 1x. As

shown in Figure 2 (top panel), the DSF thermal denaturation curve of tCBS (marked with 'a') displays an unusually high fluorescence of the dye at the initial temperature (20 °C), indicating either a partial unfolding of the protein or a possible interference from a protein component in the assay. Data were best fitted (line 'a' in Figure 2, top panel) with two consecutive transitions with very close values: T_{m1} = 45.7 °C (60%) and T_{m2} = 49.8 °C (40%), yielding a weighted mean value $T_{m\_'Ave'}$ = 47.4 °C. To check whether tCBS was partly unfolded at the initial temperature of 20 °C, thermal unfolding was also monitored by Far-UV CD spectropolarimetry. As shown in Figure 2 (top panel), according to the CD thermal denaturation profile acquired at 222 nm (marked with 'b'), there is no indication of denatured protein at the initial temperature of 20 °C. Moreover, the protein displays an apparent T_m of 58.6 °C. DSF was employed to screen the effect of the pyridine derivatives at 200 μM concentration on the thermal denaturation profile of tCBS. Statistical validation of the assay was obtained by incubating tCBS with 200 μM AOAA as the negative control (N = 25; 6 independent experiments), to be compared with the non-incubated enzyme as positive control (N = 23; 6 independent experiments) (Supplementary Figure S1 and Supplementary Table S1). The assay displayed Z'-factors of -1.58, +0.08 and -0.28 for T_{m1}, T_{m2} and $T_{m\_'Ave'}$, respectively. Compounds C9, C10, C19 and C23 resulted in aberrant thermal denaturation profiles, precluding any type of analysis. The remaining compounds had a limited impact on the tCBS thermal denaturation (Supplementary Figure S2). While none of the compounds exhibited |Z-score| ≥ 3.0 for any of the analysed parameters (T_{m1}, T_{m2} and $T_{m\_'Ave'}$), four compounds, namely C2, C14, C28 and C29, yielded $|\Delta T_{m\_'Ave'}| \geq 1.0$ °C.

The CSE thermal denaturation profile obtained in the DSF experiments (marked with 'a' in Figure 2, middle panel) presented a basal fluorescence at 20 °C even higher than observed for tCBS. The initial drop preceded two fluorescence increases (at 45-60 °C and 70-80 °C) interspaced by a major drop (at 60-70 °C). By analysing the CSE thermal unfolding monitored by CD spectropolarimetry (marked with 'b' in Figure 2, middle panel), a single transition was detected, with a T_m at 70.4 °C. While precluding reliable estimates of apparent T_m values, the DSF thermal denaturation profiles still allow analysing relative changes upon compounds screening, particularly in terms of the high basal fluorescence measured at 20 °C and intensity of each transition. To quantitatively analyse the effect of the pyridine derivatives on CSE thermal denaturation, we established two parameters based on fluorescence ratios along the thermal denaturation profile (marked with Greek letters along the curve in Figure 2, middle panel, line a): Ratio A = α/β and Ratio B = γ/β. Statistical validation of the assay for CSE was obtained by incubating the enzyme with 200 μM AOAA as the negative control (N = 26; 6 independent experiments), to be compared with the non-incubated enzyme as positive control (N = 26; 6 independent experiments) (Supplementary Figure S1 and Supplementary Table S2). The assay displayed Z'-factors of +0.53 and +0.31 for Ratios A and B, respectively. Compounds C10, C18, C19 and C23 resulted in aberrant thermal denaturation profiles, precluding any type of analysis. By analysing the effect of the other tested pyridine derivatives on the thermal denaturation profile of CSE (Supplementary Figure S3), C1, C2, C9, C17, C30 and C31 were identified as the only compounds exhibiting |Z-score| ≥ 3.0 for both Ratio A and Ratio B (Supplementary Table S2).

The MST thermal denaturation profiles obtained by DSF and CD (Figure 2, bottom panel) exhibited two well separated transitions with nearly matching T_m values between the two methods: T_{m1} = 42.4 °C (60%) and T_{m2} = 56.2 °C (40%) by DSF yielding $T_{m\_'Ave'}$ = 48.2 °C, to be compared with T_{m1} = 45.0 °C (60%) and T_{m2} = 58.8 °C (40%) by CD spectropolarimetry yielding T_{m_ave} = 50.5 °C. Possible interactions of the pyridine derivatives with MST were evaluated by DSF (Supplementary Figure S4 and Supplementary Table S3). Statistical validation of the assay for MST was obtained by incubating the enzyme with 3-mercaptopyruvate (3MP, at 2 mM) as the negative control (N = 28; 6 independent experiments), to be compared with the non-incubated enzyme as positive control (N = 31; 6 independent experiments) (Supplementary Figure S1 and Supplementary Table S3). As shown in Supplementary Figure S1, the major effect of 3MP was to significantly decrease the relative amplitude of the first transition ('Frac' in Supplementary Table S3), while decreasing both T_m values. The assay displayed Z'-factors of +0.50, -0.32, +0.68, and -0.06, for Frac, T_{m1}, T_{m2} and $T_{m\_'Ave'}$, respectively. Compounds C19 and C23 resulted in aberrant thermal denaturation profiles, precluding any type of analysis. Compounds C2, C30 and C31 exhibited $|\Delta T_{m1}| \geq 1.0$ °C with |Z-score| ≥ 3.0, while all but six compounds exhibited a |Z-score| ≥ 3.0 with respect to T_{m2} (Supplementary Table S3). Five compounds (C5, C13, C26, C27, and C30) resulted in a shift of $|\Delta T_{m\_'Ave'}| \geq 1.0$ °C and, notably, out of them only compound C30 exhibited a shift in both T_{m1} and T_{m2} with |Z-score| ≥ 3.0.

The synthetic compounds were also screened for their ability to bind CBS, CSE and MST by SPR. This is an optical methodology based on the physical

principle of refractive index changes at the biospecific sensor surface upon complex formation [287]-[291]. After immobilizing the enzymes on the chips, the tested pyridine derivatives were assayed at four concentrations: 25, 50, 100 and 200 µM. No Z'-factor could be measured for these assays due to lack of adequate controls under the selected experimental conditions. Under those conditions, several compounds (C9, C10, C18, C19 and C23) displayed poor solubility, thus precluding an analysis of their interaction with the target proteins by SPR. Moreover, the results obtained for several compounds revealed solubility issues affecting differently the sensorgrams for the three enzymes (Supplementary Figures S5, S6 and S7): C1 (MST), C11-C14 (tCBS and CSE), C16 (tCBS and CSE), C17 (all), C20-22 (tCBS and CSE), C24-26 (tCBS and CSE), C27-28 (all), and C31 (tCBS). For the remaining compounds, due to the fast kinetics observed for the studied interactions, no association or dissociation rate constants could be determined. We thus identified compounds yielding sensorgrams where the steady-state response units were proportional to the compound concentration (in the tested range) and did not exceed the expected maximal value (Rmax, based on the compound molecular weight and surface density), thus avoiding any misidentification by superstoichiometric binding behaviour. As shown in Figure 3, five compounds (C1, C3, C5, C6 and C7) proved to interact with tCBS, two (C7 and C31) with CSE, and three (C5, C7, C14) with MST, in a concentration-dependent mode. The fact that the corresponding steady-state response units linearly increase with the compound concentration up to 200 µM points to low-affinity interactions. Similarly, weak interactions were also observed between AOAA and both tCBS and CSE (Supplementary Figure S8).

Inhibition of human CBS, CSE and MST analyzed by fluorimetric and colorimetric assays

The screening was complemented with activity measurements to test the inhibitory efficacy of the synthetic compounds towards the target enzymes. A fluorescence-based assay using the H_2S-detecting dye AzMC was initially attempted with tCBS alone. A Z'-factor of +0.78 was obtained for this assay by measuring the fluorescence signal of the dye in the absence of tCBS (negative control; $N = 16$; 3 independent experiments) and in its presence (positive control; $N = 16$; 3 independent experiments) (Supplementary Table S4). All pyridine derivatives were first screened at a single concentration of 200 μM. Under these conditions, sixteen compounds appeared to lower the dye signal (Supplementary Table S4) and were thus assayed in a concentration range between 15.6 μM and 1 mM. As shown in Figure 4, out of them, twelve seemed rather effective (apparent EC_{50} values in the range of 41.6 - 229.9 μM). However, all the sixteen compounds tested were found to interfere with the AzMc probe, as they markedly decreased the dye signal (see Supplementary Table S5) in control experiments carried out with the H_2S releaser GYY4137 in place of tCBS, under otherwise identical experimental conditions (Z'-factor = +0.85, $N = 16$; 3 independent experiments for both positive and negative controls). This led us to quit with assays based on the AzMc fluorescent probe and screen the whole compound library on each target enzyme (tCSB, CSE and MST) by detecting H_2S with the colorimetric methylene blue (MB) assay.

To rule out possible interferences in the MB assay and/or direct reactivity of the compounds with H_2S, each derivative was tested in preliminary control assays using GYY4137 as the H_2S source (Z'-factor = +0.84, $N = 9$; 3 independent experiments for both positive and negative controls). As shown in Supplementary Table S6, in these assays none of the 31 compounds caused a marked decrease in the colorimetrically detected H_2S. The MB method was therefore employed to evaluate the effect of each compound on the H_2S-producing activity of tCBS, CSE and MST (respectively, with Z'-factors = +0.57, +0.78 and +0.51; $N \geq 9$ in at least 3 independent experiments for both positive and negative controls, see Table 2). By screening the effect of the whole compound library on the activity of each target enzyme, it was found that, whereas none of the tested derivatives has inhibitory effect towards MST, C30 and C31 are poor inhibitors of both tCBS and CSE (Table 2). Indeed, while 1 mM C30 inhibits tCBS and CSE by approx. 50% and 40%, respectively, 0.5 mM C31 accounts for tCBS and CSE inhibition by approx. 40% and 60%, respectively.

DISCUSSION

Hydrogen sulfide (H_2S) is endogenously produced to accomplish the regulation of numerous physiological processes, ranging from neoangiogenesis [95], vasorelaxation and blood pressure [292] to cardioprotective [293], antinflammatory [294] and antioxidant [112] effects. Altered H_2S metabolism is associated with multiple human pathologies, such as cardiovascular [282] and inflammatory [47] disorders, neurodegeneration [114] and cancer [77, 120]. Therefore, the development of compounds targeting the three H_2S-synthesizing

enzymes, namely CBS, CSE and MST, may prove beneficial for future therapeutic strategies, as posited for CBS [75, 286]. To date, only unspecific or relatively weak inhibitors have been reported for CBS. While AOAA displays a half-maximal inhibitory concentration (IC_{50}) of approximately 3 μM for human recombinant CBS, it also inhibits human CSE with even higher potency, as well as other PLP-dependent enzymes [122]. Whereas benserazide appears more specific towards CBS, it exhibits lower potency [125]. The present work attempted to identify new CBS, CSE and MST inhibitor scaffolds, using combined biophysical and biochemical approaches. The tested compounds were assembled in a composite library of 31 pyridine derivatives.

A combination of orthogonal biophysical and biochemical methods was applied to provide a robust and effective platform to identify putative ligands. Despite the fact that both DSF and SPR are able to detect protein-ligand interactions, though through different mechanisms, frequently in compound screenings the lists of hits identified by either method are only partially overlapping. Both methodologies are typically employed due to the ease of setting up such assays, and to the relatively low amounts of protein required (reviewed e.g. in [288, 295, 296]). The usage of both methodologies thus affords a more robust approach [297].

Herein, DSF data required a rather elaborate analysis due to different factors. The DSF denaturation profiles of tCBS presented a relatively high basal fluorescence (unrelated to protein destabilization at the initial temperature as judged by the CD-monitored thermal denaturation profile) and were best fitted with two apparent T_m values (Figure 2). The discrepancy between the CD- and

DSF-monitored thermal denaturation profiles and corresponding T_m values could be due to interference of the tCBS cofactors, through fluorescence increase and/or quenching by PLP and heme iron, respectively. Regardless of cofactor interference, DSF could still be employed to evaluate the effect produced by each compound on the protein thermal denaturation profile and four compounds (C2, C14, C28 and C29) were found to mildly affect tCBS thermal stability ($|\Delta T_{m\_'Ave'}| \geq 1.0$ °C), though with |Z-score| < 3.0 (Supplementary Table S1).

Similarly to tCBS, CSE showed high basal fluorescence intensity at resting temperature, possibly related to the presence of the PLP cofactor. Indeed, the CD-monitored thermal denaturation profile revealed CSE to be remarkably stable, ruling out protein instability at resting temperature (Figure 2). Despite the unconventional DSF thermal denaturation profile, it was still employed to survey possible interactions of the pyridine derivatives with CSE. Based on two parameters (Ratio A and B) quantitatively evaluating profile shape changes, both statistically validated by using the CSE inhibitor AOAA as negative control, six compounds (C1, C2, C9, C17, C30 and C31) were identified as putative interactors for CSE (Supplementary Table S2). These compounds indeed proved to be the only ones causing changes in both parameters with |Z-score| ≥ 3.0.

MST revealed a better agreement between the DSF and CD thermal denaturation profiles, with two well defined transitions likely associated with the two homologous domains that compose MST [39] and other transulfurases, like rhodanese [51]. From the four analysed parameters (Frac, T_{m1}, T_{m2}, $T_{m\_'Ave'}$), compounds putatively interacting with MST were identified based on a combination of defined criteria related to T_m shifts and corresponding Z-score

values. According to these criteria, only two compounds (C2 and C30) were found to cause shifts in both T_{m1} and T_{m2} with |Z-score| ≥ 3.0, and notably C30 caused the greatest $\Delta T_{m\_'Ave'}$ (-1.4°C) among all tested compounds (Supplementary Table S3).

Despite the limited identification of strong hits within the tested compound library, DSF assays under the experimental conditions used in this study proved to be suitable to screen compounds, at least for CSE and MST, while further optimization of the assay seems to be required in the case of tCBS, particularly for high-throughput screenings. Indeed, for the assay on CSE, according to [57], Ratio A exhibited a Z'-factor (+0.53) consistent with an excellent assay, while Ratio B exhibited a slightly lower Z'-factor (+0.31), yet consistent with a good assay (Supplementary Table S1). Likewise, for the assay on MST, two parameters (Frac and T_{m2}) were found to be characterized by Z'-factors (+0.50 and +0.68, respectively) consistent with an excellent assay (Supplementary Table S2). In contrast, for the assay on tCBS, only T_{m2} exhibited a slightly positive Z'-factor (+0.08), unlike T_{m1} and and $T_{m\_'Ave'}$ (displaying Z'-factor values of -1.58 and -0.28) (Supplementary Table S3).

In parallel with the DSF assays, putative interactions of the tested compounds with the three H_2S-synthesizing enzymes were investigated by surface plasmon resonance (SPR). The disadvantages of using a fluorescence-based technique involving an added dye are overcome by SPR, which is a label-free methodology. Herein a CM5 chip was employed to immobilize all target proteins, based on covalent linkage to the carboxymethylated surface of exposed lysine residues distributed through the protein surface, thus offering different possible

binding orientations. Pyridine derivatives were screened at four concentrations, from 25 to 200 μM, which already proved to be above the desired solubility for 15 compounds (approximately half of this library). Despite this limitation and the current lack of adequate controls to statistically validate the use of SPR for high-throughput screening, we observed interactions for a limited number of compounds, based on the proportionality between steady-state response units and compound concentration: 15% of the compounds in the library for tCBS, ~6% for CSE and ~10% for MST (Figure 3). For these compounds, however, it was not possible to extrapolate binding affinities, as the steady-state response units linearly increased with the compound concentration pointing to low-affinity interactions. The results herein obtained for the pyridine derivatives suggest that the use of SPR in future compound screenings targeting tCBS, CSE and MST would require further optimization and proper statistical validation.

The 31 pyridine derivatives were then assayed for their ability to inhibit H_2S production by tCBS using the H_2S-selective fluorescent probe AzMC [125]. While 16 compounds were selected as 'positive hits' based on a detailed kinetic analysis evaluating these compounds in a wide concentration range (Figure 4), control experiments were performed replacing tCBS with the H_2S donor GYY4137, revealing that all the tested compounds strongly interfered with AzMc detection of GYY4137-generated H_2S (Supplementary Table S5 and Supplementary Figure S9). This apparent drawback, similar to the interference of reference CBS inhibitor NSC67078 [285] with the AzMc probe reported by Druzhyna and co-workers [125], further highlights the caveat of fluorescence-based methods, particularly when dealing with compounds and/or fragments with

aromatic moieties. The discovery that the presumed 16 'hit' pyridine derivatives interfered with the AzMc fluorescence-based method prompted us to employ the MB method in 96-well plates as described in [125], adapted to prevent H_2S loss upon addition of zinc acetate. After confirming that none of the 31 compounds interfered with MB detection of H_2S released by GYY4137 (Supplementary Table S6), the compounds were screened against the three target proteins. Whereas none of the pyridine derivatives affected MST (Table 2), compounds C30 and C31 appeared to partially inhibit both CBS and CSE (Table 2), albeit only at relatively high concentrations (respectively, 1 and 0.5 mM). Interestingly, C30 and C31 share the same molecular scaffold (Figure 1). It is worth noting that all fluorimetric and colorimetric assays herein described under the experimental conditions used in the present study proved to be suitable even for high-throughput screenings based on the determined Z'-factor values [57] (Table 2 and Supplemental Tables S4, S5 and S6).

Herein, orthogonal biophysical screening methods, based both on protein-compound interaction (DSF and SPR) and on enzymatic inhibition (H_2S-detection assays), were employed for the first time for the three human H_2S-synthesizing enzymes CBS, CSE and MST altogether. Testing a library of 31 pyridine derivatives, a relatively low overlap was observed between DSF and SPR outputs in terms of compounds possibly interacting with the target enzymes. The possibility of including functional approaches such as enzymatic inhibition assays in screening campaigns increases the robustness of the resulting hit compound identification. Herein, only two out of the 31 tested compounds, namely C30 and C31, displayed a weak inhibitory activity towards both tCBS and CSE. Notably,

compound C31 was also identified by DSF as a hit compound for CSE and likely interactor of the same protein by SPR.

In conclusion, the drug discovery process can be viewed as a bumpy ride where methodological limitations may lead to the identification of false positives as hit molecules. In this regard, the present study further highlights the importance in compound screening campaigns of crossing the read-outs from complementary methodological approaches, ranging from the investigation of biophysical dynamic aspects (such as protein-ligand binding) to the implementation of more functional assays (enzymatic activity). From this perspective, we hope that the experimental setup herein presented, that integrates analysis of protein-ligand interactions by both DSF and SPR, and protein thermal denaturation investigation by Far-UV CD, with activity assays based on fluorimetric and colorimetric H_2S detection methods, offers a robust platform for the discovery of hit compounds to develop selective and potent inhibitors of the three human H_2S-synthesizing enzymes.

METHODS

Chemicals

All chemicals were purchased from Sigma, except GYY4137 (from CAYMAN), the Protein Thermal Shift Dye Kit ™ (from Applied Biosystems) and the SPR Amine Coupling Kit, type 2 (from GE Healthcare).

Synthesis and characterization of pyridine derivative compounds

Herein, a composite library of thirty-one pyridine derivatives was assembled (Table 1 and Figure1), based on newly synthesized (C16-C19 and C25-C28) and previously reported compounds (C1-15, C20-24 and C29-C31) [298-304]. Compound purity was assessed by high-performance liquid chromatography in a Waters Alliance system coupled to a Waters 2485 UV/Vis detector.

2,6-Dimethyl-1,4-dihydropyridine-3,4,5-tricarboxylic acid 4-carbamoylmethylester 3,5-diethylester (C16)

To the mixture of 0.3 g (1 mmol) 2,6-dimethyl-1,4-dihdropyridine-3,4,5-tricarboxylic acid 3,5-diethyl ester in 5 ml of dimethylformamide, 0.37 g (2 mmol) potassium carbonate and 0.19 g (1 mmol) iodoacetamide were added. The reaction mixture was heated at 60 ºC for 3 h. Afterwards, the reaction mixture was evaporated, and the residue was dissolved in water and extracted with dichloromethane. The dichloromethane layer was dried over magnesium sulfate, filtered and evaporated. Residue was crystallized with diethyl ether and 0.2 g (56.5 %) of compound C16 was obtained.

Compound C16: ^{1}H-NMR (400MHz, DMSO-d_6): 8.98 (s, 1H), 7.36 (s, 1H), 6.85 (s, 1H), 4.71 (s, 1H), 4.32 (s, 2H), 4.16-4.02 (m, 4H), 2.23 (s, 6H), 1.19 ppm (t, *J*=7.04 Hz, 6H).

m/z = 353[M-H]$^{-}$. Mp. = 183-184 ºC.

Calculated for $C_{16}H_{22}N_2O_7$: C, 54.23; H, 6.26; N, 7.91. Found: C, 54.25; H, 6.22; N, 7.80.

2,6-Dimethyl-1,4-dihydropyridine-3,4,5-tricarboxylic acid 4-ethoxycarbonylmethyl ester 3,5-diethylester (C17)

To the mixture of 1 g (3.3 mmol) 2,6-dimethyl-1,4-dihdropyridine-3,4,5-tricarboxylic acid in 35 ml acetone, 1.36 g (9.9 mmol) potassium carbonate was added. The obtained mixture was stirred and refluxed, and 0.56 g (3.3 mmol) of bromo-acetic acid ethyl ester was added. Then, the reaction mixture was refluxed for 4 h, cooled to room temperature and the formed potassium bromide was filtered off. The filtrate was evaporated, dissolved in 15 ml of ethanol and left for 12h in the refrigerator for crystallization. After filtration and crystallization of the obtained precipitate from benzene, 0.78 g (61%) of compound C17 was obtained. Compound C17: ^{1}H-NMR (400MHz, $CDCl_3$): 5.84 (s, 1H), 4.98 (s, 1H), 4.53 (s, 2H), 4.25-4.12 (m, 6H), 2.32 (s, 6H), 1.29-1.21 ppm (m, 9H).
m/z = 382$[M-H]^-$. Mp. = 110-111 ºC.
Calculated for $C_{18}H_{25}NO_8$: C, 56.39; H, 6.57; N, 3.65. Found: C, 56.54; H, 6.55: N, 3.52.

2,6-Dimethyl-1,4-dihydropyridine-3,4,5-tricarboxylic acid 3,5-diethylester 4-(2-oxo-2-phenylethyl)ester (C18)

Compound C18 (58% yield) was prepared similarly to C17.

Compound C18: ^{1}H-NMR (400MHz, $CDCl_3$): 7.86-7.42 (m, 5H), 6.19 (s, 1H), 5.23 (s, 2H), 5.05 (s, 1H), 4.26-4.14 (m, 4H), 2.30 (s, 6H), 1.27 ppm (t, *J*=7.04 Hz, 6H).

m/z = 414$[M-H]^-$. Mp. = 126-128 ºC.

Calculated for $C_{22}H_{25}NO_7$: C, 63.61; H, 6.7; N, 3.33. Found: C, 63.70; H, 6.03; N, 3.32.

2,6-Dimethyl-1,4-dihydropyridine-3,4,5-tricarboxylic acid-3,5-diethylester-4-[2-(4-methoxy-phenyl)-2-oxo-ethyl] ester (C19)

Compound C19 (57% yield) was prepared similarly to C17.

Compound C19: ^{1}H-NMR (400MHz, DMSO-d_6): 8.96 (s, 1H), 7.87 (d, *J*=4 Hz, 2H), 7.03 (d, *J*=4 Hz, 2H), 5.26 (s, 2H), 4.84 (s,1H), 4.16-4.03 (m, 4H), 3.84 (s, 3H), 2.24 (s, 6H), 1.19 ppm (t, *J*=7.04 Hz, 6H).

m/z = 444$[M-H]^-$. Mp. = 155-156 ºC.

Calculated for $C_{23}H_{27}NO_8$: C, 62.01; H, 6.11; N, 3.14. Found: C, 61.72; H, 6.02; N, 3.04.

2,7,7-Trimethyl-5-oxo-1,4,5,6,7,8-hexahydroquinoline-3,4-dicarboxylic acid 3-ethyl ester (C25)

Sodium hydroxide (0.5 g, 12.5 mmol) in 3 ml of water was added to a solution of 2 g (6 mmol) ester C26 in 10 ml of ethanol and mixed for 40 min. Then, the reaction mixture was evaporated and the residue dissolved in water. The water solution was acidified to pH=5 with hydrochloric acid, and the obtained precipitate

was filtered and crystallized from ethanol. 1.06 g (58 %) of compound C25 was obtained.

Compound C25: ^{1}H-NMR (400MHz, DMSO-d_6): 11.79 (s, 1H), 9.10 (s, 1H), 4.52 (s, 1H), 4.13-4.00 (m, 2H), 2.35 (dd, *J*=17.2 Hz, 2H), 2.22 (s, 3H), 2.16 (dd, *J*=17.2 Hz, 2H), 1.18 (t, *J*=7.0 Hz, 3H), 1.02 (s, 3H), 1.00 ppm (s, 3H).

m/z = 308$[M+H]^+$. Mp. = 165-170 ºC.

Calculated for $C_{16}H_{21}NO_5 \cdot H_2O$: C, 59.07; H, 7.13; N, 4.30. Found: C, 59.58; H, 7.07; N, 4.26.

2,7,7-Trimethyl-5-oxo-1,4,5,6,7,8-hexahydroquinoline-3,4-dicarboxylic acid diethyl ester (C26)

To 13 g (0.1 mol) of ethylacetoacetate in 0.2 ml of piperidine, 0.2 ml acetic acid and 20.4 ml (0.1 mol) of a 50% solution of ethyl glyoxalate in toluene was added. The obtained solution was mixed for 48 h at room temperature. Then, 13.9 g (0.1 mol) of dimedone enamine in 30 ml of ethanol was added to the reaction mixture and refluxed for 1h. After cooling, the mixture began to form precipitates which were filtered and crystallized from ethanol and as a result 10 g (30%) of compound C26 was obtained.

Compound C26: ^{1}H-NMR (400MHz,$CDCl_3$): 5.95 (s, 1H), 4.85 (s, 1H), 4.23-4.01 (m, 4H), 2.33 (dd, *J*=17.2 Hz, 2H), 2.30 (s, 3H), 2.27 (dd, *J*=16.4 Hz, 2H), 1.18 (t, *J*=7.0 Hz, 3H), 1.11 (s, 3H), 1.09 ppm (s, 3H).

m/z = 336$[M+H]^+$. Mp. = 194-196 ºC.

Calculated for $C_{18}H_{25}NO_5$: C, 64.46; H, 7.51; N, 4.18. Found: C, 64.41; H, 7.41; N, 4.12.

2,7,7-Trimethyl-5-oxo-4-thiophen-2-yl-1,4,5,6,7,8-hexahydroquinoline 3-carboxylic acid ethoxycarbonylmethyl ester (C27)

A mixture of 0.7 g (5 mmol) of 3-amino-5,5-dimethyl-cyclohex-2-enone, 0.56 g (5 mmol) of 2-thiophene carboxaldehyde and 0.95 g (5 mmol) of 3-oxo-butyric acid ethoxycarbonylmethyl ester in 10 ml of ethanol was stirred at room temperature for 3 days. The reaction mixture was cooled to -10 ºC and the product crystallization was observed. The crude product was recrystallized from ethanol and 0.85g (42%) of C27 was obtained.

Compound C27: ^{1}H-NMR (400MHz, DMSO-d_6): 9.36 (s, 1H), 7.17 (m, 1H), 6.81 (m, 1H), 6.72 (m, 1H), 5.20 (s, 1H), 4.65 (d, *J*=16 Hz, 2H), 4.10 (kv, *J*=7.0 Hz, 2H), 2.37 (dd, *J*=17.2 Hz, 2H), 2.27 (s, 3H), 2.15 (dd, *J*=16.0 Hz, 2H), 1.17 (t, *J*=7.0 Hz, 3H), 1.02 (s, 3H), 0.93 ppm (s, 3H).

m/z = 404$[M+H]^+$. Mp. = 188-190 ºC.

Calculated for $C_{21}H_{25}NO_5S$: C, 62.51; H, 6.25; N, 3.47. Found: C, 62.41; H, 6.34; N, 3.34.

2,7,7-Trimethyl-5-oxo-4-thiophen-2-yl-1,4,5,6,7,8-hexahydroquinoline 3-carboxylic acid carboxymethyl sodium salt (C28)

To a hot solution of 0.3 g (0.74 mmol) of methylester C27 in 7 ml of ethanol, a solution containing 0.033 g (0.83 mmol) of sodium hydroxide in 0.8 ml of water was added and boiled for 3 minutes. The solvent was evaporated. The obtained precipitates of crude product were suspended in diethyl ether. After filtration and washing with diethyl ether, 0.26 g (90%) of sodium salt C28 was obtained.

Compound C28: ^{1}H-NMR (400MHz, DMSO-d_6): 7.11 (m, 1H), 6.79-6.76 (m, 2H), 5.21 (s, 1H), 4.15 (dd , *J*=14.4 Hz, 2H), 2.35 (dd, *J*=16.0 Hz, 2H), 2.27 (s, 3H), 2.15 (dd, *J*=16.0 Hz, 2H), 1.01 (s, 3H), 0.94 ppm (s, 3H).
m/z = 374[M-Na+H]$^{-}$. Mp. = 195-196 ºC.
Calculated for $C_{19}H_{20}NNaO_5S \cdot 2{,}5H_2O$: C, 51.57; H, 5.65; N, 3.16. Found: C, 51.24; H, 5.10; N, 3.03.

Protein expression and purification

A truncated version of human CBS (tCBS), lacking the *S*-adenosyl-L-methionine-binding regulatory domain, was expressed and purified as described in [26]. Human CSE and MST were expressed and purified as described in Sun et al [22] and in Yadav et al [39], respectively.

Differential scanning fluorimetry (DSF)

DSF allows to gain information on ligand binding to a target protein from the observed changes in the protein thermal denaturation profile [141]. Using 96-to-1536-well plates in an RT-PCR instrument, protein denaturation is monitored as a function of temperature increase by making use of a fluorescent dye that emits light upon binding to the buried hydrophobic amino acid residues that become exposed as the protein unfolds. Typically, thermal denaturation profiles are sigmoidal and the protein melting temperature (T_m) is estimated from the inflexion point. Ligand binding is evaluated from the ability of a given compound to either stabilize or destabilize the target protein, which is reflected in an increase or decrease in the T_m. Here, DSF measurements were carried out in 384-well plates

in an Applied Biosystems QuantStudio™ 7 Flex Real-Time PCR. Prior to testing the compounds, the assay was optimized for each target protein in terms of concentration of the proteins (1 to 6 μM) and the fluorescent dye (1x, 2x and 4x; the Protein Thermal Shift Dye from Applied Biosystems is commercially available in a 1000 x concentration, without disclosing the actual molar concentration). Once conditions were optimized (see Results), the compounds were assayed by mixing in each well 14 μl of tCBS (2 μg/well; ~2 μM), CSE (1 μg/well; ~1 μM), or MST (2 μg/well; ~3 μM) in Buffer A (10 mM HEPES, 150 mM NaCl, 1 mM tris(2-carboxyethyl)phosphine [TCEP], pH 7.2), with 2 μl of compound solution (typically 2 mM in 10% dimethyl sulfoxide [DMSO], yielding a final compound concentration of 200 μM). The microplate was incubated at 4 °C for 2 hours to favour possible interactions with the target proteins. Prior to the measurement, the fluorescent dye was pre-diluted in Buffer A to a 5x working concentration, and 4 μl of the dye solution were dispensed into each well. The microplate was sealed with optical adhesive covers (Applied Biosystems) and centrifuged for 30 s at 500 x *g*. Using the QuantStudio™ 7 Flex Real-Time PCR System, the microplates were incubated at increasing temperatures, from 20 °C to 90 °C with increments of 1 °C/min. Protein unfolding was monitored with the ROX filter (excitation wavelength = 580 ± 10 nm and emission wavelength = 623 ± 14 nm). Data from triplicate curves were averaged and the melting temperatures were determined by fitting the data to biphasic sigmoidal curves. For statistical validation of the DSF assays towards these protein targets, control assays were performed employing 200 μM AOAA as negative control both for tCBS and CSE, and 2 mM 3-

mercaptopyruvate for MST, with the compound-free enzymes being used as positive controls.

Far-UV circular dichroism

Far-UV circular dichroism (CD) thermal denaturation curves were recorded in a Jasco J-815 spectropolarimeter equipped with a Jasco CDF-426S Peltier temperature controller, in a 0.1 cm path length quartz cuvette. CSE was diluted to 0.15 mg/mL in 50 mM NaPi buffer, 300 mM NaCl, 0.5 mM TCEP, 10% glycerol, pH 7.5, while tCBS and MST were diluted to 0.2 mg/mL in 10 mM Hepes buffer, 150 mM NaCl, 1 mM TCEP, pH 7.2. CD spectropolarimeter experimental setup: λ = 222 nm; temperature range, 20-90 °C; slope, 1 °C/min; data pitch, 0.5 min; data integration time, 1 s; bandwidth, 1 nm; nitrogen flow, 4 L/min. Thermal denaturation curves were analyzed with Graphpad (Prism), fitting the data to a monophasic (tCBS and CSE) or biphasic (MST) sigmoidal curve.

Surface plasmon resonance (SPR)

Putative interactions of the tested compounds with tCBS, CSE, and MST were investigated by surface plasmon resonance (SPR). Assays were carried out in a Biacore 4000 instrument (GE Healthcare) at 25 °C. At first, a pH scouting was performed on a CM5 chip for immobilization optimization using the following buffers: 10 mM sodium acetate pH 5.0, 5.5 and 5.8, 10 mM Bis-Tris pH 6.0 and 6.5, 10 mM sodium phosphate pH 7.0, 10 mM HEPES pH 7.5, or 10 mM Tris-HCl pH 7.5.

tCBS, CSE and MST were diluted to 5 µg/mL (tCBS) or 10 µg/mL (CSE and MST) in their corresponding immobilization buffer (10 mM sodium acetate pH 5.8 for CBS, and 10 mM Bis-Tris pH 6.0 for CSE and MST) and immobilized onto CM5 sensor chips using the standard amine coupling procedure. HBS-N, which consisted of 10 mM Hepes pH 7.4 and 150 mM NaCl, was used as the background buffer. Prior to immobilization, the carboxymethylated surface of the chip was activated with 20 mM 1-ethyl-3-(3-dimethylaminopropyl)-carbodiimide and 5 mM *N*-hydroxysuccinimide for 1.5 min. Proteins were coupled to the surface with a 5 to 10 min injection time at a flow rate of 10 µL min^{-1} in order to reach 5000 to 10000 response units (RU). The remaining activated carboxymethylated groups were blocked with a 5 min injection of 1 M ethanolamine pH 8.5.

Compounds (analytes) were directly diluted in running buffer (10 mM HEPES, 150 mM NaCl, 1 mM TCEP, 0.1 mM EDTA, 0.05 % (v/v) TWEEN-20, 5 mM $MgCl_2$, pH 7.2.) and injected at four different concentrations using 2-fold dilutions series, with the highest concentration tested being 200 µM. Interactions were qualitatively assessed from the obtained plots of steady-state analyte binding levels against the concentration, making use of the provided Biacore 4000 evaluation software (GE Healthcare)**.**

Fluorimetric H_2S-producing activity assays

Fluorimetric H_2S production activity assays were adapted from Thorson et al. [139]. Assays were carried out in 96-well black plates, using the H_2S-selective fluorescent probe AzMC and a FLUOstar Optima BMG Labtech plate reader. The reaction mixture, in 200 mM Tris-HCl pH 8.0, contained 1.12 µg recombinant

human tCBS per well (100 nM), 0.5 mM homocysteine, 50 µM PLP, and 50 µM AzMc (diluted from a 49.7 mM stock in DMSO). Compounds dissolved in DMSO were added to each well to yield a final concentration ranging from 15.6 µM to 1 mM (5% DMSO) in a total assay volume of 250 µl. The plate was incubated at 37 °C for 10 min and the reaction was then triggered by adding the 10 mM L-cysteine. The increase in the probe fluorescence ($\lambda_{excitation}$ = 340 nm; $\lambda_{emission}$ = 460 nm) was monitored over 1 hour at 37 °C. The CBS inhibitor AOAA (1 mM) and DMSO (7%) were used as positive and negative control, respectively. The reader was set up to automatically shake the plate for 5 seconds prior to each data acquisition. Data were analysed using Excel and activity was calculated from the initial slope of the fluorescence increase after L-cysteine addition. Control experiments to evaluate a possible interference of the tested compounds with the probe were done by replacing tCBS with the H_2S donor GYY4137 (3 mM in DMSO, final concentration).

Counterscreen using the methylene blue assay

The colorimetric methylene blue assay, commonly used to detect H_2S, was adapted to 96-well plates, as reported by Druzhyna et al. for CBS [125], and improved in order to i) avoid H_2S escape from the reaction mixture and headspace before trapping sulfide with zinc acetate, and ii) be extended to the other two H_2S-synthesizing enzymes (CSE and MST). Prior to the enzymatic inhibition assays, control absorbance measurements were performed in 96-well plates: at λ = 600 nm to evaluate the compounds solubility under the assays conditions, and at λ =

690 nm to evaluate their interference with the methylene blue read outs (and employ a correction factor whenever needed).

For CBS- and CSE-catalyzed H_2S production assays, 110 µL of reaction mixture contained 0.5 mM or 1 mM of tested compound, tCBS (10 µg/well) or CSE (30 µg/well) in 50 mM Tris-HCl pH 8.0, and 5 µM PLP. In the case of CBS, 2 mM homocysteine was also added. After keeping the plate on ice for 30 min, the reactions by CBS and CSE were respectively triggered by adding either L-cysteine (10 mM final concentration) alone or plus homocysteine (2 mM final concentration), The plate was sealed with vinyl adhesive films and incubated for 2 h at 37 °C. AOAA (1 mM) or DMSO were used as positive and negative control, respectively. Regarding MST, a 110 µL-reaction mixture contained 0.5 mM or 1 mM of each compound, 30 µg/well MST in 50 mM Tris-HCl pH 8.0, and 10 mM dithiothreitol. DMSO was used as negative control. After keeping the plate on ice for 30 min, the reaction was triggered by adding 1.5 mM sodium 3-mercaptopyruvate. The plate was sealed with vinyl adhesive films and incubated for 1 h at 37 °C. After the above mentioned incubation times, the CBS, CSE and MST reaction plates were kept on ice for 15 min. Then, 110 µl of 4% zinc acetate were dispensed to each well by punching a hole through the strip with a gas-tight Hamilton syringe. After 15-min incubation on ice, the films were removed and 15 µl of 60 mM NNDPD (3.6 mM final concentration) and 15 µl of 90 mM $FeCl_3$ (5.4 mM final concentration) were dispensed to each well (final volume: 250 µl). The plate was incubated for 10 min at room temperature in the dark and the absorbance measured afterwards at 690 nm. Data were acquired using the plate reader Thermo Scientific Appliskan Multimode.

Statistical Analysis

The Z'-factor was evaluated for each assay as described in [57]. Data were reported in the tables with their corresponding Z-score and coefficient of variation (CV). A |Z-score| threshold value of 3 was assumed to evaluate the effect of the screened compounds. All calculations were performed using Excel (Microsoft).

DATA AVAILABILITY

The datasets generated and/or analysed during the current study are available from the corresponding author on reasonable request.

ACKNOWLEDGMENTS

JBV acknowledges IF/01004/2014/CP1244/CT0011 Grant from Fundação para a Ciência e Tecnologia (FCT) and iNOVA4Health Research Unit (LISBOA-01-0145-FEDER-007344), which is cofunded by FCT / Ministério da Ciência e do Ensino Superior, through national funds, and by FEDER under the PT2020 Partnership Agreement. The grants PNR-CNR Aging Program 2012–2014 and PRIN 20158EB2CM_003 by Ministero dell'Istruzione, dell'Università della Ricerca of Italy are acknowledged by AG. Support of Latvian State Program "Biomedicine" (2014 – 2018) for synthesis of compounds is acknowledged by ZK, IB, EB, BV and GD. The authors are grateful to Dr. Matthias Frech (Head of Molecular Interaction & Biophysics at Merck KGaA, Darmstadt, Germany), for fruitful discussions regarding the statistical analysis.

AUTHOR CONTRIBUTIONS

JBV, AG, LS, and KZ conceived the study and designed the experimental plan. KZ and JBV produced the recombinant enzymes. ZK, IB, EB, BV and GD synthesized and characterized the pyridine derivatives. PMFS, KZ, ARL and JBV designed, performed and analyzed the SPR and DSF assays. KZ, GP, JBV and AG designed, performed and analyzed the fluorimetric and colorimetric H_2S production assays. KZ, PMFS, TMB, AG, and JBV wrote the paper. All authors reviewed the results, contributed to data interpretation and critical revision of the manuscript, and approved the final version of the manuscript.

FIGURE LEGENDS

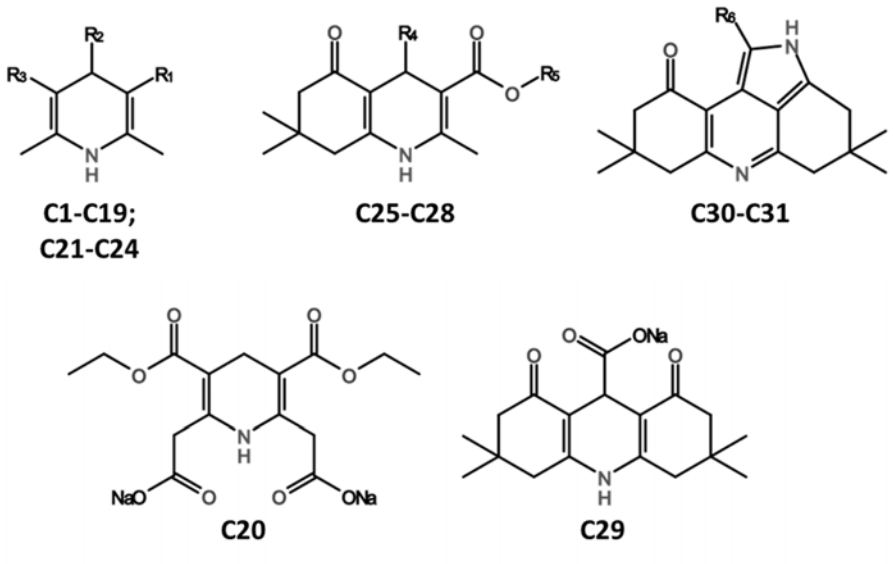

Figure 1. Chemical structures of pyridine derivatives.

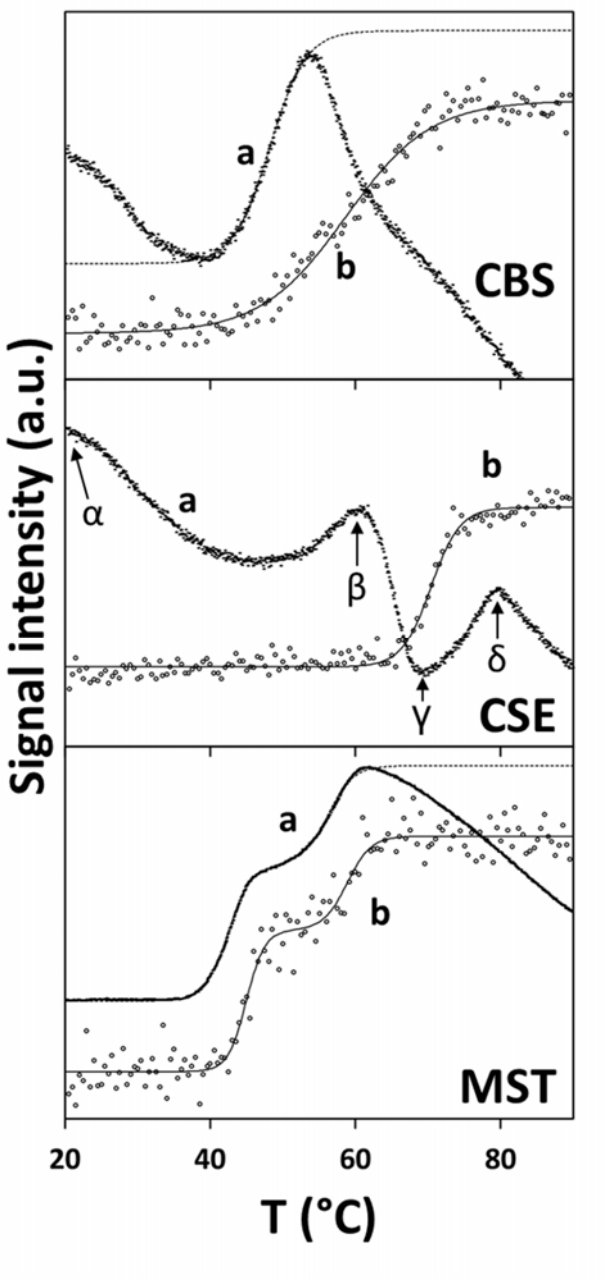
Signal intensity (a.u.)
a
b
CBS
α
a
β
b
δ
γ
CSE
a
b
MST
20
40
60
80
T (°C)

Figure 2. Thermal denaturation profiles of human H_2S-synthesizing enzymes. Thermal denaturation profiles of recombinant human cystathionine β-synthase (CBS, *top panel*), cystathionine γ-lyase (CSE, *middle panel*) and 3-mercaptopyruvate sulfurtransferase (MST, *bottom panel*), obtained by differential scanning fluorimetry (DSF, short dashed points, curves marked with 'a') or Far-UV circular dichroism spectropolarimetry (CD, hollow circles, curves marked with 'b').

CBS

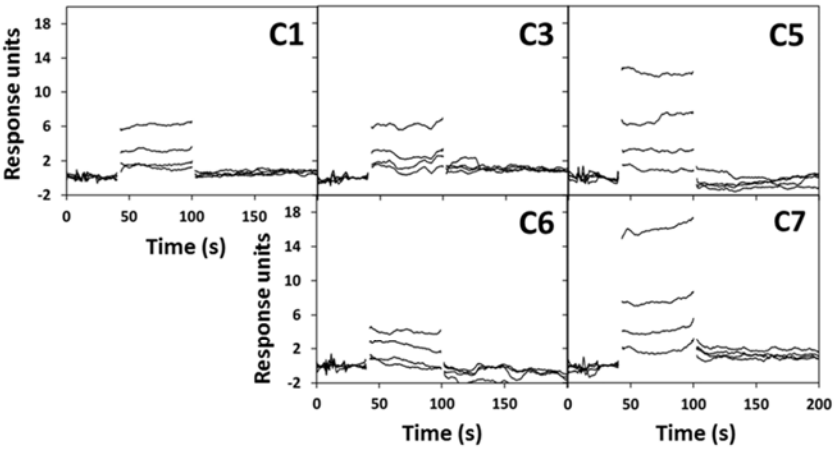
C1
C3
C5
C6
C7
Response units
Time (s)

CSE

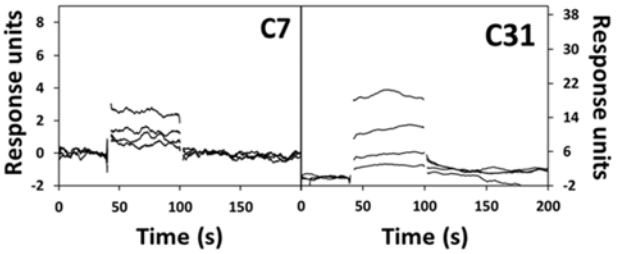
C7
C31
Response units
Time (s)

MST

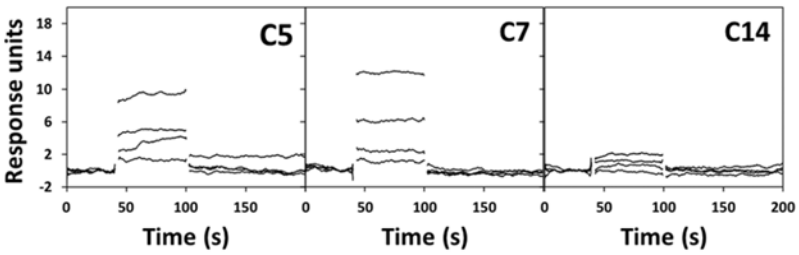
C5
C7
C14
Response units
Time (s)

Figure 3. Identification of interacting compounds by surface plasmon resonance. SPR sensorgrams obtained for the interaction between immobilized recombinant human cystathionine β-synthase (CBS, t*op panel*), cystathionine γ-lyase (CSE, *middle panel*) or 3-mercaptopyruvate sulfurtransferase (MST, *bottom panel*) with the indicated pyridine derivatives at 25, 50, 100 and 200 μM.

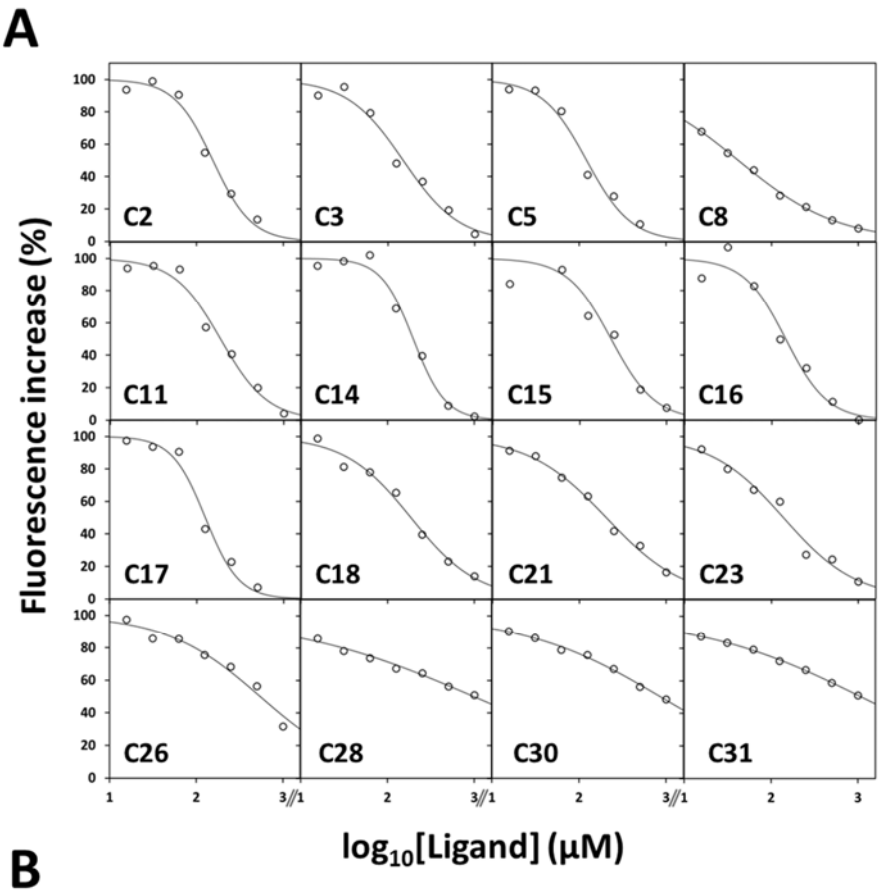
A
Fluorescence increase (%)
C2
C3
C5
C8
C11
C14
C15
C16
C17
C18
C21
C23
C26
C28
C30
C31
log10[Ligand] (μM)
B
Fluorescence increase (%)
* p<0.05
** p<0.01
*** p<0.001
GYY4137
Blank
C2
C3
C5
C8
C11
C14
C15
C16
C17
C18
C21
C23
C26
C28
C30
C31

Figure 4. Effect of compounds on fluorimetric H_2S detection. Effect of the indicated pyridine derivatives on the H_2S-selective fluorescent probe AzMC. Initial slope of the fluorescence increase on reaction of the probe with H_2S synthesized by tCBS. Experimental conditions as described in the Materials and Methods section.

Table 1. Pyridine derivatives screened against human H_2S-synthesizing enzymes.

Comp	R1	R2	R3	R4	R5	Ref.
C1	$COOC_2H_5$	COONa	$COOC_2H_5$	n/a	n/a	[301]
C2	$COOCH(CH_3)_2$	COONa	$COOCH(CH_3)_2$	n/a	n/a	[301]
C3	CN	COONa	CN	n/a	n/a	[301]
C4	$COCH_3$	COONa	$COCH_3$	n/a	n/a	[301]
C5	$COOC_2H_5$	$COOC_2H_5$	$COOC_2H_5$	n/a	n/a	[301]
C6	$COOCH_2COONa$	H	$COOCH_2COONa$	n/a	n/a	[302]
C7	$COOCH_2COOC_2H_5$	H	$COOCH_2COOC_2H_5$	n/a	n/a	[302]
C8	$COOCH_2COONa$	CH_3	$COOCH_2COONa$	n/a	n/a	[302]
C9	$COOCH_2COOC_2H_5$	CH_3	$COOCH_2COOC_2H_5$	n/a	n/a	[302]
C10	$COOCH_2COOC_2H_5$	C_2H_5	$COOCH_2COOC_2H_5$	n/a	n/a	[302]
C11	$COOCH_2COONa$	C_2H_5	COOCH2COONa	n/a	n/a	[302]
C12	$COOC_2H_5$	$CH(COONa)(CH_2)_2COONa$	$COOC_2H_5$	n/a	n/a	[299]
C13	$COOC_2H_5$	$CONH(CH_2)_2SO_3Na$	$COOC_2H_5$	n/a	n/a	[299]
C14	$COOC_2H_5$	$CONH(CH_2)_3COONa$	$COOC_2H_5$	n/a	n/a	[299]
C15	$COOC_2H_5$	$CONH(CH_2)_2COOH$	$COOC_2H_5$	n/a	n/a	[299]
C16	$COOC_2H_5$	$COOCH_2CONH_2$	$COOC_2H_5$	n/a	n/a	This work
C17	$COOC_2H_5$	$COOCH_2COOC_2H_5$	$COOC_2H_5$	n/a	n/a	This work
C18	$COOC_2H_5$	$COOCH_2COC_6H_5$	$COOC_2H_5$	n/a	n/a	This work
C19	$COOC_2H_5$	$COOCH_2COC_6H_4OCH_3$-4	$COOC_2H_5$	n/a	n/a	This work
C20	n/a	n/a	n/a	n/a	n/a	[304]
C21	$COO(CH_2)_2COONa$	$COOCH_3$	$COO(CH_2)_2COONa$	n/a	n/a	[303]
C22	$COOCH_2COOCH_3$	COOH	$COOCH_2COOCH_3$	n/a	n/a	[303]
C23	$COOCH_2COOC_2H_5$	thienyl	$COOCH_2COOC_2H_5$	n/a	n/a	[303]
C24	$COOCH_2COONa$	thienyl	$COOCH_2COONa$	n/a	n/a	[303]
C25	n/a	n/a	n/a	COOH	C_2H_5	This work
C26	n/a	n/a	n/a	$COOC_2H_5$	C_2H_5	This work
C27	n/a	n/a	n/a	thienyl	$CH_2COOC_2H_5$	This work
C28	n/a	n/a	n/a	thienyl	CH_2COONa	This work
C29	n/a	n/a	n/a	n/a	n/a	[300]
C30	n/a	n/a	n/a	n/a	n/a	[298]
C31	n/a	n/a	n/a	n/a	n/a	[298]

Table 2. Effect of pyridine derivatives on the H_2S-synthesizing activity of tCBS, CSE and MST.

	tCBS			CSE			MST		
	H_2S production (%) (Z' factor: 0.60)	**CV**	**Z-score**	**H_2S production (%) (Z' factor: 0.78)**	**CV**	**Z-score**	**H_2S production (%) (Z' factor: 0.51)**	**CV**	**Z-score**
Control	100.0 (N = 18)	11.6	---	100.0 (N=9)	12.0	---	100.0 (N=9)	6.8	
Blank	5.4 (N=18)	37.2	8.2	5.2 (N=9)	27.5	7.9	16.9 (N=9)	48.5	12.1
AOAA	8.8	12.1	**7.9**	6.7	59.7	**7.8**	---	---	---
C1*	98.4	3.4	0.1	102.3	2.8	-0.2	103.0	7.8	-0.4
C2	92.4	4.2	0.7	98.4	2.7	0.1	102.5	0.5	-0.4
C3	89.5	5.7	0.9	96.7	2.5	0.3	103.9	5.3	-0.6
C4	77.4	8.2	2.0	101.0	3.0	-0.1	100.0	4.1	0.0
C5	93.5	7.9	0.6	122.0	0.0	-1.8	107.5	0.6	-1.1
C6*	79.8	6.6	1.7	92.6	0.9	0.6	99.7	4.0	0.0
C7	95.1	2.1	0.4	97.3	1.8	0.2	99.9	6.8	0.0
C8	92.4	9.8	0.7	94.0	1.4	0.5	87.4	7.5	1.8
C9	97.1	1.7	0.2	90.3	3.6	0.8	96.5	3.4	0.5
C10	103.8	11.9	-0.3	98.0	1.0	0.2	98.0	3.7	0.3
C11	108.6	7.3	-0.7	106.9	8.4	-0.6	89.6	0.5	1.5
C12*	97.0	16.7	0.3	90.8	5.4	0.8	103.6	4.0	-0.5
C13	97.9	8.7	0.2	89.8	2.4	0.9	93.1	3.7	1.0
C14	85.0	2.8	1.3	93.0	6.5	0.6	106.3	7.4	-0.9
C15	80.7	1.1	1.7	92.6	2.4	0.6	91.2	2.1	1.3
C16	122.5	1.7	-2.0	93.8	15.3	0.5	104.8	7.9	-0.7
C17	109.2	3.9	-0.8	97.2	7.6	0.2	102.3	3.9	-0.3
C18	105.2	13.2	-0.5	94.4	2.3	0.5	101.9	2.1	-0.3
C19	118.4	3.2	-1.6	96.6	4.4	0.3	103.9	6.6	-0.6
C20*	101.5	1.3	-0.1	116.2	18.8	-1.4	103.4	9.0	-0.5
C21*	79.0	7.6	1.8	101.0	1.0	-0.1	103.3	3.1	-0.5
C22	68.3	4.2	2.7	100.6	8.2	-0.1	107.7	1.8	-1.1
C23	115.8	8.7	-1.4	91.3	3.3	0.7	103.4	2.0	-0.5
C24*	94.7	5.5	0.5	112.2	1.6	-1.0	101.6	3.6	-0.2
C25	94.7	14.1	0.5	102.9	21.7	-0.2	106.6	3.5	-1.0

C26	97.5	23.2	0.2	99.8	1.5	0.0	97.2	4.0	0.4
C27	104.8	4.9	-0.4	96.2	3.6	0.3	98.8	1.3	0.2
C28	93.8	16.7	0.5	91.8	14.0	0.7	108.0	2.7	-1.2
C29	81.3	22.5	1.6	97.4	5.3	0.2	107.6	6.4	-1.1
C30	50.3	12.9	**4.3**	64.2	9.7	**3.0**	130.3	2.3	-4.4
C31*	60.7	24.6	**3.4**	38.4	5.1	**5.1**	119.1	6.8	-2.8

* Compounds tested at a final concentration of 500 µM rather than 1 mM

SUPPLEMENTARY INFORMATIONS

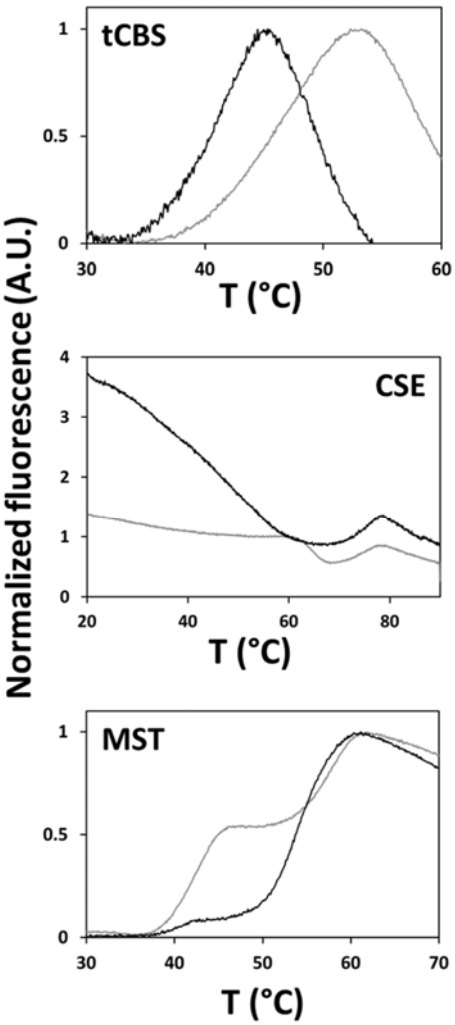

Supplementary Figure S1. Positive and negative controls for differential scanning fluorimetry thermal denaturation profiles of human H_2S-synthesizing enzymes. Thermal denaturation profiles of recombinant human

cystathionine β-synthase (tCBS, *top panel*), cystathionine γ-lyase (CSE, *middle panel*) and 3-mercaptopyruvate sulfurtransferase (MST, *bottom panel*), obtained by differential scanning fluorimetry (DSF) in the absence (grey line; positive control) or presence (black line; negative control) of 200 μM aminooxyacetic acid (for tCBS and CSE) or 2 mM 3-mercaptopyruvate (for MST).

Supplementary Table S1 - Differential scanning fluorimetry analysis of the interaction between human tCBS and pyridine derivatives

	T_{m1} (Z' factor: -1.58)				T_{m2} (Z' factor: 0.08)				$T_{m'Ave'}$ (Z' factor: -0.28)			
	Mean (°C)	CV (%)	Z-score	ΔT_{m1} (°C)	Mean (°C)	CV (%)	Z-score	ΔT_{m2} (°C)	Mean (°C)	CV (%)	Z-score	$\Delta T_{m'Ave'}$ (°C)
Positive control (DMSO; $N = 23$)	**42.3**	**4.0**	---	---	**48.4**	**1.5**	---	---	**45.6**	**1.8**	---	---
Negative control (AOAA in DMSO; $N = 25$)	**37.7**	**5.9**	**2.7**	**-4.6**	**42.2**	**2.8**	**8.5**	**-6.2**	**40.3**	**3.7**	**6.5**	**-5.3**
C1	42.6	4.7	-0.1	0.2	49.4	1.1	-1.3	1.0	46.5	1.8	-1.1	0.9
C2	39.5	3.9	1.6	-2.8	48.5	0.5	-0.2	0.1	44.6	2.6	1.2	**-1.0**
C3	40.7	3.4	0.9	-1.6	48.9	0.5	-0.7	0.5	45.5	0.4	0.2	-0.1
C4	40.0	4.5	1.4	-2.4	48.7	0.5	-0.5	0.4	45.3	1.5	0.4	-0.3
C5	41.8	1.8	0.3	-0.5	48.7	0.3	-0.4	0.3	45.9	0.0	-0.3	0.3
C6	40.8	4.7	0.9	-1.6	48.8	0.5	-0.6	0.4	45.7	0.6	-0.2	0.1
C7	41.6	0.8	0.5	-0.8	48.7	0.2	-0.4	0.3	45.6	1.1	0.0	0.0
C8	41.4	0.6	0.5	-0.9	48.8	0.6	-0.5	0.4	45.7	0.3	-0.2	0.1
C9	---	---	---	---	---	---	---	---	---	---	---	---
C10	---	---	---	---	---	---	---	---	---	---	---	---
C11	40.5	2.4	1.1	-1.8	48.7	0.5	-0.4	0.3	45.9	0.6	-0.3	0.3
C12	40.1	4.9	1.3	-2.2	48.8	0.5	-0.6	0.4	45.5	0.8	0.2	-0.1
C13	42.8	2.5	-0.3	0.5	49.2	0.5	-1.1	0.8	46.4	0.9	-1.0	0.8
C14	43.4	7.1	-0.6	1.0	49.4	1.5	-1.4	1.0	46.7	2.4	-1.3	**1.1**
C15	41.9	2.0	0.3	-0.5	48.7	0.5	-0.4	0.3	46.0	0.4	-0.5	0.4
C16	41.5	1.8	0.5	-0.9	48.7	0.4	-0.5	0.3	45.9	1.2	-0.3	0.3
C17	41.1	1.5	0.7	-1.2	48.6	0.2	-0.3	0.2	45.5	0.5	0.1	-0.1
C18	39.3	2.3	1.8	-3.1	48.4	1.6	-0.1	0.0	45.1	0.8	0.6	-0.5
C19	---	---	---	---	---	---	---	---	---	---	---	---
C20	39.7	4.0	1.6	-2.7	48.6	0.7	-0.3	0.3	45.5	1.3	0.1	-0.1
C21	40.9	1.9	0.8	-1.4	48.7	0.2	-0.5	0.4	46.0	0.2	-0.4	0.4
C22	39.8	3.7	1.5	-2.5	48.5	0.8	-0.1	0.1	45.2	0.8	0.5	-0.4
C23	---	---	---	---	---	---	---	---	---	---	---	---
C24	42.6	1.2	-0.2	0.3	48.9	0.4	-0.7	0.5	46.1	0.2	-0.6	0.5
C25	42.8	2.9	-0.3	0.4	49.2	0.7	-1.1	0.8	46.3	0.9	-0.8	0.7
C26	43.4	1.9	-0.6	1.0	49.5	0.5	-1.5	1.1	46.5	1.0	-1.1	0.9
C27	43.2	2.1	-0.5	0.8	48.9	0.3	-0.7	0.5	45.9	1.2	-0.4	0.3
C28	43.6	4.4	-0.8	1.3	49.6	1.2	-1.6	1.2	47.4	0.8	-2.1	**1.8**
C29	44.3	4.1	-1.2	2.0	49.8	1.2	-1.9	1.4	47.0	1.4	-1.7	**1.4**
C30	42.5	2.8	-0.1	0.1	48.8	1.1	-0.5	0.4	46.0	1.7	-0.5	0.4
C31	42.2	2.3	0.1	-0.2	48.4	0.4	0.0	0.0	45.9	1.4	-0.3	0.3

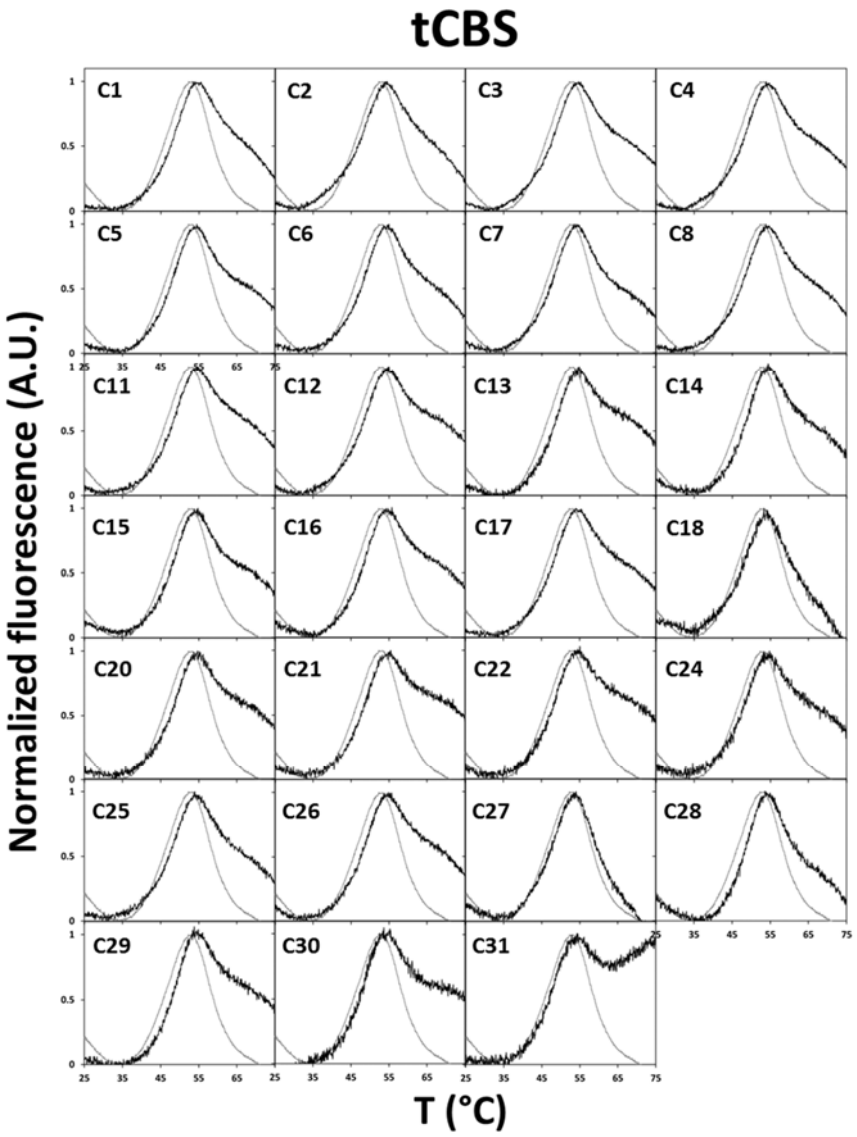

Supplementary Figure S2. Differential scanning fluorimetry thermal

denaturation profiles of human tCBS incubated with pyridine derivatives.

Experimental conditions as described in the Materials and Methods section.

Supplementary Table S2 - Differential scanning fluorimetry analysis of the interaction between human CSE and pyridine derivatives

	Ratio A (Z' factor: 0.53)			Ratio B (Z' factor: 0.31)		
	Mean	CV (%)	Z-score	Mean	CV (%)	Z-score
Positive control (DMSO; *N* = 26)	1.4	7.9	---	0.6	8.1	---
Negative control (AOAA in DMSO; *N* = 26)	3.8	7.1	**-22.1**	0.9	3.5	**-7.3**
C1	2.1	22.7	**-6.2**	0.4	2.9	**3.7**
C2	2.1	18.0	**-6.3**	0.4	7.1	**3.9**
C3	1.7	28.6	-2.4	0.4	5.1	**4.0**
C4	1.7	22.9	-2.6	0.4	1.2	2.9
C5	1.6	17.5	-2.1	0.4	2.9	**3.7**
C6	1.6	23.6	-2.1	0.4	5.5	**3.4**
C7	1.6	10.2	-2.0	0.4	8.0	**4.2**
C8	1.5	8.3	-1.5	0.4	8.2	**3.6**
C9	2.2	2.8	**-7.2**	0.4	6.8	**3.8**
C10	---	---	---	---	---	---
C11	1.4	3.7	0.2	0.4	1.7	2.9
C12	1.3	3.2	1.0	0.4	6.7	**3.3**
C13	1.2	6.4	1.8	0.4	5.7	2.8
C14	1.3	2.6	0.8	0.5	4.0	2.4
C15	1.4	10.8	-0.3	0.5	6.3	2.0
C16	1.4	4.4	-0.4	0.4	2.8	2.9
C17	1.7	21.0	**-3.3**	0.4	3.9	**3.6**
C18	---	---	---	---	---	---
C19	---	---	---	---	---	---
C20	1.3	3.5	1.0	0.5	2.0	1.6
C21	1.3	6.2	1.1	0.4	5.2	2.6
C22	1.3	10.3	0.4	0.5	1.2	1.6
C23	---	---	---	---	---	---
C24	1.4	7.1	-0.2	0.5	8.2	1.8
C25	1.3	2.4	0.5	0.4	5.9	2.8
C26	1.4	4.1	-0.1	0.4	4.4	**3.2**
C27	1.3	9.7	0.5	0.6	1.0	-1.4
C28	1.3	13.1	0.5	0.5	4.9	2.5
C29	1.2	6.7	2.1	0.6	1.8	-1.5
C30	1.0	2.0	**3.2**	0.7	1.4	**-3.8**
C31	1.0	4.6	**3.6**	0.8	1.2	**-4.0**

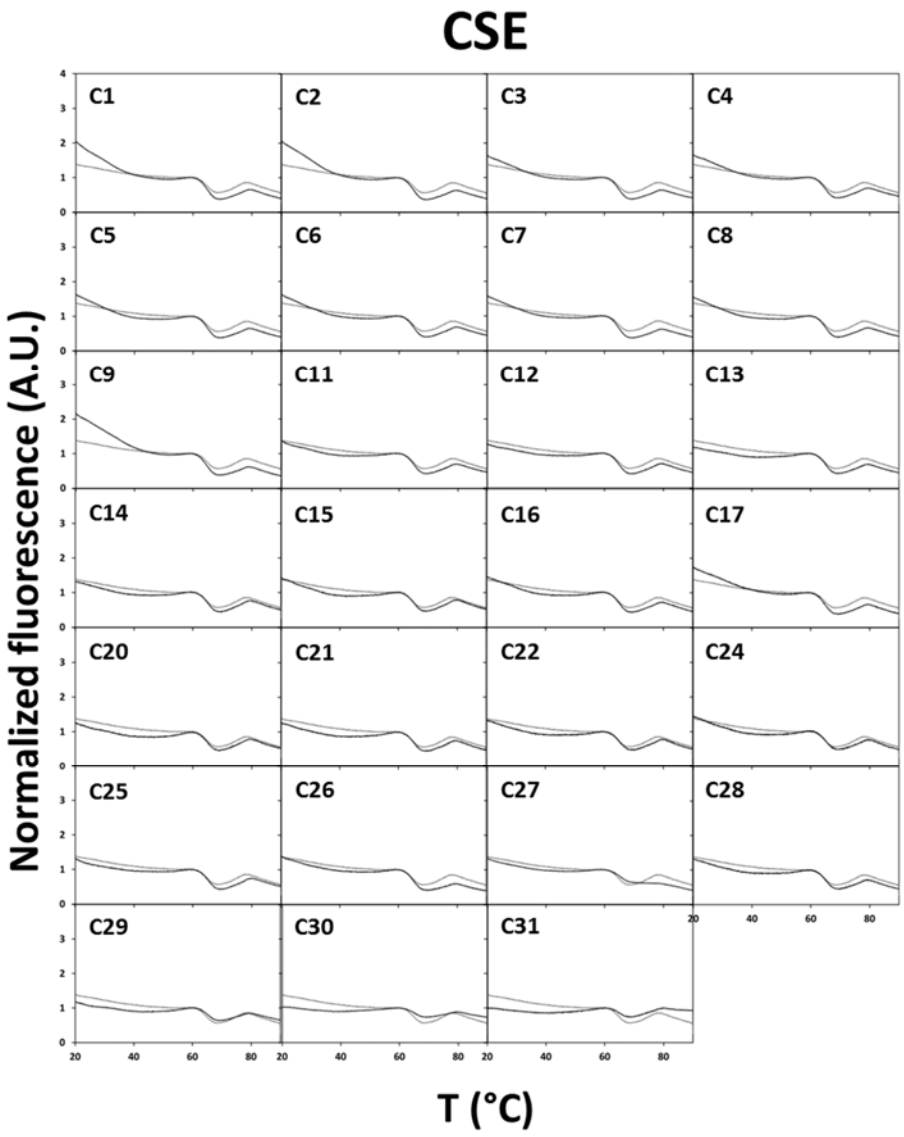

Supplementary Figure S3. Differential scanning fluorimetry thermal

denaturation profiles of human CSE incubated with pyridine derivatives. Experimental conditions as described in the Materials and Methods section.

Supplementary Table S3 - Differential scanning fluorimetry analysis of the interaction between human MST and pyridine derivatives

	Frac (Z' factor: 0.50)			T_{m1} (Z' factor: -0.32)				T_{m2} (Z' factor: 0.68)				$T_{m'Ave'}$ (Z' factor: -0.06)			
	Mean	CV (%)	Z-score	Mean (°C)	CV (%)	Z- score	ΔT_{m1} (°C)	Mean (°C)	CV (%)	Z-score	ΔT_{m2} (°C)	Mean (°C)	CV (%)	Z-score	$\Delta T_{m'Ave'}$ (°C)
Positive control (N = 31)	**0.54**	**10.9**	---	**41.9**	**0.6**	---	**0**	**57.2**	**0.3**	---	**0**	**49.2**	**2.4**	---	**0**
Negative control (N = 28)	**0.05**	**46.0**	**8.3**	**40.4**	**1.0**	**6.0**	**-1.5**	**54.1**	**0.3**	**19.5**	**-3.1**	**53.5**	**0.6**	**-3.6**	**4.3**
C1	0.51	9.6	0.5	41.3	0.3	2.4	-0.6	56.6	0.2	**4.0**	-0.6	48.7	1.6	0.4	-0.5
C2	0.48	7.6	1.0	40.6	0.4	**5.2**	**-1.3**	56.5	0.3	**4.2**	-0.7	48.8	1.2	0.3	-0.4
C3	0.53	5.6	0.2	42.1	0.2	-0.6	0.2	56.7	0.2	**3.5**	-0.5	48.9	0.9	0.2	-0.3
C4	0.52	6.7	0.3	41.8	0.2	0.6	-0.2	56.8	0.2	2.7	-0.4	48.9	0.9	0.2	-0.3
C5	0.59	3.8	-0.7	42.2	0.5	-1.3	0.3	56.6	0.3	**4.0**	-0.6	48.2	0.4	0.8	**-1.0**
C6	0.55	3.1	-0.1	42.3	0.2	-1.5	0.4	56.8	0.2	2.4	-0.4	48.8	0.5	0.3	-0.3
C7	0.57	3.5	-0.5	41.9	0.5	-0.1	0.0	56.7	0.2	**3.4**	-0.5	48.3	0.6	0.8	-0.9
C8	0.58	6.0	-0.7	42.2	0.3	-1.2	0.3	56.8	0.1	2.9	-0.4	48.3	1.0	0.7	-0.9
C9	0.53	2.3	0.2	42.1	0.5	-0.6	0.2	56.4	0.2	**5.3**	-0.8	48.8	0.3	0.3	-0.4
C10	0.49	14.1	0.9	41.9	0.2	-0.1	0.0	56.4	0.0	**5.4**	-0.8	49.3	2.1	-0.1	0.1
C11	0.51	6.2	0.5	42.1	0.1	-0.9	0.2	56.6	0.1	**3.7**	-0.6	49.2	0.9	0.0	0.0
C12	0.54	3.9	0.0	42.4	0.1	-1.9	0.5	56.7	0.1	**3.3**	-0.5	48.9	0.7	0.2	-0.3
C13	0.59	4.2	-0.8	42.4	0.4	-1.9	0.5	56.6	0.1	**3.6**	-0.6	48.2	0.8	0.8	**-1.0**
C14	0.54	5.2	0.0	42.2	0.4	-1.0	0.3	56.7	0.2	**3.0**	-0.5	48.8	0.7	0.3	-0.4
C15	0.56	3.8	-0.2	42.1	0.3	-0.6	0.2	56.8	0.1	2.7	-0.4	48.6	0.8	0.5	-0.6
C16	0.56	9.4	-0.3	42.3	0.1	-1.5	0.4	56.7	0.1	**3.3**	-0.5	48.6	1.5	0.5	-0.6
C17	0.54	2.2	0.1	42.3	0.1	-1.4	0.4	56.6	0.1	**4.0**	-0.6	48.9	0.3	0.2	-0.3
C18	0.57	5.6	-0.5	42.3	0.1	-1.5	0.4	56.6	0.0	**3.6**	-0.6	48.4	0.9	0.6	-0.8
C19	---	---	---	---	---	---	---	---	---	---	---	---	---	---	---
C20	0.56	7.0	-0.2	42.1	0.1	-0.7	0.2	56.7	0.3	**3.5**	-0.5	48.6	1.3	0.5	-0.6
C21	0.57	6.7	-0.4	42.2	0.7	-1.2	0.3	56.5	0.1	**4.6**	-0.7	48.4	1.4	0.6	-0.8
C22	0.53	4.5	0.2	42.3	0.4	-1.7	0.4	56.7	0.4	**3.2**	-0.5	49.1	0.9	0.1	-0.1
C23	---	---	---	---	---	---	---	---	---	---	---	---	---	---	---
C24	0.50	5.8	0.6	42.4	1.6	-1.9	0.5	56.5	0.1	**4.2**	-0.7	49.4	0.7	-0.2	0.2
C25	0.57	4.2	-0.5	42.0	0.2	-0.4	0.1	56.8	0.1	2.3	-0.4	48.3	0.7	0.7	-0.8
C26	0.60	6.1	-1.0	42.4	0.1	-1.8	0.5	56.7	0.2	**3.4**	-0.5	48.1	1.1	0.9	**-1.1**
C27	0.61	7.8	-1.1	42.5	0.4	-2.1	0.5	56.7	0.2	**3.0**	-0.5	48.1	1.5	0.9	**-1.1**
C28	0.56	5.2	-0.3	42.3	0.5	-1.6	0.4	56.7	0.1	**3.2**	-0.5	48.6	0.8	0.5	-0.5
C29	0.53	11.0	0.3	42.3	0.5	-1.7	0.4	56.3	0.5	**5.9**	-0.9	48.9	1.3	0.2	-0.2
C30	0.55	0.4	-0.2	40.8	0.2	**4.4**	**-1.1**	56.4	0.4	**4.8**	-0.8	47.8	0.3	1.1	**-1.4**
C31	0.43	15.5	1.9	40.2	0.1	**6.7**	**-1.7**	57.0	0.3	1.2	-0.2	49.8	2.5	-0.5	0.6

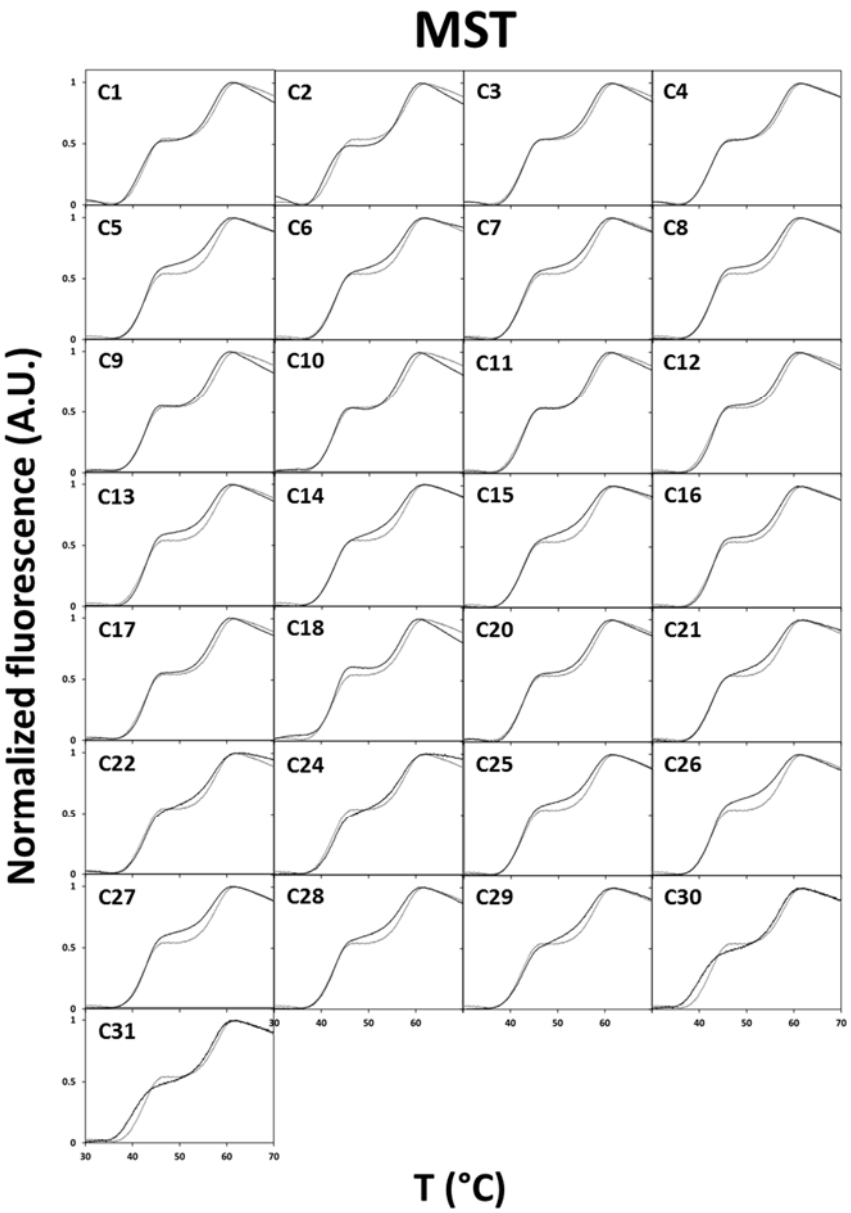

Supplementary Figure S4. Differential scanning fluorimetry thermal denaturation profiles of human MST incubated with pyridine derivatives. Experimental conditions as described in the Materials and Methods section.

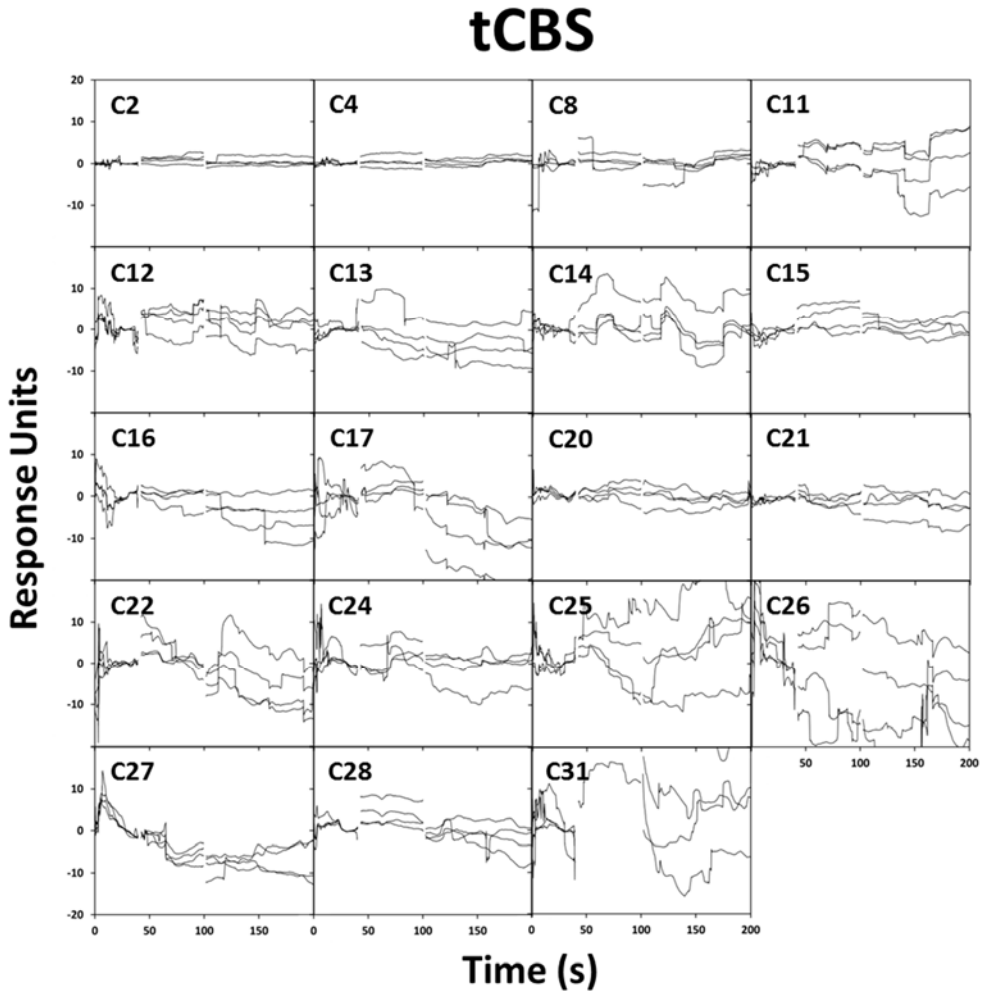

Supplementary Figure S5. Surface plasmon resonance sensorgrams for human tCBS incubated with pyridine derivatives. Experimental conditions as described in the Materials and Methods section.

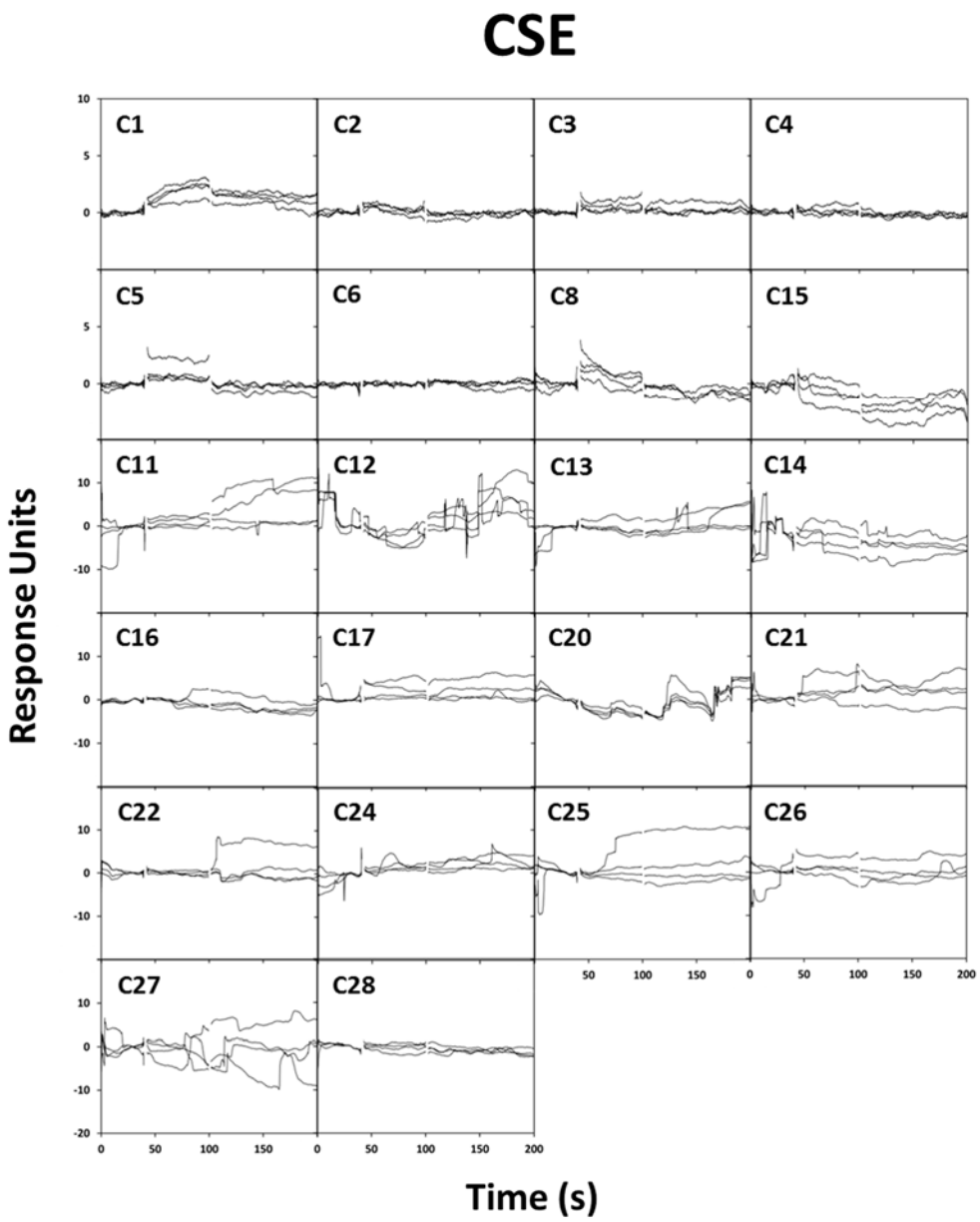

Supplementary Figure S6. Surface plasmon resonance sensorgrams for human CSE incubated with pyridine derivatives. Experimental conditions as described in the Materials and Methods section.

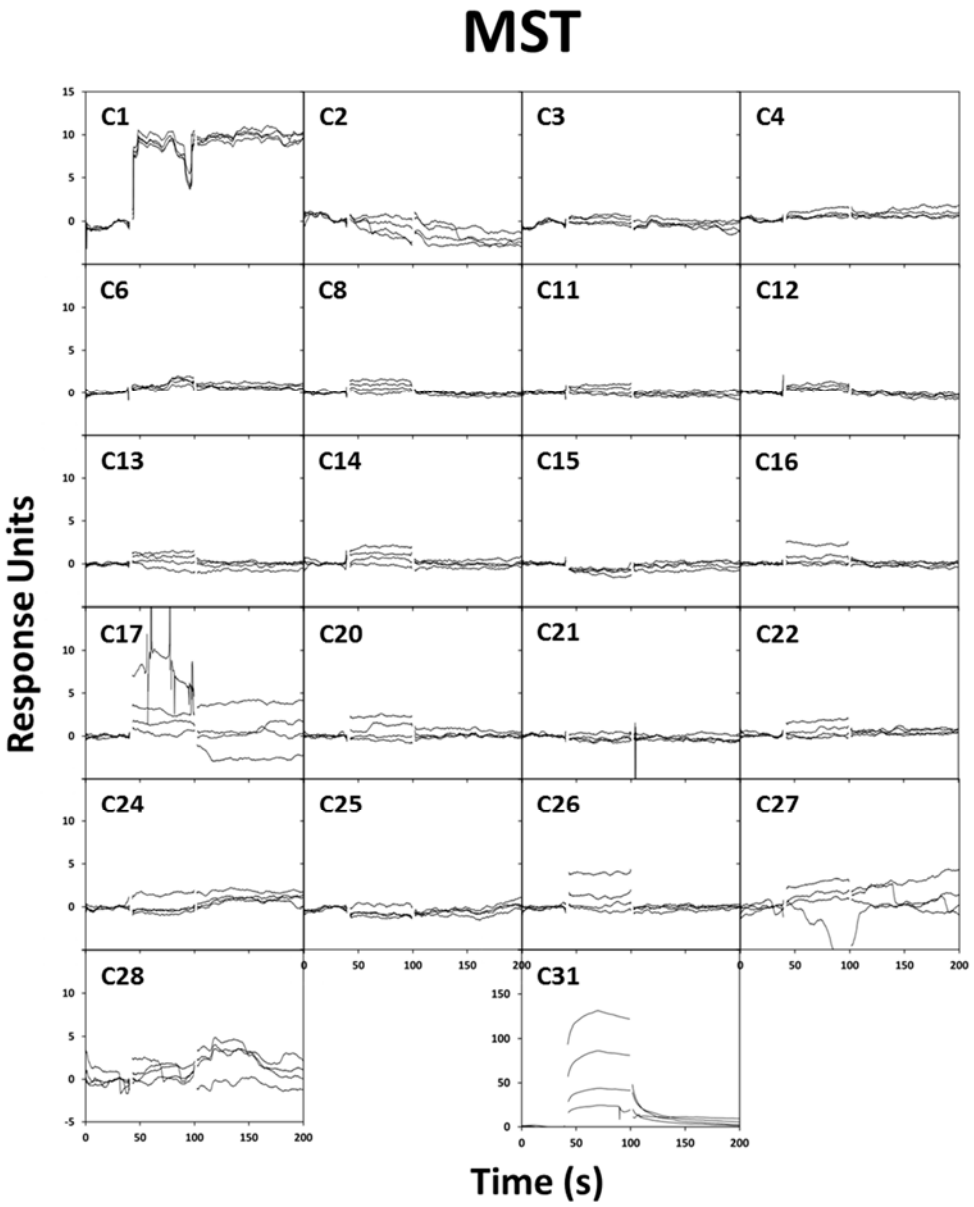

Supplementary Figure S7. Surface plasmon resonance sensorgrams for human MST incubated with pyridine derivatives. Experimental conditions as described in the Materials and Methods section.

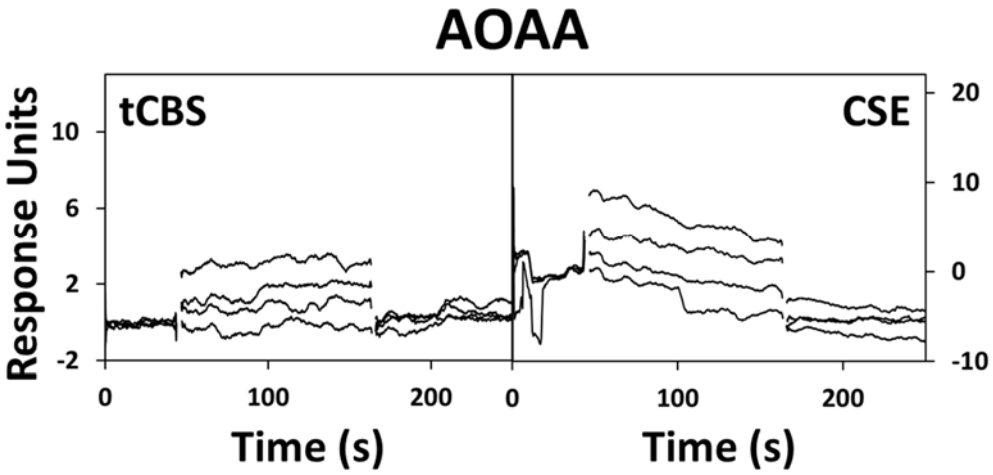

Supplementary Figure S8. Surface plasmon resonance sensorgrams for human tCBS and CSE incubated with AOAA. Experimental conditions as described in the Materials and Methods section.

Supplementary Table S4 - Effect of compounds on fluorimetric detection of H_2S produced by tCBS. Experiments aimed at evaluating the possible effect of pyridine derivatives on the H_2S-synthesizing activity of tCBS, making use of the H_2S-selective fluorescent probe AzMC. Experimental conditions as described in the Materials and Methods section. Unless otherwise indicated, data represent mean values of triplicate determinations. Compounds were tested at a final concentration of 200 μM.

	Frac (Z' factor: 0.78)		
	Fluorescence (%)	**CV (%)**	**Z-score**
Positive control (*N* = 16)	**100.0**	**6.6**	**---**
Negative control (*N* = 16)	**2.8**	**14.2**	**14.5**
C2	52.8	4.9	7.0
C3	49.4	6.9	7.6
C5	46.6	5.6	8.0
C8	31.2	4.9	10.3
C11	50.2	78.1	7.4
C14	52.6	20.3	7.1
C15	43.0	14.6	8.5
C16	28.2	6.4	10.7
C17	40.9	4.4	8.8
C18	46.7	6.8	8.0
C21	37.6	13.1	9.3
C23	34.9	4.2	9.7
C26	41.9	7.2	8.7
C28	51.3	7.4	7.3
C30	46.5	7.4	8.0
C31	49.9	5.3	7.5

Supplementary Table S5 - Effect of compounds on fluorimetric detection of H_2S released by GYY4137. Experiments showing interference of pyridine derivatives with detection of GYY4137-released H_2S by the selective fluorescent probe AzMC. Experimental conditions as described in the Materials and Methods section. Unless otherwise indicated, data represent mean values of triplicate determinations. Compounds were tested at a final concentration of 500 μM.

	Frac (Z' factor: 0.85)		
	Fluorescence (%)	**CV (%)**	**Z-score**
Positive control (*N* = 16)	100.00	7.9	––
Negative control (*N* = 16)	12.3	6.5	11.9
C2	30.9	8.1	**8.7**
C3	38.9	5.0	**7.7**
C5	27.7	6.8	**9.1**
C8	16.6	6.2	**10.5**
C11	65.7	9.7	**4.3**
C14	20.5	13.9	**10.1**
C15	27.3	11.1	**9.2**
C16	24.0	5.4	**9.6**
C17	22.6	23.1	**9.8**
C18	31.1	9.6	**8.7**
C21	20.8	9.1	**10.0**
C23	15.9	23.0	**10.6**
C26	11.7	13.2	**11.2**
C28	22.6	17.3	**9.8**
C30	32.3	6.7	**8.6**
C31	31.7	7.0	**8.6**

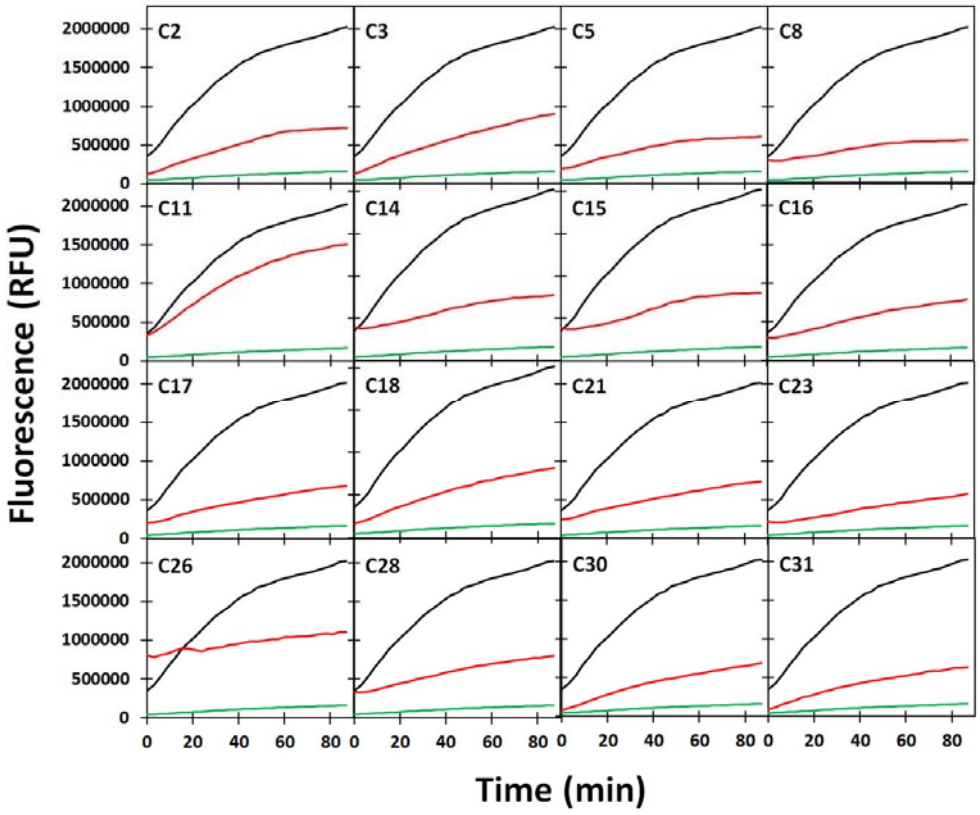

Supplementary Figure S9. Interaction between selected pyridine derivatives and the H_2S detecting fluorescent probe AzMc. H_2S release by GYY 4137 detected by the fluorescent probe AzMc in the absence (black lines) and presence (red lines) of pyridine derivatives. Green line, blank control lacking GYY 4137. Experimental conditions as described in the Materials and Methods section.

Supplementary Table S6 - Effect of compounds on colorimetric detection of H_2S released by GYY4137. Experiments showing no interference of

pyridine derivatives with detection of GYY4137-released H_2S by the methylene blue method. Experimental conditions as described in the Materials and Methods section. Unless otherwise indicated, data represent mean values of triplicate determinations. The asterisk denotes the compounds tested at 500 μM instead of 1 mM final concentration.

	Frac (Z' factor: 0.84)		
	Absorbance (%)	**CV (%)**	**Z-score**
Positive control (*N* = 9)	100,0	7,5	**---**
Negative control (*N* = 9)	4,3	2,9	12.8
C1*	88.7	8.3	1.5
C2	91.7	3.6	1.1
C3	91.7	1.4	1.1
C4	92.8	2.8	1.0
C5	92.9	5.1	0.9
C6*	103.1	3.0	-0.4
C7	100.9	4.7	-0.1
C8	101.7	1.3	-0.2
C9	96.9	5.3	0.4
C10	100.8	2.6	-0.1
C11	82.7	6.0	2.3
C12*	100.2	16.5	0.0
C13	102.7	12.5	-0.4
C14	93.6	9.6	0.9
C15	95.0	9.6	0.7
C16	94.4	13.9	0.8
C17	101.4	0.5	-0.2
C18	103.6	0.8	-0.5
C19	104.0	2.5	-0.5
C20*	91.7	2.2	1.1
C21*	93.3	5.7	0.9
C22	98.6	5.8	0.2
C23	99.0	4.9	0.1

C24*	94.1	2.9	0.8
C25	97.1	7.1	0.4
C26	96.2	3.5	0.5
C27	96.1	2.0	0.5
C28	95.6	1.4	0.6
C29	94.9	3.0	0.7
C30	99.1	7.1	0.1
C31*	96.7	2.8	0.4

RESULTS AND DISCUSSION

PAPER 5

Hydrogen sulfide mediates ALS-related damages in *Drosophila melanogaster* models and human cells

Karim Zuhra[a,b,#], Michela Di Salvio[a,#], Elena Forte[b], Alessandro Giuffrè[a,*] , Gianluca Cestra[a,*]

[a)] *CNR Institute of Molecular Biology and Pathology, Rome, Italy*
[b)] *Department of Biochemical Sciences, Sapienza University of Rome, Rome, Italy*

[#] These authors contributed equally

*To whom correspondence should be addressed:
Dr. Alessandro Giuffrè, Institute of Molecular Biology and Pathology (IBPM), National Research Council of Italy (CNR), Piazzale Aldo Moro 5, I-00185 Rome, Italy. alessandro.giuffre@uniroma1.it

Dr. Gianluca Cestra, Institute of Molecular Biology and Pathology (IBPM), National Research Council of Italy (CNR), Piazzale Aldo Moro 5, I-00185 Rome, Italy. gianluca.cestra@cnr.it

ABSTRACT

Hydrogen sulfide (H_2S), once merely known as a toxic gas, has been shown to be a neuromodulator and to provide cytoprotection in the nervous system, raising the possibility that dysregulation of its metabolism could contribute to neurodegeneration. Abnormal sulfide levels were observed in Parkinson's and Alzheimer's diseases and, more recently, in amyotrophic lateral sclerosis (ALS). In the present study, working on *Drosophila melanogaster* and HeLa cell models of ALS, we explored the possibility that a modulation of H_2S metabolism could reduce ALS-associated neurotoxicity. Here, we report that knocking down or pharmacological inhibition of the two H_2S-synthetizing enzymes cystathionine β-synthase (CBS) and cystathionine

γ-lyase (CSE) resulted in ameliorative phenotypes. These data may contribute to shed light on the molecular mechanism underlying the selective degeneration of motoneurons in ALS patients, which so far remains an unsolved question.

ABBREVIATIONS

Amyotrophic lateral sclerosis (ALS), cystathionine β-synthase (CBS), cystathionine γ-lysase (CSE), hydrogen sulfide (H_2S), integrated stress response (ISR), motoneurons (MNs), nitric oxide (NO), protein phosphatase-1 (PP1c), stress granules (SGs), TAR DNA-binding protein 43 (TDP43).

1. INTRODUCTION

In the last few decades, gasotransmitters such as hydrogen sulfide (H_2S) and nitric oxide (NO), have emerged as virtually ubiquitous in all body systems and involved in the regulation of different physiological processes, such as blood flow, energy metabolism, inflammation and stress response [15, 277]. The role of H_2S in the nervous system has been extensively studied, being implicated in both neuromodulation and neuroprotection [4, 109]. Unlike other neurotransmitters and due to its gaseous nature, H_2S cannot be pooled in vesicles, but it is stored as zero-valent sulfur species also called sulfane sulfur species, including persulfides and polysulfides [305]. The signalling function of H_2S is mainly achieved *via* persulfidation of reactive cysteine thiols of target proteins [14, 57]. In this respect, it has been demonstrated persulfides and polysulfides are more reactive than H_2S, and the biological effects of sulfide were suggested to be at least in part mediated by sulfane sulfur species [306-308]. H_2S is biosynthesized by two cytosolic enzymes, cystathionine β-synthase (CBS) and cystathionine γ-lysase (CSE) [127], and by 3-

mercaptopyruvate sulfurtranferase, partly localized in the mitochondrion [39]. The tissue distribution of these enzymes is not homogeneous, as confirmed for instance by the lack of CBS in the cardiovascular and respiratory systems where, in turn, CSE is abundantly expressed. Interestingly, the three H_2S synthesizing enzymes are all present in the central nervous system, where CBS seems to play a major role. CBS is mainly expressed in astrocytes, while CSE was reported to be localized in neurons, and MST in both neurons and astrocytes [16]. H_2S is oxidatively catabolized in mitochondria where, acting as a substrate of the electron transport chain, it sustains cellular bioenergetics by stimulating ATP synthesis [5, 46]. On the other hand, at higher concentration H_2S inhibits cytochrome *c* oxidase, thereby mimicking hypoxia and, eventually leading to mitochondrial respiration failure [24, 30]. The pivotal role of H_2S is proven by the tight regulation of its metabolism at transcriptional, translational and post-translational level, involving also an intricate crosstalk between gasotransmitters. It has been reported that H_2S and NO are intertwined, both sharing analogous biological targets and mutually modulating each other's metabolism [5, 309]. Dysregulated sulfide metabolism has been repeatedly observed in oncological diseases [54], for which CBS has been recognized as a potential therapeutic target [75, 140]. Benserazide-mediated inhibition of CBS has been shown to induce tumor xenograft growth impairment and reduction of colon cancer cell proliferation [125]. The pivotal signalling role of H_2S in neurophysiology is proven by the still growing evidence associating altered sulfide metabolism with several neurological diseases, such as Alzheimer's, Parkinson's, Huntington's disease and amyotrophic lateral sclerosis (ALS) [63, 310].

ALS is a disorder characterized by a gradual degeneration of the brain and spinal cord motoneurons (MNs), resulting in progressive muscle atrophy

with a clinical course culminating in a fatal outcome. The mechanism behind the selective MNs impairment is still unknown. It has been recognized that the ALS phenotype is mostly associated to mutations of key genes such as C9orf72, SOD1, TARDBP and FUS, causing mitochondrial dysfunction and impairment of RNA metabolism [311]. In this respect, one of the most studied protein is TAR DNA-binding protein 43 (TDP43), which is a multitask protein involved in the transcription, splicing and transport of mRNA from the nucleus to the cytoplasm [311]. The localization of TDP43 is mainly nuclear, but under stress conditions, such as oxidative stress, osmotic damage or hypoxia, it translocates to the cytosol where it colocalizes in the so-called stress granules (SGs) [312, 313]. These cytoplasmic structures mediate translational silencing of mRNA aiming to transiently arrest protein synthesis, thus prioritizing an adequate response to stress [314]. The size of SGs and their superstructures with diameters ranging from 0.1 μM to 4 μM seems to increase along with the stress type and duration [315-317]. Accordingly, recovery from exposure to sublethal concentration of arsenite or sorbitol, widely used compounds inducing ALS-like damage in cells and tissues, is characterized by a progressive disassembly of SGs followed by TDP43 countermigration to the nucleus [312, 318]. TDP43 aggregates due to mutation or overexpression, leading to cytotoxicity. Particularly, it was suggested that SGs may act as a trigger of TDP43 aggregation [319]. Hence, SGs generation has emerged as a potential pharmacological target for ALS treatment [320, 321]. The main actors involved in the control of SGs formation are TIA-1 and TIAR, which are recruited upstream by the phosphorylated form of eIF2α (eIF2α-P), which is in turn activated in stress conditions by a group of kinases, including PERK [322]. Conversely, in unstressed conditions, low basal levels of eIF2α-P are kept under control by protein phosphatase-1 (PP1c) [323]. Given the central

role of eIF2α, modulation of its phosphorylation state by targeting either PERK or PP1c has been suggested to be a key element in the activation of integrated stress response (ISR) associated with neurodegenerative diseases [321, 324]. Particularly, it was reported that ISR activation induced by pharmacological inhibition of eIF2α de-phosphorylation correlated with prolonged survival of the SOD1-G93A mouse model of ALS [325-327]. On the other hand, it is believed that one of the contributors to neurodegeneration is the uncontrolled and prolonged activation of ISR. Indeed, it was shown that both in *Drosophila melanogaster* and in neuronal cell models of ALS, pharmacological inhibition of eIF2α phosphorylation or knock-down of PERK rescued TDP43-mediated cytotoxicity [328]. Accordingly, increased eIF2α-P has been proposed to mediate neurodegeneration in C9orf72 ALS models, by enhancing expression of dipeptide-repeat-containing proteins [329]. Moreover, in Alzheimer's and Parkinson's disease, overexpression of eIF2α-P phosphatase restored prosteostasis, whereas phosphatase inhibition increased eIF2α-P levels, exacerbating neurotoxicity [330]. Recently, it has been shown that a physiological mechanism mediating PP1c inhibition is the protein persulfidation at Cys-127, thus offering a mechanistic insight on the engaging of H_2S in the ISR activation [331]. Currently, in line with the Janus-faced character of H_2S, it has been recognized that either increased or decreased H_2S levels are associated to ALS. Nonetheless, in both cases CBS seems to play a central role [61, 310]. In cerebrospinal fluid and plasma of ALS patients high homocysteine levels were measured [332]. As suggested by Miyamoto et al., as CBS is a key enzyme in homocysteine catabolism, its downregulation and the resulting decreased H_2S levels could be key in ALS pathogenesis [126]. On the other hand, high sulfide levels were found in the spinal fluid of ALS patients and cultures of the spinal cord mouse cells expressing SOD1G93A

mutation, suggesting that, during the inflammatory process, hyperactivation of the astroglia leads to H_2S overproduction, which may participate to MNs damage [119]. This apparent discrepancy is somewhat reconciled by the bell-shaped character of H_2S, that is known to exert deleterious effect both at lower and higher than physiological concentrations [333]. This notwithstanding, currently the evidence supporting a potential role of H_2S in ALS progression is still scarce. Here, we investigated the effect of CBS and CSE silencing in a TDP43-overexpressing *Drosophila melanogaster* model of ALS. Furthermore, after inducing ALS-like stress in HeLa cells, we have evaluated the ability of benserazide to revert SGs formation. We report in *vitro* and in *vivo* evidence suggesting that H_2S could be a potential target for the pharmacological treatment of ALS.

2. MATERIALS AND METHODS

The human cervix adenocarcinoma cell line HeLa was purchased from the American Type Culture Collection (ATCC no. CCL-2™). Benserazide (B7283) and the Dulbecco's Modified Eagle Medium (DMEM) cell culture medium (D6546) were purchased from Sigma. Fetal bovine serum (FBS), L-glutamine, streptomycin and penicillin were from Biowest. Anti-TIAR antibody (610352) was from BD Biosciences and the anti-mouse secondary antibody (green) from Hybridoma.

2.1. Cultivation of Drosophila melanogaster and phenotypic study

Drosophila flies were grown on a standard cornmeal, yeast, glucose agar medium at 25°C. All the fly stocks were purchased from Bloomington Drosophila Stock Centre. Particularly, Oregon and GMR-GAL4-wtTDP43 (stock # 51370) were used as healthy and ALS model, respectively. Transgenic

stocks producing dsRNA for RNAi of CBS or CSE *Drosophila* homologs under UAS control were UAS-CBS^{RNAi1} (stock # 36767), UAS-CBS^{RNAi2} (stock # 41877), UAS-CSE^{RNAi1} (stock # 36766) and UAS-CSE^{RNAi3} (stock # 41876). In order to generate the lines GMR-TDP43; UAS-CBS^{RNAi1}, GMR-TDP43; UAS-CBS^{RNAi2}, GMR-TDP43; UAS- CSE^{RNAi1} and GMR-TDP43; UAS-CSE^{RNAi3}, males from the RNAi stock were allowed to mate with virgin females of GMR-TDP43 over 10 days. Phenotypic studies were carried out on F1 progeny flies, which were daily observed and transferred to fresh food. Images of eyes were captured with a Carl Zeiss Stemi 508 microscope equipped with an Axiocam 105 color using a Zen 2 core software. Images were analysed with Photoshop CS4.

2.2.Cell culture and immunofluorescence

HeLa cells were cultured in DMEM containing 4.5 $g \cdot L^{-1}$ glucose, supplemented with 2 mM L-glutamine, 10% (v/v) heat-inactivated FBS, 100 $U \cdot mL^{-1}$ penicillin and 100 $\mu g \cdot mL^{-1}$ streptomycin. Cells (75×10^6 cells/well; 1 ml final volume) were plated on sterile 12 mm glass coverslips (Thermo Fisher), positioned on the bottom of a 24-well plate (Costar), and grown overnight at 37°C and 5% CO_2. Prior to inducing stress, cells were treated for 6 hours with 25 µM, 50 µM or 100 µM benserazide, a CBS inhibitor. Sublethal oxidative stress was induced by treating cells with 1 mM sodium arsenite (NaAS) for 30 min at 37 °C. Adherent cells were washed three times in pre-filtered PBS and fixed with 500 µl of 4% p-formaldeide for 20 min, washed in PBS, and then permeabilized with 0.25 % Triton X-100 in PBS. Sample were blocked with 3% BSA in 0.1% Tween-20 in PBS (blocking solution) and incubated over 1 hour. SGs were targeted by incubation with anti-TIAR antibody diluted in blocking solution (1:100) for 2 hours in humidity chamber.

After three washing steps, samples were incubated with the secondary antibody diluted 1:200 in blocking solution. Finally, after three additional washing steps, coverslips were mounted onto microscope slides with 3 µl of Vectashield mounting medium with DAPI (Vector Laboratories). Microscopy was performed with a Carl Zeiss Axioplan fluorescence microscope, using Image J software and images were analysed with Photoshop CS4. SGs formation was evaluated by randomly capturing images of at least 100 cells. Once established the observational window, the same limits were applied for all the conditions and replicates. Total cell number was evaluated by nuclear staining with DAPI, while cells labelled with anti-TIAR immunostaining were considered positive for SGs formation.

3. RESULTS

CBS knock-down rescues the ALS phenotype in Drosophila melanogaster

In order to evaluate the neurodegeneration associated to overexpression of wtTDP43, we employed *Drosophila melanogaster* using GMR-GAL4 driver to address the phenotypical changes specifically in developing eyes. As shown in Fig. 1, in comparison with control animals (Oregon), the first generation of wtTDP43 flies displayed clear signs of neurodegeneration, presenting tissue abnormalities such as loss of pigmentation and necrotic patches, indicative of considerable cell death. To explore whether the TDP-43-mediated phenotype was dependent on H_2S, we generated CBS- or CSE-knocked down flies by mating GMR-wtTDP43 line with RNAi lines with the aim of obtaining the production of dsRNA in eye imaginal discs during F1 larval development. Interestingly, the F1 progeny of GMR-TDP43;UAS-CBS^{RNAi1}, GMR-TDP43;UAS-CSE^{RNAi1} and GMR-TDP43;UAS-CSE^{RNAi3}

flies partially recovered from ommatidial disorganization, depigmentation, and necrosis. However, targeting CBS with the construct CBS^{RNAi2} did not produce an ameliorative phenotype, necrotic areas being still visible.

SGs formation is reduced upon pharmacological inhibition of CBS

SGs formation was studied by inducing oxidative stress in HeLa cells with sodium arsenite (NaAs). As shown in Fig. 2A, treatment with NaAs strongly induced formation of SGs, as detected by immunofluorescence microscopy using TIAR as SGs marker. Pre-treatment of HeLa cells with 50 μM benserazide significantly reduced size, distribution and frequency of SGs. Particularly, a rescue effect was observed in ≈30 % of the cells (Fig. 2C). However, this effect was not seen either at lower or higher benserazide concentrations. Indeed, at 25 μM benserazide no difference was observed as compared to cells treated with NaAs only, while 100 μM benserazide seemed to induce a change in size but not in frequency of SGs (Fig. 2A, C). Cells treated with the sole benserazide showed signs of stress in a concentration-dependent manner: the drug was ineffective at 25 μM, but induced an occasional or a marked formation of SGs at 50 μM or 100 μM, respectively (Fig. 2B, C).

4. DISCUSSION

In the last decade, substantial progresses have been done in the understanding of the pathogenesis of ALS and in the identification of its causes [334]. Yet, several questions are still unanswered. The dichotomy one pathology-one phenotype is an oversimplification, above all when dealing with neurological diseases, which are usually characterized by an ensemble of disorders. ALS-related mutations have been reported for different genes, often

causing different phenotypes. For instance, mutation of SOD1 gene has been associated to muscular atrophy, while mutation of C9ORF72 and TARDBP genes was observed in ALS patients with frontotemporal dementia and parkinsonism (as reviewed in [311]). Interestingly, a relatively high number of RNA-binding proteins were found to be dysregulated in ALS models, suggesting that defective RNA metabolism might play a central role in the pathogenesis of ALS [335]. For instance, mutation or overexpression of TDP43 induces massive migration of the protein to the cytosol, resulting in nuclear TDP43 depletion and formation of cytoplasmic aggregates. Yet, it is unclear whether cytotoxicity is related to a cytoplasmic TDP43 gain-of-function or nuclear TDP43 loss-of-function, but most likely both of them [319]. The triggering event promoting TDP43 aggregation has been suggested to be the formation of SGs, which is a hallmark of the ISR [319]. From a mechanistic perspective, SGs assembly is coordinated by the nuclear RNA-binding molecules TIAR and TIA-1, which under stress conditions form cytoplasmic inclusion bodies harbouring untranslated mRNA [314]. TDP43 and other proteins involved in shuttling mRNA from the nucleus to the cytosol were found to co-localize with SGs, thus shutting protein synthesis down. The signalling cascade orchestrated by TIAR and TIA-1 is regulated by phosphorylation of eIF2α [324]. Recently, H_2S has been shown to play a role in this process. Indeed, by inhibiting PP1c via persulfidation, H_2S shifts the balance towards eIF2α-P, thus sparking the ISR [331]. In the brain, the cytoprotective effect of H_2S has been extensively explored, this gasotransmitter being involved in the regulation and redistribution of glutathione levels and thus in the scavenging of reactive oxygen species [109, 111]. It is believed that sulfide provides protection under hypoxic/ischemic conditions by upregulation of CBS and CSE [251, 264]. Consistently with its

bell-shaped effect, it was observed that low oxygen availability promotes SQR overexpression, pointing out the importance of keeping sulfide levels under control by enhancing H_2S detoxification [336]. In this light, it is likely that the lack of sulfide oxidizing activity in neuronal cells makes nervous tissues more sensitive to H_2S toxicity [46]. According to Davoli et al., higher H_2S levels may induce hypoxia-like condition, thus suggesting a role for dysregulated sulfide metabolism in MNs degeneration in ALS models [119]. Of relevance for ALS, different in *vitro* and in *vivo* studies have shown that MNs are more vulnerable to hypoxia as compared to other neuronal types [337, 338]. SGs assembly takes place in the presence of environmental stressors like hypoxia, thus making of H_2S a potential actor in ALS neurodegeneration, contributing to activation of ISR. To test this working hypothesis, we worked with TDP43-overexpressing *Drosophila melanogaster*, a well-accepted model of ALS [339, 340]. One of the reasons of the successful employment of this organism in neuroscience, is the possibility to produce fly models of neurodegenerative diseases expressing transgenes in specific tissue using the UAS-GAL4 binary system [341]. Particularly, the GMR-GAL4 driver is commonly employed to target eyes, thus allowing an easy assessment of changing phenotypes [342]. As shown in Fig. 1, the healthy control animals (Oregon) showed ommatidia, the functional units of the fruit fly eyes, characterized by a red pigmentation with the typical mosaic-like distribution. Conversely, flies overexpressing wtTDP43 displayed a widespread necrosis along with a strong depigmentation, likely due to death of retinal pigment cells, overall suggesting a severe neurodegeneration. Indeed, Hanson et al. had previously characterized TDP43-induced eye degeneration in *Drosophila melanogaster* ALS model, reporting a dose-dependent MNs impairment and a marked reduction of lifespan [339]. To determine whether H_2S could exert a role in TDP-43-mediated toxicity, we

knocked down the endogenous CBS or CSE *Drosophila* homologs via transcription of a short hairpin RNA [343]. The F1 progeny, generated by mating wtTDP43-overexpressing and CBS^{RNAi1} lines, revealed a partial recovery of the red pigmentation along with disappearance of necrotic spots, overall indicating an ameliorative phenotype (Fig. 1). Nevertheless, the UAS-CBS^{RNAi2} was much weaker in eliciting the loss-of-function phenotype in F1 progeny, since ommatidial disorganization and necrotic tissue were still clearly visible. This discrepancy could be ascribed to different efficiencies between the different dsRNAs targeting the same gene, leading to off-target effects [344]. Therefore, as CBS was reported to be typically expressed in the astrocytes, this finding supports the hypothesis that microglia plays a role in neurodegeneration by activating ISR in MNs through release of proinflammatory cytokines and signalling molecule such as NO [345, 346]. Conversely, CSE was reported to be mostly localized in neurons, although its expression in the central nervous system is much lower than CBS [347]. This prompted us to explore the effect of downregulation of CSE too, thus reducing the H_2S intrinsically produced in MNs. Consistently, the rescue effect of CSE knock-down observed in the transgenic lines GMR-TDP43;UAS-CSE^{RNA1} and GMR-TDP43;UAS-CSE^{RNA2} was even more evident as compared to UAS-CBS^{RNA1}, showing an enhanced recovery of ommatidial pigmentation and distribution.

To gain more mechanistic insight in ALS-associated neurological damage, we studied the putative involvement of H_2S in mediating SGs formation in HeLa cells. Although concerns may be raised about HeLa cells suitability as a cellular model for neurological disease, currently the use of cancer cell lines in ALS research is quite widespread, as ALS-like damage can be easily induced by exposure to oxidative stressors like NaAs [318]. As shown

in Fig. 2A, treatment of HeLa cells with NaAs resulted in the appearance of large and numerous SGs, as visualized by immunofluorescent staining of TIAR, a known SGs marker. Interestingly, pre-inhibition of CBS with 50 μM benserazide, significantly reduced the size, distribution and frequency of SGs, overall suggesting that CBS inhibition may attenuate arsenite-induced cytotoxicity. However, benserazide effect on SGs assembly seemed to have a short window, being ineffective at 25 μM and toxic at 100 μM, as proven by the SGs formation in absence of NaAs. Indeed, 50 μM benserazide alone sporadically displayed SGs formation, suggesting that this concentration is barely tolerated (Fig. 2B, C).

To our knowledge, this is the first study reporting a mechanistic insight into the possible role of H_2S in mediating ALS-related neurodegeneration, providing direct association between SGs formation and H_2S metabolism. The occurrence of increased sulfide levels in ALS patients and its implication in the regulation of the eIF2α phosphorylation state point to H_2S as a plausible mediator of SGs formation. The *in vivo* and in *vitro* data reported here support this hypothesis, but need to be strengthened and expanded.

FIGURES

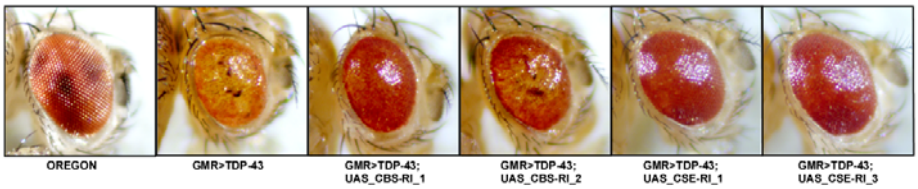

Figure 1. RNAi-mediated knock-down of CBS or CSE partially reverts TDP-43-induced toxicity. External eye phenotype of control (Oregon) and GMR-TDP-43-expressing (ALS model) flies. Transgenic flies with CBS^{RNAi1}, CSE^{RNAi1} and CSE^{RNAi3} displayed a partial reversal of the TDP43-dependent toxicity. CBS^{RNAi2} failed in eliciting substantial phenotypic changes. The observations presented here were typically confirmed in 15 different individuals and reproduced in, at least, two independent mating.

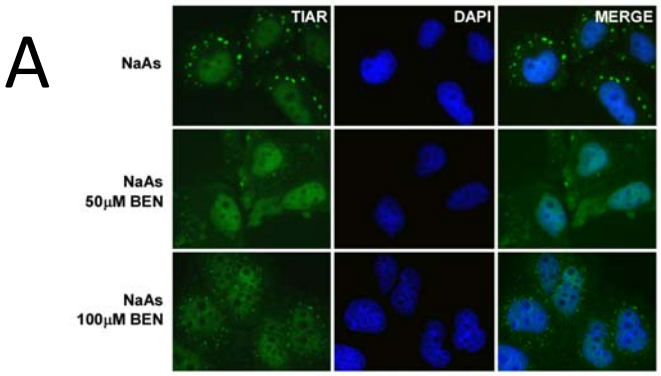

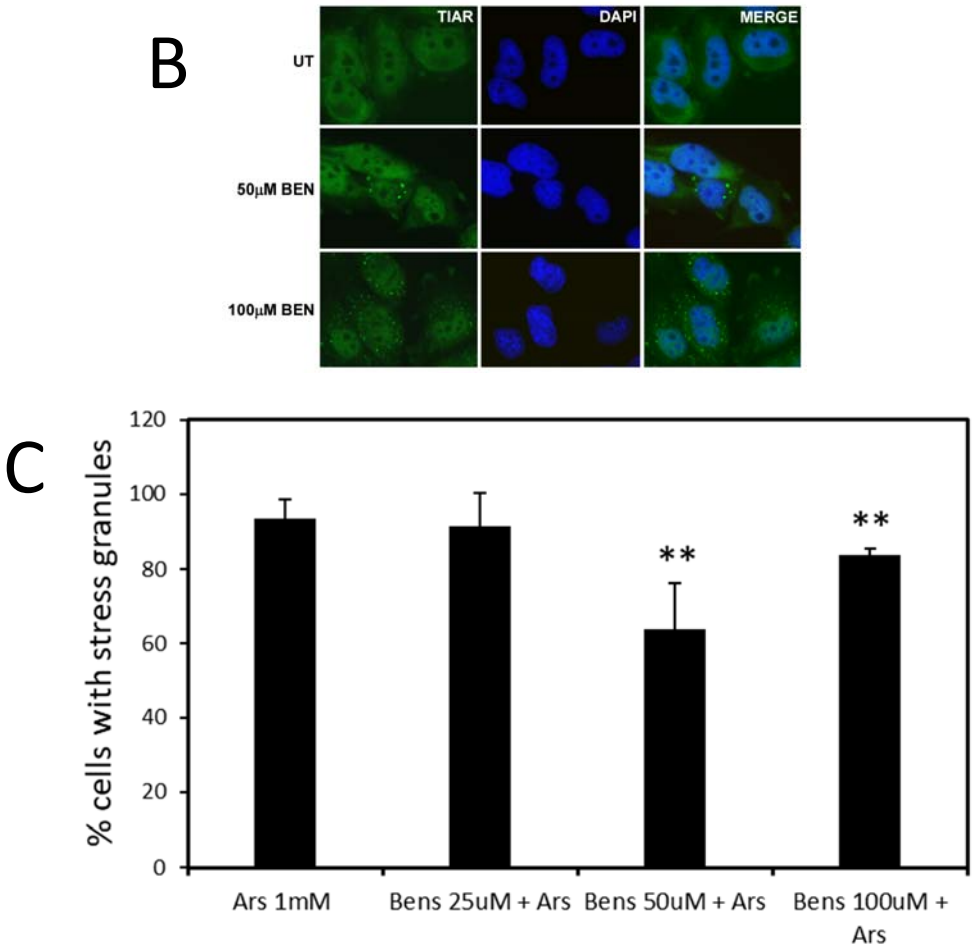

Figure 2. Benserazide treatment reduces stress granules formation (SGs). A) SGs induced by treatment of HeLa cells with 1 mM sodium arsenite (NaAs) were visualized by immunofluorescent staining of TIAR (*green*), while cellular nuclei were stained with DAPI (*blue*). Unlike 100 μM benserazide, pre-treatment with 50 μM benserazide partly prevented SGs formation. B) Benserazide alone promotes a widespread SGs formation at 100 μM, while being weakly toxic at 50 μM. C) Statistical analysis of the randomized cell counting (as reported in Materials and Methods section). ** $p \leq 0.01$.

CONCLUSIONS

Recent years have witnessed an increasing interest in the role of H_2S in human physiology and pathophysiology. This stimulated remarkable efforts to identify new inhibitors of the three human H_2S-synthesizing enzymes which might be suitable for pharmacological applications. In the present thesis, we provided insights into the involvement of H_2S in colorectal cancer and ALS-related neurodegeneration. Furthermore, we proposed a methodological platform to be employed for high-throughput screening of inhibitors against the human H_2S-synthesizing enzymes. The new knowledge acquired here, while deepening our understanding of the role of H_2S in human (patho)physiology and, more specifically, in tumorigenesis and neurodegeneration, will hopefully set the basis for innovative diagnostic and therapeutic approaches.

Conclusion 1

The cysteine prodrug N-acetylcysteine (NAC) has been recently shown to owe its antioxidant and cytoprotective effects to its ability to generate sulfane sulfur species. Herein, working on SW480 colon cancer cells, we evaluated the effect of NAC on H_2S metabolism and found that cell exposure to 10 mM NAC for 24 hours induced enhanced expression and activity of both MST and SQR. Furthermore, NAC has proven to act as a substrate for human MST, as shown working on the isolated enzyme recombinantly produced (*paper 1*). The reported evidence that chronic exposure of colon cancer cells to NAC stimulates H_2S metabolism sheds new light on the mechanism of action of this antioxidant drug, while providing a possible explanation for its failure in anticancer therapy.

Conclusion 2

H_2S levels have been shown to increase in response to low O_2 availability, such that H_2S is currently recognized as an O_2 sensor able to mediate the cellular response to hypoxia. So far, this adaptive regulatory mechanism has been ascribed to upregulation of the H_2S-synthetizing enzymes, while the possible involvement of the H_2S catabolic pathway has remained elusive. Herein, we have investigated the effect of hypoxia on the mitochondrial catabolism of H_2S, evaluating the maximal sulfide oxidizing activity of living cells by high-resolution respirometry. SW480 colon cancer cells exposed for 24 hours to hypoxia (1% O_2), as compared to control (air O_2), have shown a reduced mitochondrial mass, overall accounting for a reduced sulfide catabolism. However, in cells exposed to hypoxia mitochondria have proven to be enriched in the H_2S-consuming enzyme SQR and, thus, to be better equipped to detoxify H_2S. This may represent an adaptive mechanism to ensure higher H_2S levels with pro-survival effects, and concomitantly, protection of mitochondria from H_2S toxicity (*paper 2*). Additionally, available information on the role of H_2S in tumour microenvironment was summarized in a review article (*paper 3*).

Conclusion 3

Increased H_2S due to CBS upregulation has been associated to ALS-related neurodegeneration. Herein, we attempted to unveil the molecular mechanism underlying the involvement of H_2S in ALS development. RNA silencing of either CBS or CSE correlated with an ameliorative phenotype in a *Drosophila melanogaster* ALS model. In a cellular model in which ALS-like damage was induced with sodium arsenite, benserazide-mediated inhibition of CBS exerted a rescue effect, resulting in decreased formation of stress granules. Overall, these preliminary data, while confirming an involvement of

H_2S in ALS etiology, will hopefully contribute to better understand the molecular mechanisms underlying the selective degeneration of motoneurons taking place in ALS (*paper 5*).

Conclusion 4

Given the growingly recognized pivotal role of H_2S in both oncological and neurological diseases, there is an urgent need for drugs able to selectively and effectively target the three human H_2S-synthetizing enzymes. Herein, employing a combination of orthogonal biophysical and biochemical methodologies, we screened a library of synthetic pyridine derivatives for their ability to bind and inhibit the target enzymes. This study led the identification of two weak inhibitors of CSE and CBS and the set-up of a robust platform to be used in future high-throughput compound screenings for the identification of inhibitors of the human H_2S-synthesizing enzymes (*paper 4*).

ABBREVIATIONS

3MP	3-mercaptopyruvate
7AzC	7-azido-4-methylcoumarin
AD	Alzheimer's disease
AdoMet	S-adenosylmethionine
ALS	amyotrophic lateral sclerosis
AOAA	aminooxyacetic acid
BCA	bicinchoninic acid
BSA	bovine serum albumin
CARSs	cysteinyl-tRNA synthetases
CAT	cysteine aminotransferase
CBS	cystathionine β-synthase
CcOx	cytochrome *c* oxidase
CD	circular dichroism
CO	carbon monoxide
CoA	coenzyme A
CoQ	coenzyme Q
CoQ_1	coenzyme Q_1
CS	citrate synthase
CSE	cystathionine γ-lyase
CV	coefficient of variation
Cys	L-cysteine
CysSSH	cysteine persulfide
DMEM	Dulbecco's Modified Eagle Medium
DMSO	dimethyl sulfoxide
DS	Down's syndrome
DSF	differential scanning fluorimetry
DTNB	5,5'-dithiobis-[2-nitrobenzoic acid]

ECM	extracellular matrix
ECs	endothelial cells
eIF2α	eukaryotic translation initiation factor 2α
eIF2α-P	phosphorylated form of eIF2α
ERK	extracellular-regulated kinase
ETC	electron transport chain
ETHE1	persulfide dioxygenase
FAD	flavin adenine dinucleotide
FBS	fetal bovine serum
$FeCl_3$	ferric chloride
GAPDH	glyceraldehyde-3-phosphate dehydrogenase
GSH	glutathione
GSSH	glutathione persulfide
H_2S	hydrogen sulfide
Hcy	L-homocysteine
HIF	hypoxia-inducible factor
HIF-1α	hypoxia-inducible factor-1α
IPTG	isopropyl-1-thio-ß-D-galactopyranoside
ISR	integrated stress response
LB	Luria Bertani broth
LDH	D-lactic dehydrogenase
LDH-A	isoform A of lactate dehydrogenase
LMW	low-molecular weight
MAPK	mitogen activated protein kinase
MB	methylene blue
MMPs	metalloproteases
MNs	motoneurons

MST	3-mercaptopyruvate sulfurtransferase
MTT	thiazolyl blue tetrazolium bromide
Na_2S	sodium sulfide
NaAs	sodium arsenite
NAC	N-acetylcysteine
NADH	reduced β-nicotinamide adenine dinucleotide
NEM	n-ethylmaleimide
NF-κB	nuclear factor kappa-light-chain-enhancer of activated B cells
NMR	nuclear magnetic resonance
NNDPD	N,N-dimethyl-p-phenylenediamine
NO	nitric oxide
Nrf2	nuclear factor erythroid 2-related factor
NTB^-	5-thio-2-nitrobenzoate anion
O_2	dioxygen
OAA	oxaloacetate
OCR	oxygen consumption rate
OXPHOS	oxidative phosphorylation
PARP-1	Poly [ADP-ribose] polymerase 1
PBS	phosphate buffered saline
PCA	perchloric acid
PD	Parkinson's disease
PBS-T	phosphate buffered saline with 0.1% Tween 20 [v/v]
PI3K/Akt	phosphoinositide-3-kinase/protein kinase B
PLP	pyridoxal 5'-phosphate
PMFS	phenylmethylsulfonyl fluoride
PP1c	protein phosphatase-1
PPG	propargylglycine

Rhod	thiosulfate sulfurtransferase
RNS	reactive nitrogen species
ROS	reactive oxygen species
RP-HPLC	reverse phase high performance liquid chromatography
RU	response units
$S_2O_3^{2-}$	thiosulfate
SEM	standard error of the mean
SGs	stress granules
SO_4^{2-}	sulfate
SOU	sulfide oxidizing unit
SOx	sulfite oxidase
SPR	surface plasmon resonance
SQR	sulfide:quinone oxidoreductase
TCEP	tris[2-carboxyethyl]phosphine
TDP43	TAR DNA-binding protein 43
T_m	melting temperature
TST	thiosulfate sulfurtransferase
VEGF	vascular endothelial growth factor

REFERENCES

1. Moss, G.A., *Water and health: a forgotten connection?* Perspect Public Health, 2010. **130**(5): p. 227-32.
2. Matz, H., E. Orion, and R. Wolf, *Balneotherapy in dermatology.* Dermatol Ther, 2003. **16**(2): p. 132-40.
3. Banerjee, S.K. and S.K. Maulik, *Effect of garlic on cardiovascular disorders: a review.* Nutr J, 2002. **1**: p. 4.
4. Abe, K. and H. Kimura, *The possible role of hydrogen sulfide as an endogenous neuromodulator.* J Neurosci, 1996. **16**(3): p. 1066-71.
5. Giuffre, A. and J.B. Vicente, *Hydrogen Sulfide Biochemistry and Interplay with Other Gaseous Mediators in Mammalian Physiology.* Oxid Med Cell Longev, 2018. **2018**: p. 6290931.
6. Cuevasanta, E., M.N. Moller, and B. Alvarez, *Biological chemistry of hydrogen sulfide and persulfides.* Arch Biochem Biophys, 2017. **617**: p. 9-25.
7. Riahi, S. and C.N. Rowley, *Why can hydrogen sulfide permeate cell membranes?* J Am Chem Soc, 2014. **136**(43): p. 15111-3.
8. Nagy, P., et al., *Chemical aspects of hydrogen sulfide measurements in physiological samples.* Biochim Biophys Acta, 2014. **1840**(2): p. 876-91.
9. Hancock, J.T. and M. Whiteman, *Hydrogen sulfide signaling: interactions with nitric oxide and reactive oxygen species.* Ann N Y Acad Sci, 2016. **1365**(1): p. 5-14.
10. Ono, K., et al., *Redox chemistry and chemical biology of H2S, hydropersulfides, and derived species: implications of their possible biological activity and utility.* Free Radic Biol Med, 2014. **77**: p. 82-94.
11. Everett, S.A. and P. Wardman, *Perthiols as antioxidants: radical-scavenging and prooxidative mechanisms.* Methods Enzymol, 1995. **251**: p. 55-69.
12. Edwards, J.O. and R.G. Pearson, *The Factors Determining Nucleophilic Reactivities.* Journal of the American Chemical Society, 1962. **84**(1): p. 16-24.
13. Fukuto, J.M., et al., *Small molecule signaling agents: the integrated chemistry and biochemistry of nitrogen oxides, oxides of carbon, dioxygen, hydrogen sulfide, and their derived species.* Chemical research in toxicology, 2012. **25**(4): p. 769-793.
14. Nagy, P., *Mechanistic chemical perspective of hydrogen sulfide signaling.* Methods Enzymol, 2015. **554**: p. 3-29.
15. Wang, R., *Gasotransmitters: growing pains and joys.* Trends Biochem Sci, 2014. **39**(5): p. 227-32.
16. Wang, R., *Physiological implications of hydrogen sulfide: a whiff exploration that blossomed.* Physiol Rev, 2012. **92**(2): p. 791-896.
17. Vitvitsky, V., O. Kabil, and R. Banerjee, *High turnover rates for hydrogen sulfide allow for rapid regulation of its tissue concentrations.* Antioxid Redox Signal, 2012. **17**(1): p. 22-31.

18. Wang, R., *Two's company, three's a crowd: can H2S be the third endogenous gaseous transmitter?* Faseb j, 2002. **16**(13): p. 1792-8.
19. Chen, X., K.H. Jhee, and W.D. Kruger, *Production of the neuromodulator H2S by cystathionine beta-synthase via the condensation of cysteine and homocysteine.* J Biol Chem, 2004. **279**(50): p. 52082-6.
20. Singh, S., et al., *Relative contributions of cystathionine beta-synthase and gamma-cystathionase to H2S biogenesis via alternative trans-sulfuration reactions.* J Biol Chem, 2009. **284**(33): p. 22457-66.
21. Ida, T., et al., *Reactive cysteine persulfides and S-polythiolation regulate oxidative stress and redox signaling.* Proc Natl Acad Sci U S A, 2014. **111**(21): p. 7606-11.
22. Sun, Q., et al., *Structural basis for the inhibition mechanism of human cystathionine gamma-lyase, an enzyme responsible for the production of H(2)S.* J Biol Chem, 2009. **284**(5): p. 3076-85.
23. Ereno-Orbea, J., et al., *Structural basis of regulation and oligomerization of human cystathionine beta-synthase, the central enzyme of transsulfuration.* Proc Natl Acad Sci U S A, 2013. **110**(40): p. E3790-9.
24. Vicente, J.B., et al., *Bioenergetic relevance of hydrogen sulfide and the interplay between gasotransmitters at human cystathionine beta-synthase.* Biochim Biophys Acta, 2016. **1857**(8): p. 1127-1138.
25. Vicente, J.B., et al., *NO* binds human cystathionine beta-synthase quickly and tightly.* J Biol Chem, 2014. **289**(12): p. 8579-87.
26. Vicente, J.B., et al., *S-Adenosyl-l-methionine Modulates CO and NO* Binding to the Human H2S-generating Enzyme Cystathionine beta-Synthase.* J Biol Chem, 2016. **291**(2): p. 572-81.
27. Banerjee, R. and C.G. Zou, *Redox regulation and reaction mechanism of human cystathionine-beta-synthase: a PLP-dependent hemesensor protein.* Arch Biochem Biophys, 2005. **433**(1): p. 144-56.
28. Niu, W.N., et al., *S-glutathionylation enhances human cystathionine beta-synthase activity under oxidative stress conditions.* Antioxid Redox Signal, 2015. **22**(5): p. 350-61.
29. Niu, W., et al., *Allosteric control of human cystathionine beta-synthase activity by a redox active disulfide bond.* J Biol Chem, 2018. **293**(7): p. 2523-2533.
30. Olson, K.R., *Hydrogen sulfide as an oxygen sensor.* Antioxid Redox Signal, 2015. **22**(5): p. 377-97.
31. Teng, H., et al., *Oxygen-sensitive mitochondrial accumulation of cystathionine beta-synthase mediated by Lon protease.* Proc Natl Acad Sci U S A, 2013. **110**(31): p. 12679-84.
32. Kabil, O., Y. Zhou, and R. Banerjee, *Human Cystathionine β-Synthase Is a Target for Sumoylation.* Biochemistry, 2006. **45**(45): p. 13528-13536.

33. Bao, L., et al., *Identification and tissue distribution of human cystathionine beta-synthase mRNA isoforms.* Arch Biochem Biophys, 1998. **350**(1): p. 95-103.
34. Kabil, O., et al., *The quantitative significance of the transsulfuration enzymes for H2S production in murine tissues.* Antioxid Redox Signal, 2011. **15**(2): p. 363-72.
35. Enokido, Y., et al., *Cystathionine beta-synthase, a key enzyme for homocysteine metabolism, is preferentially expressed in the radial glia/astrocyte lineage of developing mouse CNS.* Faseb j, 2005. **19**(13): p. 1854-6.
36. Kabil, O., V. Yadav, and R. Banerjee, *Heme-dependent Metabolite Switching Regulates H2S Synthesis in Response to Endoplasmic Reticulum (ER) Stress.* J Biol Chem, 2016. **291**(32): p. 16418-16423.
37. Mikami, Y., et al., *Hydrogen sulfide is produced by cystathionine gamma-lyase at the steady-state low intracellular Ca(2+) concentrations.* Biochem Biophys Res Commun, 2013. **431**(2): p. 131-5.
38. Fu, M., et al., *Hydrogen sulfide (H2S) metabolism in mitochondria and its regulatory role in energy production.* Proc Natl Acad Sci U S A, 2012. **109**(8): p. 2943-8.
39. Yadav, P.K., et al., *Structure and kinetic analysis of H2S production by human mercaptopyruvate sulfurtransferase.* J Biol Chem, 2013. **288**(27): p. 20002-13.
40. Mikami, Y., et al., *Thioredoxin and dihydrolipoic acid are required for 3-mercaptopyruvate sulfurtransferase to produce hydrogen sulfide.* Biochem J, 2011. **439**(3): p. 479-85.
41. Cao, X., et al., *A Review of Hydrogen Sulfide Synthesis, Metabolism, and Measurement: Is Modulation of Hydrogen Sulfide a Novel Therapeutic for Cancer?* Antioxid Redox Signal, 2019. **31**(1): p. 1-38.
42. Tomita, M., N. Nagahara, and T. Ito, *Expression of 3-Mercaptopyruvate Sulfurtransferase in the Mouse.* Molecules, 2016. **21**(12).
43. Carbonero, F., A.C. Benefiel, and H.R. Gaskins, *Contributions of the microbial hydrogen economy to colonic homeostasis.* Nat Rev Gastroenterol Hepatol, 2012. **9**(9): p. 504-18.
44. Shen, X., et al., *Microbial regulation of host hydrogen sulfide bioavailability and metabolism.* Free Radic Biol Med, 2013. **60**: p. 195-200.
45. Blachier, F., et al., *Luminal sulfide and large intestine mucosa: friend or foe?* Amino Acids, 2010. **39**(2): p. 335-47.
46. Lagoutte, E., et al., *Oxidation of hydrogen sulfide remains a priority in mammalian cells and causes reverse electron transfer in colonocytes.* Biochim Biophys Acta, 2010. **1797**(8): p. 1500-11.
47. Bhatia, M., *H2S and Inflammation: An Overview.* Handb Exp Pharmacol, 2015. **230**: p. 165-80.

48. Szabo, C., et al., *Regulation of mitochondrial bioenergetic function by hydrogen sulfide. Part I. Biochemical and physiological mechanisms.* Br J Pharmacol, 2014. **171**(8): p. 2099-122.
49. Linden, D.R., et al., *Sulphide quinone reductase contributes to hydrogen sulphide metabolism in murine peripheral tissues but not in the CNS.* Br J Pharmacol, 2012. **165**(7): p. 2178-90.
50. Olson, K.R. and K.D. Straub, *The Role of Hydrogen Sulfide in Evolution and the Evolution of Hydrogen Sulfide in Metabolism and Signaling.* Physiology (Bethesda), 2016. **31**(1): p. 60-72.
51. Libiad, M., et al., *Organization of the human mitochondrial hydrogen sulfide oxidation pathway.* J Biol Chem, 2014. **289**(45): p. 30901-10.
52. Jackson, M.R., P.J. Loll, and M.S. Jorns, *X-Ray Structure of Human Sulfide:Quinone Oxidoreductase: Insights into the Mechanism of Mitochondrial Hydrogen Sulfide Oxidation.* Structure, 2019. **27**(5): p. 794-805 e4.
53. Hildebrandt, T.M. and M.K. Grieshaber, *Three enzymatic activities catalyze the oxidation of sulfide to thiosulfate in mammalian and invertebrate mitochondria.* Febs j, 2008. **275**(13): p. 3352-61.
54. Szabo, C., *Gasotransmitters in cancer: from pathophysiology to experimental therapy.* Nat Rev Drug Discov, 2016. **15**(3): p. 185-203.
55. Shefa, U., et al., *Role of Gasotransmitters in Oxidative Stresses, Neuroinflammation, and Neuronal Repair.* BioMed research international, 2017. **2017**: p. 1689341-1689341.
56. Andreadou, I., et al., *The role of gasotransmitters NO, H2S and CO in myocardial ischaemia/reperfusion injury and cardioprotection by preconditioning, postconditioning and remote conditioning.* British journal of pharmacology, 2015. **172**(6): p. 1587-1606.
57. Paul, B.D. and S.H. Snyder, *H(2)S signalling through protein sulfhydration and beyond.* Nat Rev Mol Cell Biol, 2012. **13**(8): p. 499-507.
58. Akaike, T., et al., *Cysteinyl-tRNA synthetase governs cysteine polysulfidation and mitochondrial bioenergetics.* Nat Commun, 2017. **8**(1): p. 1177.
59. Akaike, T., et al., *Cysteinyl-tRNA synthetase governs cysteine polysulfidation and mitochondrial bioenergetics.* 2017. **8**(1): p. 1177.
60. Mishanina, T.V., M. Libiad, and R. Banerjee, *Biogenesis of reactive sulfur species for signaling by hydrogen sulfide oxidation pathways.* Nat Chem Biol, 2015. **11**(7): p. 457-64.
61. Paul, B.D. and S.H. Snyder, *Gasotransmitter hydrogen sulfide signaling in neuronal health and disease.* Biochemical pharmacology, 2018. **149**: p. 101-109.
62. Nicholls, P., et al., *Sulfide inhibition of and metabolism by cytochrome c oxidase.* Biochem Soc Trans, 2013. **41**(5): p. 1312-6.
63. Panthi, S., S. Manandhar, and K. Gautam, *Hydrogen sulfide, nitric oxide, and neurodegenerative disorders.* Transl Neurodegener, 2018. **7**: p. 3.

64. Modis, K., et al., *S-Sulfhydration of ATP synthase by hydrogen sulfide stimulates mitochondrial bioenergetics.* Pharmacol Res, 2016. **113**(Pt A): p. 116-124.
65. Mustafa, A.K., et al., *H2S signals through protein S-sulfhydration.* Sci Signal, 2009. **2**(96): p. ra72.
66. Jarosz, A.P., et al., *Glyceraldehyde 3-phosphate dehydrogenase (GAPDH) is inactivated by S-sulfuration in vitro.* Free Radic Biol Med, 2015. **89**: p. 512-21.
67. Petersen, L.C., *The effect of inhibitors on the oxygen kinetics of cytochrome c oxidase.* Biochim Biophys Acta, 1977. **460**(2): p. 299-307.
68. Warburg, O., *On respiratory impairment in cancer cells.* Science, 1956. **124**(3215): p. 269-70.
69. Warburg, O., *On the origin of cancer cells.* Science, 1956. **123**(3191): p. 309-14.
70. Hanahan, D. and R.A. Weinberg, *Hallmarks of cancer: the next generation.* Cell, 2011. **144**(5): p. 646-74.
71. Giampazolias, E. and S.W. Tait, *Mitochondria and the hallmarks of cancer.* FEBS J, 2016. **283**(5): p. 803-14.
72. Kumari, S., et al., *Reactive Oxygen Species: A Key Constituent in Cancer Survival.* Biomark Insights, 2018. **13**: p. 1177271918755391.
73. Galadari, S., et al., *Reactive oxygen species and cancer paradox: To promote or to suppress?* Free Radic Biol Med, 2017. **104**: p. 144-164.
74. Nunes, S.C., et al., *Cysteine allows ovarian cancer cells to adapt to hypoxia and to escape from carboplatin cytotoxicity.* 2018. **8**(1): p. 9513.
75. Hellmich, M.R., et al., *The therapeutic potential of cystathionine beta-synthetase/hydrogen sulfide inhibition in cancer.* Antioxid Redox Signal, 2015. **22**(5): p. 424-48.
76. Sen, S., et al., *Role of cystathionine beta-synthase in human breast Cancer.* Free Radic Biol Med, 2015. **86**: p. 228-38.
77. Szabo, C., et al., *Tumor-derived hydrogen sulfide, produced by cystathionine-beta-synthase, stimulates bioenergetics, cell proliferation, and angiogenesis in colon cancer.* Proc Natl Acad Sci U S A, 2013. **110**(30): p. 12474-9.
78. Bhattacharyya, S., et al., *Cystathionine beta-synthase (CBS) contributes to advanced ovarian cancer progression and drug resistance.* PLoS One, 2013. **8**(11): p. e79167.
79. Wang, L., et al., *Cystathionine-γ-lyase promotes the metastasis of breast cancer via the VEGF signaling pathway.* International journal of oncology, 2019. **55**(2): p. 473-487.
80. Fu, Y., et al., *Antioxidants decrease the apoptotic effect of 5-Fu in colon cancer by regulating Src-dependent caspase-7 phosphorylation.* Cell Death Dis, 2014. **5**: p. e983.
81. Ezerina, D., et al., *N-Acetyl Cysteine Functions as a Fast-Acting Antioxidant by Triggering Intracellular H2S and Sulfane Sulfur Production.* Cell Chem Biol, 2018. **25**(4): p. 447-459 e4.

82. Untereiner, A.A., et al., *H2S-induced S-sulfhydration of lactate dehydrogenase a (LDHA) stimulates cellular bioenergetics in HCT116 colon cancer cells.* Biochem Pharmacol, 2017. **136**: p. 86-98.
83. Untereiner, A.A., et al., *Drug resistance induces the upregulation of H(2)S-producing enzymes in HCT116 colon cancer cells.* Biochemical pharmacology, 2018. **149**: p. 174-185.
84. Stokes, E., et al., *Efflux inhibition by H2S confers sensitivity to doxorubicin-induced cell death in liver cancer cells.* Life Sci, 2018. **213**: p. 116-125.
85. Rose, P., et al., *Hydrogen sulfide protects colon cancer cells from chemopreventative agent beta-phenylethyl isothiocyanate induced apoptosis.* World J Gastroenterol, 2005. **11**(26): p. 3990-7.
86. Sekiguchi, F., et al., *Endogenous Hydrogen Sulfide Enhances Cell Proliferation of Human Gastric Cancer AGS Cells.* Biol Pharm Bull, 2016. **39**(5): p. 887-90.
87. Tiong, C.X., M. Lu, and J.S. Bian, *Protective effect of hydrogen sulphide against 6-OHDA-induced cell injury in SH-SY5Y cells involves PKC/PI3K/Akt pathway.* Br J Pharmacol, 2010. **161**(2): p. 467-80.
88. Zhen, Y., et al., *Exogenous hydrogen sulfide exerts proliferation/anti-apoptosis/angiogenesis/migration effects via amplifying the activation of NF-kappaB pathway in PLC/PRF/5 hepatoma cells.* Int J Oncol, 2015. **46**(5): p. 2194-204.
89. Sen, N., et al., *Hydrogen sulfide-linked sulfhydration of NF-kappaB mediates its antiapoptotic actions.* Mol Cell, 2012. **45**(1): p. 13-24.
90. Erez, N., et al., *Cancer-Associated Fibroblasts Are Activated in Incipient Neoplasia to Orchestrate Tumor-Promoting Inflammation in an NF-kappaB-Dependent Manner.* Cancer Cell, 2010. **17**(2): p. 135-47.
91. Hanahan, D. and R.A. Weinberg, *The hallmarks of cancer.* Cell, 2000. **100**(1): p. 57-70.
92. Balkwill, F.R., M. Capasso, and T. Hagemann, *The tumor microenvironment at a glance.* J Cell Sci, 2012. **125**(Pt 23): p. 5591-6.
93. Wu, D., et al., *Hydrogen sulfide acts as a double-edged sword in human hepatocellular carcinoma cells through EGFR/ERK/MMP-2 and PTEN/AKT signaling pathways.* Sci Rep, 2017. **7**(1): p. 5134.
94. Kugeratski, F.G. and S.J. Atkinson, *Hypoxic cancer-associated fibroblasts increase NCBP2-AS2/HIAR to promote endothelial sprouting through enhanced VEGF signaling.* 2019. **12**(567).
95. Papapetropoulos, A., et al., *Hydrogen sulfide is an endogenous stimulator of angiogenesis.* Proc Natl Acad Sci U S A, 2009. **106**(51): p. 21972-7.
96. Mustafa, A.K., et al., *Hydrogen sulfide as endothelium-derived hyperpolarizing factor sulfhydrates potassium channels.* Circ Res, 2011. **109**(11): p. 1259-68.

97. Karakashev, S.V. and M.J. Reginato, *Progress toward overcoming hypoxia-induced resistance to solid tumor therapy.* Cancer management and research, 2015. **7**: p. 253-264.
98. Krock, B.L., N. Skuli, and M.C. Simon, *Hypoxia-induced angiogenesis: good and evil.* Genes & cancer, 2011. **2**(12): p. 1117-1133.
99. Semenza, G.L., *Hypoxia-inducible factors: mediators of cancer progression and targets for cancer therapy.* Trends Pharmacol Sci, 2012. **33**(4): p. 207-14.
100. Wu, B., et al., *Interaction of Hydrogen Sulfide with Oxygen Sensing under Hypoxia.* Oxid Med Cell Longev, 2015. **2015**: p. 758678.
101. Bir, S.C., et al., *Hydrogen sulfide stimulates ischemic vascular remodeling through nitric oxide synthase and nitrite reduction activity regulating hypoxia-inducible factor-1alpha and vascular endothelial growth factor-dependent angiogenesis.* J Am Heart Assoc, 2012. **1**(5): p. e004093.
102. Beaumont, M., et al., *Detrimental effects for colonocytes of an increased exposure to luminal hydrogen sulfide: The adaptive response.* Free Radic Biol Med, 2016. **93**: p. 155-64.
103. Liu, X., et al., *Hypoxia-inducible factor-1alpha is involved in the pro-angiogenic effect of hydrogen sulfide under hypoxic stress.* Biol Pharm Bull, 2010. **33**(9): p. 1550-4.
104. Reichard, A. and K. Asosingh, *The role of mitochondria in angiogenesis.* Mol Biol Rep, 2019. **46**(1): p. 1393-1400.
105. Magierowski, M., et al., *Exogenous and Endogenous Hydrogen Sulfide Protects Gastric Mucosa against the Formation and Time-Dependent Development of Ischemia/Reperfusion-Induced Acute Lesions Progressing into Deeper Ulcerations.* Molecules, 2017. **22**(2).
106. Zhu, Y., et al., *Increased autophagic degradation contributes to the neuroprotection of hydrogen sulfide against cerebral ischemia/reperfusion injury.* Metab Brain Dis, 2017. **32**(5): p. 1449-1458.
107. Abou-Hamdan, A., et al., *Positive feedback during sulfide oxidation fine-tunes cellular affinity for oxygen.* Biochim Biophys Acta, 2016. **1857**(9): p. 1464-1472.
108. Solaini, G., et al., *Hypoxia and mitochondrial oxidative metabolism.* Biochim Biophys Acta, 2010. **1797**(6-7): p. 1171-7.
109. Whiteman, M., et al., *The novel neuromodulator hydrogen sulfide: an endogenous peroxynitrite 'scavenger'?* J Neurochem, 2004. **90**(3): p. 765-8.
110. Whiteman, M. and B. Halliwell, *Protection against peroxynitrite-dependent tyrosine nitration and alpha 1-antiproteinase inactivation by ascorbic acid. A comparison with other biological antioxidants.* Free Radic Res, 1996. **25**(3): p. 275-83.
111. Kimura, Y., Y. Goto, and H. Kimura, *Hydrogen sulfide increases glutathione production and suppresses oxidative stress in mitochondria.* Antioxid Redox Signal, 2010. **12**(1): p. 1-13.

112. Kimura, Y. and H. Kimura, *Hydrogen sulfide protects neurons from oxidative stress.* Faseb j, 2004. **18**(10): p. 1165-7.

113. Yang, G., et al., *Hydrogen sulfide protects against cellular senescence via S-sulfhydration of Keap1 and activation of Nrf2.* Antioxid Redox Signal, 2013. **18**(15): p. 1906-19.

114. Paul, B.D., et al., *Cystathionine gamma-lyase deficiency mediates neurodegeneration in Huntington's disease.* Nature, 2014. **509**(7498): p. 96-100.

115. Xuan, A., et al., *Hydrogen sulfide attenuates spatial memory impairment and hippocampal neuroinflammation in beta-amyloid rat model of Alzheimer's disease.* J Neuroinflammation, 2012. **9**: p. 202.

116. Vandiver, M.S., et al., *Sulfhydration mediates neuroprotective actions of parkin.* Nat Commun, 2013. **4**: p. 1626.

117. Tiranti, V. and M. Zeviani, *Altered sulfide (H(2)S) metabolism in ethylmalonic encephalopathy.* Cold Spring Harb Perspect Biol, 2013. **5**(1): p. a011437.

118. Ichinohe, A., et al., *Cystathionine beta-synthase is enriched in the brains of Down's patients.* Biochem Biophys Res Commun, 2005. **338**(3): p. 1547-50.

119. Davoli, A., et al., *Evidence of hydrogen sulfide involvement in amyotrophic lateral sclerosis.* Ann Neurol, 2015. **77**(4): p. 697-709.

120. Hellmich, M.R. and C. Szabo, *Hydrogen Sulfide and Cancer.* Handb Exp Pharmacol, 2015. **230**: p. 233-41.

121. Augsburger, F. and C. Szabo, *Potential role of the 3-mercaptopyruvate sulfurtransferase (3-MST)-hydrogen sulfide (H2S) pathway in cancer cells.* Pharmacol Res, 2018.

122. Asimakopoulou, A., et al., *Selectivity of commonly used pharmacological inhibitors for cystathionine beta synthase (CBS) and cystathionine gamma lyase (CSE).* Br J Pharmacol, 2013. **169**(4): p. 922-32.

123. Thornburg, J.M., et al., *Targeting aspartate aminotransferase in breast cancer.* Breast Cancer Res, 2008. **10**(5): p. R84.

124. Son, J., et al., *Glutamine supports pancreatic cancer growth through a KRAS-regulated metabolic pathway.* Nature, 2013. **496**(7443): p. 101-5.

125. Druzhyna, N., et al., *Screening of a composite library of clinically used drugs and well-characterized pharmacological compounds for cystathionine beta-synthase inhibition identifies benserazide as a drug potentially suitable for repurposing for the experimental therapy of colon cancer.* Pharmacol Res, 2016. **113**(Pt A): p. 18-37.

126. Miyamoto, R., et al., *Neuronal regulation of expression of hydrogen sulfide-producing enzyme cystathionine beta-synthase in rat spinal cord astrocytes.* Neurosci Res, 2015. **97**: p. 52-9.

127. Kabil, O. and R. Banerjee, *Enzymology of H2S biogenesis, decay and signaling.* Antioxid Redox Signal, 2014. **20**(5): p. 770-82.

128. Jackson, M.R., S.L. Melideo, and M.S. Jorns, *Human sulfide:quinone oxidoreductase catalyzes the first step in hydrogen sulfide metabolism and produces a sulfane sulfur metabolite.* Biochemistry, 2012. **51**(34): p. 6804-15.

129. Paul, B.D. and S.H. Snyder, *H2S: A Novel Gasotransmitter that Signals by Sulfhydration.* Trends Biochem Sci, 2015. **40**(11): p. 687-700.

130. Bjelakovic, G., et al., *Antioxidant supplements for prevention of gastrointestinal cancers: a systematic review and meta-analysis.* Lancet, 2004. **364**(9441): p. 1219-28.

131. Casazza, A., et al., *Tumor stroma: a complexity dictated by the hypoxic tumor microenvironment.* Oncogene, 2014. **33**(14): p. 1743-54.

132. Fernandez-Vizarra, E., et al., *Isolation of mitochondria for biogenetical studies: An update.* Mitochondrion, 2010. **10**(3): p. 253-62.

133. Nashef, A.S., D.T. Osuga, and R.E. Feeney, *Determination of hydrogen sulfide with 5,5'-dithiobis-(2-nitrobenzoic acid), N-ethylmaleimide, and parachloromercuribenzoate.* Anal Biochem, 1977. **79**(1-2): p. 394-405.

134. Brundu, S., et al., *Validation of a Reversed-Phase High Performance Liquid Chromatography Method for the Simultaneous Analysis of Cysteine and Reduced Glutathione in Mouse Organs.* Oxid Med Cell Longev, 2016. **2016**: p. 1746985.

135. Rivero-Gutierrez, B., et al., *Stain-free detection as loading control alternative to Ponceau and housekeeping protein immunodetection in Western blotting.* Anal Biochem, 2014. **467**: p. 1-3.

136. Srere, P.A., *[1] Citrate synthase: [EC 4.1.3.7. Citrate oxaloacetate-lyase (CoA-acetylating)]*, in *Methods in Enzymology*. 1969, Academic Press. p. 3-11.

137. Valentine, W.N. and J.K. Frankenfeld, *3-Mercaptopyruvate sulfurtransferase (EC 2.8.1.2): a simple assay adapted to human blood cells.* Clin Chim Acta, 1974. **51**(2): p. 205-10.

138. Theissen, U. and W. Martin, *Sulfide : quinone oxidoreductase (SQR) from the lugworm Arenicola marina shows cyanide- and thioredoxin-dependent activity.* Febs j, 2008. **275**(6): p. 1131-9.

139. Thorson, M.K., et al., *Identification of cystathionine beta-synthase inhibitors using a hydrogen sulfide selective probe.* Angew Chem Int Ed Engl, 2013. **52**(17): p. 4641-4.

140. Zuhra, K., et al., *Screening Pyridine Derivatives against Human Hydrogen Sulfide-synthesizing Enzymes by Orthogonal Methods.* Sci Rep, 2019. **9**(1): p. 684.

141. Niesen, F.H., H. Berglund, and M. Vedadi, *The use of differential scanning fluorimetry to detect ligand interactions that promote protein stability.* Nat Protoc, 2007. **2**(9): p. 2212-21.

142. Kabil, O. and R. Banerjee, *Enzymology of H_2S biogenesis, decay and signaling.* Antioxid. Redox Signal., 2014. **20**(5): p. 770-82.

143. Ono, K., et al., *Redox chemistry and chemical biology of H_2S, hydropersulfides, and derived species: implications of their possible biological activity and utility.* Free Radic. Biol. Med., 2014. **77**: p. 82-94.

144. Cuevasanta, E., M.N. Moller, and B. Alvarez, *Biological chemistry of hydrogen sulfide and persulfides.* Arch. Biochem. Biophys., 2017. **617**: p. 9-25.

145. Filipovic, M.R., et al., *Chemical biology of H_2S signaling through persulfidation.* Chem. Rev., 2018. **118**(3): p. 1253-1337.

146. Cooper, C.E. and G.C. Brown, *The inhibition of mitochondrial cytochrome oxidase by the gases carbon monoxide, nitric oxide, hydrogen cyanide and hydrogen sulfide: chemical mechanism and physiological significance.* J. Bioenerg. Biomembr., 2008. **40**(5): p. 533-9.

147. Pietri, R., E. Roman-Morales, and J. Lopez-Garriga, *Hydrogen sulfide and hemeproteins: knowledge and mysteries.* Antioxid. Redox Signal., 2011. **15**(2): p. 393-404.

148. Olson, K.R., *H_2S and polysulfide metabolism: Conventional and unconventional pathways.* Biochem. Pharmacol., 2018. **149**: p. 77-90.

149. Giuffrè, A. and J. Vicente, *Hydrogen sulfide biochemistry and interplay with other gaseous mediators in mammalian physiology.* Oxid. Med. Cell Longev., 2018. **2018**: p. 6290931.

150. Puranik, M., et al., *Dynamics of carbon monoxide binding to cystathionine beta-synthase.* J. Biol. Chem., 2006. **281**(19): p. 13433-8.

151. Gherasim, C., et al., *Nitrite reductase activity and inhibition of H(2)S biogenesis by human cystathionine beta-synthase.* PLoS One, 2014. **9**(1): p. e85544.

152. Vicente, J.B., et al., *NO* binds human cystathionine beta-synthase quickly and tightly.* J. Biol. Chem., 2014. **289**(12): p. 8579-87.

153. Vicente, J.B., et al., *S-Adenosyl-L-methionine modulates CO and NO* binding to the human H_2S-generating enzyme cystathionine beta-synthase.* J. Biol. Chem., 2016. **291**(2): p. 572-81.

154. Vicente, J.B., et al., *A clinically relevant variant of the human hydrogen sulfide-synthesizing enzyme cystathionine beta-synthase: increased CO reactivity as a novel molecular mechanism of pathogenicity?* Oxid. Med. Cell. Longev., 2017. **2017**: p. 8940321.

155. Hildebrandt, T.M. and M.K. Grieshaber, *Three enzymatic activities catalyze the oxidation of sulfide to thiosulfate in mammalian and invertebrate mitochondria.* FEBS J., 2008. **275**(13): p. 3352-61.

156. Goubern, M., et al., *Sulfide, the first inorganic substrate for human cells.* FASEB J., 2007. **21**(8): p. 1699-706.

157. Mishanina, T.V., et al., *Transient kinetic analysis of hydrogen sulfide oxidation catalyzed by human sulfide quinone oxidoreductase.* J. Biol. Chem., 2015. **290**(41): p. 25072-80.

158. Landry, A.P., D.P. Ballou, and R. Banerjee, *H_2S oxidation by nanodisc-embedded human sulfide quinone oxidoreductase.* J. Biol. Chem., 2017. **292**(28): p. 11641-11649.

159. Augustyn, K.D., M.R. Jackson, and M.S. Jorns, *Use of Tissue Metabolite Analysis and Enzyme Kinetics To Discriminate between Alternate Pathways for Hydrogen Sulfide Metabolism.* Biochemistry, 2017. **56**(7): p. 986-996.

160. Landry, A.P., D.P. Ballou, and R. Banerjee, *Modulation of catalytic promiscuity during hydrogen sulfide oxidation.* ACS Chem. Biol., 2018. **13**(6): p. 1651-1658.

161. Lagoutte, E., et al., *Oxidation of hydrogen sulfide remains a priority in mammalian cells and causes reverse electron transfer in colonocytes.* Biochim. Biophys. Acta, 2010. **1797**(8): p. 1500-11.

162. Weisiger, R.A., L.M. Pinkus, and W.B. Jakoby, *Thiol S-methyltransferase: suggested role in detoxication of intestinal hydrogen sulfide.* Biochem. Pharmacol., 1980. **29**(20): p. 2885-7.

163. Bouillaud, F. and F. Blachier, *Mitochondria and sulfide: a very old story of poisoning, feeding, and signaling?* Antioxid. Redox Signal., 2011. **15**(2): p. 379-91.

164. Szabo, C., et al., *Regulation of mitochondrial bioenergetic function by hydrogen sulfide. Part I. Biochemical and physiological mechanisms.* Br. J. Pharmacol., 2014. **171**(8): p. 2099-122.

165. Abou-Hamdan, A., et al., *Oxidation of H_2S in mammalian cells and mitochondria.* Methods Enzymol., 2015. **554**: p. 201-28.

166. Vicente, J.B., et al., *Bioenergetic relevance of hydrogen sulfide and the interplay between gasotransmitters at human cystathionine beta-synthase.* Biochim. Biophys. Acta, 2016. **1857**(8): p. 1127-38.

167. Mimoun, S., et al., *Detoxification of H(2)S by differentiated colonic epithelial cells: implication of the sulfide oxidizing unit and of the cell respiratory capacity.* Antioxid. Redox Signal., 2012. **17**(1): p. 1-10.

168. Hellmich, M.R., et al., *The therapeutic potential of cystathionine beta-synthetase/hydrogen sulfide inhibition in cancer.* Antioxid. Redox Signal., 2015. **22**(5): p. 424-48.

169. Hellmich, M.R. and C. Szabo, *Hydrogen sulfide and cancer.* Handb. Exp. Pharmacol., 2015. **230**: p. 233-41.

170. Cao, X., et al., *A review of hydrogen sulfide synthesis, metabolism, and measurement: Is modulation of hydrogen sulfide a novel therapeutic for cancer?* Antioxid. Redox Signal., 2018: p. in press.

171. Szabo, C., et al., *Tumor-derived hydrogen sulfide, produced by cystathionine-beta-synthase, stimulates bioenergetics, cell proliferation, and angiogenesis in colon cancer.* Proc. Natl. Acad. Sci. U S A, 2013. **110**(30): p. 12474-9.

172. Chakraborty, P.K., et al., *Role of cystathionine beta synthase in lipid metabolism in ovarian cancer.* Oncotarget, 2015. **6**(35): p. 37367-84.

173. Sen, S., et al., *Role of cystathionine beta-synthase in human breast cancer.* Free Radic. Biol. Med., 2015. **86**: p. 228-38.

174. Szczesny, B., et al., *Inhibition of hydrogen sulfide biosynthesis sensitizes lung adenocarcinoma to chemotherapeutic drugs by inhibiting mitochondrial DNA repair and suppressing cellular bioenergetics.* Sci. Rep., 2016. **6**: p. 36125.

175. Druzhyna, N., et al., *Screening of a composite library of clinically used drugs and well-characterized pharmacological compounds for cystathionine beta-synthase inhibition identifies benserazide as a drug potentially suitable for repurposing for the experimental therapy of colon cancer.* Pharmacol Res., 2016. **113**(Pt A): p. 18-37.

176. Panza, E., et al., *Role of the cystathionine gamma lyase/hydrogen sulfide pathway in human melanoma progression.* Pigment Cell Melanoma Res., 2015. **28**(1): p. 61-72.

177. Gai, J.W., et al., *Expression profile of hydrogen sulfide and its synthases correlates with tumor stage and grade in urothelial cell carcinoma of bladder.* Urol. Oncol., 2016. **34**(4): p. 166 e15-20.

178. Muz, B., et al., *The role of hypoxia in cancer progression, angiogenesis, metastasis, and resistance to therapy.* Hypoxia (Auckl), 2015. **3**: p. 83-92.

179. Masson, N. and P.J. Ratcliffe, *Hypoxia signaling pathways in cancer metabolism: the importance of co-selecting interconnected physiological pathways.* Cancer Metab., 2014. **2**(1): p. 3.

180. Xie, H. and M.C. Simon, *Oxygen availability and metabolic reprogramming in cancer.* J. Biol. Chem., 2017. **292**(41): p. 16825-16832.

181. Samanta, D. and G.L. Semenza, *Metabolic adaptation of cancer and immune cells mediated by hypoxia-inducible factors.* Biochim. Biophys. Acta, 2018: p. in press.

182. Zhang, H., et al., *Mitochondrial autophagy is an HIF-1-dependent adaptive metabolic response to hypoxia.* J. Biol. Chem., 2008. **283**(16): p. 10892-903.

183. Solaini, G., et al., *Hypoxia and mitochondrial oxidative metabolism.* Biochim. Biophys. Acta, 2010. **1797**(6-7): p. 1171-7.

184. Wu, H. and Q. Chen, *Hypoxia activation of mitophagy and its role in disease pathogenesis.* Antioxid. Redox Signal., 2015. **22**(12): p. 1032-46.

185. Olson, K.R., *Hydrogen sulfide as an oxygen sensor.* Antioxid. Redox Signal., 2015. **22**(5): p. 377-97.

186. Wu, B., et al., *Interaction of hydrogen sulfide with oxygen sensing under hypoxia.* Oxid. Med. Cell. Longev., 2015. **2015**: p. 758678.

187. Takano, N., et al., *Hypoxia-inducible factors regulate human and rat cystathionine beta-synthase gene expression.* Biochem. J., 2014. **458**(2): p. 203-11.

188. Wang, M., Z. Guo, and S. Wang, *Regulation of cystathionine gamma-lyase in mammalian cells by hypoxia.* Biochem. Genet., 2014. **52**(1-2): p. 29-37.

189. Teng, H., et al., *Oxygen-sensitive mitochondrial accumulation of cystathionine beta-synthase mediated by Lon protease.* Proc. Natl. Acad. Sci. U S A, 2013. **110**(31): p. 12679-84.

190. Morikawa, T., et al., *Hypoxic regulation of the cerebral microcirculation is mediated by a carbon monoxide-sensitive hydrogen sulfide pathway.* Proc. Natl. Acad. Sci. U S A, 2012. **109**(4): p. 1293-8.

191. Yuan, G., et al., *Protein kinase G-regulated production of H_2S governs oxygen sensing.* Sci. Signal., 2015. **8**(373): p. ra37.

192. Bos, E.M., et al., *Hydrogen sulfide: physiological properties and therapeutic potential in ischaemia.* Br. J. Pharmacol., 2015. **172**(6): p. 1479-93.

193. Jensen, A.R., et al., *Hydrogen sulfide: a potential novel therapy for the treatment of ischemia.* Shock, 2017. **48**(5): p. 511-524.

194. Nagy, P., et al., *Chemical aspects of hydrogen sulfide measurements in physiological samples.* Biochim. Biophys. Acta, 2014. **1840**(2): p. 876-91.

195. Nashef, A.S., D.T. Osuga, and R.E. Feeney, *Determination of hydrogen sulfide with 5,5'-dithiobis-(2-nitrobenzoic acid), N-ethylmaleimide, and parachloromercuribenzoate.* Anal. Biochem., 1977. **79**(1-2): p. 394-405.

196. Srere, P.A., *[1] Citrate synthase: [EC 4.1.3.7. Citrate oxaloacetate-lyase (CoA-acetylating)].* Methods Enzymol., 1969. **13**: p. 3-11.

197. Rivero-Gutierrez, B., et al., *Stain-free detection as loading control alternative to Ponceau and housekeeping protein immunodetection in Western blotting.* Anal. Biochem., 2014. **467**: p. 1-3.

198. Zhong, H. and J.W. Simons, *Direct comparison of GAPDH, beta-actin, cyclophilin, and 28S rRNA as internal standards for quantifying RNA levels under hypoxia.* Biochem. Biophys. Res. Commun., 1999. **259**(3): p. 523-6.

199. Heerlein, K., et al., *Hypoxia decreases cellular ATP demand and inhibits mitochondrial respiration of a549 cells.* Am. J. Respir. Cell. Mol. Biol., 2005. **32**(1): p. 44-51.

200. Helmy, N., et al., *Oxidation of hydrogen sulfide by human liver mitochondria.* Nitric Oxide, 2014. **41**: p. 105-12.

201. Larsen, S., et al., *Biomarkers of mitochondrial content in skeletal muscle of healthy young human subjects.* J. Physiol., 2012. **590**(14): p. 3349-60.

202. Olson, K.R., et al., *Hydrogen sulfide as an oxygen sensor/transducer in vertebrate hypoxic vasoconstriction and hypoxic vasodilation.* J. Exp. Biol., 2006. **209**(Pt 20): p. 4011-23.

203. Fawcett, E.M., et al., *Hypoxia disrupts proteostasis in Caenorhabditis elegans.* Aging Cell, 2015. **14**(1): p. 92-101.

204. Hine, C., et al., *Endogenous hydrogen sulfide production is essential for dietary restriction benefits.* Cell, 2015. **160**(1-2): p. 132-44.

205. Marutani, E., et al., *Thiosulfate mediates cytoprotective effects of hydrogen sulfide against neuronal ischemia.* J. Am. Heart Assoc., 2015. **4**(11).
206. Leskova, A., et al., *Role of thiosulfate in hydrogen sulfide-dependent redox signaling in endothelial cells.* Am. J. Physiol. Heart Circ. Physiol., 2017. **313**(2): p. H256-H264.
207. Olson, K.R., et al., *Thiosulfate: a readily accessible source of hydrogen sulfide in oxygen sensing.* Am. J. Physiol. Regul. Integr. Comp. Physiol., 2013. **305**(6): p. R592-603.
208. Zhao, W., et al., *The vasorelaxant effect of H(2)S as a novel endogenous gaseous K(ATP) channel opener.* EMBO J., 2001. **20**(21): p. 6008-16.
209. Papapetropoulos, A., et al., *Hydrogen sulfide is an endogenous stimulator of angiogenesis.* Proc. Natl. Acad. Sci. U S A, 2009. **106**(51): p. 21972-7.
210. Beaumont, M., et al., *Detrimental effects for colonocytes of an increased exposure to luminal hydrogen sulfide: The adaptive response.* Free Radic. Biol. Med., 2016. **93**: p. 155-64.
211. Matallo, J., et al., *Sulfide-inhibition of mitochondrial respiration at very low oxygen concentrations.* Nitric Oxide, 2014. **41**: p. 79-84.
212. Abou-Hamdan, A., et al., *Positive feedback during sulfide oxidation fine-tunes cellular affinity for oxygen.* Biochim. Biophys. Acta, 2016. **1857**(9): p. 1464-72.
213. Filipovic, M.R., et al., *Chemical Biology of H2S Signaling through Persulfidation.* Chem Rev, 2018. **118**(3): p. 1253-1337.
214. Libiad, M., et al., *Hydrogen sulfide perturbs mitochondrial bioenergetics and triggers metabolic reprogramming in colon cells.* J Biol Chem, 2019.
215. Tang, G., et al., *Direct stimulation of K(ATP) channels by exogenous and endogenous hydrogen sulfide in vascular smooth muscle cells.* Mol Pharmacol, 2005. **68**(6): p. 1757-64.
216. Cai, W.J., et al., *The novel proangiogenic effect of hydrogen sulfide is dependent on Akt phosphorylation.* Cardiovasc Res, 2007. **76**(1): p. 29-40.
217. Zhao, K., et al., *S-sulfhydration of MEK1 leads to PARP-1 activation and DNA damage repair.* EMBO Rep, 2014. **15**(7): p. 792-800.
218. Wang, L., et al., *A pharmacological probe identifies cystathionine beta-synthase as a new negative regulator for ferroptosis.* Cell Death Dis, 2018. **9**(10): p. 1005.
219. Szczesny, B., et al., *Inhibition of hydrogen sulfide biosynthesis sensitizes lung adenocarcinoma to chemotherapeutic drugs by inhibiting mitochondrial DNA repair and suppressing cellular bioenergetics.* Sci Rep, 2016. **6**: p. 36125.
220. Untereiner, A.A., et al., *Drug resistance induces the upregulation of H2S-producing enzymes in HCT116 colon cancer cells.* Biochem Pharmacol, 2018. **149**: p. 174-185.
221. Nunes, S.C., et al., *Cysteine allows ovarian cancer cells to adapt to hypoxia and to escape from carboplatin cytotoxicity.* Sci Rep, 2018. **8**(1): p. 9513.

222. Ianaro, A., G. Cirino, and J.L. Wallace, *Hydrogen sulfide-releasing anti-inflammatory drugs for chemoprevention and treatment of cancer.* Pharmacol Res, 2016. **111**: p. 652-658.

223. Reis, A., A. Stern, and H.P. Monteiro, *S-nitrosothiols and H2S donors: Potential chemo-therapeutic agents in cancer.* Redox Biol, 2019: p. 101190.

224. Zuhra, K., et al., *Screening Pyridine Derivatives against Human Hydrogen Sulfide-synthesizing Enzymes by Orthogonal Methods.* Sci Rep, 2019. **9**(1): p. 684.

225. Wallace, J.L., et al., *Hydrogen Sulfide-Releasing Therapeutics: Translation to the Clinic.* Antioxid Redox Signal, 2018. **28**(16): p. 1533-1540.

226. Puccinelli, M.T. and S.D. Stan, *Dietary Bioactive Diallyl Trisulfide in Cancer Prevention and Treatment.* Int J Mol Sci, 2017. **18**(8).

227. Yagdi, E., et al., *Garlic-derived natural polysulfanes as hydrogen sulfide donors: Friend or foe?* Food Chem Toxicol, 2016. **95**: p. 219-33.

228. Frasdorf, B., C. Radon, and S. Leimkuhler, *Characterization and interaction studies of two isoforms of the dual localized 3-mercaptopyruvate sulfurtransferase TUM1 from humans.* J Biol Chem, 2014. **289**(50): p. 34543-56.

229. McCorvie, T.J., et al., *Inter-domain communication of human cystathionine beta-synthase: structural basis of S-adenosyl-L-methionine activation.* J Biol Chem, 2014. **289**(52): p. 36018-30.

230. Ereno-Orbea, J., et al., *Structural insight into the molecular mechanism of allosteric activation of human cystathionine beta-synthase by S-adenosylmethionine.* Proc Natl Acad Sci U S A, 2014. **111**(37): p. E3845-52.

231. Kumar, A., et al., *Heme interaction of the intrinsically disordered N-terminal peptide segment of human cystathionine-beta-synthase.* Sci Rep, 2018. **8**(1): p. 2474.

232. Banerjee, R., *Catalytic promiscuity and heme-dependent redox regulation of H2S synthesis.* Curr Opin Chem Biol, 2017. **37**: p. 115-121.

233. Pettinati, I., et al., *Crystal structure of human persulfide dioxygenase: structural basis of ethylmalonic encephalopathy.* Hum Mol Genet, 2015. **24**(9): p. 2458-69.

234. Pietri, R., E. Roman-Morales, and J. Lopez-Garriga, *Hydrogen sulfide and hemeproteins: knowledge and mysteries.* Antioxid Redox Signal, 2011. **15**(2): p. 393-404.

235. Rios-Gonzalez, B.B., et al., *Hydrogen sulfide activation in hemeproteins: the sulfheme scenario.* J Inorg Biochem, 2014. **133**: p. 78-86.

236. Smith, R.P. and R.E. Gosselin, *On the mechanism of sulfide inactivation by methemoglobin.* Toxicol Appl Pharmacol, 1966. **8**(1): p. 159-72.

237. Vitvitsky, V., et al., *Sulfide oxidation by a noncanonical pathway in red blood cells generates thiosulfate and polysulfides.* J Biol Chem, 2015. **290**(13): p. 8310-20.

238. Cooper, C.E. and G.C. Brown, *The inhibition of mitochondrial cytochrome oxidase by the gases carbon monoxide, nitric oxide, hydrogen cyanide and hydrogen sulfide: chemical mechanism and physiological significance.* J Bioenerg Biomembr, 2008. **40**(5): p. 533-9.

239. Giuffre, A., et al., *Nitric oxide reacts with the single-electron reduced active site of cytochrome c oxidase.* J Biol Chem, 2002. **277**(25): p. 22402-6.

240. Mastronicola, D., et al., *Control of respiration by nitric oxide in Keilin-Hartree particles, mitochondria and SH-SY5Y neuroblastoma cells.* Cell Mol Life Sci, 2003. **60**(8): p. 1752-9.

241. Sarti, P., et al., *The Chemical Interplay between Nitric Oxide and Mitochondrial Cytochrome c Oxidase: Reactions, Effectors and Pathophysiology.* Int J Cell Biol, 2012. **2012**: p. 571067.

242. Kasamatsu, S., et al., *Redox Signaling Regulated by Cysteine Persulfide and Protein Polysulfidation.* Molecules, 2016. **21**(12).

243. Millikin, R., et al., *The chemical biology of protein hydropersulfides: Studies of a possible protective function of biological hydropersulfide generation.* Free Radic Biol Med, 2016. **97**: p. 136-147.

244. Bianco, C.L., et al., *The chemical biology of the persulfide (RSSH)/perthiyl (RSS.) redox couple and possible role in biological redox signaling.* Free Radic Biol Med, 2016. **101**: p. 20-31.

245. Kimura, Y., et al., *3-Mercaptopyruvate sulfurtransferase produces potential redox regulators cysteine- and glutathione-persulfide (Cys-SSH and GSSH) together with signaling molecules H2S2, H2S3 and H2S.* Sci Rep, 2017. **7**(1): p. 10459.

246. Yadav, P.K., et al., *Biosynthesis and Reactivity of Cysteine Persulfides in Signaling.* J Am Chem Soc, 2016. **138**(1): p. 289-99.

247. Goncalves-Dias, C., et al., *Mercapturate Pathway in the Tubulocentric Perspective of Diabetic Kidney Disease.* Nephron, 2019: p. 1-7.

248. Leschelle, X., et al., *Adaptative metabolic response of human colonic epithelial cells to the adverse effects of the luminal compound sulfide.* Biochim Biophys Acta, 2005. **1725**(2): p. 201-12.

249. Malagrino, F., et al., *Hydrogen Sulfide Oxidation: Adaptive Changes in Mitochondria of SW480 Colorectal Cancer Cells upon Exposure to Hypoxia.* Oxid Med Cell Longev, 2019. **2019**: p. 8102936.

250. Goubern, M., et al., *Sulfide, the first inorganic substrate for human cells.* Faseb j, 2007. **21**(8): p. 1699-706.

251. Wang, M., Z. Guo, and S. Wang, *Regulation of cystathionine gamma-lyase in mammalian cells by hypoxia.* Biochem Genet, 2014. **52**(1-2): p. 29-37.

252. Abdollahi Govar, A., et al., *3-Mercaptopyruvate sulfurtransferase supports endothelial cell angiogenesis and bioenergetics.* Br J Pharmacol, 2019.

253. Augsburger, F. and C. Szabo, *Potential role of the 3-mercaptopyruvate sulfurtransferase (3-MST)-hydrogen sulfide (H2S) pathway in cancer cells.* Pharmacol Res, 2018: p. 104083.

254. Modis, K., et al., *Intramitochondrial hydrogen sulfide production by 3-mercaptopyruvate sulfurtransferase maintains mitochondrial electron flow and supports cellular bioenergetics.* Faseb j, 2013. **27**(2): p. 601-11.

255. Valvona, C.J., et al., *The Regulation and Function of Lactate Dehydrogenase A: Therapeutic Potential in Brain Tumor.* Brain Pathol, 2016. **26**(1): p. 3-17.

256. Masson, N. and P.J. Ratcliffe, *Hypoxia signaling pathways in cancer metabolism: the importance of co-selecting interconnected physiological pathways.* Cancer Metab, 2014. **2**(1): p. 3.

257. Xie, H. and M.C. Simon, *Oxygen availability and metabolic reprogramming in cancer.* J Biol Chem, 2017. **292**(41): p. 16825-16832.

258. Samanta, D. and G.L. Semenza, *Metabolic adaptation of cancer and immune cells mediated by hypoxia-inducible factors.* Biochim Biophys Acta Rev Cancer, 2018. **1870**(1): p. 15-22.

259. Semenza, G.L., *Regulation of physiological responses to continuous and intermittent hypoxia by hypoxia-inducible factor 1.* Exp Physiol, 2006. **91**(5): p. 803-6.

260. Yee Koh, M., T.R. Spivak-Kroizman, and G. Powis, *HIF-1 regulation: not so easy come, easy go.* Trends Biochem Sci, 2008. **33**(11): p. 526-34.

261. Budde, M.W. and M.B. Roth, *Hydrogen sulfide increases hypoxia-inducible factor-1 activity independently of von Hippel-Lindau tumor suppressor-1 in C. elegans.* Mol Biol Cell, 2010. **21**(1): p. 212-7.

262. Kai, S., et al., *Hydrogen sulfide inhibits hypoxia- but not anoxia-induced hypoxia-inducible factor 1 activation in a von hippel-lindau- and mitochondria-dependent manner.* Antioxid Redox Signal, 2012. **16**(3): p. 203-16.

263. Wu, B., et al., *Hydrogen sulfide inhibits the translational expression of hypoxia-inducible factor-1alpha.* Br J Pharmacol, 2012. **167**(7): p. 1492-505.

264. Takano, N., et al., *Hypoxia-inducible factors regulate human and rat cystathionine beta-synthase gene expression.* Biochem J, 2014. **458**(2): p. 203-11.

265. Rockwell, S., et al., *Hypoxia and radiation therapy: past history, ongoing research, and future promise.* Curr Mol Med, 2009. **9**(4): p. 442-58.

266. Zhang, J., et al., *Hydrogen sulfide contributes to hypoxia-induced radioresistance on hepatoma cells.* J Radiat Res, 2011. **52**(5): p. 622-8.

267. Bos, E.M., et al., *Hydrogen sulfide: physiological properties and therapeutic potential in ischaemia.* Br J Pharmacol, 2015. **172**(6): p. 1479-93.

268. Leskova, A., et al., *Role of thiosulfate in hydrogen sulfide-dependent redox signaling in endothelial cells.* Am J Physiol Heart Circ Physiol, 2017. **313**(2): p. H256-H264.

269. Marutani, E., et al., *Thiosulfate Mediates Cytoprotective Effects of Hydrogen Sulfide Against Neuronal Ischemia.* J Am Heart Assoc, 2015. **4**(11).

270. Lencesova, L., et al., *Hypoxic conditions increases H(2)S-induced ER stress in A2870 cells.* Mol Cell Biochem, 2016. **414**(1-2): p. 67-76.

271. Olson, K.R., et al., *Hydrogen sulfide as an oxygen sensor/transducer in vertebrate hypoxic vasoconstriction and hypoxic vasodilation.* J Exp Biol, 2006. **209**(Pt 20): p. 4011-23.

272. Morikawa, T., et al., *Hypoxic regulation of the cerebral microcirculation is mediated by a carbon monoxide-sensitive hydrogen sulfide pathway.* Proc Natl Acad Sci U S A, 2012. **109**(4): p. 1293-8.

273. Yuan, G., et al., *Protein kinase G-regulated production of H2S governs oxygen sensing.* Sci Signal, 2015. **8**(373): p. ra37.

274. Wu, H. and Q. Chen, *Hypoxia activation of mitophagy and its role in disease pathogenesis.* Antioxid Redox Signal, 2015. **22**(12): p. 1032-46.

275. Zhang, H., et al., *Mitochondrial autophagy is an HIF-1-dependent adaptive metabolic response to hypoxia.* J Biol Chem, 2008. **283**(16): p. 10892-903.

276. Bianco, S., et al., *Hypoxia and hydrogen sulfide differentially affect normal and tumor-derived vascular endothelium.* Redox Biol, 2017. **12**: p. 499-504.

277. Kajimura, M., et al., *Gas biology: tiny molecules controlling metabolic systems.* Respir Physiol Neurobiol, 2012. **184**(2): p. 139-48.

278. Rose, P., P.K. Moore, and Y.Z. Zhu, *H2S biosynthesis and catabolism: new insights from molecular studies.* Cell Mol Life Sci, 2017. **74**(8): p. 1391-1412.

279. Giuffre, A. and J.B. Vicente, *Hydrogen sulfide biochemistry and interplay with other gaseous mediators in mammalian physiology.* Oxid Med Cell Longev, 2018(In press).

280. Abou-Hamdan, A., et al., *Oxidation of H2S in mammalian cells and mitochondria.* Methods Enzymol, 2015. **554**: p. 201-28.

281. Vicente, J.B., et al., *A Clinically Relevant Variant of the Human Hydrogen Sulfide-Synthesizing Enzyme Cystathionine beta-Synthase: Increased CO Reactivity as a Novel Molecular Mechanism of Pathogenicity?* Oxid Med Cell Longev, 2017. **2017**: p. 8940321.

282. Yang, G. and R. Wang, *H2S and Blood Vessels: An Overview.* Handb Exp Pharmacol, 2015. **230**: p. 85-110.

283. Untereiner, A.A., et al., *Drug resistance induces the upregulation of H2S-producing enzymes in HCT116 colon cancer cells.* Biochem Pharmacol, 2017.

284. Hanaoka, K., et al., *Discovery and Mechanistic Characterization of Selective Inhibitors of H2S-producing Enzyme: 3-Mercaptopyruvate Sulfurtransferase (3MST) Targeting Active-site Cysteine Persulfide.* Sci Rep, 2017. **7**: p. 40227.

285. Zhou, Y., et al., *High-throughput tandem-microwell assay identifies inhibitors of the hydrogen sulfide signaling pathway.* Chem Commun (Camb), 2013. **49**(100): p. 11782-4.
286. Chao, C., et al., *Cystathionine-beta-synthase inhibition for colon cancer: Enhancement of the efficacy of aminooxyacetic acid via the prodrug approach.* Mol Med, 2016. **22**.
287. Ciulli, A., *Biophysical screening for the discovery of small-molecule ligands.* Methods Mol Biol, 2013. **1008**: p. 357-88.
288. Lamoree, B. and R.E. Hubbard, *Current perspectives in fragment-based lead discovery (FBLD).* Essays Biochem, 2017. **61**(5): p. 453-464.
289. Niu, W., et al., *Discovery of selective cystathionine [small beta]-synthase inhibitors by high-throughput screening with a fluorescent thiol probe.* MedChemComm, 2017. **8**(1): p. 198-201.
290. Fogo, J.K. and M. Popowsky, *Spectrophotometric Determination of Hydrogen Sulfide - Methylene Blue Method.* Analytical Chemistry, 1949. **21**(6): p. 732-734.
291. Nguyen, H.H., et al., *Surface plasmon resonance: a versatile technique for biosensor applications.* Sensors (Basel), 2015. **15**(5): p. 10481-510.
292. Yang, G., et al., *H2S as a physiologic vasorelaxant: hypertension in mice with deletion of cystathionine gamma-lyase.* Science, 2008. **322**(5901): p. 587-90.
293. Calvert, J.W., et al., *Hydrogen sulfide mediates cardioprotection through Nrf2 signaling.* Circ Res, 2009. **105**(4): p. 365-74.
294. Whiteman, M., et al., *The effect of hydrogen sulfide donors on lipopolysaccharide-induced formation of inflammatory mediators in macrophages.* Antioxid Redox Signal, 2010. **12**(10): p. 1147-54.
295. Abell, C. and C. Dagostin, *Different Flavours of Fragments*, in *Fragment-Based Drug Discovery*, S. Howard and C. Abell, Editors. 2015, The Royal Society of Chemistry: Cambridge. p. 1-18.
296. van Montfort, R.L.M. and P. Workman, *Structure-based drug design: aiming for a perfect fit.* Essays Biochem, 2017. **61**(5): p. 431-437.
297. Redhead, M., et al., *A combinatorial biophysical approach; FTSA and SPR for identifying small molecule ligands and PAINs.* Anal Biochem, 2015. **479**: p. 63-73.
298. Bisenieks, é.A., et al., *Octahydropyrrolo[4,3,2-m,n]acridine derivatives. I. Synthesis and molecular structure of derivatives of 2,3,4,5,7,8,9,10-octahydropyrrolo[4,3,2-m,n]acridin-10-one, a new heterocyclic system.* Chemistry of Heterocyclic Compounds, 1987. **23**(1): p. 88-92.
299. Biseniex, E.A., et al., *2-(2,6-Dimethyl-3,5-diethoxycarbonyl-1,4-dihydropyridine-4-carboxamide glutaric acid its disodium salt and method of their preparation*. 1984, Google Patents.

300. Bundule, M.F., et al., *Preparation, molecular-crystal structure, and chemical peculiarities of the potassium salt of 3,3,6,6-tetramethyl-1,8-dioxo-1,2, 3,4,5,6,7,8,9,10-decahydroacridine-9-carboxylic acid.* Chemistry of Heterocyclic Compounds, 1980. **16**(5): p. 519-525.

301. Dubur, G.Y. and Y.R. Uldrikis, *Preparation of 3,5-diethoxycarbonyl-2,6-dimethyl-1,4-dihydro-isonicotinic acid and 3,5-diacetyl-2,6-dimethyl-1,4-dihydroisoni-cotinic acid and their salts.* Chemistry of Heterocyclic Compounds, 1972. **5**(6): p. 762-763.

302. Dubur, G., et al., *Pharmaceutical combination of 5-fluorouracil and derivate of 1,4-dihydropyridine and its use in the treatment of cancer*. 2013, Google Patents.

303. Stonans, I., et al., *Derivatives of 1,4-dihydropyridine possessing antiviral efficacy*. 2013, Google Patents.

304. Tirzit, G.D., E.Y. Kazush, and G.Y. Dubur, *Influence of 1,4-dihydropyridine derivatives on the generation of hydroxyl radicals.* Chemistry of Heterocyclic Compounds, 1992. **28**(4): p. 435-437.

305. Kimura, H., *Hydrogen sulfide: its production, release and functions.* Amino Acids, 2011. **41**(1): p. 113-21.

306. Greiner, R., et al., *Polysulfides link H2S to protein thiol oxidation.* Antioxid Redox Signal, 2013. **19**(15): p. 1749-65.

307. Kimura, H., *Physiological role of hydrogen sulfide and polysulfide in the central nervous system.* Neurochem Int, 2013. **63**(5): p. 492-7.

308. Kimura, Y., et al., *Polysulfides are possible H2S-derived signaling molecules in rat brain.* Faseb j, 2013. **27**(6): p. 2451-7.

309. Kolluru, G.K., X. Shen, and C.G. Kevil, *A tale of two gases: NO and H2S, foes or friends for life?* Redox Biol, 2013. **1**: p. 313-8.

310. Shefa, U., M.S. Kim, and N.Y. Jeong, *Antioxidant and Cell-Signaling Functions of Hydrogen Sulfide in the Central Nervous System.* Oxid Med Cell Longev. , 2018. **2018**: p. 1873962.

311. Robberecht, W. and T. Philips, *The changing scene of amyotrophic lateral sclerosis.* Nat Rev Neurosci, 2013. **14**(4): p. 248-64.

312. Dewey, C.M., et al., *TDP-43 is directed to stress granules by sorbitol, a novel physiological osmotic and oxidative stressor.* Mol Cell Biol, 2011. **31**(5): p. 1098-108.

313. McDonald, K.K., et al., *TAR DNA-binding protein 43 (TDP-43) regulates stress granule dynamics via differential regulation of G3BP and TIA-1.* Hum Mol Genet, 2011. **20**(7): p. 1400-10.

314. Spriggs, K.A., M. Bushell, and A.E. Willis, *Translational regulation of gene expression during conditions of cell stress.* Mol Cell, 2010. **40**(2): p. 228-37.

315. Mahboubi, H., M. Kodiha, and U. Stochaj, *Automated detection and quantification of granular cell compartments.* Microsc Microanal, 2013. **19**(3): p. 617-28.

316. Wheeler, J.R., et al., *Distinct stages in stress granule assembly and disassembly.* eLife, 2016. **5**: p. e18413.

317. Anderson, P. and N. Kedersha, *Stress granules.* Curr Biol, 2009. **19**(10): p. R397-8.

318. Aulas, A. and C. Vande Velde, *Alterations in stress granule dynamics driven by TDP-43 and FUS: a link to pathological inclusions in ALS?* Front Cell Neurosci, 2015. **9**: p. 423.

319. Dewey, C.M., et al., *TDP-43 aggregation in neurodegeneration: are stress granules the key?* Brain Res, 2012. **1462**: p. 16-25.

320. Neumann, M., et al., *Ubiquitinated TDP-43 in frontotemporal lobar degeneration and amyotrophic lateral sclerosis.* Science, 2006. **314**(5796): p. 130-3.

321. Cestra, G., et al., *Control of mRNA Translation in ALS Proteinopathy.* Front Mol Neurosci, 2017. **10**: p. 85.

322. Baird, T.D. and R.C. Wek, *Eukaryotic initiation factor 2 phosphorylation and translational control in metabolism.* Adv Nutr, 2012. **3**(3): p. 307-21.

323. Novoa, I., et al., *Feedback inhibition of the unfolded protein response by GADD34-mediated dephosphorylation of eIF2alpha.* J Cell Biol, 2001. **153**(5): p. 1011-22.

324. Kedersha, N.L., et al., *RNA-binding proteins TIA-1 and TIAR link the phosphorylation of eIF-2 alpha to the assembly of mammalian stress granules.* The Journal of cell biology, 1999. **147**(7): p. 1431-1442.

325. Das, I., et al., *Preventing proteostasis diseases by selective inhibition of a phosphatase regulatory subunit.* Science, 2015. **348**(6231): p. 239-42.

326. Saxena, S., E. Cabuy, and P. Caroni, *A role for motoneuron subtype-selective ER stress in disease manifestations of FALS mice.* Nat Neurosci, 2009. **12**(5): p. 627-36.

327. Wang, L., et al., *Guanabenz, which enhances the unfolded protein response, ameliorates mutant SOD1-induced amyotrophic lateral sclerosis.* Neurobiol Dis, 2014. **71**: p. 317-24.

328. Kim, H.-J., et al., *Therapeutic modulation of eIF2α phosphorylation rescues TDP-43 toxicity in amyotrophic lateral sclerosis disease models.* Nature genetics, 2014. **46**(2): p. 152-160.

329. Green, K.M., et al., *RAN translation at C9orf72-associated repeat expansions is selectively enhanced by the integrated stress response.* Nat Commun, 2017. **8**(1): p. 2005.

330. Moreno, J.A., et al., *Sustained translational repression by eIF2alpha-P mediates prion neurodegeneration.* Nature, 2012. **485**(7399): p. 507-11.

331. Yadav, V., et al., *Hydrogen sulfide modulates eukaryotic translation initiation factor 2alpha (eIF2alpha) phosphorylation status in the integrated stress-response pathway.* J Biol Chem, 2017. **292**(32): p. 13143-13153.

332. Valentino, F., et al., *Elevated cerebrospinal fluid and plasma homocysteine levels in ALS.* Eur J Neurol, 2010. **17**(1): p. 84-9.

333. Szabo, C. and A. Papapetropoulos, *International Union of Basic and Clinical Pharmacology. CII: Pharmacological Modulation of H2S Levels: H2S Donors and H2S Biosynthesis Inhibitors.* Pharmacol Rev, 2017. **69**(4): p. 497-564.

334. Taylor, J.P., R.H. Brown, Jr., and D.W. Cleveland, *Decoding ALS: from genes to mechanism.* Nature, 2016. **539**(7628): p. 197-206.

335. Lemmens, R., et al., *RNA metabolism and the pathogenesis of motor neuron diseases.* Trends Neurosci, 2010. **33**(5): p. 249-58.

336. Malagrino, F., et al., *Hydrogen Sulfide Oxidation: Adaptive Changes in Mitochondria of SW480 Colorectal Cancer Cells upon Exposure to Hypoxia.* 2019. **2019**: p. 8102936.

337. O'Reilly, J.P., C. Jiang, and G.G. Haddad, *Major differences in response to graded hypoxia between hypoglossal and neocortical neurons.* Brain Res, 1995. **683**(2): p. 179-86.

338. Pierrefiche, O., et al., *Hypoxic response of hypoglossal motoneurones in the in vivo cat.* J Physiol, 1997. **505 (Pt 3)**: p. 785-95.

339. Hanson, K.A., et al., *Ubiquilin modifies TDP-43 toxicity in a Drosophila model of amyotrophic lateral sclerosis (ALS).* J Biol Chem, 2010. **285**(15): p. 11068-72.

340. Zhan, L., et al., *Identification of genetic modifiers of TDP-43 neurotoxicity in Drosophila.* PLoS One, 2013. **8**(2): p. e57214.

341. Casci, I. and U.B. Pandey, *A fruitful endeavor: modeling ALS in the fruit fly.* Brain Res, 2015. **1607**: p. 47-74.

342. Li, W.Z., et al., *A broad expression profile of the GMR-GAL4 driver in Drosophila melanogaster.* Genet Mol Res, 2012. **11**(3): p. 1997-2002.

343. Kennerdell, J.R. and R.W. Carthew, *Heritable gene silencing in Drosophila using double-stranded RNA.* Nat Biotechnol, 2000. **18**(8): p. 896-8.

344. Birmingham, A., et al., *3' UTR seed matches, but not overall identity, are associated with RNAi off-targets.* Nat Methods, 2006. **3**(3): p. 199-204.

345. Ferri, A., et al., *Cell death in amyotrophic lateral sclerosis: interplay between neuronal and glial cells.* Faseb j, 2004. **18**(11): p. 1261-3.

346. Philips, T. and W. Robberecht, *Neuroinflammation in amyotrophic lateral sclerosis: role of glial activation in motor neuron disease.* Lancet Neurol, 2011. **10**(3): p. 253-63.

347. Morikawa, T., et al., *Hypoxic regulation of the cerebral microcirculation is mediated by a carbon monoxide-sensitive hydrogen sulfide pathway.* Proceedings of the National Academy of Sciences of the United States of America, 2012. **109**(4): p. 1293-1298.